Developmentally Regulated and Environmentally Induced Programmed Cell Death (PCD) in the Lace Plant (*Aponogeton madagascariensis*)

by

Christina Ella Nickerson Lord

Submitted in partial fulfilment of the requirements
for the degree of Doctor of Philosophy

at

Dalhousie University
Halifax, Nova Scotia
March 2013

DALHOUSIE UNIVERSITY

DEPARTMENT OF BIOLOGY

The undersigned hereby certify that they have read and recommend to the Faculty of Graduate Studies for acceptance a thesis entitled "Developmentally Regulated and Environmentally Induced Programmed Cell Death (PCD) in the Lace Plant (*Aponogeton madagascariensis*)" by Christina Ella Nickerson Lord in partial fulfillment of the requirements for the degree of Doctor of Philosophy.

Dated: March 8th 2013

External Examiner: _____

Research Supervisor: _____

Examining Committee: _____

_____

Departmental Representative: _____

DALHOUSIE UNIVERSITY

DATE: March 8th 2013

AUTHOR: Christina Ella Nickerson Lord

TITLE: Developmentally Regulated and Environmentally Induced Programmed Cell Death (PCD) in the Lace Plant (*Aponogeton madagascariensis*)

DEPARTMENT OR SCHOOL: Department of Biology

DEGREE: PhD CONVOCATION: May YEAR: 2013

_____

Signature of Author

For my parents, all four of whom raised me to believe I could accomplish this.

Table of Contents

List of Tables

List of Figures

Abstract

Programmed cell death (PCD) is pervasive in eukaryotes, playing a fundamental role in development. PCD in animals has been studied in detail, partly due to *Caenorhabditis elegan*s, a worm whose anatomy allowed for the investigation of exactly 131 cells that die via PCD. Elucidating this complex pathway in this simple worm laid the foundation for further insights into mammalian PCD. Overall, less is known regarding PCD in plants, where cell death is broadly separated into developmentally regulated and environmentally induced. The lace plant (*Aponogeton madagascariensis)* undergoes developmentally regulated PCD to form perforations between longitudinal and transverse veins over its leaf surface. The optimization of protoplast isolation and induced cell death via heat shock (HS) in the lace plant is detailed here. Following HS, protoplasts displayed characteristics of PCD including: Terminal deoxynucleotidyl transferase-mediated dUTP nick-end labeling (TUNEL) positive nuclei, increases in vesicles as well as Brownian motion, and plasma membrane blebbing. Additionally, mitochondrial dynamics were investigated, and a role for the mitochondrial permeability transition pore (MPTP) was indirectly established via cyclosporine A (CsA) experimentation. The main focus of this dissertation was to elucidate cellular dynamics during developmentally regulated PCD in the lace plant, which is visibly discernable during the window stage of leaf development. A single areole within a window stage leaf was further divided into three areas based on the progression of PCD; non-PCD (NPCD) cells, early PCD (EPCD) cells, and late PCD (LPCD) cells. Using this gradient, mitochondria were delineated into four stages based on distribution, motility, and membrane potential. Additionally, it was determined that the MPTP also played a role in developmental lace plant PCD, as inhibition of the pore with CsA not only reduced caspase-like proteases (CLPs) but also stopped perforation formation. Furthermore, the actin cytoskeleton was also investigated, with evidence suggesting it as a possible target for CLPs. The novel use of lace plant leaves for long-term live cell imaging allowed for the establishment of a timeline of cellular events that occur during developmental PCD. Major conclusions of this dissertation reveal various similarities between environmental induced and developmentally regulated PCD in this one plant species.

List of Abbreviations Used

2, 4-D	2, 4-dichlorophenoxyacetic acid
$\Delta\Psi_m$	membrane potential
ABC	ATP-binding cassette
ADP	adenosine diphosphate
$AlC1_3$	aluminum chloride
AIF	apoptosis-inducing factor
ANT	adenine nucleotide translocase
Apaf-1	apoptosis activating factor-1
Arg	arginine
Asp	aspartate
ATP	adenosine triphosphate
Avr	avirulence
Bcl	b-cell-lymphoma
Cd	cadmium
CARD	caspase recruitment domain
Caspase	cysteine aspartate-specific proteases
CEM	cephalic male sensory
Ced	cell death abnormal
Ces	cell death specification
CLP(s)	caspase-like protease(s)
CMXRos	chloromethyl-X-rosamine
CsA	cyclosporine A
Cyt-*c*	cytochrome *c*
CyP-D	cyclophilin D
DAPI	4', 6-diamidino-2-phenylindole
DED	death effector domain
DEVD	Asp-Glu-Val-Asp
DIC	differential interference contrast
DISC	death-inducing signalling complex

Egl	egg-laying defective
Endo G	endonuclease G
EPCD	early programmed cell death
ER	endoplasmic reticulum
ETC	electron transport chain
FDA	fluorescein diacetate
FITC	fluorescein isothiocyanate
GA	glutaraldehyde
Gln	glutamine
HR	hypersensitive response
HS	heat shock
HSN	hermaphrodite-specific neurons
IMM	inner mitochondrial membrane
IMS	intermembrane space
Jasp	jasplakinolide
Lat B	latrunculin B
LPCD	late programmed cell death
LRRs	leucine-rich repeats
Lys	lysine
LZ	leucine zipper
MES	2-N-morpholino-ethanesulfonic acid
MPT	mitochondrial permeability transition
MPTP	mitochondrial permeability transition pore
MS	Murashige and Skoog
NPCD	non-programmed cell death
Nuc	nuclease
NSM	neurosecretory motor
OMM	outer mitochondrial membrane
OsO_4	osmium tetroxide
PCD	programmed cell death
PI	propidium iodide

PM	plasma membrane
Prf gene	pathogen resistance gene
Pro	proline-rich repeat motif
Q-PCR	quantitative polymerase chain reaction
R genes	resistance genes
ROS	reactive oxygen species
SAM	shoot apical meristem
SI	self-incompatibility
TE	treachery element
TEM	transmission electron microscopy
TIR	drosophila toll, mammalian interleukin-1 receptor
TMV	tobacco mosaic virus
TRITC	tetramethyl rhodamine isothiocyanate
TUNEL	terminal deoxynucleotidyl transferase mediated dUTP nick-end labeling
TVS	transvacuolar strand
VDAC	voltage dependent anion channel
VPE	vacuolar processing enzyme
YVAD	Tyr-Val-Ala-Asp
ZN	zinc finger motif

Acknowledgments

I thank my supervisor, and good friend Dr. Arunika Gunawardena. Your passion and expertise in the field of botany inspired me to take my own passion more seriously. I am grateful for your high expectations, which instilled within me a work ethic that will stay with me for the remainder of my life. Thank you for believing in me, and often giving me opportunities that although challenged me, taught me more than most graduate students would ever encounter. I would also like to sincerely thank the other members of my committee, Dr. Gefu Wang-Pruski, and Dr. Bill Pohajdak for their assistance at all levels of this work.

To my lifetime best friend Jessica Ells, thank you for your never-ending encouragement, patience and understanding. Like family you supported me in times of struggle and celebrated with me in times of triumph. You are my sanity, and in many ways this is your achievement as well. Also, many thanks to Adrian Dauphinee and Allison King; you were motivating confidants who made this experience even more exceptional for me. Thank you to Brendan Reese, Tyler Legere, Matt Lynch and Richard Redden, although you may not realize it, your presence and support keeps me grounded, and each of you has shaped this work in your own little way. Lastly, thank you to my brother Anthony Lord and his partner Wendy Krkosek, you are both amazing role models and I could not think of two people more deserving of admiration.

The work presented in this thesis was supported by grants to Dr. Arunika Gunawardena from the Natural Sciences and Engineering Research Council (NSERC) of Canada and also from the Canadian Foundation for Innovation (CFI). I also gratefully acknowledge NSERC for its support in the form of a Postgraduate Scholarship (PGS) doctoral scholarship awarded to me in my last three years of study.

Chapter 1 Introduction

Large portions of this introduction are published as:

Lord CEN, Gunawardena AHLAN. Programmed cell death in *C. elegans*, mammals and plants. European Journal of Cell Biology 91: (2012) 603-613

1.1 Types of Cell Death: Necrosis vs. Programmed Cell Death

Cell death is an omnipresent process that occurs throughout the eukaryotic kingdom, and exists in multiple forms, including necrosis and programmed cell death (PCD). Necrotic cell death has been described in both plant (McCabe et al. 1997; reviewed by McCabe and Leaver 2000; Evans 2004; reviewed by Chowdhury et al. 2008; Lord and Gunawardena 2011) and animal (reviewed by Golstein and Kroemer 2007; Kroemer et al. 2009) systems and is characterized morphologically by an overall gain in cell volume, the swelling of organelles, and plasma membrane (PM) rupture leading to subsequent degradation of remaining intracellular contents (reviewed by McCabe and Leaver 2000; Kroemer et al. 2009; Lord and Gunawardena 2011). Although necrosis has generally been considered to be an uncontrolled process, evidence is now emerging suggesting it may be more organized than once thought (reviewed by Golstein and Kroemer 2007; Kroemer et al. 2009; reviewed by Kacprzyk et al. 2011; van Doorn et al. 2011). Work reviewed by Golstein and Kroemer (2007) demonstrated that following the initial cell death signal, necrotic cells displayed signs of a controlled process, including mitochondrial dysfunction and enhanced generation of reactive oxygen species (ROS).

Conversely to necrosis, PCD, as its name suggests, is the regulated removal of cells within a multicellular organism. Within animal systems PCD is usually divided into two categories: 1. apoptosis, characterized by chromatin condensation, nuclear fragmentation and the formation of apoptotic bodies and 2. autophagy, usually occurring in the absence of chromatin condensation, and involving the accumulation of double/multi membrane autophagic vacuoles (Kroemer et al. 2009; Kacprzyk et al. 2011). The delineation of plant PCD into categories has been challenging in the past. Fukuda

(2000) keyed three forms of plant PCD: 1. apoptotic-like, a fast process characterized by the initial shrinkage of the nucleus and followed by chromatin condensation, nuclear fragmentation and DNA laddering 2. cell death occurring during senescence, a slow process characterized by the initial loss of chloroplasts and followed by nuclear and vacuolar breakdown and 3. PCD in which the vacuole plays the central role, this process is intermediate in length between the aforementioned examples and is characterized by vacuole enlargement followed by disruption of the tonoplast and PM leading to inevitable degradation of organelles. In 2005 van Doorn and Woltering compared plant PCD with three previously described morphological categories of metazoan cell death 1. autophagy, involving three distinct forms of the process, micro-, macro- and mega-autophagy. Micro-autophagy is the uptake of small portions of the cytoplasm by a lytic compartment, usually the vacuole in plant cells. Macro-autophagy involves the formation of a double membrane structure known as the autophagosome, which will then fuse with a lytic compartment, again usually the vacuole in plant cells. Lastly, mega-autophagy is accomplished by the permeabilization or rupture of tonoplast. 2. apoptosis, defined by the presence of nuclear fragmentation, apoptotic bodies and the final degradation of the apoptotic bodies by the lysosome of another cell and 3. non-lysosomal PCD, involving the inhibition of major biosynthetic pathways leading to cell death. These authors concluded that no examples of plant PCD conformed to the second category, apoptotic cell death, given no true apoptotic bodies, or lysosomes, are found within plant systems (van Doorn and Woltering 2005). In 2008 Reape et al. as well as Reape and McCabe continued with the use of the term apoptotic-like cell death, referring to occurrences of PCD following both abiotic stress and developmental signals (McCabe et al. 1997). In

(2011) both van Doorn et al. and van Doorn proposed two changes to the terminology used to describe plant PCD based on morphological characteristics. Initially van Doorn et al. (2011) suggested the implementation of two categories: 1. vacuolar cell death, characterized by the removal of cell contents through a combination of autophagy-like processes and the release of hydrolases from collapsed vacuoles and 2. necrotic cell death, characterized by early rupture of the PM, shrinkage of the protoplast, and the lack of vacuolar cell death features. It is pertinent to note that by this van Doorn et al. (2011) definition some examples of plant PCD cannot be described via these major classes, including self-incompatibility (SI) and PCD of the cereal endosperm, lending to the fact that caution should be taken when categorizing plant PCD (van Doorn et al. 2011).

By this van Doorn et al. (2011) example, necrosis is defined as a form of PCD; this has not been an overwhelmingly putative classification in the past; as noted above. Evidence has been widely presented and accepted that PCD and necrosis are two different processes although they can occur independently, sequentially, or simultaneously (reviewed by Elmore 2007). It has been demonstrated that it is the stimuli or the degree of stimuli, which determines whether a cell will undergo necrosis or PCD. For instance at low doses a variety of stimuli, including hypoxia and heat shock (HS) induce PCD, however at high doses these same stimuli can result in necrotic cell death (McCabe et al. 1997; reviewed by McCabe and Leaver 2000; Evans 2004; reviewed by Elmore 2007). This author believes the theory that PCD and necrosis are separate processes; the discussion presented by van Doorn et al. (2011) in which necrotic cell death in plants is a form of PCD requires future investigation.

Additionally in (2011) van Doorn proposed another ammendment to the classification system of plant PCD, citing that the category 'vacuolar cell death' defind in the van Doorn et al. (2011) manuscript was inherintently incorrect given that the vacuole is also involved during PCD in examples that were ascribed to other categories. Hence, two new forms of PCD were suggested: 1. autolytic, which shows features of tonoplast rupture and the susbsequent rapid degradation of the cytosolic components and 2. non-autolytic that can include tonoplast permebilization or rupture, but does not portray rapid cytosolic clearnace. These categories, autolytic and non-autolytic, are suggested to correspond with the categrories of 'autophagy' and 'necrosis' in animal PCD systems respectively. Overall it is obvious that there is a lack of consistenty with regards to classifying plant PCD based on morphology; consequently this point will be addressed further within the discussion.

1.2 Molecular and Cellular Characteristics of Programmed Cell Death

1.2.1 Programmed Cell Death in Mammals

Mammalian cells that undergo apoptotic cell death display distinct morphological and molecular characteristics, in brief they include but are not limited to: alterations in mitochondrial dynamics (reviewed by Jones 2000; reviewed by Wang and Youle 2009), influx of Na^{2+} leading to PM depolarization and subsequent efflux of K^{+} cations (Benítez-Rangel et al. 2011), up regulation of caspases (*C*ysteine *ASP*artate-specific prote*ASES;* reviewed by Denault and Salvesen 2002; Potten and Wilson 2004), actin cytoskeleton modulations (reviewed by Franklin-Tong and Gourlay 2008), formation of apoptotic bodies, cellular condensation and shrinkage, nuclear fragmentation detectable by terminal

deoxynucleotidyl transferase mediated dUTP nick-end labeling (TUNEL) staining, and chromatin condensation leading to DNA laddering into 180 bp nucleosomal units (Potten and Wilson 2004; Widlak and Garrard 2005; reviewed by Jan et al. 2008; reviewed by Conradt 2009). Given that PCD plays such a distinct role in the life cycle of many mammals several of the key players in the process have been examined in detail.

1.2.1.1 Bcl-2 Family Members

B-cell-lymphoma (Bcl-2) family proteins serve as critical regulators to the PCD pathway in mammals (reviewed by Gross et al. 1999). Over 20 members of the Bcl-2 family of proteins have been identified in humans, all of which act as either pro- or anti-apoptotic (reviewed by Gross et al. 1999; Pepper and Bentley 2000). Examples of pro-apoptotic family members include: Bak, Bad, Bax, Bik and Bid, while examples of anti-apoptotic family members include: Bcl-2 and Bcl-x_L (Pepper and Bentley 2000; Potten and Wilson 2004; reviewed by Jan et al. 2008). Whether pro- or anti-apoptotic, three general functions for Bcl-2 family members have been identified: 1. dimerization with other Bcl-2 family proteins; 2. interactions with proteins to control mitochondrial homeostasis, and 3. the formation of ion channels or pores in the outer mitochondrial membrane (OMM; Pepper and Bentley 2000). The majority of the Bcl-2 proteins contain C-terminal hydrophobic transmembrane domains that cause them to post-transcriptionally insert themselves into membranes including the OMM, the nuclear envelope and the endoplasmic reticulum (ER; Figure 1.1; reviewed by Hengartner 2000; Potten and Wilson 2004).

1.2.1.2 Mitochondrial Involvement During Mammalian PCD

In almost all examples of mammalian PCD the mitochondria is known to play an imperative role. It has been demonstrated experimentally that the PCD pathway is amplified by the release of apoptotic molecules from the mitochondrial intermembrane space (IMS; reviewed by Crompton 1999; reviewed by Jones 2000; reviewed by Wang and Youle 2009). These proteins are able to exit the mitochondria through two main pathways (Figure 1.2). One being the mitochondrial permeability transition pore (MPTP; Figure. 1.2A), and the second via pro-apoptotic pore forming Bcl-2 family proteins mentioned above, which in some cases can also involve the voltage dependent anion channel (VDAC; Figure 1.2B; reviewed by Crompton 1999; Halestrap et al. 2000; reviewed by Jones 2000; Potten and Wilson 2004; reviewed by Kroemer et al. 2007; reviewed by Wang and Youle 2009).

The MPTP is a considerably simple structure that is between 2.0-2.6 nm in diameter and can transport molecules $\leq$ 1.5 kDa. It is made up primarily of three components: 1. the inner mitochondrial membrane (IMM) localized adenine nucleotide translocase (ANT); 2. the matrix localized cyclophilin D (CyP-D); and 3. the OMM localized VDAC. ANT is an antiporter that catalyzes the exchange of adenosine diphosphate (ADP) for adenosine triphosphate (ATP) across the IMM. CyP-D is known to bind to the ANT, and in the presence of increased cytosolic Ca^{2+} converts the exclusive pore into a nonspecific transporter (Halestrap et al. 2000). The VDAC is also known to attach to the ANT and outside of its position in the MPTP behaves as a general diffusion pore for the transport of hydrophilic molecules (reviewed by Hengartner 2000). A strong MPTP pore inhibitor known as cyclosporine A (CsA) has been used extensively to inhibit

programmed cell death. Radioactively labeled CsA has been shown to bind to CyP-D *in vivo* and has been demonstrated to prevent the MPTP from opening (reviewed by Crompton 1999; Potten and Wilson 2004).

MPTP formation in mammals is generally a consequence of mitochondrial Ca^{2+} overload (reviewed by Crompton 1999; Halestrap et al. 2000; reviewed by Gunter et al. 2000; reviewed by Jones 2000). In healthy cells Ca^{2+} enters the mitochondria via a Ca^{2+} uniporter and exits via exchange with either a Na^{+} dependent or independent carrier (reviewed by Gunter et al. 2000). Ca^{2+} moving in this manner results in a continuous cycling of Ca^{2+} across the IMM. Oxidative stress can bring about a progressive increase in free Ca^{2+} within the cytosol of the cell. A change in cytosolic Ca^{2+} of 1-3μM is considered an overload and results in a decrease in efflux versus influx of Ca^{2+} in and out of the mitochondria; subsequently causing the formation of the MPTP (reviewed by Crompton 1999; reviewed by Gunter et al. 2000). Following MPTP formation solutes rush into the mitochondrial matrix, causing the mitochondrial permeability transition (MPT) of the IMM and causing a concurrent drop in mitochondrial membrane potential ($\Delta\Psi_m$). Oxidative phosphorylation is also disassociated from the electron transport chain (ETC) and matrix swelling is thought to occur. This matrix swelling then disrupts the OMM causing it to be permeabilized or rupture (Figure 1.2).

Succeeding the permeabilization or rupture of the OMM, apoptotic factors are released from the IMS, which include: cytochrome *c* (cyt-*c*), apoptosis-inducing factor (AIF) and endonuclease G (Endo G; Figure 1.2). Cyt-*c*, a respiratory chain protein bound on the outer face of the IMM binds with apoptosis activating factor-1 (Apaf-1) once in the cytosol forming the apoptosome (Figure 1.3 and 1.4; reviewed by Bratton and

Salvesen 2010). Apaf-1 contains a WD-40 repeat domain, which can act as scaffolding for protein-protein interactions, and is thought to be the location of cyt-*c* binding (Figure 1.3). Apaf-1 also contains a nucleotide binding domain (NB-ARC), which is thought to bind and hydrolyze ATP (Figure 1.3). Following the formation of the apoptosome it then binds specific proteases, to further the PCD process (reviewed by Hengartner 2000; reviewed by Shi 2001; Potten and Wilson 2004; Kim et al. 2005; Bajt et al. 2006; reviewed by Wang and Youle 2009).

AIF and Endo G are IMS nucleases that are also brought from the mitochondria to the cytosol following the formation of the MPTP. Once in the cytosol they relocate to the nucleus where AIF causes chromatin condensation and DNA fragmentation into high molecular weight fragments (50-300 kb; reviewed by Hengartner 2000; Joza et al. 2001; Bajt et al. 2006; reviewed by Wang and Youle 2009; Figure 1.4), while Endo G causes DNA fragmentation, but into oligonucleosomal size portions, thought to be responsible for DNA laddering during agarose gel electrophoresis (fragment size 180-190 bp; reviewed by Hengartner 2000; Zhang et al. 2003; Widlak and Garrard 2005; Bajt et al. 2006; Figure 1.4). Overall, each of these mitochondrial IMS proteins appears to play a significant role in the PCD process.

1.2.1.3 Cysteine Aspartic-Specific Proteases (Caspases)

Another main distinction of mammalian PCD is the occurrence of a family of death inducing proteases known as cysteine aspartic-specific proteases (caspases). Caspases consist of an N-peptide region, a large subunit (20kDa), a linker and a small subunit (10kDa) and are referred to as procaspases prior to activation (Figure 1.5). The large and small subunits on the C-terminus are catalytic domains. The N-peptide region

varies in length and within it are regulatory domains that act as protein-protein interaction modules, such as the caspase recruitment domain (CARD) and the death effector domain (DED). These regulatory domains within the N-peptide region are responsible for specific recruitment of caspases to different cell death pathways (Stennicke 2000; Uren et al. 2000; reviewed by Denault and Salvesen 2002; Potten and Wilson 2004; Figure 1.5). In all, approximately fourteen caspases have been identified in humans (Stennicke 2000). Caspases are often divided into three major groups (Figure 1.5): 1. cytokine activators (CASP 1, 4, 5, 11, 12 and 13): 2. initiator caspases (CASP 2, 8, 9 and 10): and 3. effector caspases (CASP 3, 6, 7 and 14; Stennicke 2000; reviewed by Denault and Salvesen 2002; Potten and Wilson 2004; reviewed by Chowdhury et al. 2008).

Activation of procaspases requires selective proteolytic cleavage of the protease at two cleavage sites (Figure 1.6)[1]. The active caspase then consists of two heterodimers, each containing one large and one small subunit, existing as a tetramer. Procaspases can be activated by two different mechanisms: 1. homo-activation, which requires the recruitment of the procaspase to selected factors within the cell or 2. Hetero-activation, that requires another protease to act upon the pro-caspase resulting in its' activation. Homo-activation is based mainly on the induced proximity hypothesis in which the increased concentration of procaspases possessing intrinsic enzymatic activity forces activation, hence no outside protease is required; homo-activation is common amongst initiator caspases. Homo-activation occurs in caspase 8 and 9 where activation transpires by recruitment to the death-inducing signalling complex (DISC), a multi protein complex

[1] This figure is supplemental to the figures published in European Journal of Cell Biology and aimed to clarify the activation of procaspases.

usually assembled on the PM. The apoptosome, a cytosolic multi-protein complex, constitutes another homo-activation mechanism. This complex allows the attachment of pro-caspase 9, which is in turn activated (Stennicke 2000; reviewed by Hengartner 2000; reviewed by Shi 2001; Potokar et al. 2006).

Hetero-activation is the activation of procaspases by initiator caspases or other proteases, and is common amongst effector caspases (Stennicke 2000; reviewed by Hengartner 2000; reviewed by Denault and Salvesen 2002). Once activated, effector caspases have the ability to discriminate between substrates for cleavage. Overall, this cleavage is based on the recognition of Aspartate (Asp) in the P_1 position (Asp being directly N-terminal to site of cleavage) on the substrate by catalytic domains on the caspase. In the caspase structures examined thus far, the small and large subunits contain at least seven residues that can play a role in substrate recognition of P_1 Asp: Arginine (Arg) 179, Glutamine (Gln) 283 and Arg 341 are three depicted in Figure 1.5 (Stennicke 2000; reviewed by Chowdhury et al. 2008).

Cytokine activators, also often described as initiator caspases, are activated within a complex termed the inflammasome. The inflammasome is composed of procaspase-1 and 5, as well as a CARD containing protein. The formation of this complex results in the activation of these caspases, which in turn process cytokines, playing a central role in immune response and apoptosis (reviewed by Chowdhury et al. 2008).

1.2.1.4 The Actin- Cytoskeleton

In mammalian cells, organization and shape is maintained by the cytoskeleton, consisting of filamentous networks of actin, intermediate filaments and microtubules (reviewed by Franklin-Tong and Gourlay 2008). Actin dynamics have recently been

shown to play a role in the regulation of specific morphological features of PCD. Actin has been shown to be a target for caspase activity during apoptosis in animal cells, leading to the production of actin N-terminal 32 kDa and 15 kDa fragments (Utsumi et al. 2003; reviewed by Franklin-Tong and Gourlay 2008). Also, through the application of actin depolymerizing drugs such as latrunculin B (Lat B) apoptosis was stimulated in ischaemic kidney cells (Genescà et al. 2006; reviewed by Franklin-Tong and Gourlay 2008). Subsequently the application of the F-actin stabilizing drug Jasplakinolide (Jasp) to the same kidney cells was able to alleviate cell death (Genescà et al. 2006; reviewed by Franklin-Tong and Gourlay 2008). Interestingly, in several systems, including Jurkat T-cells, the application of Jasp has been shown to induce apoptosis (Odaka et al. 2000). Overall it appears that caspases can alter actin dynamics, which in turn can modulate apoptotic signals.

1.2.2 Programmed Cell Death in Caenorhabditis elegans

PCD analyses in *C. elegans* have been extensive throughout the years and have led to the identification of many key players in cell death pathways as a whole (reviewed by Conradt and Xue 2005). This investigation of PCD has been made possible due to the biology of this model worm. PCD in *C. elegans* occurs during both embryonic and post-embryonic development in the soma, and also in the gonads of adult hermaphroditic worm (Sulston and Horvitz 1977; Ellis and Horvitz 1986; reviewed by Conradt and Xue 2005). Cell death within this system has been designated apoptotic and can be seen very clearly via differential interference contrast (DIC) microscopy or Nomarski optics. These characteristics of cell death allowed for the elucidation of PCD in *C. elegans* where 1090

cells will develop within the whole hermaphroditic organism and 131 will die via PCD, leaving a total of 959 cells in an adult worm (Gartner et al. 2003; reviewed by Lettre and Hengartner 2006; reviewed by Darland-Ransom et al. 2009). Like in mammals, these dying cells display distinct morphological characteristics including changes in the refractivity of the nucleus and cytoplasm until they resemble flat, round disks, cell shrinkage, chromatin condensation and phagocytosis of the corpse (Gartner et al. 2003; reviewed by Conradt and Xue 2005; reviewed by Darland-Ransom et al. 2009).

The detailed knowledge of the timing and location of PCD during development in *C. elegans* has led to the screening of mutants that affect the regulation of the cell death process. Analysis of these mutants suggests that PCD genes within *C. elegans* fall into one of four categories: 1. genes involved in the selection of cell types that are to die, including cell death specification 1 and 2 (*ces-1* and *-2*); 2. genes involved in the killing of selected cells, including cell death abnormal 3, 4, 8 and 9 (*ced-3, -4, -8* and *-9*) and egg-laying defective 1 (*egl-1*); 3. genes involved in coding for proteins required for the recognition, engulfment and removal of the cell corpse including *ced-1, -2, -5, -6, -7, -10 and -12;* and 4. genes involved in the degradation of genomic DNA in dead or dying cells, including nuclease 1 (nuc-1; Gartner et al. 2003; reviewed by Conradt and Xue 2005; reviewed by Lettre and Hengartner 2006; reviewed by Darland-Ransom et al. 2009).

1.2.2.1 'Selection Gene' Regulation

Products encoded for by genes *ces-1* and *2* are important in determining the fates of three specific cell types within *C. elegans* including: 1. neurosecretory motor (NSM's) neurons in the pharynx; 2. hermaphrodite-specific neurons (HSN's) that develop in both

hermaphrodites and males and undergo PCD in the latter; and 3. cephalic male sensory (CEM's) neurons, that develop in both hermaphrodites and males and undergo PCD in the former, CEM's inevitably become sensory neurons (reviewed by Darland-Ransom et al. 2009).

1.2.2.2 'Killer Gene' Regulation

Two genes, *ced-3* and *ced-4* are instrumental in nearly all PCD pathways in *C. elegans* (Hengartner and Bryant 2000). Loss of function mutations in either one of these genes causes the survival of all 131 cells, which are normally destined to die; conversely, gain of function mutations cause extensive cell death. *Ced-3* encodes a protein with similarity to mammalian caspases (reviewed by Darland-Ransom et al. 2009). Like other caspases, CED-3 contains a CARD and is synthesized as a pro-enzyme that is proteolytically cleaved to generate an active protease (Stennicke 2000; Uren et al. 2000; reviewed by Denault and Salvesen 2002; Figure 1.5). Like some mammalian caspases, *C. elegans* CED-3 is activated by an Apaf-1 homolog CED-4 and has been shown to bind to human Apaf-1 *in vitro* (Potten and Wilson 2004).

Examinations of protein databases reveal significant sequence similarities between *C. elegans* CED-4 and mammalian Apaf-1 (Figure 1.3). Both CED-4 and Apaf-1 contain a CARD and nucleotide binding motifs that are critical for the function of these proteins (Hengartner and Bryant 2000; Joza et al. 2001; reviewed by Inohara et al. 2002; Potokar et al. 2006; Figure 1.3). The similarities of *ced-3* and *ced-4* to mammalian genes have been confirmed through the transfection and overexpression of *ced-3* and *ced-4* into mammalian systems, which in turn triggers PCD (Chinnaiyan 1997).

Both pro and anti-apoptotic forms of Bcl-2 family proteins also exist within *C. elegans*. *Ced-9* encodes a protein possessing anti-apoptotic capabilities, with 25% sequence similarity to that of Bcl-2 and Bcl-x_L (Jabbour et al. 2006; Figure 1.1). Despite the less than half sequence similarity, human anti-apoptotic Bcl-2 family proteins can partially rescue *ced-9* mutant worms from PCD, thus suggesting that action may be more important than sequence similarity (Figure 1.1; Jabbour et al. 2006). *Egl-1* acts upstream of *ced-9* and encodes a relatively small protein of 91 amino acids with a BH3 motif that has been found in all death promoting Bcl-2 family members (reviewed by Conradt and Xue 2005; reviewed by Nehme and Conradt 2008; reviewed by Conradt 2009).

In cells that are destined to survive, CED-3 and CED-4 are kept at bay by the binding of CED-4 to CED-9 on the OMM (Figure 1.7; Hengartner and Bryant 2000; reviewed by Conradt and Xue 2005; reviewed by Lettre and Hengartner 2006; reviewed by Darland-Ransom et al. 2009). In cells that are programmed or signalled to die, an execution signal is sent to EGL-1. EGL-1 is then proposed to bind to CED-9 causing a conformational change thereby releasing CED-4 (Figure 1.7; reviewed by Conradt and Xue 2005; reviewed by Nehme and Conradt 2009). In this way this system does vary from the components of the mammalian system, due to the fact that anti-apoptotic Bcl-2 does not directly interact with Apaf-1 *in vivo.* Upon liberation from CED-9, CED-4 travels to the nucleus where it confers with CED-3 activating this caspase-like protease and initiating the PCD process (Figure 1.7; Hengartner and Bryant 2000; reviewed by Conradt and Xue 2005; reviewed by Lettre and Hengartner 2006; reviewed by Darland-Ransom et al. 2009). However, more recently, evidence has been presented that these components may not interact as previously thought (Pourkarimi et al. 2011). Pourkarimi

et al. (2011) demonstrated that CED-9 does associate with OMM but in areas that do not overlap with the location of CED-4. Furthermore, it was concluded that CED-4 is predominantly perinuclear and does not appear to localize to the OMM frequently. These results suggest that the protection from PCD conferred by CED-9 cannot solely be attributed to direct CED-4 binding, although further research needs to be completed in order to concretize these findings.

1.2.2.3 'Engulfment' Gene Regulation

At least two classes of engulfment genes exist: 1. *ced-1, 6* and *7;* and 2. *ced-2, 5, 10* and *12.* Group one is involved in cell corpse recognition. CED-7 is similar to the mammalian ATP-binding cassette (ABC), a group of proteins that bind and hydrolyze ATP in order to transport molecules across cellular membranes (reviewed by Darland-Ransom et al. 2009). Group two genes appear to encode conserved components of the mammalian Rac GTPase signalling pathway; CED-10 is a *C. elegans* homologue of mammalian Rac GTPase that controls cytoskeletal dynamics (reviewed by Darland-Ransom et al. 2009).

1.2.2.4 'Nuclease' Gene Regulation

The degradation of nuclear DNA is thought to be a vital step in PCD and therefore 4', 6-diamidino-2-phenylindole (DAPI) and TUNEL staining have been used to visualize nuclei within cells of *C. elegans.* Mutant embryos over expressing the gene nuclease-1 (*nuc-1*), a mammalian DNase II homologue, show an increase in TUNEL positive nuclei as compared to wild type embryos. Overexpression of the CED-3 protease suppressor (*cps-6*), a homologue of mammalian mitochondrial Endo G, also increases the

amount of TUNEL positive nuclei (reviewed by Conradt and Xue 2005; reviewed by Darland-Ransom et al. 2009). Similarly, worm AIF homologue-1 (*wah-1*) is known to interact with *cps-6* and enhances its' endonuclease activity. Overall these findings suggest that genes, *nuc-1, cps-6,* and *wah-1* play a role in nuclear degradation during cell death in *C. elegans* (Gartner et al. 2003; reviewed by Conradt and Xue 2005; reviewed by Darland-Ransom et al. 2009).

1.2.2.5 Mitochondrial Involvement During C. elegans PCD

Several homologs of mammalian mitochondrial genes have been identified in *C. elegans* including those mentioned above, *cps-6* and *wah-1.* Interestingly, the discovery of *cps-6* was the first indication that mitochondria were involved in PCD within the nematode worm (Widlak and Garrard 2005). Like CPS-6 and human AIF, *C. elegans* WAH-1 also localizes to the mitochondria. *Egl-1* expression induced WAH-1 translocation from the mitochondria to the nucleus in a CED-3 dependent manner, thus suggesting that the role of the mitochondria in the regulation of nuclear degradation in cell death is conserved (Parrish et al. 2001). Furthermore it is evident that the mitochondria may be playing a role in the PCD process based on CED-9 dependent localization of CED-4 to the mitochondria (Schwartz 2007). Additionally, although there are two copies of cyt-*c* encoded for in the worms genome, currently it is unknown whether or not OMM permeabilization or the release of cyt-*c* from the mitochondria plays a role in *C. elegans* PCD (Hengartner and Bryant 2000; Gartner et al. 2003).

1.2.2.6 The Actin- Cytoskeleton

Surprisingly little literature is available on actin-cytoskeleton dynamics during

PCD in *C. elegans.* When cells die within this system they tend to condense away from the cell body, leaving cell corpses. It has been shown in previous experiments that CED-10 (a mammalian Rac-GTPase homologue) promotes actin cytoskeleton rearrangement during phagocytosis of these corpses (Kinchen et al. 2005; reviewed by Lettre and Michael Hengartner 2006; reviewed by Darland-Ransom et al. 2009). Therefore, the role of actin filaments during PCD is generally discussed in relation to engulfment of this dead matter. Kinchen et al. (2005) confirmed YFP::actin 'halos' around early apoptotic corpses in wild-type germ cells. Mutant worms, which depicted increased cell death also showed increase numbers of apoptotic cells and actin halos surrounding them. Interestingly, mutant worms lacking caspase-like activity (knockdown of homologue *ced-3*) showed no apoptotic cells, or actin halos. Overall, this evidence not only suggests that the actin cytoskeleton plays a role in cell corpse maintenance during *C. elegans* PCD, but also points to *ced-3,* or caspase-like activity as playing some role in the process.

1.2.3 Programmed Cell Death in Plants

Plant cells that undergo PCD display many of the same morphological and physiological properties as cells undergoing PCD in *C. elegans* and mammals (reviewed by Conradt 2009) including but not limited to: alterations in mitochondrial dynamics (Scott and Logan 2008), cellular K^+ efflux (reviewed by Shabala 2009), up regulation of caspase-like proteases (reviewed by Chowdhury et al. 2008), modulations of the actin cytoskeleton (reviewed by Franklin-Tong and Gourlay 2008), increased formation of vesicles and transvacuolar strands (TVS; Reisen et al. 2005) cytoplasmic condensation, nuclear condensation, DNA fragmentation detectable by TUNEL staining (Gunawardena

et al. 2004; Yao et al. 2004) and chromatin fragmentation leading to DNA laddering in several systems (Balk et al. 2003). Despite the number of examples, less is known regarding the genetics of the PCD in plants as compared to animals.

1.2.3.1 'Bcl-2 Like' Family Members

Although no specific Bcl-2 family proteins have been identified in plants, evidence for Bcl-2 like proteins certainly exists (Figure 1.1). With regards to anti-apoptotic members, Dion et al. (1997) revealed the presence of a protein immunoreacting with anti-bcl-2 antibodies in tobacco leaves via Western blotting. Transgenic tobacco expressing human *Bcl-2* or nematode *ced-9* is also resistant to a wide range of pathogens, while wild type tobacco is still very susceptible (Dickman et al. 2001; Gray 2004; Chen and Dickman 2004). The expression of *ced*-9 in tobacco was also able to inhibit aluminum-induced vacuolar processing enzyme (VPE) activity, which is a crucial executor of PCD in tobacco (Wang et al. 2009). Also, Bcl-x_L and *ced-9* expression in tomato produced a tolerance to viral induced and stress induced PCD; this symptom suppression was correlated with increasing transgenic expression levels (Xu et al. 2004). Xu and Reed (1998) reported the discovery of a *Bax-inhibitor-1 (BI-1)* gene in humans, generally located within the ER membrane, which was able to inhibit the toxicity of Bax *in vivo* (reviewed by Hetz and Glimcher 2008). In 2004 Eichmann et al. was able to isolate a *BI-1* homologue from barley, which was up regulated during fungal pathogen infection. In 2001 Kawai-Yamada et al. reported that a gene encoding for a homologue of *BI-1* was isolated from Arabidopsis, including *Arabidopsis BI-1* (*AtBI-1*; Figure 1.1) and could inhibit Bax mammalian action *in Planta*. Other BI-1 related proteins have also been discovered in Arabidopsis, including AtBI-2 and AtBI-3 (Xu and Reed 1998).

With regards to pro-apoptotic Bcl-2 family or *egl-1* homologues, few have been characterized in plants, although evidence has been presented to suggest they exist. Kawai-Yamada et al. (2001) demonstrated that mammalian Bax was able to induce plant cell death in *Arabidopsis*, and was actually able to be suppressed via AtBI-1; thus providing evidence for a Bax-like homologue in plants. Given an obvious lack of sequence similarity, alternative approaches will have to begin to be used in order to identify functional plant homologues of PCD regulators. Overall evidence for Bcl-2 like proteins in plants is substantial. Given *ced-9* and Bcl-2 can functionally substitute for one another, despite having only 25% sequence homology lends to the point that divergent sequences can produce similar protein folds relevant to cell death regulation, thus perhaps explaining the inability of sequence comparisons to detect identical Bcl-2 homologs within plant genomes (Vaux et al. 1992).

1.2.3.2 Mitochondrial Involvement During Plant PCD

The mitochondria have been highly implicated during plant PCD (Tiwari et al. 2002; Arpagaus et al. 2002; Yao et al. 2004; Diamond and McCabe 2007; Scott and Logan 2007; Scott and Logan 2008). Like animals it appears that in plants, the initiation of PCD leads to the formation of a MPTP, causing a subsequent MPT and decrease in $\Delta\Psi_m$. This decrease in $\Delta\Psi_m$ is thought to be followed by the release of IMS proteins promoting PCD further. The release of cyt-*c* from the mitochondria of animals, as noted above, is a key regulator in the PCD process, and has also been demonstrated in a variety of plant systems including: potato (Arpagaus et al. 2002), cucumber (Balk et al. 1999), sunflower (Balk and Leaver 2001), sycamore (Contran et al. 2007), oats (Curtis and Wolpert 2002), BY2 tobacco cells (Vacca et al. 2006) and *Arabidopsis* (Balk et al. 2003;

Yao et al. 2004). Additionally this release lends more to other analogies between the systems including the need for an Apaf-1/CED-4 homolog to form an apoptosome-like structure (Jan et al. 2008).

The use of CsA to block MPTP opening, and subsequent PCD in plants has also been successful in both environmentally induced (Arpagaus et al. 2002; Contran et al. 2007; Scott and Logan 2008; Lord and Gunawardena 2011) as well as developmentally regulated cell death (Lord et al. 2011). In the latter example, the use of 10 μM CsA was shown to significantly reduce the amount of perforation formation within lace plant leaves; the consequence of CsA in this approach points further to an equivalent role for the mitochondria within plant and animal PCD. Plant mitochondria also often display distinct structural attributes common of PCD in animals, including aggregation (Yao et al. 2004; Gao et al. 2008; Lord et al. 2011; Lord and Gunawardena 2011) swelling (Arpagaus et al. 2002; Scott and Logan 2008) decrease in $\Delta\Psi_m$ (Curtis and Wolpert 2002; Yao et al. 2004; Gao et al. 2008; Lord et al. 2011; Lord and Gunawardena 2011), loss of electron density and cristae, and compromised inner and outer membranes (reviewed by Crompton 1999; Scott and Logan 2008; Lord et al. 2011). The mitochondria have also been shown to form small aggregates with chloroplasts and assemble in a ring-like structure surrounding the nucleus within lace plant developmental PCD, although the purpose of this structure is still unknown (Wright et al. 2009; Lord et al. 2011). Furthermore the mitochondria in plants, like in animals are also capable of producing large amounts of ROS (Diamond and McCabe 2007; Gao et al. 2008; Zhang et al. 2009) leading to hastened cell death.

1.2.3.3 Plant Apaf-1 or Ced-4 Homologue

The plant genes most closely related to mammalian *Apaf-1* and nematode *ced-4* include pathogen resistance (*Prf*) genes and resistance (*R)* genes; here we will focus on the latter, although the structure of the *Prf* gene product is still detailed for reference in Figure 1.3. In plants, *R* genes are mainly encoded for during disease resistance (Kim et al. 2005; Figure 1.3) and are involved extensively in the recognition of pathogens. *R* genes encode both membrane bound and cytosolic proteins and have been shown to mediate the hypersensitive response (HR) through initiating localized cell death at the site of pathogen infection (Inohara et al. 2002). van der Biezen and Jones (1998) detailed similar findings regarding *R* genes and concluded that their products may function as controlling adaptors in a plant apoptosome-like structure. This apoptosome-like structure would be activated by the pathogens avirulence (*avr)* signals and *R* gene products could then aid in activating caspase-like proteases to further cell death. The leucine-rich repeats (LRRs) of *R* gene products could play a role in protein-protein interactions or protein activation just as WD-40 repeats in Apaf-1. Apaf-1, CED-4 and *R* gene products also all share a NB-ARC domain as well as amino-terminal effector domains including a leucine zipper (LZ) or a Drosophila Toll, mammalian interleukin-1 receptor (TIR). Further research must be conducted in order to determine the significance of these homologies, which may indicate the conservation of a regulatory mechanism for PCD in *C. elegans,* mammals and plants (van der Biezen and Jones 1998; Figure 1.3).

1.2.3.4 'Caspase- Like' Proteases

Although true caspases are yet to be described in plants, two broad groups of caspase-like proteases (CLPs) have been identified: 1. cysteine endopeptidases (Rojo et

al. 2004) and 2. serine endopeptidases (Coffeen and Wolpert 2004). Cysteine endopeptidases are involved in plant cell death and possess caspase-like activity. These endopeptidases can be further divided into two groups including, metacaspases (reviewed by Sanmartin et al. 2005; Bozhkov and Jansson 2007; reviewed by Piszczek and Gutman 2007; reviewed by Bozhkov et al. 2010) and vacuolar processing enzymes (VPEs; reviewed by Sanmartin et al. 2005; Hara-Nishimura et al. 2005; reviewed by Piszczek and Gutman 2007). Although both the primary and tertiary protein structure of metacaspases do resemble that of animal caspases, evidence suggests that there is limited sequence similarity between VPEs and true caspases (Hara-Nishimura et al. 2005; Hatsugai et al. 2006). VPEs have been shown to cleave at both Asp as well as Asparagine (Asn) residues. However, metacaspases do not cleave at the typical Asp residue, but instead at an Arg or Lysine (Lys) residue (reviewed by Piszczek and Gutman 2007). Given this substrate specificity there has been much debate about whether or not metacaspases are true caspases. A paper published by Enoksson and Salvesen (2010) appears to have settled the argument by noting that within the original definition, proteases are to be defined by both their catalytic mechanism and substrate specificity (Alnemri et al. 1996); given metacaspases cleave at basic Arg and Lys residues, not the usual acidic Asp, it is definitive that they are not true caspases. However, this argument then prompts the question, are VPEs true caspases? VPEs, possess both a cysteine active site and Asp substrate specificity (cleave YVAD containing substrates and therefore are thought to resemble caspase-1 or initiator type caspases; Hatsugai et al. 2006) and therefore fit the mould of the original definition of a true caspase described over 16 years ago (Alnemri et al. 1996). Conceivably, it is the varying location of these proteases,

VPEs in the vacuole, and true caspases in the cytosol, or the fact VPEs were originally regarded as asparaginyl endopeptidases, that causes these proteases to not be coined as true caspases, although further research on this topic would be timely and valuable.

Metacaspases fall within two classes, type I and type II, based on overall structure and the level of sequence similarity to true caspases (Figure 1.5). Type I metacaspases from fungi and plants have prodomains with a zinc finger motif (ZN), and proline-rich repeat motif (Pro; Uren et al. 2000; Figure 1.5). Type II metacaspases, found exclusively in plants, have no pro-domain but an insertion of approximately 20 amino acids directly C-terminal to their p20 like subunit (Figure 1.5). Examining plant caspase-like activity during the HR in tobacco plant infection revealed that caspase-specific peptide inhibitors Ac-YVAD-CMK and Ac-DEVD-CHO could abolish bacteria induced PCD (Del Pozo and Lam 1998). Also, tobacco expressing *C. elegans ced-3* portrayed an accelerated PCD phenotype (Tristán 2008). Serine endopeptidases are the other form of CLP found within plant systems and include saspases, which contain a serine residue at their active site, instead of a cysteine (reviewed by Sanmartin et al. 2005).

1.2.3.5 The Actin- Cytoskeleton

Like in mammals the cytoskeleton of plants helps to facilitate cell shape and organization, however, in plants, no intermediate filaments are present. The actin cytoskeleton has been highly implicated in plant PCD including during cell death of *Picea abies* (Norway Spruce) embryonic tissues (Smertenko et al. 2003) as well as during SI in *Papaver rhoeas* L (field poppy; reviewed by Franklin-Tong and Gourlay 2008). During embryogenesis, like in mammals, depolymerization of the actin cytoskeleton with Lat B resulted in the production of abnormal embryos, accompanied by high levels of cell

death and DNA fragmentation (Smertenko et al. 2003; reviewed by Franklin-Tong and Gourlay 2008). During the SI in poppy pollen, extensive and sustained F-actin depolymerization, followed by stabilization to produce punctate foci could be visualized (Snowman et al. 2002; reviewed by Franklin-Tong and Gourlay 2008). Moreover, transient depolymerization of actin in pollen using Lat B triggered PCD and was shown to involve caspase-3-like activity. Surprisingly, like in mammalian cells, treatment with the actin stabilizer Jasp has also been shown to trigger PCD in *Papaver* pollen; thus suggesting that any change in actin dynamics may play a role in initiating PCD (Thomas et al. 2006; reviewed by Franklin-Tong and Gourlay 2008).

1.3 Developmentally Regulated and Environmentally Induced PCD in Plants

PCD occurs throughout plant development from embryogenesis to the death of the whole plant (Gray 2004; reviewed by Rogers 2005). Besides the divisions of plant PCD based on morphological characteristics described above, PCD in plant systems can also be divided into two broader categories based on the method of induction, including environmentally induced or developmentally regulated (reviewed by Gunawardena 2008). Environmentally induced PCD is usually a consequence of external factors including HS (Balk et al. 2003; Zhang et al. 2009; Lord and Gunawardena 2011), pathogen infection leading to the HR (del Pozo and Lam 1998; reviewed by Lam et al. 2001), as well low oxygen treatment leading to the formation of aerenchyma (Gunawardena et al. 2001). Prominent examples of developmentally regulated PCD in plants include, but are not limited to, deletion of the embryonic suspensor (Giuliani 2002; reviewed by Rogers 2005), anther dehiscence (reviewed by Rogers 2005; Senatore et al. 2009; reviewed by Wilson et al. 2011), xylem differentiation (Fukuda 1997; Obara and

Fukuda 2004), leaf senescence (reviewed by Lim et al. 2007; Michele et al. 2009), flower senescence (reviewed by Rogers 2006) and leaf morphogenesis as is seen in the lace plant or *Aponogeton madagascariensis* (reviewed by Gunawardena 2008; Wright et al. 2009; Elliott and Gunawardena 2010; Lord et al. 2011).

1.4 The Lace Plant (*Aponogeton madagascariensis*)

The lace plant (*Aponogeton madagascariensis*) is one of forty species in the monogeneric family Aponogetonaceae, and is the only species in the family that produces perforations in its leaves through the PCD process. The lace plant is native to the river systems of Madagascar and is a fully submerged freshwater aquatic. It is secured in gravel substrate at the bottom of rivers by roots borne adventitiously on a spherical corm. A shoot apex in the centre of this corm gives rise to the lace plant leaves. Lace plant leaves form via a heteroblastic series; therefore the first three leaves that form are juvenile leaves and will never undergo PCD, and conversely, the leaves which form after this are adult leaves and will undergo PCD. Within an adult lace plant leaf, longitudinal and transverse veins form a network of small, roughly square segments known as areoles; it is within these areoles where perforations caused by PCD initiate. The perforations radiate outward until cell death is halted four to five cells from the perimeter veins, creating a lattice-like pattern over the entire leaf surface (Gunawardena et al. 2004, 2007; Gunawardena and Dengler 2006; Gunawardena 2008; Wright et al. 2009).

The lace plant makes an excellent model system for the study of developmentally regulated PCD for several reasons (Gunawardena et al. 2004, 2007; Gunawardena and Dengler 2006; Gunawardena 2008; Wright et al. 2009). Firstly, perforation formation within the leaf is predictable, with perforations forming at very specific stages of leaf

development and only between longitudinal and transverse veins. Given this predictability, the developmental morphology of the adult perforated lace plant leaf has been well documented and has been divided into five stages (Gunawardena et al. 2004). Initially stage 1 (pre-perforation) involves longitudinally rolled, often pink leaves where no perforations are present. This pink coloration is due to the pigment anthocyanin, which is found in the vacuole of the mesophyll cells (Figure 1.8A). Stage 2 (window) is characterized by distinct transparent regions in the centre of the vascular tissue, due to the loss of pigments such as chlorophyll and anthocyanin (Figure 1.8B); stage 3 (perforation formation) involves the degradation of the cytoplasm and the cell wall of the cell, resulting in the loss of transparent cells in the centre of the window (Figure 1.8C); stage 4 (perforation expansion) is characterized by the expansion of the perforation within the areole (Figure 1.8D); lastly, stage 5 (mature perforation) results in a completed perforation (Figure 1.8E; Gunawardena et al. 2004). A single areole within a window stage leaf has also been divided into three areas based on the progression of PCD; cells closet to the vasculature, will not undergo PCD (NPCD); these cells are markedly pink again due to pigment anthocyanin found within their vacuoles. The next layers of cells inward are in the early stages of PCD (EPCD); these cells are markedly green in colour due to the pigment chlorophyll found within chloroplasts. Lastly cells towards the center of the areole are in the late stages of PCD (LPCD); these cells are generally clear in colour due to loss of pigments. The lace plant leaf tissue is also very thin, approximately four to five cell layers thick, making whole-mount *in vivo* examination via microscopy possible. This thin structure makes the leaf nearly transparent, allowing for long term live cell imaging within the plant. Lastly, there is a well-developed protocol for the sterile

culture of the lace plant (Figure 1.8F), allowing for a large amount of experimental plant material with no microbial contamination (Gunawardena and Dengler 2006). These sterile cultures are also ideal for pharmacological experimentation, including the addition of calcium (Elliott and Gunawardena 2010), ethylene, and caspase-like protease inhibitors, whose substrates are thought to be involved in PCD in plants.

1.5 Objectives

The overall objective of this dissertation was to use the novel lace plant (*Aponogeton madagascariensis*) as a new model organism to study both environmentally induced and developmentally regulated PCD. In order to achieve this aim my research objectives have been separated into four categories as follows.

1.5.1 Protoplast Isolation and Environmentally Induced PCD

The initial objective of this research was to investigate environmentally induced PCD in the lace plant through HS of protoplasts. Protoplasts serve as a highly valuable and versatile cell based systems that have been used to observe many cellular processes. Following the optimization of protoplast isolation, PCD was induced via a HS treatment at 55°C for 20 min. Cellular changes that occurred following HS were examined, with an emphasis placed on the role of the mitochondria within this lace plant PCD system. This induced PCD system also provided the first ever opportunity to compare and contrast both induced and regulated PCD within one species of plant. As a subset of these goals the induction of necrosis, the uncontrolled form of cell death, was also accomplished, by applying a more intense version of the same HS stimulus.

1.5.2 Developmentally Regulated PCD: A Mitochondrial Focus

Following the investigation of induced PCD in lace plant protoplasts the objective of this research was to elucidate the role of mitochondrial dynamics in relation to other organelles during regulated PCD in the lace plant using various forms of microscopy. As a subset of this goal long-term live cell imaging within the plant was perfected allowing for *in vivo* video recording, aiding in further investigation of organelle dynamics.

1.5.3 Developmentally Regulated PCD: Caspase-Like Proteases and Actin Dynamics

Research involving animal PCD places emphasis on the roles of caspases and the cytoskeleton during cell death. This research aimed to elucidate the role of caspase-like proteases and the actin cytoskeleton during PCD in the lace plant. From previous research it was clear that alterations in mitochondrial dynamics occurred early in the lace plant PCD process; given the knowledge that mitochondrial alterations can activate caspases in animal tissue, the relationship between the mitochondria, caspase-like proteases and the actin cytoskeleton was investigated to uncover a link that has been rarely examined in plants in the past.

1.5.4 Developmentally Regulated PCD: Delineating the Order of Organelle Events

Various cellular morphological characteristics have been examined throughout the process of cell death within the lace plant; however the detailed characterization of the order of organelle and cellular events occurring throughout the entire process had yet to be investigated and amalgamated. The aim of this final research was to utilize the novel

lace plant system as well as *in vivo* short- and long-term live cell imaging, to delineate the possible order of cellular changes that occur during developmental PCD.

Figure 1.1 Protein Schematic of B-cell-Lymphoma (Bcl-2) Family Members, CED-9, and Arabidopsis Bax Inhibitor-1 (AtBI-1) From Mammals, *C. elegans* and Plants Respectively

Mammalian Bcl-2 family members are either pro- or anti-apoptotic. Many Bcl-2 family proteins contain C-terminal hydrophobic transmembrane domains that cause them to post transcriptionally insert themselves into membranes. *C. elegans* ced-9 encodes a protein with anti-apoptotic capabilities, with 25% sequence homology to that of Bcl-2 and Bcl-xL. Although no specific Bcl-2 family protein has been identified in plants, proteins immunoreacting with anti-Bcl-2 antibodies have been identified. Genes encoding for homologs of BI-1 have been isolated from Arabidopsis, including Arabidopsis BI-1 (AtBI-1). Figure modified from (Gross et al. 1999; Lam et al. 2001).

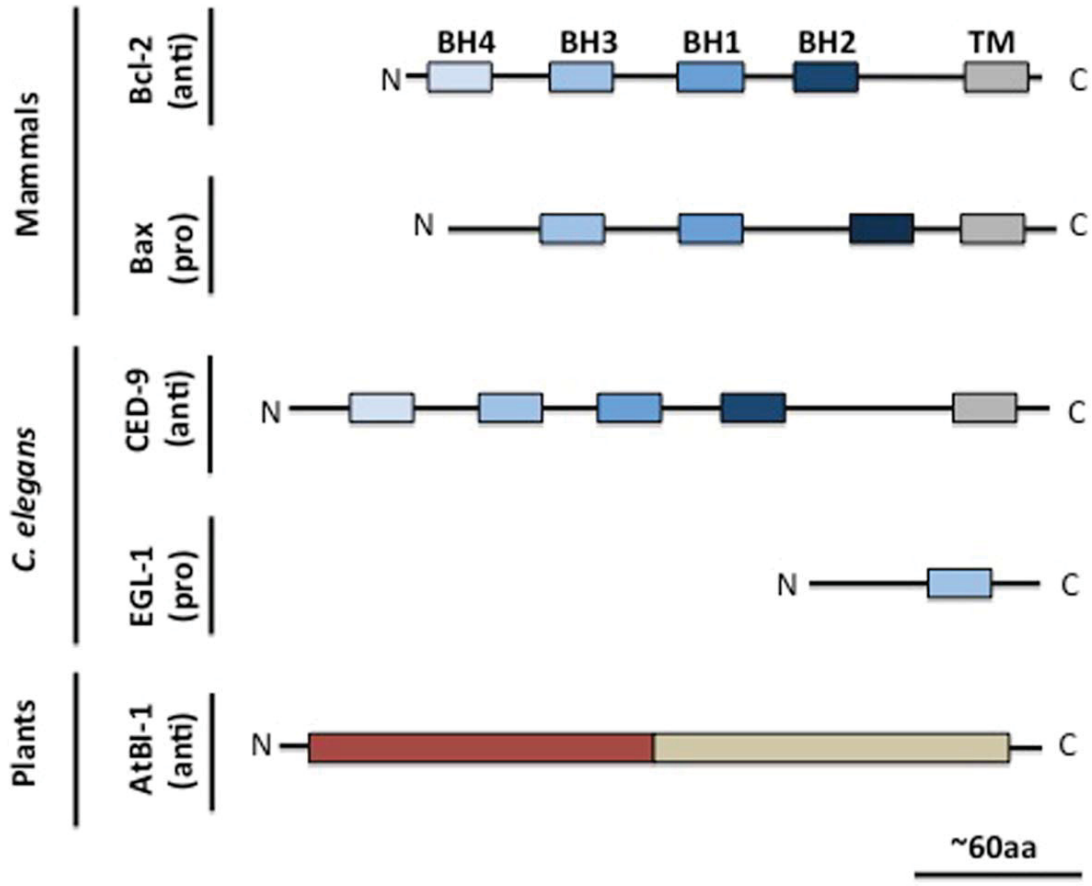

Figure 1.1 Protein Schematic of B-cell-Lymphoma (Bcl-2) Family Members, CED-9, and Arabidopsis Bax Inhibitor-1 (AtBI-1) From Mammals, *C. elegans* and Plants Respectively

Figure 1.2 The Role of the Mitochondria During PCD in Mammals

Intermembrane[2] space (IMS) proteins are believed to exit the mitochondria through two main pathways; the mitochondrial permeability transition pore (MPTP; A) or through pro-apoptotic pore forming Bcl-2 family members, and or the voltage dependent ion channel (VDAC; B). Increases in cytosolic Ca^{2+} cause the formation of the MPTP, [composed of the inner mitochondrial membrane (IMM) localized adenine nucleotide translocase (ANT) and the matrix localized cyclophilin D (CyP-D)] following which solutes rush into the matrix, initiating the mitochondrial permeability transition (MPT) in the IMM and causing a subsequent drop in mitochondrial membrane potential (Ψm). Oxidative phosphorylation is then disassociated from the ETC and matrix swelling occurs disrupting the OMM and causing the release of IMS proteins (A). A second pathway involves homodimerization and insertion of pro-apoptotic Bcl-2 proteins into the OMM via C-terminal transmembrane domains allowing for the release of IMS proteins. Additionally the VDAC, outside of its role in the MPTP, also behaves as a general diffusion pore and can be influenced by Bcl-2 family members (B). Figure modified from (Jones 2000).

[2] Amended from "inner membrane space" as published in European Journal of Cell Biology.

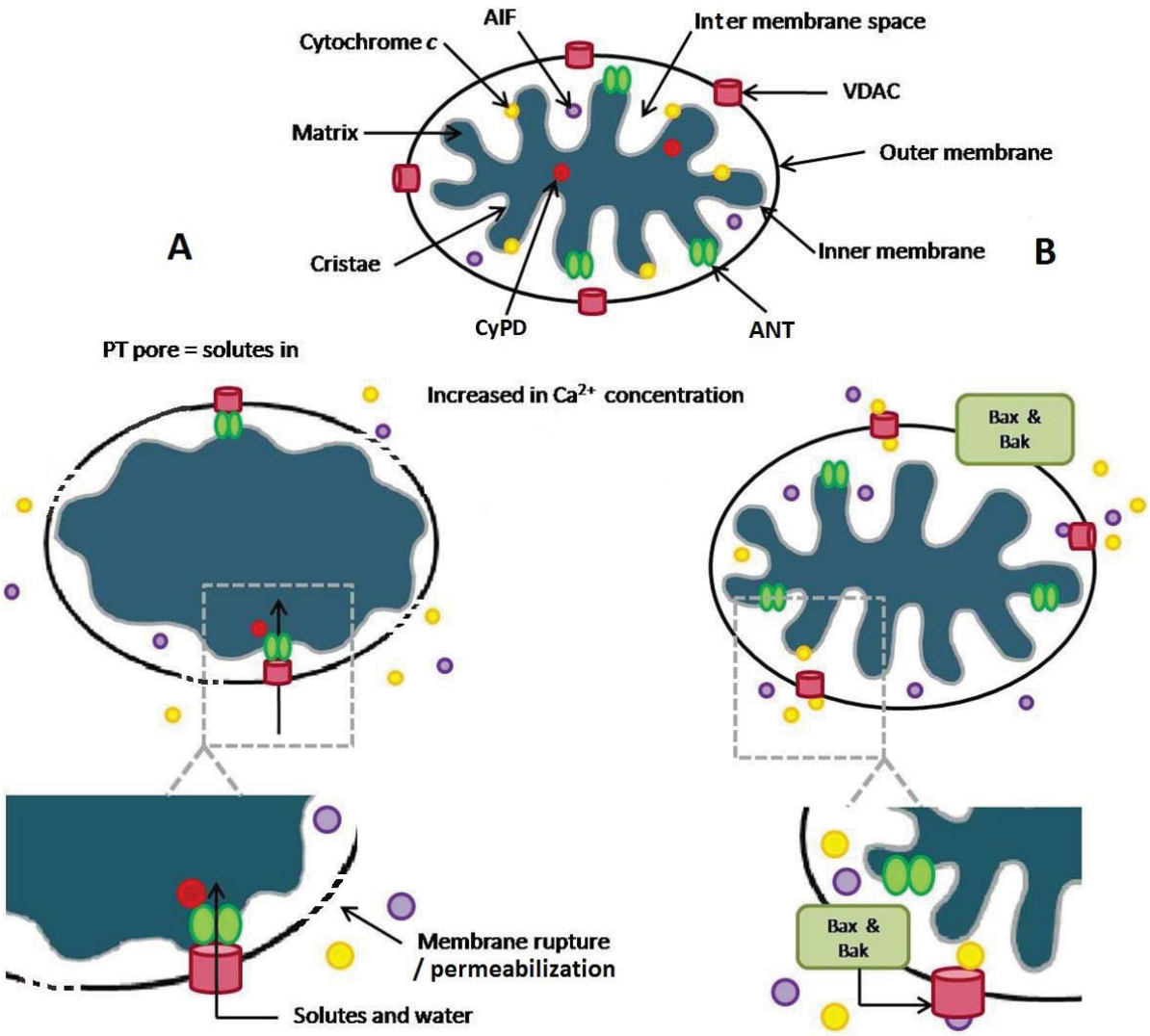

Figure 1.2 The Role of the Mitochondria During PCD in Mammals

Figure 1.3 Protein Schematic of Apoptosis Activating Factor-1 (APAF-1), CED-4, and Both Pathogen Resistance (PRF) and Resistance (R) Proteins From Mammals, *C. elegans* and Plants Respectively

Mammalian APAF-1 and *C. elegans* CED-4 protein domains are very similar but with CED-4 lacking WD-40 repeats at the C-terminus. The structures of both PRF and R proteins are also similar to CED-4 and APAF-1. R proteins have amino-terminal effector domains including a leucine zipper (LZ) or a Drosophila Toll, mammalian interleukin-1 receptor (TIR) similar to the CARDs found in APAF- 1 and CED-4. Both PRF and R proteins also have an NB-ARC domain closer to their N-terminus and C-terminal leucine-rich repeats (LRRs) which are similar to the WD- 40 repeats found in APAF-1 that aid in protein–protein interactions. The amino- terminal domain of PRF is shown fourfold smaller to fit into the figure modified from (Inohara et al. 2002; Hoeberichts and Woltering 2003).

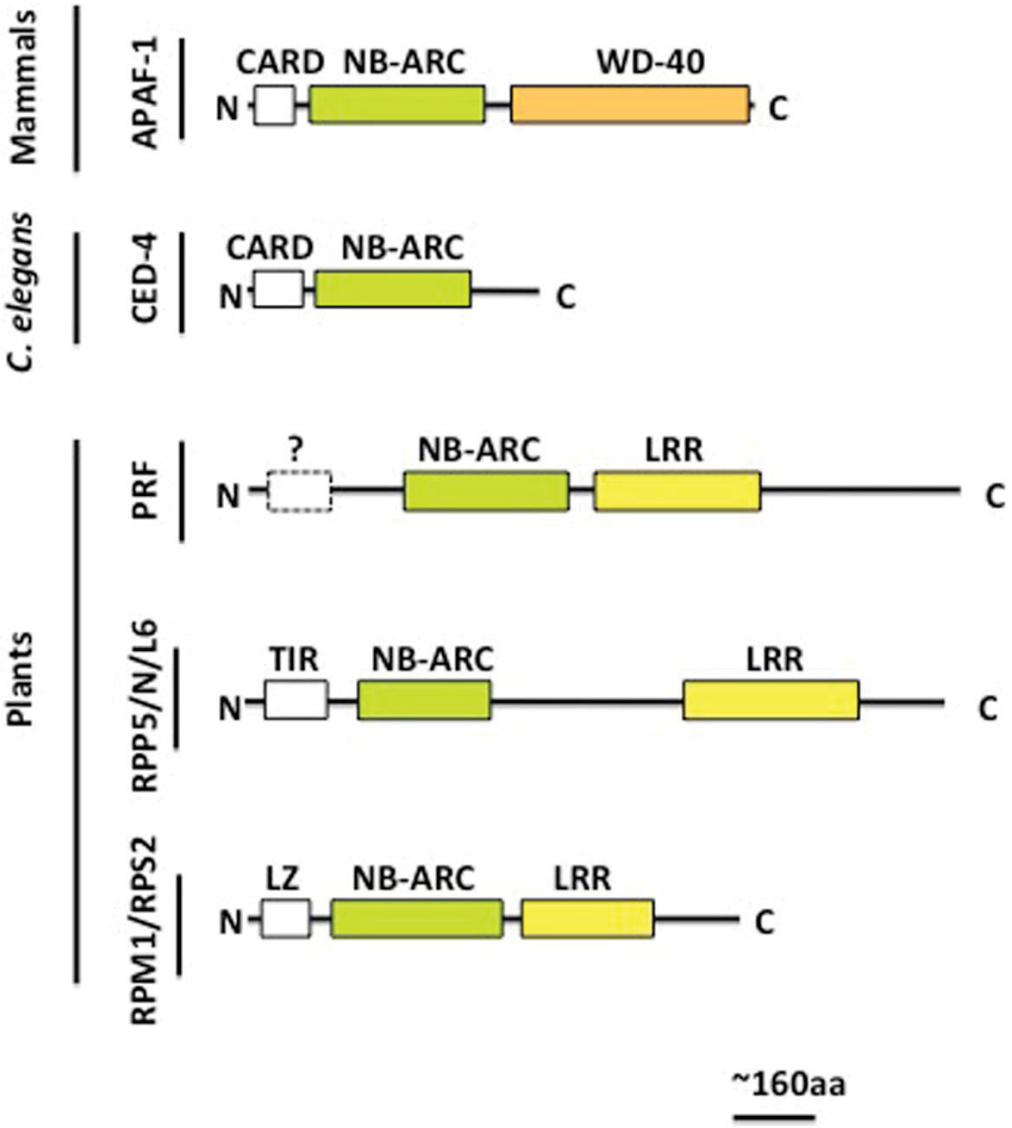

Figure 1.3 Protein Schematic of Apoptosis Activating Factor-1 (APAF-1), CED-4, and Both Pathogen Resistance (PRF) and Resistance (R) Proteins From Mammals, *C. elegans* and Plants Respectively

Figure 1.4 Schematic Model of the PCD Pathway in Mammals

A PCD signal is received by the cell. The death inducing signalling complex (DISC) found on the surface of the PM recruits multiple pro-caspase 8 molecules resulting in caspase 8 activation through induced proximity. The mitochondrial pathway (right) is used extensively in response to PCD signalling as noted in Fig. 3. Pro-apoptotic Bcl-2 family members can form pores in the outer mitochondrial membrane (OMM); however, the up-regulation of anti-apoptotic Bcl-2 family members can hasten pro-apoptotic activity through heterodimerization or the recruitment of cytosolic proteins such as Raf-1 to the OMM where it phosphorylates Bad and subsequently inactivates it. IMS proteins can also be released through the mitochondrial permeability transition pore (MPTP) or via the voltage dependent ion channel (VDAC). The MPTP forms due to an increase in cytosolic Ca^{2+}. Principally among the IMS proteins released is cytochrome *c* (cyt-c), which once released joins with apoptosis activating factor-1 (APAF-1) and possibly other proteins (including pro-caspase 9) to form the apoptosome. The apoptosome can independently activate pro-caspase 9 leading to downstream PCD processes. Also released from the IMS are proteins including apoptosis inducing factor (AIF) and endonuclease G (Endo G), which act upon the nucleus to trigger chromatin cleavage. UV radiation can act independently of the above-mentioned pathways (requiring no caspase activity) causing direct DNA damage. Crosstalk between the DISC and mitochondrial pathways is provided by the pro-apoptotic family member Bid; caspase 8 activation of Bid increases PCD activity by commencing its translocation to the mitochondria where is promotes IMS protein release; however, it is important to note that these pathways normally work independently of one another. Figure modified from (Gross et al. 1999; Hengartner 2000; Potten and Wilson 2004; Kim et al. 2005; Diamond and McCabe 2007).

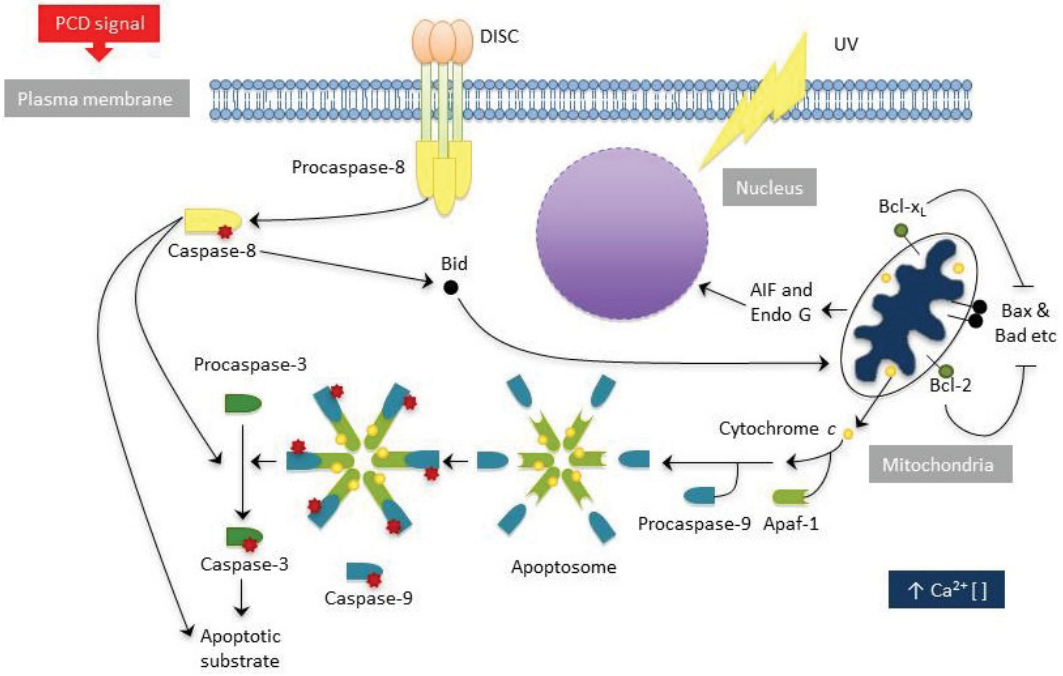

Figure 1.4 Schematic Model of the PCD Pathway in Mammals

Figure 1.5 Protein Schematic of Caspases, CED-3, and Caspase-Like Proteases From Mammals, *C. elegans* and Plants Respectively

Caspases generally consist of regulatory domains including an N-peptide region and catalytic domains including a large and small subunit connected by a linker. *C. elegans ced-3* encodes a protein with similarity to mammalian caspases. One of two groups of caspase-like proteases identified in plants is detailed, cysteine endopeptidases, that can be divided into two groups including, metacaspases and vacuolar processing enzymes (VPEs); both of which contain cysteine at their active sites. Figure modified from (Kinoshita et al. 1995; Stennicke andSalvesen 2000; Uren et al. 2000; Kuroyanagi et al. 2002; Sanmartin et al. 2005; Hara-Nishimura et al. 2005).

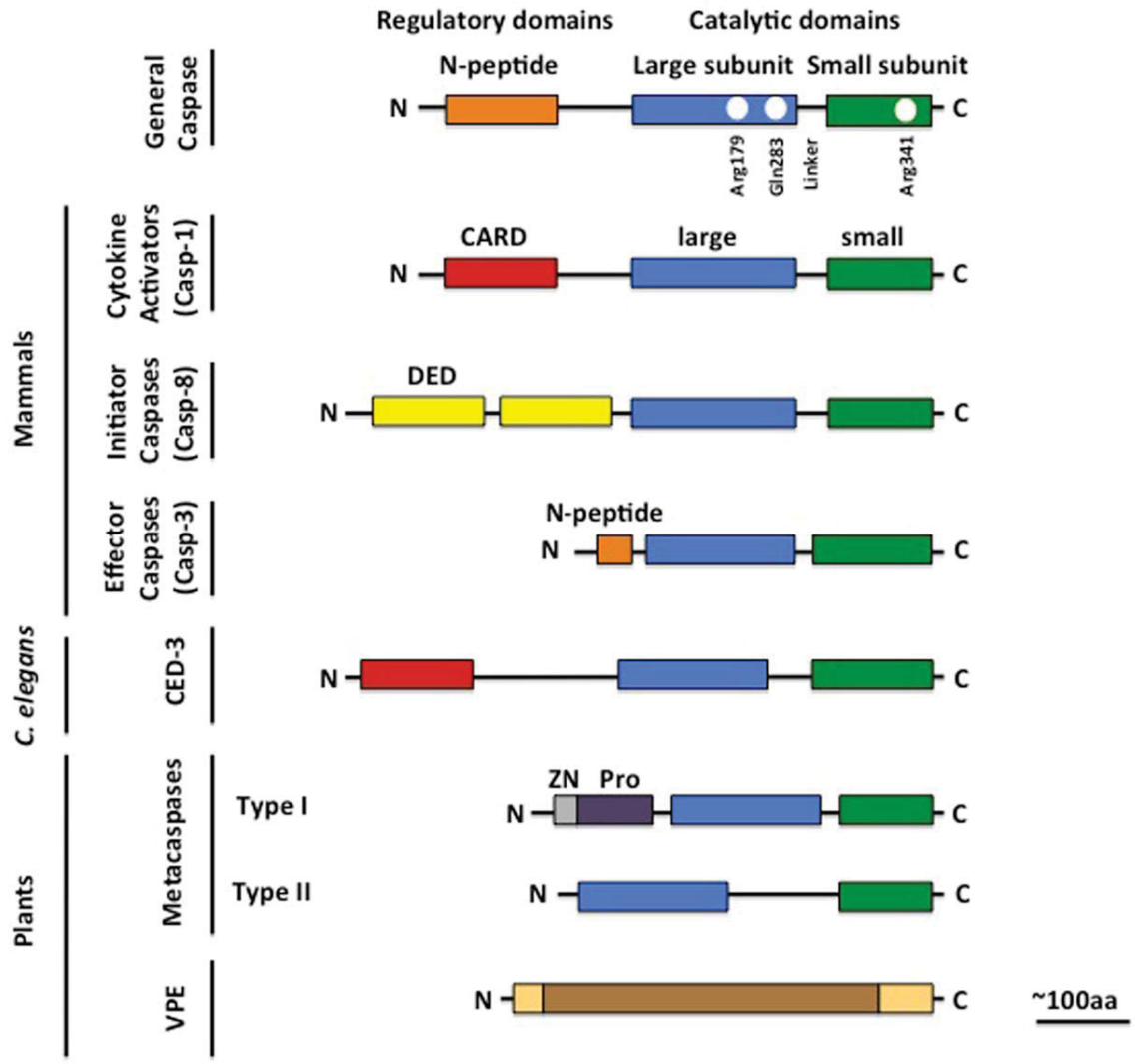

Figure 1.5 Protein Schematic of Caspases, CED-3, and Caspase-Like Proteases From Mammals, *C. elegans* and Plants Respectively

Figure 1.6 Protein Schematic of a Procaspase and Activated Mature Caspase Tetramer[3]

Following cleavage of the procaspase at designated cleavage sites a heterodimer is formed; two heterodimers then come together to form a single active caspase tetramer. R, H and C represent active site residues, which will aid in substrate recognition. The conserved catalytic cysteine site is an essential component of the cysteine endopeptidases family.

[3] This figure is supplemental to the figures published in European Journal of Cell Biology and aimed to clarify the activation of procaspases.

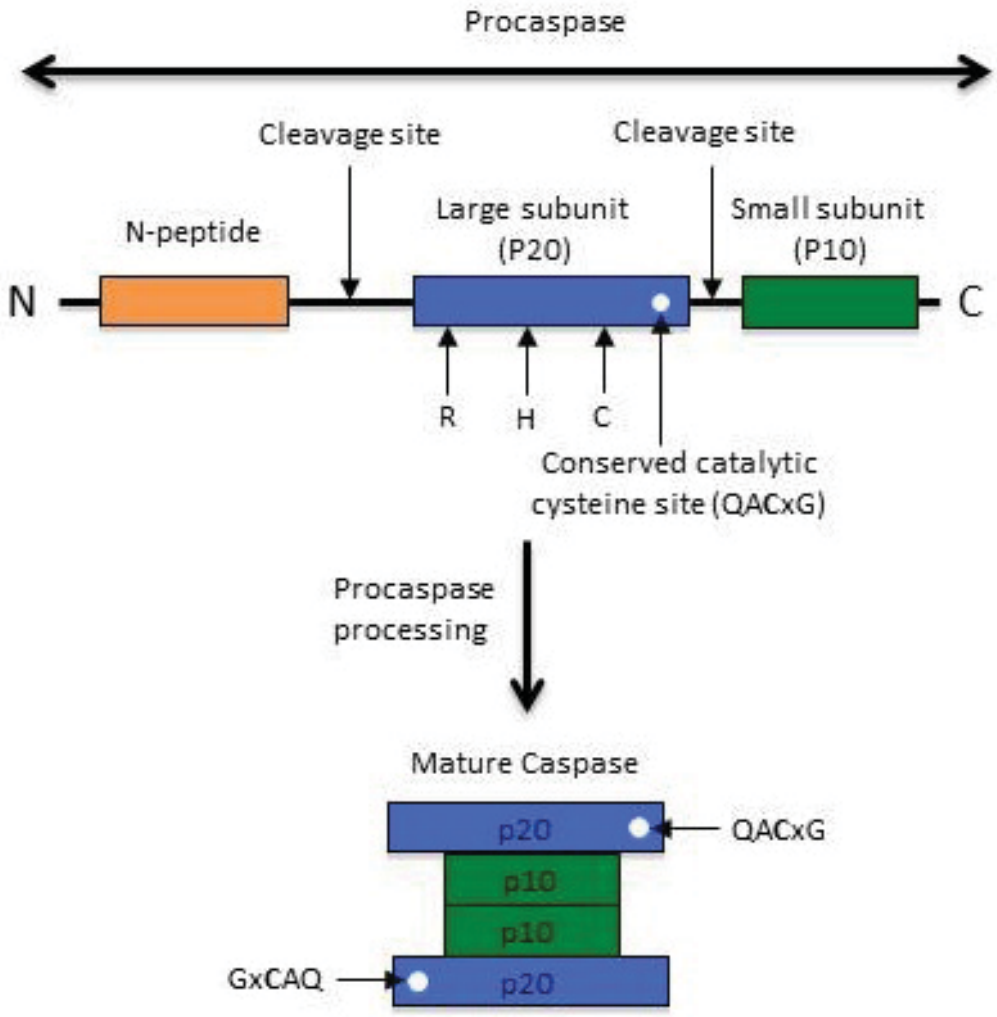

Figure 1.6 Protein Schematic of a Procaspase and Activated Mature Caspase Tetramer

Figure 1.7 Model of PCD Activation in *C. elegans* Emphasizing Protein Interactions

In cells that are destined to survive, CED-4 and CED-3 are kept at bay by the binding of CED-4 to CED-9 on the outer mitochondrial membrane (OMM). In cells that are programmed or signalled to die, an execution signal is sent to EGL-1, which is then proposed to bind to CED-9 causing a conformational change releasing CED-4. Upon liberation CED-4 travels to the nucleus where it associates with CED-3 activating it and initiating the PCD process. Figure modified from (Gartner et al. 2003; Conradt and Xue 2005; Wang and Youle 2009).

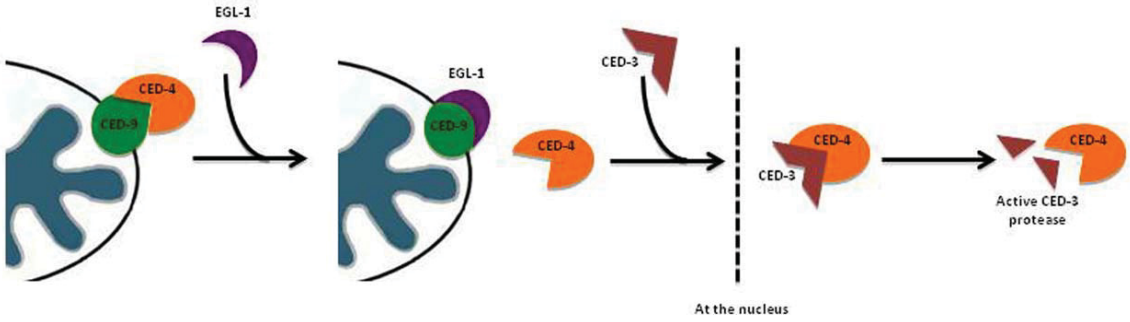

Figure 1.7 Model of PCD Activation in *C. elegans* Emphasizing Protein Interactions

Figure 1.8 The Lace Plant or *Aponogeton madagascariensis*[4]

Five stages of leaf morphogenesis in lace plant leaves as PCD progresses. (A) Stage 1, or pre-perforation, note the abundance of the pink pigment anthocyanin (B) Stage 2, or "window" stage, note the distinct cleared area in the center of the vasculature tissue indicating a loss of pigments anthocyanin and chlorophyll. (C) Stage 3, or perforation formation. The cells in the center of the areole have begun to break away, forming a hole. (D) Stage 4, or perforation expansion, note that cell death has stopped approximately four-five cells from the vascular tissue. (E) Stage 5, or mature stage. The cells bordering the perforation have transdifferentiated to become epidermal cells. (F) Whole plant growing in sterile culture in a magenta box filled with liquid and solid Murashige and Skoog (MS) medium. (A-E) = 500 μm; (F) = 1 cm.

[4] This figure is supplemental to the figures published in European Journal of Cell Biology and aimed to clarify the five stages of leaf development.

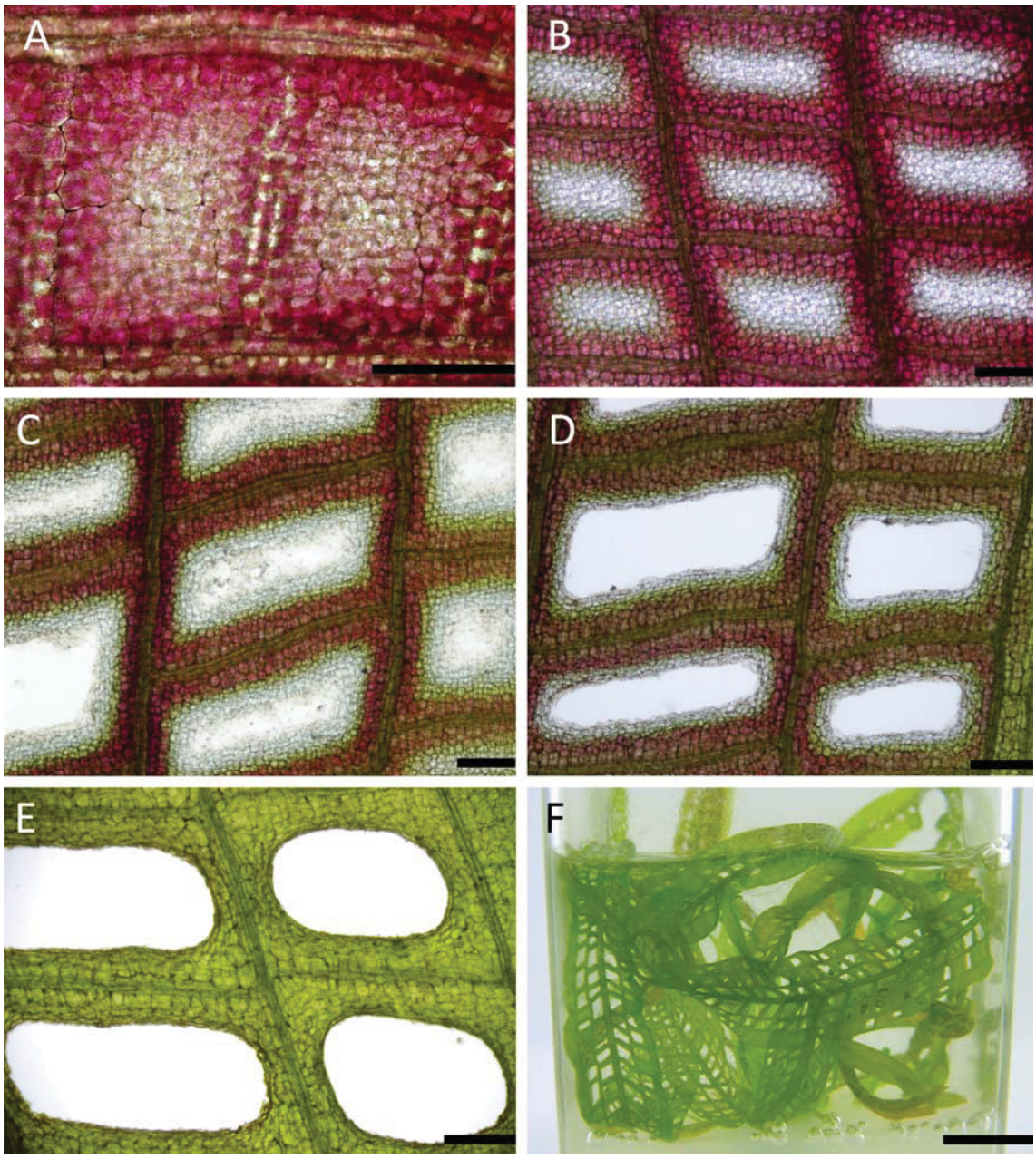

Figure 1.8 The Lace Plant or *Aponogeton madagascariensis*

Chapter 2 Isolation of Leaf Protoplasts From the Submerged Aquatic Monocot *Aponogeton madagascariensis*

Published as:

Lord CEN, Gunawardena AHLAN. Isolation of Leaf Protoplasts From the Submerged Aquatic Monocot *Aponogeton madagascariensis.* The Americas Journal of Plant Science and Biotechnology 4: (2010) (special issue 2) 6-11 (www.globalsciencebooks.info)

2.1 Abstract

Aponogeton madagascariensis is the only aquatic plant which forms perforations in its leaves through a process known as programmed cell death (PCD). Although PCD can be studied *in vivo*, isolated protoplasts maintain many of the same physiological properties of the intact plant and, due to their accessibility and reduced complexity, make ideal research tools to investigate plant processes including PCD. The conditions for the isolation of protoplasts from the lace plant were examined. Several factors including leaf age, carbohydrate source, and enzyme incubation time all significantly influenced protoplast yield and viability from lace plant tissue. Viable protoplasts were successfully isolated from leaf tissue approximately 1 month in age, using an enzyme mixture comprised of 2% w/v cellulase onozuka R10 and 0.5% pectolyase Y-23 dissolved in 0.005 M MES and 0.6 M sorbitol, pH 5.5. Approximately 60.35 ± 1.08 x 10^5 protoplasts/g fresh weight, with a viability of 92.75 ± 2.25%, were obtained from 4 hr isolations in the dark. Following successful isolation, these lace plant protoplasts can be used as an excellent model system for the study of environmentally induced PCD and can provide the first ever opportunity to compare this form of PCD with its developmentally regulated counterpart within one species of plant.

2.2 Introduction

2.2.1 Protoplasts

Protoplasts are essentially naked plant cells lacking a cell wall. They are spherical in shape with the cytoplasm contained within a plasma membrane (PM). Protoplasts serve as a highly valuable and versatile cell based system and have been used to observe

cellular processes and activities such as cell wall degradation, synthesis and communication, embryogenesis, cell division, photosynthetic activity and particle uptake, as well as stress and hormone responses in a variety of plant species (Pongchawee et al. 2006; Yoo et al. 2007)

The processes of protoplast isolation and regeneration have been of specific interest to the cereal industry given they represent some of the most economically important groups of plants for man. Protoplast isolation, culture and regeneration have been reported in the monocotyledonous cereals rice (Yamada et al. 1986), maize (Sheen 1993), pearl millet (Vasil and Vasil 1974), wheat (Harris et al. 1988) and sorghum (Battraw and Hall 1991). Protoplast manipulation has also been perfected in the model dicotyledonous species *Arabidopsis thaliana* (Yoo et al. 2007). To date, there are few reports of protoplast isolation and culture from freshwater aquatic plant species. The few species of freshwater plants which have been studied include the monocotyledonous angiosperm *Potamogeton lucens* L. (Staal et al. 1988), the dicotyledonous angiosperm *Ranunculus penicillatus* ssp. *Pseudofluitans* (Newman and Raven 1999), the monocotyledonous aquarium species *Anubias nana* Engler (Pongchawee et al. 2006) and *Cryptocoryne wendtii* De Wit (Pongchawee et al. 2007) and, as will be discussed here, the submerged monocotyledonous angiosperm *Aponogeton madagascariensis*.

2.2.2 The Lace Plant

The lace plant (*Aponogeton madagascariensis*) is an aquatic monocot native to the river systems of Madagascar. The lace plant is secured in gravel substrate by roots borne adventitiously on a spherical corm. Leaves are produced from a shoot apical

meristem (SAM) at the apex of the corm. The leaves of the lace plant form in a heteroblastic series; the first one-three leaves produced by the SAM are the juvenile leaves in the heteroblastic series and do not form perforations (Figure 2.1A and B); the following leaves produced by the SAM are adult leaves, which do form perforations. There are only two families in the vascular plant kingdom that produce perforations in their leaves via PCD: the Araceae and Aponogetonaceae. The lace plant is one of 40 species in the monogeneric family Aponogetonaceae and is the only species that produces perforations in its leaves through the PCD process (Gunawardena and Dengler 2006).

2.2.3 PCD and the Lace Plant

Programmed cell death is the regulated death of cells within an organism. PCD is omnipresent throughout the eukaryotes, occurring in both unicellular and multicellular organisms. PCD in plants can be either environmentally induced or developmentally regulated (reviewed by Gunawardena 2008). Environmentally induced PCD is an outcome of external biotic and abiotic factors and can be induced by such factors as heat shock (McCabe et al. 1997; reviewed by McCabe and Leaver 2000), UV radiation (Danon and Gallois 1998), pathogens (Mittler and Lam 1997), low oxygen (Gunawardena et al. 2001), and density and salinity changes (McCabe et al. 1997). In contrast, developmentally regulated PCD occurs as part of normal, unperturbed development and presumably is a response to internal signals. Examples of developmentally regulated PCD include elimination of transitory organs and tissues (Browder and Iten 1998), xylem differentiation (Fukuda et al. 1998), and leaf morphogenesis (Gunawardena et al. 2004, 2005) as is seen in the lace plant. In the lace

plant, each leaf reaches a length of approximately two cm before PCD is initiated. Through the PCD process, a simple, tongue-shaped leaf is converted to a more complex structure characterized by open perforations located between longitudinal and transverse veins. The perforations radiate outward before they stop growth four to five cells from the perimeter veins, creating a lattice like pattern over the entire leaf surface (Gunawardena et al. 2004, 2006, 2007; reviewed by Gunawardena 2008; Wright et al. 2009).

The developmental morphology of the adult perforated lace plant leaf has been divided into five stages. Initially, stage 1 (tissue pattern) involves longitudinally rolled pink leaves where no perforations are present. This pink coloration is due to the pigment anthocyanin, which is found in the vacuole of the mesophyll cells; interestingly this pigment is not found in the epidermal cells. Stage 2 (window) is characterized by distinct transparent regions forming in the center of the vascular tissue due to the loss of pigments such as chlorophyll and anthocyanin (Figure 2.1C); stage 3 (perforation formation) involves the degradation of the cytoplasm and the cell wall, resulting in the loss of transparent cells in the center of the window; stage 4 (perforation expansion) is characterized by the expansion of the perforation within the areole and lastly, stage 5 (mature) results in a completed perforation (Figure 2.1D; Gunawardena et al. 2004). Despite being a fully submerged macrophyte a cuticle is present on the leaves, commencing as very thin in the window stage and thickening moderately into the mature stage.

The lace plant is an excellent model system for the study of developmentally regulated PCD in plants (Gunawardena et al. 2004, 2006, 2007; reviewed by

Gunawardena 2008; Wright et al. 2009; Elliott and Gunawardena 2010). Perforation formation within the leaf is predictable, with perforations forming at very specific stages of leaf development and only between longitudinal and transverse veins. The leaf tissue is also very thin, approximately four to five cell layers thick, making examination via microscopy possible. This thin structure also makes the leaf nearly transparent, allowing for live cell imaging within the plant. There is also a well-developed protocol for the sterile culture of the lace plant (Figure 2.1A), allowing for generation of a large amount of experimental plant material with no microbial contamination (Gunawardena et al. 2006). The present study aimed to optimize the isolation of viable, high-density protoplasts from the freshwater monocot *Aponogeton madagascariensis*.

2.3 Materials and Methods

2.3.1 Subculture and Plant Materials

Lace plants used for all experimental purposes were grown in axenic culture in magenta boxes (Figure 2.1 A) as described by Gunawardena et al. (2006). Plants were maintained at 23.5°C with 12 h light/ 12 h dark cycles provided by daylight simulating fluorescent bulbs (Philips, Daylight Deluxe, F40T12/DX, Markham, Ontario) at approximately 125 $\mu mol \cdot m^{-2} \cdot s^{-1}$. All experimental plant materials were propagated via subculture according to the protocol of Gunawardena et al. (2006). All chemicals were purchased from Bio Shop (Burlington, Ontario, Canada) unless otherwise stated.

2.3.2 Protoplast Isolation

Protoplast isolation was modified from Staal et al. (1988), Pongchawee et al. (2006) and Pongchawee et al. (2007). Leaf samples from boxed plants between one-two months of age were excised and rinsed with dH_2O. The central vein from each leaf was removed and the remaining two halves were cut longitudinally into strips approximately 1 cm in width. The strips were placed in 100 mL protoplast buffer solution (0.005 M 2-*N*-morpholino-ethanesulfonic acid, MES; Sigma-Aldrich, Oakville, Ontario, Canada), 0.6 M sorbitol, pH 5.5 (adjusted with dilute potassium hydroxide) for 15-20 min (Staal et al. 1988). All strips totalling one gram in wet fresh weight were transferred to a 100 × 20 mm Petri dish containing enzyme solution. Enzyme solution consisted of 2% w/v Cellulase R10, and 0.5% Pectolyase Y-23 (Yakult Pharmaceutical Ind, Tokyo, Japan) dissolved in 10 mL protoplast buffer solution (Pongchawee et al. 2006, 2007). Leaf strips were incubated for 4 hr at 27°C in the dark; the Petri dish was shaken at 50 rpm for the final 30 min of the enzyme incubation. The suspension was then pipetted through a wet 70 μm mesh into a 50 mL centrifuge tube leaving the leaf debris in the Petri dish. This leaf debris was then rinsed with 10 mL of clean protoplast buffer and swirled for an additional 10 min at 50 rpm to release the remaining protoplasts. This suspension was then collected, pipetted through mesh and collected in the same 50 mL centrifuge tube. The combined protoplast suspension was then centrifuged at 100 × *g* for 20 min with no brake at room temperature. The pellet was rinsed with 15 mL of clean buffer solution, re-centrifuged, and re-suspended in approximately 1 mL of clean protoplast buffer.

2.3.3 Density and Viability

Protoplast density was determined via a hemocytometer technique in which protoplasts were counted in small areas under square coverslips and the data were extrapolated to the entire sample. Viability was determined through fluorescein diacetate (FDA) staining (Sigma-Aldrich, Oakville, Ontario, Canada).

2.3.4 Microscopy

Light microscopic observations were performed using glass coverslips and slides on a Nikon eclipse 90i compound light microscope (Nikon, Mississauga, Ontario, Canada) fitted with a digital camera (Nikon DXM 1200c) using NIS Elements AR 3.0 imaging software and I Control. Light microscope observations were performed using differential interference contrast (DIC) optics with any complimentary fluorescent images taken via a fluorescent B2A filter (excitation 440-520 nm and emission 485-585 nm).

Laser confocal scanning observations were performed using a droplet cell culture chamber on a Nikon Eclipse T*i* confocal microscope (Nikon, Mississauga, Ontario, Canada) fitted with a digital camera (Nikon DS-Fi1) and using EZ-C1 3.80 imaging software and Ti Control. Confocal microscope observations were performed using DIC optics with complimentary fluorescent images taken via a fluorescein isothiocyanate (FITC; excitation 460-500, nm emission 510-560 nm) or tetramethyl rhodamine Isothiocyanate (TRITC; excitation 527-552 nm, emission 577-632 nm) laser. All composite plates were assembled using Adobe Photoshop Elements version 6.0.

2.3.5 Leaf Stage, Carbohydrate Source, and Enzyme Incubation Time

Following preliminary trials in which a suitable enzyme combination for lace plant protoplast isolation was determined (data not shown), the effects of varied leaf stage (juvenile, window and mature), carbohydrate source in buffer (0.6 M sorbitol, mannitol, sucrose or glucose) and enzyme incubation time (2, 4 or 6 hr in the dark) were examined. Protoplasts were isolated and collected as previously described. Protoplast density and viability were recorded in order to determine the effect of these variables on protoplast isolation.

2.3.6 Statistical Analysis

All data were assessed by a general linear model of variance (GLM ANOVA) and the means were compared by the Tukey test at 95% confidence intervals ($P < 0.05$). All statistical analyses were carried out using Minitab 15 Statistical Software English (Minitab Inc., State College, PA, USA).

2.4 Results

2.4.1 Protoplast Isolation

Leaf stage was found to significantly affect the yield and viability of protoplast isolates ($P = 0.000$). The window stage of leaf development resulted in the highest yield ($60.50 \pm 0.80 \times 10^5$ protoplasts/ g fresh weight) and viability ($92.50 \pm 2.59\%$) of protoplasts when compared to the heteroblast and mature leaf samples (Figure 2.2) as determined by hemocytometer and FDA techniques respectively. The window stage cells were consistently spherical in shape and contained many chloroplasts and mitochondria (Figure 2.3C). Protoplast density decreased significantly when using heteroblast leaf

(0.80 ± 0.24 × 10^5/g fresh weight) and mature stage leaf samples (1.99 ± 0.44 × 10^5/g fresh weight), as compared to window stage leaf material at $P < 0.05$. Protoplast viability also decreased significantly when using heteroblast leaf (53.25 ± 3.71%) and mature stage leaf samples (52.60 ± 5.03%), as compared to window stage leaf material at $P < 0.05$.

Figure 2.3 depicts both DIC and corresponding FDA fluorescent images from all three leaf samples, illustrating both protoplast density and viability respectively. Density and viability in the juvenile leaf isolations (Figure 2.3A and B) are drastically reduced compared to window stage samples (Figure 2.3C and D), and cells also appear to be less spherical in shape. Density and viability are also reduced in the mature stage samples (Figure 2.3E and F) when compared to window stage isolates. These mature cells appear to maintain a more spherical shape than the heteroblast cells but display less chloroplasts when compared to window stage isolates. Note the presence of anthocyanin in the vacuole of some cells (Figure 2.3C and E), suggesting the presence of an intact tonoplast membrane.

Window stage protoplast isolations exhibited high yields of cells (Figure 2.4A), with organelles clearly present within the majority of isolates (Figure 2.4B and C). Chloroplasts (Figure 2.4B red arrow) and the nucleus (Figure 2.4B black arrow) can also be visualized within the cells, suggesting viable isolations. The PM can also be seen on all cell isolates (Figure 2.4C red arrow). Lastly, the tonoplast membrane (Figure 2.4C black arrow) can be seen in isolated protoplasts, once again suggesting healthy cells. Note the presence of anthocyanin in the vacuole of some cells (Figure 2.4), suggesting the presence of an intact tonoplast membrane.

Trials experimenting with four different carbohydrate sources, each at 0.6 M, in protoplast buffer and enzyme mixture depicted that sorbitol significantly influenced protoplast yield and viability ($P = 0.000$; Figure 2.5). Sorbitol at 0.6 M resulted in the highest yield ($60.42 \pm 0.89 \times 10^5$ protoplasts/ g fresh weight) and viability ($92.75 \pm 2.95\%$) when compared to other carbohydrate sources, as determined by hemocytometer and FDA techniques respectively. Using mannitol, protoplast yield ($7.85 \pm 0.53 \times 10^5$/g fresh weight) and viability ($71.25 \pm 2.04\%$) were significantly decreased when compared to sorbitol samples at $P < 0.05$ (Figure 2.5). Using glucose, protoplast yield ($4.17 \pm 0.43 \times 10^5$/g fresh weight) and viability ($52.22 \pm 3.53\%$) were also significantly decreased when compared to sorbitol samples at $P < 0.05$ (Figure 2.5). Lastly, when using sucrose, protoplast yield ($9.98 \pm 0.51 \times 10^5$/g fresh weight) and viability ($74.87 \pm 1.84\%$) were significantly decreased when compared to sorbitol samples at $P < 0.05$ (Figure 2.5).

The amount of time protoplasts were allowed to digest in enzyme solution (2, 4 and 6 hr) was found to significantly influence protoplast yield and viability ($P = 0.000$; Figure 2.6). Protoplast digestion for 4 hr resulted in the highest yield ($60.35 \pm 1.08 \times 10^5$ protoplasts/g fresh weight) and viability ($92.75 \pm 2.25\%$) when compared to 2 and 6 hr digestion times, as determined by hemocytometer and FDA techniques respectively. Digestion for 2 hr resulted in significantly lower yield ($2.02 \pm 0.27 \times 10^5$) and viability ($61.37 \pm 1.61\%$) at $P < 0.05$ when compared to 4 hr digestions (Figure 2.6). Digestion for 6 hr also resulted in significantly lower yield ($1.92 \pm 0.34 \times 10^5$) and viability ($51.55 \pm 2.94\%$) at $P < 0.05$ when compared to 4 hr digestion (Figure 2.6). There was no significant difference in protoplast yield between 2 and 6 hr digestions at $P > 0.05$,

although significant differences in viability were noted between the same two trials at $P < 0.05$ (Figure 2.6).

2.5 Discussion

2.5.1 Factors Effecting Protoplast Isolation

Several factors, including leaf age, carbohydrate source in buffer and enzyme solution, and enzyme incubation time all significantly influenced protoplast yield and viability from lace plant tissue. Window stage leaves from plants approximately 1 month of age resulted in the highest yield and viability of protoplast isolates when compared to juvenile heteroblast and mature leaf samples. This difference in yield and viability based on leaf age has been seen in other species including *Anubias nana* (Pongchawee et al. 2006), *Cryptocoryne wendtii* (Pongchawee et al. 2007) and *Sesbania bispinosa* (Yan-Xiu et al. 1995). Similar trends to *Anubias nana* and *Cryptocoryne wendtii* were seen in the lace plant in that the youngest and oldest leaves gave lower protoplast yields and viability when compared to middle aged samples. There are several reasons for this occurrence, foremost among them being that the youngest leaves often do not contain thick deposits of cellulose or pectin, resulting in the enzyme mixture degrading the leaf instead of isolating protoplasts from it. Secondly, older leaves tend to have a thicker cuticle and more lignin in their cell walls then younger leaves, making them difficult to digest. Middle stage samples such as the window stage have a very thin cuticle and generally contain low amounts of lignin, resulting in healthy, round, organelle rich protoplasts from isolation.

Using mannitol, sucrose, or glucose in protoplast buffer and enzyme mixture resulted in a significantly lower number of protoplasts isolated when compared to sorbitol. It is possible that mannitol, sucrose and glucose all resulted in hypo or hypertonic solutions, causing the burst or collapse of protoplasts, respectively. Sorbitol as a carbohydrate seemed to provide the most suitable osmotic pressure for *A. madagascariensis* protoplasts, allowing for cells to remain intact; however the factors contributing to this finding should be investigated further (Pongchawee et al. 2006, 2007).

During enzyme incubation trials the optimal time to digest lace plant leaves was determined to be 4 hr. Incubation for a shorter period of time (2 hr) led to a decrease in protoplast yield, due to the tissue not being thoroughly digested. Large pieces of tissue still remained intact following digestion at 2 hr and contained many intact protoplasts. Conversely, the 6 hr incubation resulted in excessive digestion of the leaf material. This prolonged incubation of leaves could potentially have led to the dysfunction and breaking of cells. To allow for shorter incubation times, the concentration of the enzyme solution could have been raised and to allow for longer incubation times, the concentration of the enzyme solution could have been lowered (Pongchawee et al. 2006, 2007)

2.6 Conclusions and Further Work

Initially, several protocols for the isolation of protoplasts from land plants such as *A. thaliana* (Yoo et al. 2007), maize (Sheen 1993) and wheat (Harris et al. 1988) were attempted with the lace plant, and resulted in low yield, nonviable protoplasts from the plant. Here, the first efficient protocol for the isolation of high yield, viable protoplasts from the aquatic monocot *A. madagascariensis* was developed. Protoplasts were

successfully isolated from window stage leaf tissue using an enzyme mixture comprised of 2% w/v cellulase R10 and 0.5% pectolyase Y-23 dissolved in 0.005 M MES, 0.6 M sorbitol, pH 5.5. Approximately 60.35 ± 1.08 × 10^5 protoplasts/g fresh weight, with a viability of 92.75 ± 2.25% were obtained from 4 hr isolations in the dark. Leaf age, carbohydrate source, and enzyme incubation time all significantly influenced both protoplast yield and viability.

At present time the isolated protoplasts will remain viable in culture medium consisting of 1.0 mg/L 2,4-dichlorophenoxyacetic acid (2,4-D), and 1.0 mg/L thidiazuron for up to 10 days with aggregates forming following 20 days of culture. Further research needs to be completed in order to determine precise hormone concentrations for the formation of callus and whole plant regeneration from the protoplasts. Whole plant regeneration from protoplasts would create an accelerated, cost effective method for producing sterile lace plants in large quantities. Lace plant protoplasts are also currently being utilized as a model system for the study of environmentally induced PCD. At present we are subjecting the isolated cells to heat treatments of 55°C for 20 min; following heat treatments cells are screened for morphological changes in organelles, focusing on the mitochondria, cytoskeleton, vacuole and nucleus. This environmentally induced cell death has allowed for the first ever opportunity to compare environmentally induced PCD with its developmentally regulated counterpart within one plant (Lord and Gunawardena 2011). Lastly, these protoplasts can be utilized as a system for *in vivo* transient gene expression; by transforming the cells with genes tagged with fluorescent markers and targeted to specific organelles, a more precise understanding of the order of

events occurring within a cell undergoing PCD can be determined. This tagging would also permit for characterization of organelle origin, movement and fate.

2.7 Acknowledgements

The authors thank Dr. N. Dengler (University of Toronto) for critical review of this article, Dr. Jennifer Sheen (Mass General Hospital, Molecular Biology, Boston, MA, USA) for help regarding protoplast isolation, and honours student Joey Carter (Dalhousie University) for technical assistance. The authors also greatly acknowledge the Canadian Foundation for Innovation (CFI) for the Leaders Opportunity Fund, the Natural Sciences and Engineering Research Council (NSERC) for discovery and equipment grants for A.G. and Dalhousie University for partial doctoral funding for C.L.

Figure 2.1 The Lace Plant or *Aponogeton madagascariensis*

Sterile *A. madagascariensis* in magenta box, white arrow indicating mature leaf, red arrow indicating window stage leaf, and black arrow indicating heteroblast leaf (A). Scale bar = 1 cm. Micrograph of heteroblast leaf (B) window stage leaf (C) and mature leaf (D). Scale bar (B-D) = 100 μm.

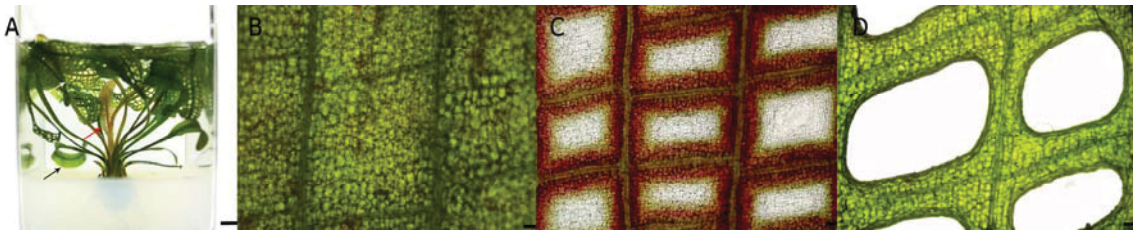

Figure 2.1 The Lace Plant or *Aponogeton madagascariensis*

Figure 2.2 Effect of Leaf Stage on Protoplast Isolation From *A. madagascariensis*

Bar graph represents average protoplast yield from each leaf stage while the line graph represents average viability. All samples were isolated with enzyme combination 2. Data represents mean ± standard error of four replicates.

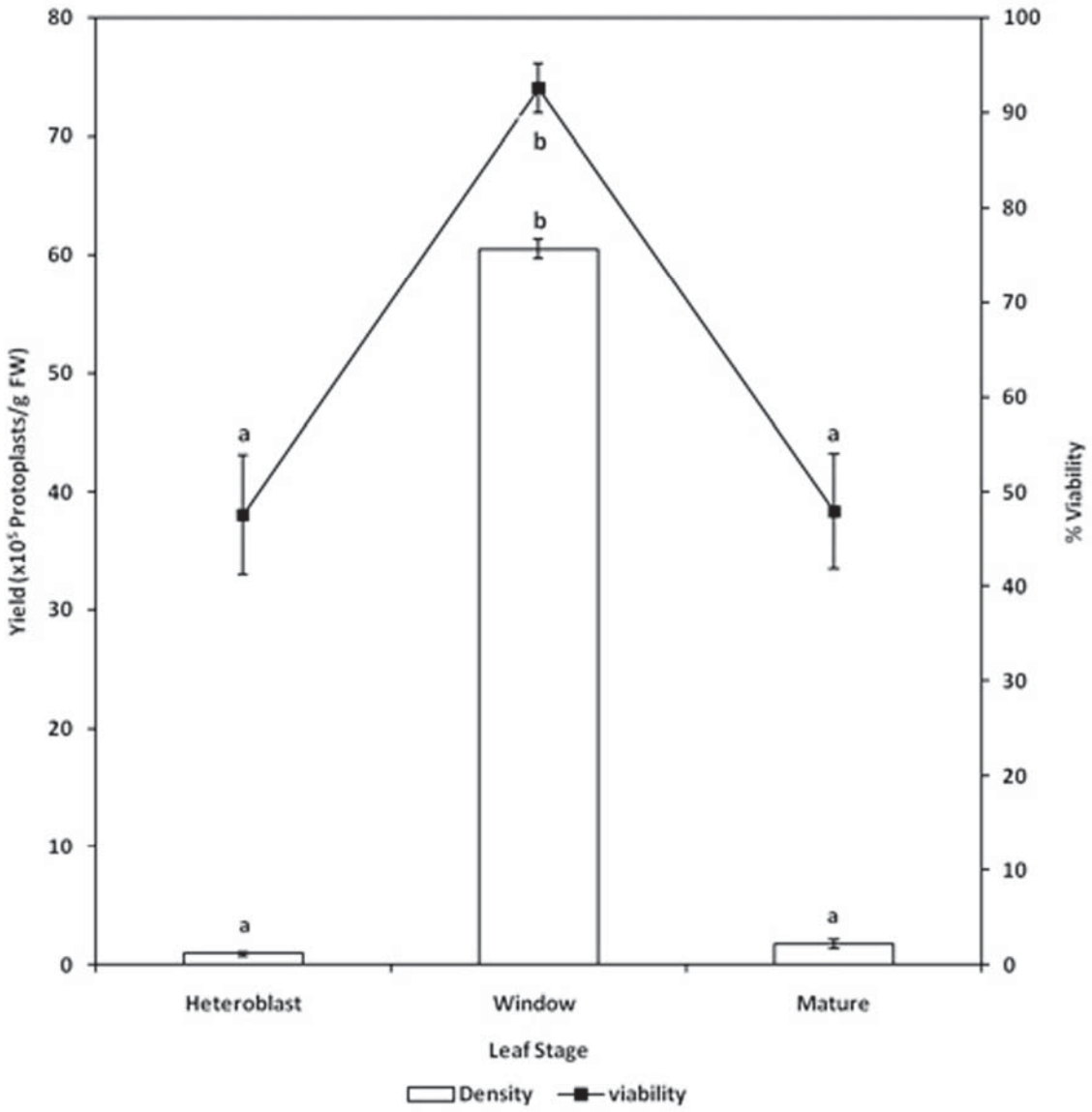

Figure 2.2 Effect of Leaf Stage on Protoplast Isolation From *A. madagascariensis*

Figure 2.3 Light Micrographs of Isolated Protoplasts From *A. madagascariensis*

Protoplasts from heteroblast leaves (A, B), window stage leaves (C, D) and mature leaves (E, F). DIC images (A, C, E) and corresponding fluorescent images depicting FDA staining of living cells (B, D, F). The pink coloration within the cells is the pigment anthocyanin; the presence of this pigment within the cells indicates an intact tonoplast membrane, and hence viable cells. These pink cells are isolated from the mesophyll of the leaf, while the clear cells are isolated from the epidermis. All scale bars = 100 μm.

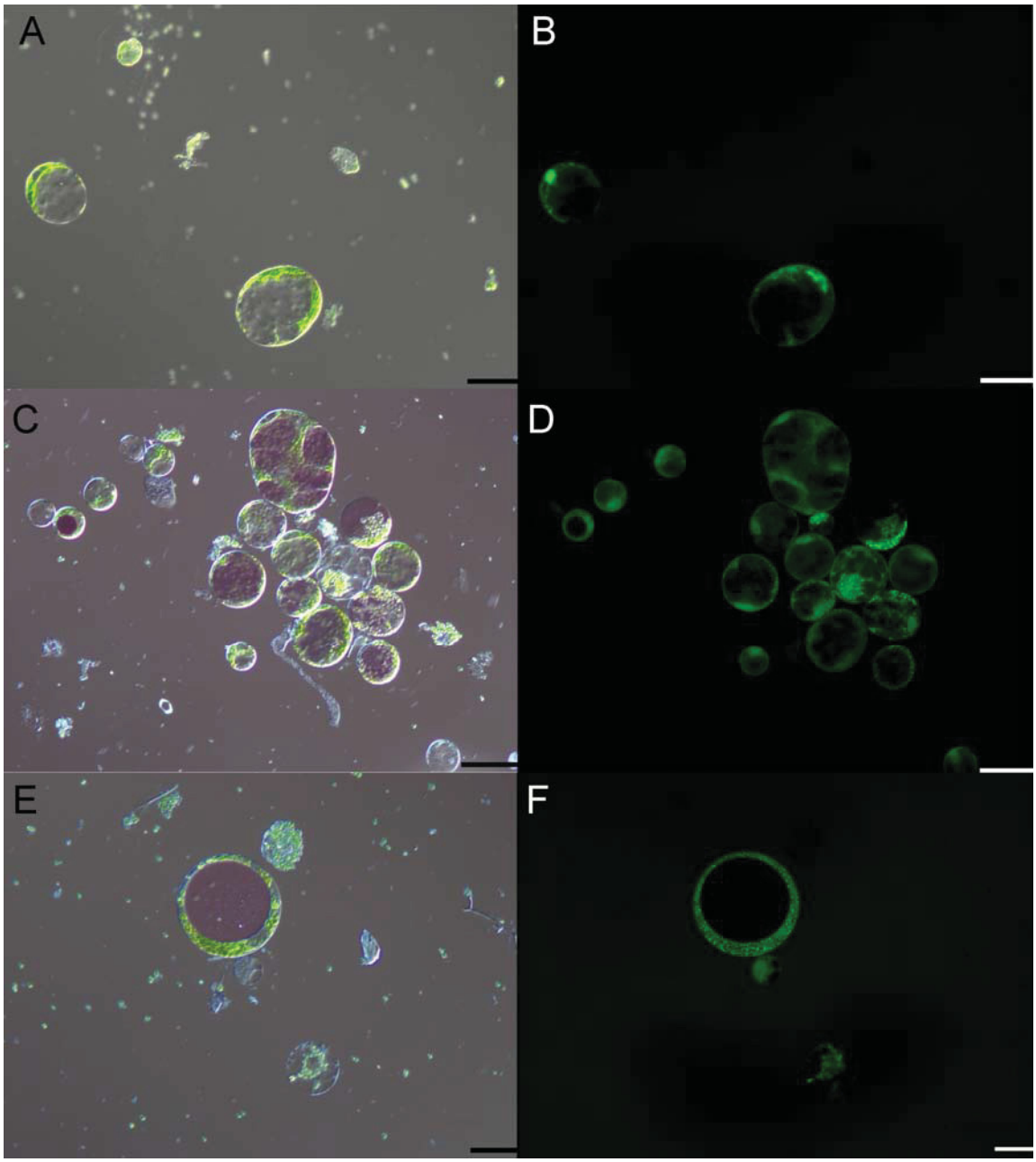

Figure 2.3 Light Micrographs of Isolated Protoplasts From *A. madagascariensis*

Figure 2.4 Confocal Micrographs of Isolated Protoplasts From a Window Stage Leaf Sample

Freshly isolated protoplasts released from window stage lace plant leaf. The pink cells are isolated from the mesophyll of the leaf, while the clear cells are isolated from the epidermis (A). Scale bar = 100 μm. Individual isolated protoplast, red arrow indicates chloroplasts, black arrow indicates nucleus (B). Individual isolated protoplast, red arrow indicates plasma membrane, black arrow indicates tonoplast membrane (C). Scale bar (B, C) = 50 μm.

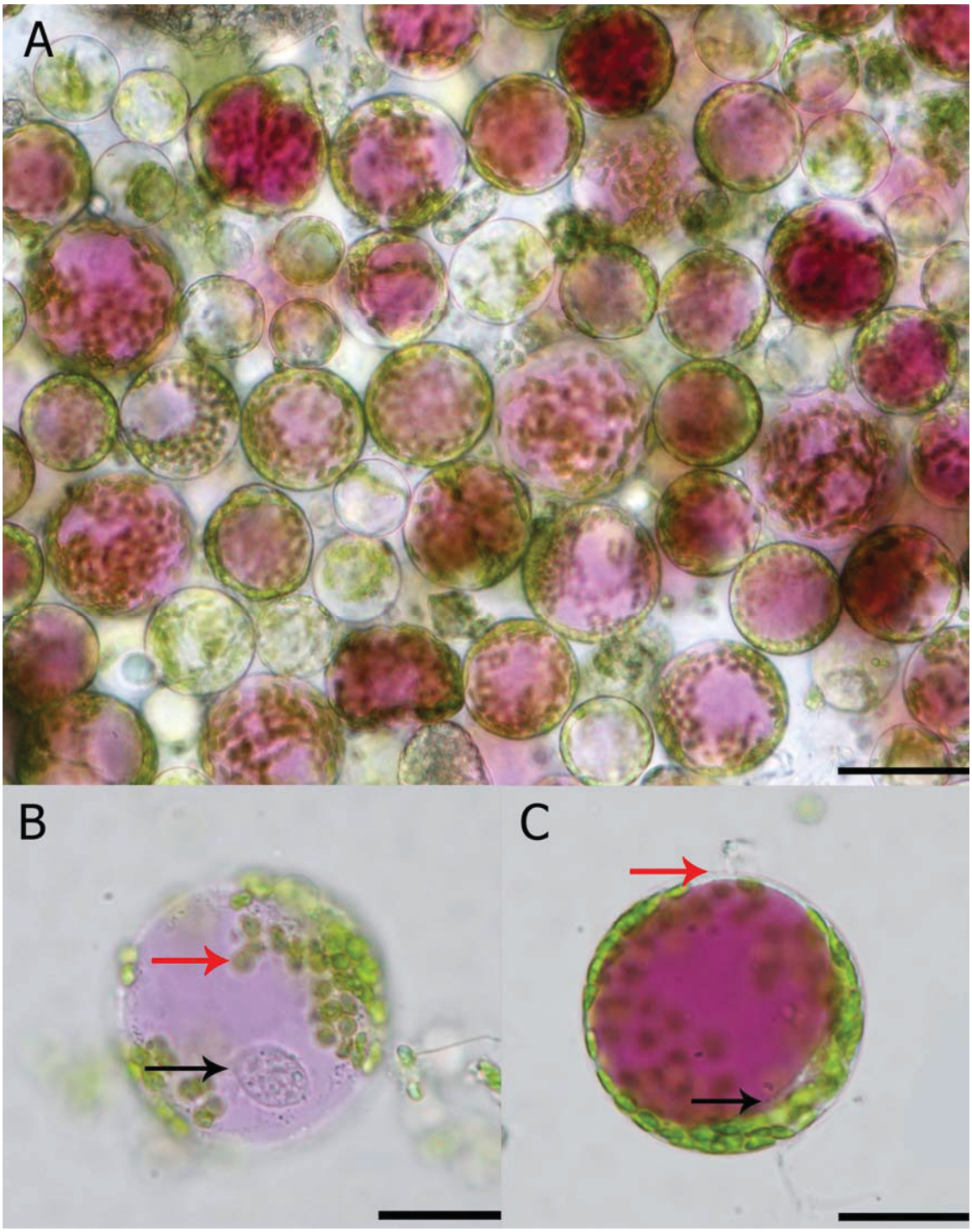

Figure 2.4 Confocal Micrographs of Isolated Protoplasts From a Window Stage Leaf Sample

Figure 2.5 Effect of Various Carbohydrate Sources on Protoplast Isolation From *A. madagascariensis* Window Stage Leaves

Bar graph represents average protoplast yield from each treatment while the line graph represents average viability. Data represents mean ± standard error of four replicates.

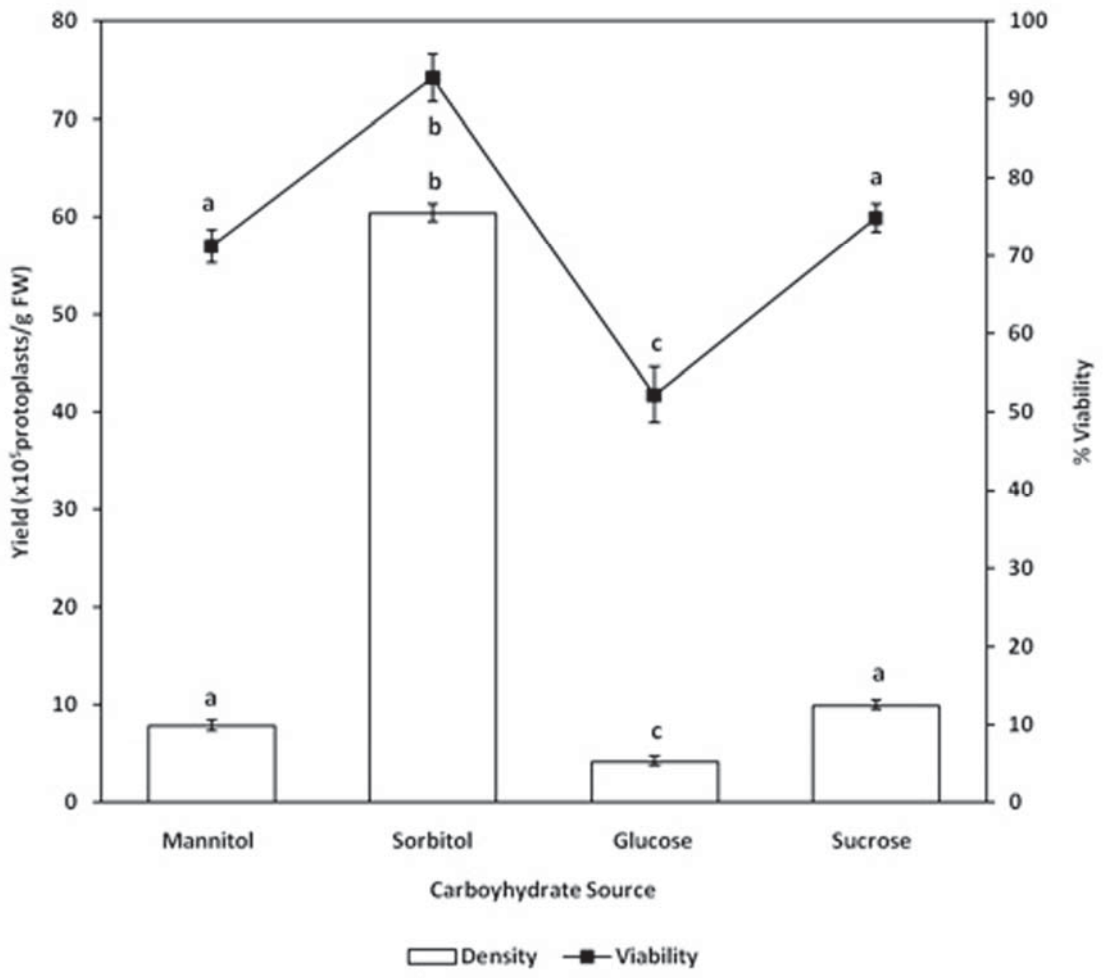

Figure 2.5 Effect of Various Carbohydrate Sources on Protoplast Isolation From *A. madagascariensis* Window Stage Leaves

Chapter 3 Environmentally Induced Programmed Cell Death in Leaf Protoplasts of *Aponogeton madagascariensis*

Published as:

Lord CEN, Gunawardena AHLAN. Environmentally Induced Programmed Cell Death in Leaf Protoplasts of *Aponogeton madagascariensis.* Planta 233: (2011) 407-421

3.1 Abstract

Within plant systems, two main forms of programmed cell death (PCD) exist; developmentally regulated and environmentally induced. The lace plant (*Aponogeton madagascariensis*) naturally undergoes developmentally regulated PCD to form perforations between longitudinal and transverse veins over its leaf surface. Developmental PCD in the lace plant has been well characterized; however environmental PCD has never before been studied in this plant species. The results presented here portray heat shock (HS) treatment at 55°C for 20 min as a promising inducer of environmental PCD within lace plant protoplasts originally isolated from non-PCD areas of the plant. HS treatment produces cells displaying many characteristics of developmental PCD, including: blebbing of the plasma membrane, increased number of hydrolytic vesicles and transvacuolar strands (TVS), nuclear condensation, terminal deoxynucleotidyl transferase mediated dUTP nick-end labeling (TUNEL) positive nuclei, as well as increased Brownian motion within the vacuole. Results presented here for the first time provide evidence of chloroplasts in the vacuole of living protoplasts undergoing environmentally induced PCD. Findings suggest the mitochondria play a critical role in the cell death process. Changes in mitochondrial dynamics were visualized in HS treated cells, including, loss of mitochondrial mobility, reduction in mitochondrial membrane potential ($\Delta\Psi_m$), as well as the proximal association with chloroplasts. The role of the mitochondrial permeability transition pore (MPTP)[5] was examined by pre-treatment with the pore agonist cyclosporine A (CsA). Overall, HS is depicted as a reliable method to

[5] PTP has been replaced with MPTP in the remainder of this manuscript in order to be consistent throughout this dissertation.

induce PCD within lace plant protoplasts, and proves to be a reliable technique to enable comparisons between environmentally induced and developmentally regulated PCD within one species of plant.

3.2 Introduction

3.2.1 Programmed Cell Death (PCD)

PCD is the regulated death of cells within an organism, and is ubiquitous in all eukaryotes (Lam and Del Pozo 2000). PCD in plants can be broadly characterized as either environmentally induced or developmentally regulated (reviewed by Gunawardena 2008). Environmentally induced PCD is an outcome of abiotic or biotic factors and includes examples such as heat shock (HS; Balk et al. 2003; reviewed by McCabe and Leaver, 2000; McCabe et al. 1997; Scott and Logan, 2008; Vacca et al. 2004; Vacca et al. 2006; Zhang et al. 2009), UV radiation (Danon and Gallois, 1998; He et al. 2008), low oxygen treatment inducing the formation of lysigenous aerenchyma (Gunawardena et al. 2001), the use of compounds and chemical elements, including aluminum chloride ($AlCl_3$) and cadmium (Cd; Iakimova et al. 2008; Yakimova et al. 2007), as well as pathogen infection (Mittler and Lam 1997). The initial four examples fit into the abiotic induced category, while pathogen infection is caused by biotic factors. Within an experimental setting, environmentally induced PCD has been demonstrated in whole tissues as well as in protoplasts (single cells lacking the cell wall; reviewed by McCabe and Leaver, 2000; reviewed by Reape and McCabe, 2008). Protoplasts have been used as a versatile cell-based system, which maintain many of the same physiological properties of an intact plant cell, despite the removal of the cell wall, but with an increased level of

manipulability (Pongchawee et al. 2007; Pongchawee et al. 2006; Scott and Logan, 2008; Yoo et al. 2007).

In contrast, developmentally regulated PCD occurs as part of normal development and presumably is a response to internal signals. Examples of developmentally regulated PCD include elimination of transitory organs and tissues (Filonova et al. 2008; Helmersson et al. 2008), xylem differentiation (reviewed by Fukuda et al. 1998; Fukuda, 2000), and leaf morphogenesis (Gunawardena et al. 2004; Gunawardena et al. 2005) as is seen in the lace plant (*Aponogeton madagascariensis*) and *Monstera*.

Both forms of PCD display distinct morphological characteristics, including plasma membrane (PM) blebbing, increased formation of vesicles and transvacuolar strands (TVS), condensation of the cytoplasm and nucleus, changes in mitochondrial dynamics, cleavage of DNA at specific sites by endonucleases, as well as a positive terminal deoxynucleotidyl transferase mediated dUTP nick-end labeling (TUNEL) response (Balk et al., 2003; reviewed by Conradt, 2009; reviewed by Danon et al. 2000; Gunawardena et al. 2004; reviewed by McCabe and Leaver, 2000; McCabe et al., 1997; Reisen et al. 2005; Yao et al. 2004).

3.2.2 Mitochondria and PCD

Mitochondria play a vital role in cellular metabolism in both plants and animals. Within animal systems, mitochondrial dynamics have been recognized to play an imperative role in the regulation of PCD, while this organelles role within plant PCD is still unclear (reviewed by Jones, 2000; Joza et al. 2001). In animal systems, mitochondria

appear to undergo one of two distinct physiological changes leading to alterations in mitochondrial membrane potential ($\Delta\Psi_m$) and the release of intermembrane space (IMS) proteins. One strategy involves the formation of the mitochondrial permeability transition pore (MPTP) by the coordination of the voltage-dependent anion channel (VDAC), adenine nucleotide translocase (ANT) and cyclophilin D (CyP-D), while the second strategy involves the Bcl family of proteins and utilizes only the VDAC (reviewed by Green and Reed 1998). To date, evidence for the presence of MPTP formation in plant PCD has been reported (Arpagaus et al. 2002; Balk et al. 1999; reviewed by Crompton, 1999; Diamond and McCabe, 2007; reviewed by Jacobson, 1996; reviewed by Jones, 2000; Zamzami et al. 1995; Zhang et al. 2009); however, there is little evidence for the involvement of Bcl family proteins in plants[6] (Balk et al. 1999; Balk and Leaver 2001). It is now known that cyclosporine A (CsA) can act in disrupting the MPTP by inhibiting the binding of CyP-D to ANT (Arpagaus et al. 2002; reviewed by Crompton, 1999; Diamond and McCabe, 2007; Lin et al. 2005) leading to advances in PCD research focusing on the mitochondria.

3.2.3 Induction of Cell Death

---

[6] As per section 1.2.3.1 within Chapter 1, this statement is not completely accurate. Evidence for Bcl-2 family proteins certainly does exist in plants. Similar anti-apoptotic proteins include *Bax-inhibitor-1 (BI-1)* homologues in barley and Arabidopsis (*AtBI-1*). Less is known regarding pro-apoptotic homologues but the up regulation of pro-apoptotic Bcl-2 family members, or *egl-1* have been shown to cause cell death associated characteristics in plants.

.

The induction of PCD through the use of environmental factors such as HS has recently become a frequently used technique in plant systems. HS is thought to alter cellular metabolism, including the disruption of electron transport chain (ETC) in the mitochondria, leading to reduced chemiosmosis and decreases in ATP production. *Arabidopsis*, tobacco BY-2 cells, and cucumber have all depicted alterations in cellular redox status, as well as disruption of mitochondrial dynamics following HS (Balk et al. 2003, 1999; Scott and Logan, 2008; Vacca et al. 2004; Yao et al. 2004; Zhang et al. 2009). These changes in mitochondrial dynamics can be visualized when mitochondria are stained with a permeability sensitive dye such as chloromethyl-X-rosamine (CMXRos MitoTracker Red), which is sequestered in the mitochondrial matrix as a function of the Nernst equation (Balk et al. 1999; Curtis and Wolpert, 2002; reviewed by Kroemer et al. 1997; Yao et al. 2004).

3.2.4 The Lace Plant

The lace plant [*A. madagascariensis* (Mirbel) H. Bruggen] is an aquatic monocot endemic to the river of Madagascar. Leaves of the plant are very thin, approximately four cell layers thick and are produced from a shoot apical meristem (SAM) at the apex of the spherical corm. The leaves of the lace plant form in a heteroblastic series; the first one to three leaves produced by the SAM are the juvenile leaves that do not form perforations, while the following leaves are adult leaves, which will form perforations. The lace plant is one of 40 species in the monogeneric family Aponogetonaceae, and is the only species which produces perforations in its leaves through the PCD process (Gunawardena et al.,

2004, 2006, 2007). Proposed hypotheses for the purpose of these perforations are reviewed in Gunawardena and Dengler (2006).

3.2.5 Developmentally Regulated PCD and the Lace Plant

In the lace plant, PCD begins between longitudinal and transverse veins in spaces known as areoles, and continues outward before stopping four to five cells (non-PCD or NPCD) from the vascular tissue, creating a lattice-like pattern over the entire leaf surface (Gunawardena et al. 2004). The developmental morphology of the adult lace plant leaf has been divided into five stages as detailed in Gunawardena et al (2004). Due to the predictability of perforation formation, *A. madagascariensis* makes an ideal model system for the study of developmentally regulated PCD in plants (Elliott and Gunawardena, 2010; reviewed in Gunawardena, 2008; Gunawardena et al. 2004, 2007, 2006; Wright et al. 2009). The present study aimed to investigate environmental PCD in the lace plant, through HS at 55°C for 20 min. Cellular changes that occurred were examined using live cell imaging and characteristics compared with the developmental counterpart within the whole leaf of the plant. An emphasis was placed on the role of the mitochondria, particularly the MPTP, and its role within the induced cell death system.

3.3 Materials and Methods

3.3.1 Plant Materials

All plant materials were grown and subcultured as described in section 2.3.1 within Chapter 2. All chemicals were purchased from Sigma-Aldrich (St Louis, MO,

USA), unless otherwise stated. All experiments were completed at least four times unless otherwise stated.

3.3.2 Confocal Laser Scanning Microscopy

All confocal observations were performed as described in section 2.3.4 within Chapter 2.

3.3.3 Protoplast Isolation

Protoplast isolation was accomplished as described in section 2.3.2 within Chapter 2. However, perforation expansion leaves were used for isolations as to eliminate the isolation of protoplasts, which were already destined to undergo developmentally regulated PCD. Protoplast density and viability calculations were performed as described in section 2.3.3 within Chapter 2. Due to the large variation in the size of lace plant protoplasts (25–100 μm), it is difficult to use a fine mesh for the separation of protoplasts and cell debris; therefore, it is common in protoplast isolations to have a small amount of cell debris present (Lord and Gunawardena 2010).

3.3.4 Heat Shock (HS) Challenge

Originally, lace plant protoplasts were heated at 25, 55 or 75°C in order to determine the temperature that most effectively induced PCD. Given results from this preliminary work, freshly prepared protoplasts were then challenged by HS at 55°C for 20 min. HS was performed using a Nikon live cell culture chamber, equipped with a Bionomic controller (20/20 technology, BC-110) regulated by a heat exchanger (20/20

technology, HEC-400; Grand Rapids, MI, USA). Breathing quality air (5 psi) was pumped into a gas purge system (20/20 technology, P-502) for regulation; air was then pumped into a small humidity chamber, which was then subsequently pumped over the sample in the culture chamber to create a humid environment, preventing cells from desiccating. Preliminary experiments tracked HS-treated protoplasts over a 6 hr period. Following this preliminary work, it was determined that allowing HS cells to recover at 24°C for 0, 30, 60, 90, or 120 min was sufficient and optimal. Controls consisted of isolated protoplasts which were not subjected to HS. Several cell samples were also heated at 75°C for 20 min in an effort to induce necrosis. This experiment was completed not only to enable the comparison of PCD cells with controls, but also to allow for comparison with the cells undergoing uncontrolled cell death. Prior to HS at 55°C for 20 min, several protoplast samples were pre-treated with 50 μM CsA for 30 min, at room temperature according to (Lin et al. 2005, 2006). All operations and staining were carried out under dark conditions to minimize possible oxidative stress caused by light.

3.3.5 TUNEL

For the LM-TUNEL assay, treated protoplasts were fixed with 4% paraformaldehyde for 1 hr at room temperature. Protoplasts were then permeabilized with 10 μg/mL proteinase K at 4°C for 2 min. The free 3`-OH groups in the DNA were labelled by a fluorescein *in situ* cell death detection kit (Roche, Boehringer Mannheim, Germany) according to manufacturer's instructions. TUNEL stained samples were excited with the FITC cube (excitation 460–500 nm, emission 510–560 nm) on the confocal microscope.

3.3.6 DNA Isolation and Electrophoresis

Genomic DNA was isolated from HS-treated protoplasts that were originally isolated from a 1 g perforation expansion leaf sample. Protoplasts isolated from this sample were divided into six 400 µl samples and frozen in liquid nitrogen at 0, 0.5, 1, 3, 5, and 24 hr post-HS. Samples were ground by hand into a fine powder. Isolation of DNA was performed using a DNeasy plant mini kit (Qiagen, Mississauga, Ontario, Canada) according to the manufacturer's instructions. To observe DNA fragmentation, samples (0.5 µg/mL lane, final concentration) were run with a 100-bp ladder on a 1% ethidium bromide agarose gel at a constant 50 V.

3.3.7 Mitochondrial Staining

Control, CsA + HS or HS-challenged protoplasts were incubated with 100 nM of the mitochondria-specific, membrane potential sensitive dye CMXRos (Molecular Probes Eugene, OR, USA; dissolved in dimethylsulfoxide, DMSO), for 10 min at 24°C in the dark. CMXRos was excited with the TRITC cube (excitation 527–552 nm, emission 577–632 nm) using the confocal microscope.

3.3.8 Transmission Electron Microscopy (TEM)

Protoplast samples for TEM were fixed using a method optimized specifically for lace plant material. Fixation was initiated by adding cells to 2% glutaraldehyde (GA) in buffer (0.05 M sodium cacodylate, 0.4 M sorbitol, pH 6.5) for 1 hr, followed by the addition (1:1, v/v) of 1% osmium tetroxide (OsO_4) in distilled water (dH_2O). Fixed protoplasts were then washed twice in buffer (0.05 M sodium cacodylate, 0.4 M sorbitol,

pH 6.5) for 20 min each and stored at 4°C overnight. Cells were then embedded in 4% agarose (Type VII-A low gelling temperature; Sigma-Aldrich), cut into small pieces (approximately 0.5 cm x 0.5 cm) and dehydrated for 10 min each in 50, 70, 80, 90, and 95% ethanol and twice for 10 min each in 100% ethanol and propylene oxide. Embedded protoplasts were infiltrated in mixed propylene oxide and poly/bed (1:1) overnight, then infiltrated in fresh epoxy for 4 hr, and transferred to fresh epoxy in capsules. Polymerization was performed in a 60°C oven for a total of 48 hr. Semi-thin sections (2 μm thick) and ultra-thin sections (50 nm thick) were stained with uranyl acetate and lead citrate before observation with a Philips Tecnai 12 transmission electron microscope (TEM; Philips Electron Optics, Eindhoven, The Nether- lands) operating at 80 kV and fitted with a Kodak (Rochester, NY, USA) Megaview II camera and software (AnalySIS, Soft Imaging System, Műnster, Germany). All composite plates were assembled using Adobe Photoshop Elements version 6.0.

3.3.9 Statistical Analysis

All data were assessed as described in section 2.3.6 within Chapter 2.

3.4 Results

The natural development of a lace plant leaf has been previously described via five developmental stages (Figure 3.1). These stages include furled stage, ‘‘window’’ stage (Figure 3.1A), perforation formation, perforation expansion (Figure 3.1B) and mature (Figure 3.1C). A method has been developed for sterile culture of plants (Figure 3.1D; Gunawardena et al. 2004), and the transparent nature of the thin leaf facilitates live cell imaging. Several common characteristics of PCD have already been described

throughout regular leaf morphogenesis in the lace plant, including PM blebbing, increased vesicle formation, condensation of the cytoplasm and nucleus, changes in mitochondrial dynamics as well as TUNEL positive nuclei.

3.4.1 Environmentally Induced PCD Characteristics

One hr following protoplast isolation, control protoplasts were still of high yield with approximately 97.75% viability (Figure. 3.2A and B) in contrast to cells allowed to rest for 1 hr post HS with approximately 31.25% viability (Figure 3.2C and D). Viability of protoplasts was determined by FDA staining. Characteristics of PCD were not seen in control protoplasts. Control cells showed intact tonoplast and PMs (Figure 3.3A, and B; Figure 3.4A), healthy nuclei (Figure 3.4B), healthy chloroplasts with intact stroma and starch granules (Figure 3.3A; Figure 3.4C), as well as healthy, and often dividing mitochondria (Figure 3.4D).

HS has been used as a practical method to induce cell death in many species of plant, but has never before been used with the lace plant. Between 20 min and 2 hr post-HS at 55°C, lace plant protoplasts displayed many key characteristics of PCD, including blebbing of the PM (Figure 3.3C; Figure 3.4E), increased vesicle formation (Figure 3.3D), nuclear condensation (Figure 3.3D; Figure 3.4F), increased Brownian motion within the vacuole (see Online Resource 3.1), circular chloroplasts with degraded inner membrane, stroma, starch granules, and thylakoids (Figure 3.4G). In approximately one dozen protoplasts (out of 30 samples), chloroplasts were seen inside the central vacuole of the protoplast (Figure 3.3E; see Online Resource 3.2). Also following HS, slightly swollen mitochondria appeared with degraded cristae (Figure 3.4H); these mitochondria

were often seen associated with compromised chloroplasts (Figure 3.4H). An increased number of TVS was observed in approximately 20% of HS-treated cells (Figure 3.3F). A detailed table regarding organelle dynamics and timing is provided in Appendix B[7]. Combined, these characteristics suggest HS as an excellent inducer for the study of environmentally induced cell death in lace plant protoplasts. In contrast, protoplasts which were heated at 75°C for 20 min to induce necrosis displayed characteristics of an uncontrolled version of cell death including cell swelling (Figure 3.3G) and cell rupture (Figure 3.3H).

Protoplast viability was tracked via PI staining at 30 min intervals over a 2 hr period; control, CsA + HS and HS protoplast viability were compared (Figure 3.5A). HS was found to significantly affect protoplast viability at 0, 30, 60, 90 and 120 min post-HS when compared to control cells ($P < 0.05$; Figure 3.5B). CsA treatment was found to significantly affect protoplast viability at 0, 30, 60, 90, and 120 min post-HS when compared to control cells ($P < 0.05$; Figure 3.5B). The percentage of dead protoplasts following HS rose exponentially and reached 97.75 ± 0.94% at 120 min post-HS (Figure 3.5A and B). This value varied significantly from both CsA + HS protoplasts (81.75 ± 1.10%) and control protoplasts (5.75 ± 0.62%) at the same time interval ($P < 0.05$ for both; Figure 3.5A and B). All cells which stained positive with PI for dead nuclei contained a shrunken, PCD appearance, and in very few cases did a protoplast appear to be swollen or have ruptured via necrosis (Figure 3.5A).

---

[7] This table is an addition to the manuscript published in Planta and was included to aid in organelle examination during lace plant PCD.

3.4.2 Cessation of Mitochondrial Streaming

Following the determination of optimal dye loading concentrations and incubation time periods, protoplasts were incubated in 100 nM CMXRos for 10 min at 25°C, in the dark. Protoplasts stained via this method displayed intense mitochondrial staining, which could be easily observed within single protoplasts. Control protoplasts displayed active mitochondrial streaming (Figure 3.6A; see Online Resource 3.3). Between approximately 20 min and 1 hr post- HS, mitochondria depicted remarkable changes in motility; HS-treated protoplasts displayed cessation of mitochondrial streaming in approximately 65% of the isolates (Figure 3.6B; Table 3.1; see Online Resource 3.3). Also in this interval of time, mitochondria within the HS cells appeared to form small aggregates, and occasionally appeared to be proximally associated with the chloroplasts (Figure 3.4H). This aggregate formation was found in approximately 30% of the HS-treated protoplasts, but not seen in control cells (Figure 3.4C and D). Protoplasts pre-treated with CsA still showed cessation of mitochondrial streaming between approximately 20 min and 1 hr post HS (Table 3.1). Further analysis of changes in mitochondria motility were performed with CMXRos-stained protoplasts by quantifying the variation in mitochondrial fluorescence in arbitrarily chosen areas indicated by ellipses (Figure 3.6A and B). Variation in fluorescence intensity within these ellipses was used as a measure of mitochondrial streaming. Oscillation in the control graph (Figure 3.6A) indicates rapid mitochondrial streaming within the cell, whereas little oscillation in the HS-treated graph (Figure 3.6B) indicates little to no mitochondrial streaming. More details of mitochondrial motility can be found within Online Resource 3.3.

3.4.3 Decrease in Mitochondrial $\Delta\Psi_m$

Control, CsA + HS and HS-treated protoplasts stained with CMXRos were also used to make inferences regarding mitochondrial $\Delta\Psi_m$ during environmentally induced cell death. Regardless of which pathway was used by the mitochondria to induce cell death, the increased release of IMS proteins during the HS challenge is indicative of a reduction in mitochondrial $\Delta\Psi_m$, and therefore can be visualized via changes in mitochondria fluorescence. Control protoplasts labelled with CMXRos showed vivid mitochondrial staining at time 0, 60, and 120 min post-isolation (Figure 3.7; Table 3.1). In contrast, protoplasts pre-treated with CsA followed by HS showed a slight decrease in mitochondrial fluorescence at 0, 60, and 120 min post-HS when compared to controls (Figure 3.7; Table 3.1). Protoplasts treated with just a HS challenge showed rapid decreases in CMXRos staining leading to almost no viable mitochondria 2 hr post-HS (Figure 3.7; Table 3.1). CsA + HS-treated protoplasts displayed an intermediate decrease in mitochondrial $\Delta\Psi_m$ between control- and HS-treated cells. It should also be noted that within HS challenged protoplast samples, the largest decrease in mitochondrial fluorescence occurred between 1 and 2 hr post-HS (Figure 3.7; Table 3.1). The results for each treatment were observed in at least 65% of the sample protoplasts.

3.4.4 TUNEL, DNA Isolation and Electrophoresis

PCD confirmation was supported by the presence of 3`-OH nick ends detected via LM fluorescent TUNEL (Figure 3.8). At 2 hr post-isolation, no TUNEL positive nuclei were present in control cells (Figure 3.8A–C). Approximately 20% of CsA + HS-treated cells, which were allowed to rest for 2 hr post-HS, had TUNEL positive nuclei (Figure

3.8D–F). Approximately 55% of HS-treated cells, which were allowed to rest for 2 hr post-HS treatment, showed TUNEL positive nuclei (Figure 3.8G–L). HS protoplasts, when allowed to rest for 18 hr post-HS, still displayed approximately 55% TUNEL positive nuclei (data not shown). No DNA laddering was visualized via electrophoresis at any interval post-HS (data not shown).

3.5 Discussion

Results presented here indicate that HS treatment at 55°C for 20 min is an excellent inducer of cell death in lace plant protoplasts, and caused an increase in cell death compared to control cells at 1 hr post-HS, as per FDA and PI staining. The decline in living cells was anticipated given the severity of the HS challenge as well as drastic changes in cellular morphology visualized in HS-treated protoplasts. These changes in cellular morphology were representative of those normally seen in cells which have undergone PCD, including the overall shrinkage of cells versus the swelling and rupture associated with necrosis (reviewed by McCabe and Leaver, 2000; McCabe et al. 1997).

3.5.1 Organelles Involved in PCD

Chloroplast degradation in the lace plant-induced cell death system mimicked many of the same characteristics seen in the developmentally regulated counterpart. Changes in chloroplast shape, size, matrix morphology and the presence of starch granules were all noted in this induced death system, and have been reported previously in the developmentally regulated system (Wright et al. 2009). Wright et al. (2009) also made inferences regarding chloroplast fate, but due to the thickness of whole lace plant leaves, and the static nature of TEM, were not able to determine if chloroplasts were

entering the vacuole to be degraded. To date, findings of chloroplasts entering the vacuole have been reported in *Arabidopsis thaliana* (Wada et al. 2009), French bean (Minamikawa et al. 2001) and wheat (Wittenbach et al. 1982), all during leaf senescence via developmentally regulated PCD. Live cell imaging evidence presented here for the first time depicts chloroplasts within the vacuole of a protoplast undergoing induced PCD (Online Resource 3.2). Unlike the findings of Wright et al. (2009), dumbbell-shaped dividing chloroplasts were only seen in control cells, and not in early stages of cell death. This lack of dividing chloroplasts may be a result of the strong stress following HS, unlike the possibly more gradual effect of developmentally regulated PCD signals. An increased number of TVS was also noted in both the induced and developmentally regulated cell death systems in the lace plant (Wright et al. 2009). An increase in TVS was also shown during induced cell death by osmotic stress in tobacco suspension cultures (Reisen et al. 2005). Increases in TVS could aid in the movement of organelles such as chloroplasts and mitochondria to the edge of the nucleus or to inside the vacuole in lace plant cells. As was anticipated, an increase in hydrolytic vesicle formation was also seen within both death systems. The increase in these vesicles would presumably aid in the degradation of dead or dying organelles as PCD progresses. Changes in nuclear shape and size were noted within both induced and developmentally regulated death systems. Nuclear condensation is a common characteristic of PCD and is possibly driven by the condensation of chromatin (Ryerson and Heath 1996; McCabe et al. 1997). TUNEL positive nuclei were seen in HS-challenged cells and increased exponentially following HS. The presence of TUNEL positive nuclei was also noted in the developmentally regulated system (Gunawardena et al. 2004). DNA laddering was not

present in the induced cell death system at any interval following HS. However, DNA laddering was seen following HS-induced death in several species, including carrot (McCabe et al. 1997) and *Arabidopsis* (reviewed by McCabe and Leaver 2000). The lack of DNA laddering has been noted previously within several developmental PCD examples including leaf morphogenesis in the whole lace plant leaves (Gunawardena et al. 2004), and treachery element differentiation in Zinnia (reviewed by Fukuda et al. 1998; Fukuda 2000).

3.5.2 The Mitochondria, an Organelle Commonly Thought to be Involved in Plant PCD

HS challenge has been demonstrated to cause PCD in a variety of plant species, including *Arabidopsis* (Balk et al. 2003; reviewed by McCabe and Leaver, 2000; Scott and Logan, 2008; Yao et al. 2004; Zhang et al. 2009), BY-2 tobacco cells (Vacca et al. 2004, 2006) and cucumber (Balk et al. 1999). Yao et al. (2004), Scott and Logan (2008) and Zhang et al. (2009) reported changes in mitochondria, such as the formation of the MPTP, the release of IMS proteins, and the MPT following the death induction signal, but preceding morphological cell changes. Within the lace plant-induced cell death system, it is evident that PCD is occurring, and given the drastic changes in mitochondrial dynamics, it is also evident that mitochondria are playing a role in the cell death process; however, the order of the death events is just beginning to be elucidated. Cessation of mitochondrial streaming appears to be one of the earliest occurrences in the lace plant-induced cell death system, between approximately 20 min and 1 hr post- HS. This cessation of streaming was also demonstrated during HS-induced cell death by

Zhang et al. (2009) in *A. thaliana* protoplasts, as well as Vacca et al. (2004, 2006) in tobacco BY-2 cells. This impairment of mitochondrial movement following HS challenge is thought to be highly correlated with the induction of PCD (Vacca et al. 2004, 2006) and is suggested to indicate an acute change in cellular redox status within the cell (Zhang et al. 2009). Within this time period, mitochondria also appear to form aggregates, and in some cases form associations with chloroplasts. This aggregate formation has been noted by both Yao et al. (2004) and Scott and Logan (2008) in *Arabidopsis* protoplasts and could be an attempt to reserve energy stores within the dying cell, or to offer the last remaining energy from the organelle to chloroplasts for further death-associated processes.

Following cessation of streaming, between 1 and 2 hr post-HS, mitochondria begin to lose their $\Delta\Psi_m$, as noted by substantial decreases in CMXRos staining. This decrease in $\Delta\Psi_m$ was noted previously in *Arabidopsis* protoplasts by Yao et al. (2004) 2–3 hr post-HS, and by Scott and Logan (2008) 1–4 hr post-HS. Preliminary work completed on whole lace plant leaves, undergoing developmental PCD, depicts similar patterns in mitochondrial dynamics as noted above. Mitochondria initially show vivid mitochondrial staining and streaming, followed by the formation of large aggregates, which move rapidly in the cytoplasm[8]. This rapid movement is followed by the loss of streaming and finally the loss of mitochondrial staining (data not shown). Overall, at the

[8] Following a more detailed investigation it was determined that the mitochondria were originally in the cytosol; they are then brought into the vacuole via some form of autophagy. Both mitochondria and chloroplasts have been identified together in aggregates undergoing Brownian motion within the vacuole; these aggregates become visibly larger as PCD progresses.

2 hr mark within lace plant protoplasts, it is realistic to assume that the mitochondria are no longer viable. This decrease in viable mitochondria presumably follows increases in hydrolytic vesicles (Appendix B), and could occur concurrently with the increase of TUNEL positive nuclei, blebbing of the PM and overall shrinkage of the protoplast (Appendix B)[9]. In general, plant mitochondria have been suggested to play a pivotal role in the integration of environmental and developmental signals that trigger cell death and must be further studied in order elucidate the role of the organelle in other non-model plant species (reviewed by Jones 2000; Balk and Leaver 2001).

3.5.3 Implications of CsA on Induced Cell Death

CsA appeared to have a strong effect on the induction and continuance of environmental cell death in the lace plant. Pre-treatment of lace plant protoplasts with 50 μM CsA for 30 min at room temperature caused a significant decrease in the amount of dead cells at 30, 60, 90, and 120 min post- HS as compared to control- and HS-treated cells. This effect of CsA is relatively rapid compared to results presented by Scott and Logan (2008), in which CsA pre- treatment only significantly decreased *Arabidopsis* cell death at 24 hr post-HS. The variation in CsA effect could be due to lower concentrations and incubation times utilized by Scott and Logan (2008). As expected, CsA pre-treatment also decreased the percentage of TUNEL positive nuclei within cell samples at 2 hr post-HS. The finding that CsA partially inhibits cell death, characterizing the cells as intermediate between control and HS-treated cells, has been noted previously in

[9] This sentence has been amended from the sentence published in Planta and was included in light of new evidence presented in Chapter 6 and amalgamated in Appendix B.

Arabidopsis (Yao et al. 2004), tobacco (Lin et al. 2005, 2006) and sycamore (Contran et al. 2007).

Pre-treatment of protoplasts with CsA prior to HS also had an effect on mitochondrial $\Delta\Psi_m$. CsA partially delayed the decrease in mitochondrial $\Delta\Psi_m$, causing CMXRos staining to be visible for longer following HS. This delayed decrease in $\Delta\Psi_m$ was also noted by Lin et al. (2005, 2006) in tobacco protoplasts, following pre-treatment with CsA. This delayed decrease in $\Delta\Psi_m$ may be directly correlated with the later onset of cell death and DNA fragmentation as noted in the previous paragraph; this supports the role of mitochondria as a key player in the induced cell death process.

Unexpectedly, pre-treatment with CsA did not have an effect on the cessation of mitochondrial streaming as compared to HS samples. Protoplasts pre-treated with CsA still showed cessation of mitochondrial streaming. This result suggests that the cessation of streaming may not be correlated with the MPTP and hence CsA has no effect on this organelle characteristic.

Overall, CsA appears to have an effect on the induction and maintenance of induced PCD within the lace plant. Given the effect of this MPTP inhibitor, it can be suggested that induced cell death within the lace plant is at least partially governed by the association between the VDAC, ANT, and the matrix localized protein CyP-D, all which form the MPTP within the mitochondria (Diamond and McCabe 2007).

3.6 Conclusions

In plants, the exact signal transduction pathway, which causes PCD is not yet fully understood. The results presented here portray HS at 55°C for 20 min in lace plants as a promising inducer of PCD within plant protoplasts, which according to our

observations can be most accurately examined between 20 min and 2 hr post-HS. HS treatment produced cells which contain many characteristic of PCD. PCD was confirmed through the use of fluorescent TUNEL, in which 3`-OH nick ends were visualized in HS-treated protoplasts beginning 2 hr post-HS[10]. TUNEL positive nuclei were not present in control samples. Results presented here demonstrate, to the best of our knowledge, the first example of chloroplasts being brought into the vacuole of protoplasts undergoing environmentally induced PCD. The results also indicate that the mitochondria, particularly the MPTP, may play a role in the induced cell death process. Thus, HS treatment proves to be a reliable technique to enable the comparison of environmentally induced and developmentally regulated PCD within one species of plant.

3.7 Acknowledgments

The authors thank Dr. M. E. Kane (University of Florida, USA) for providing the original sterile lace plant cultures, Jaime Wertman (Dalhousie University, Canada) for critical review of this article, Bruno J. Roy (Dalhousie University, Canada) for assistance in formatting supplementary videos, Dr. Nancy Dengler (University of Toronto, Canada) and Dr. Wouter G. van Doorn (Wageningen University, The Netherlands) for help throughout the manuscript, and Dr. Jennifer Sheen (Mass General Hospital, Molecular Biology, Boston, MA, USA) for help regarding protoplast isolation. The authors also greatly acknowledge the Canadian Foundation for Innovation (CFI) for the Leaders Opportunity Fund, the Natural Sciences and Engineering Research Council (NSERC) for

[10] This timing originally read "1 hr" within the manuscript published in Planta, it has been amended here for accuracy.

discovery and equipment grants for A.G., and Dalhousie University for partial doctoral funding for C.L.

3.8 Online Resources

Online Resource 3.1 Increased Brownian Motion

Small unknown objects in the vacuole of a protoplast HS at 55°C for 20 min. Scale bar = 15μm.

Online Resource 3.2 Protoplasts HS at 55°C for 20 min and Allowed to Rest for 1 hr at Room Temperature

Note chloroplasts actively entering the vacuole of a cell, followed by slight Brownian motion within the vacuole. Chloroplasts are presumably brought into the vacuole to be degraded. Chloroplast material floating freely in cell culture is cellular debris left from enzymatic isolation. Scale bar = 10μm.

Online Resource 3.3 Control Protoplast Depicting CMXRos Stained Mitochondria (red) and Chlorophyll Autofluorescence (Green)

Note actively streaming mitochondria in control protoplast. Also note the abundance of chloroplasts within the cell. Scale bar = 10μm.

Online Resource 3.4 Protoplast HS at 55°C for 20 min Followed by a 30 min Rest Period at Room Temperature

CMXRos stained mitochondria (red) and chlorophyll autofluorescence (green). Note there is no actively streaming mitochondria within the HS challenged cell, when

compared to the control sample (Online Resource 3.3). Also note the decrease in chloroplast abundance within the cell. Scale bar = 10μm.

Table 3.1 Characteristics of Mitochondria in Control, HS and HS + CsA-Treated Protoplasts

	0-1hour		1-2 hour	
	Streaming	Staining	Streaming	Staining
Control	+	+	+	+
Heat shock	-	+	-	-
CsA + heat shock	-	+	-	+

Figure 3.1 The Lace Plant (*Aponogeton madagascariensis*)[11]

Window stage lace plant leaf, displaying transparent windows where PCD is occurring (a). Perforation expansion lace plant leaf portraying the expansion of the perforated areole (b). Mature lace plant leaf showing completed perforations between longitudinal and transverse veins (c). Sterile lace plant in magenta box (d). Scale bars 400 μm (a–c), 1 cm (d). Erratum to image published (Lord and Gunawardena 2012b).

[11] Due to an error in image selection an erratum to this image has been published.

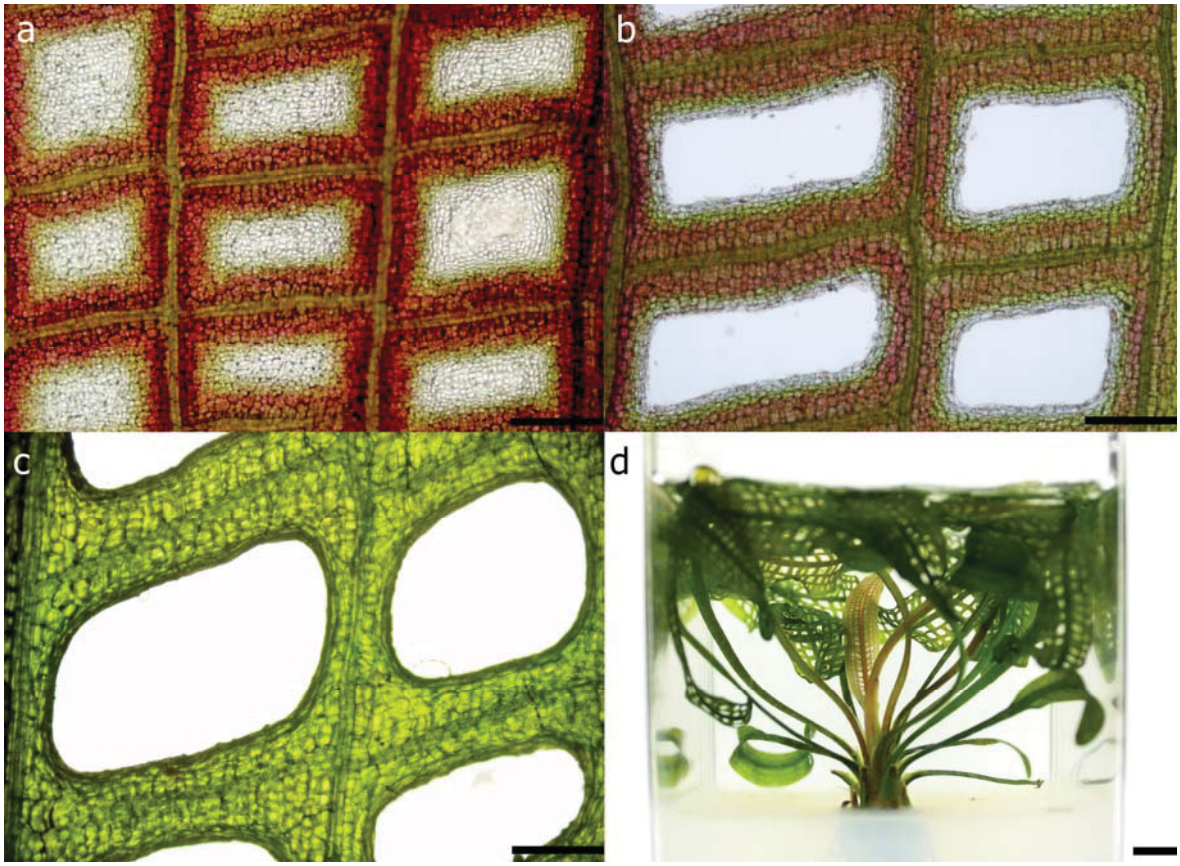

Figure 3.1 The Lace Plant (*Aponogeton madagascariensis*)

Figure 3.2 Micrograph of Lace Plant Protoplasts

Viable control protoplasts isolated from perforation expansion leaves. DIC image (a) and corresponding fluorescent image showing fluorescein diacetate (FDA) staining of living cells 1 hr post-isolation (b). Cells exposed to HS challenge at 55°C for 20 min and allowed to rest for 1 hr. DIC image (c) and corresponding fluorescent image showing FDA staining of living cells (d). Scale bars 50 μm.

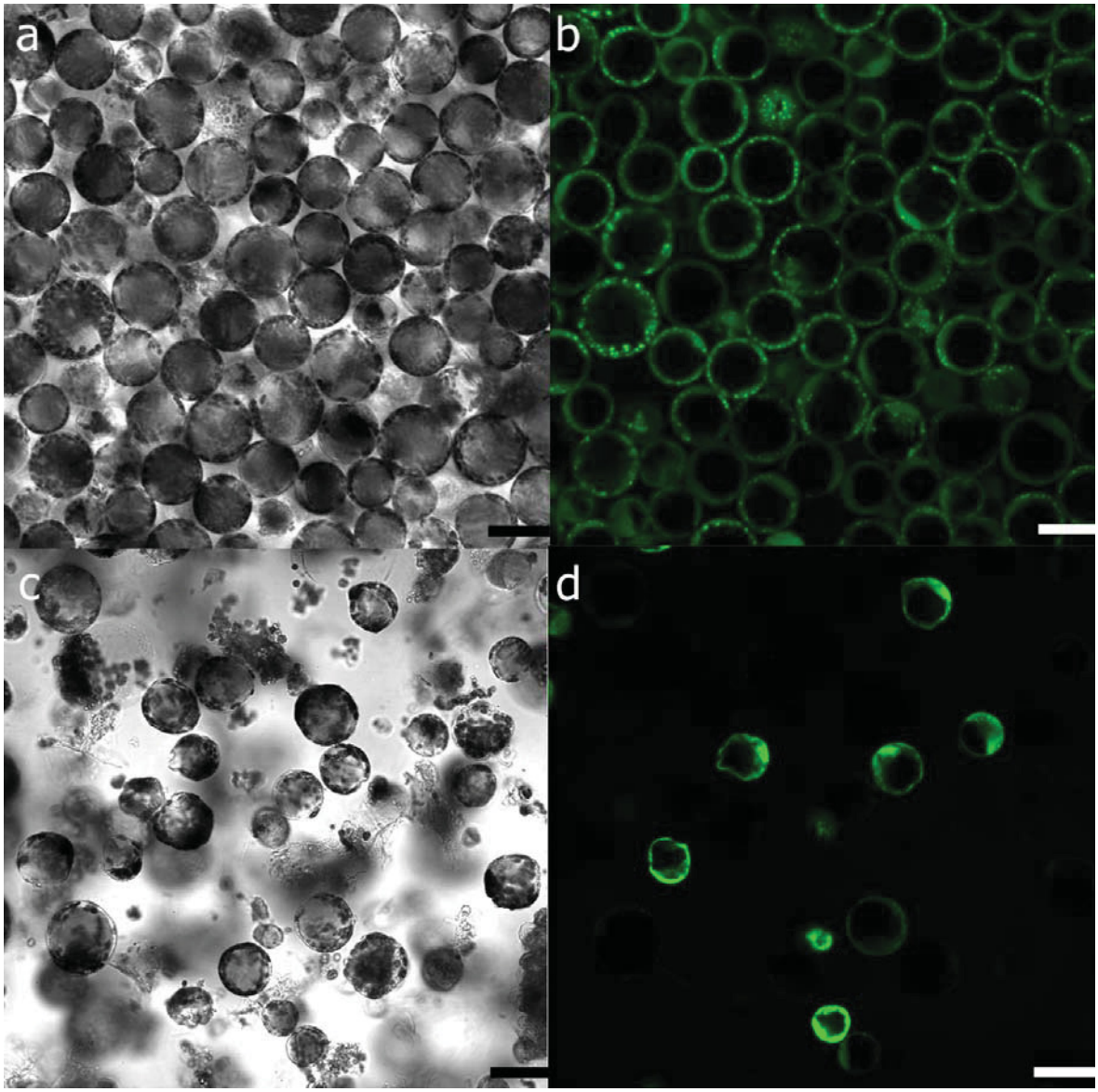

Figure 3.2 Micrograph of Lace Plant Protoplasts

Figure 3.3 Micrographs of Individual Lace Plant Protoplasts 1 Hr Post-Isolation for Controls, and 1 Hr Post-HS for PCD and Necrotic Cells

Control protoplasts without signs of PCD, intact plasma membrane (PM; black arrow, a), and healthy chloroplasts (white arrow, a), intact tonoplast membrane (black arrow, b). Protoplasts HS at 55°C for 20 min with common characteristics of PCD. Plasma membrane blebbing (black arrow, c), increased production of hydrolytic vesicles (black arrow, d), severe nuclear condensation (white arrow, d). Chloroplasts (white arrow, e) inside the vacuole, note intact tonoplast membrane (black arrow, e). Increased production of transvacuolar strands (black arrow, f). Protoplasts after HS treatment at 75°C for 20 min with common characteristics of necrosis. Swollen protoplast (black arrow, g), inevitably leading to complete cell lysis (black arrow, h). Scale bars 10 μm (c–f), 20 μm (a, b, g, h).

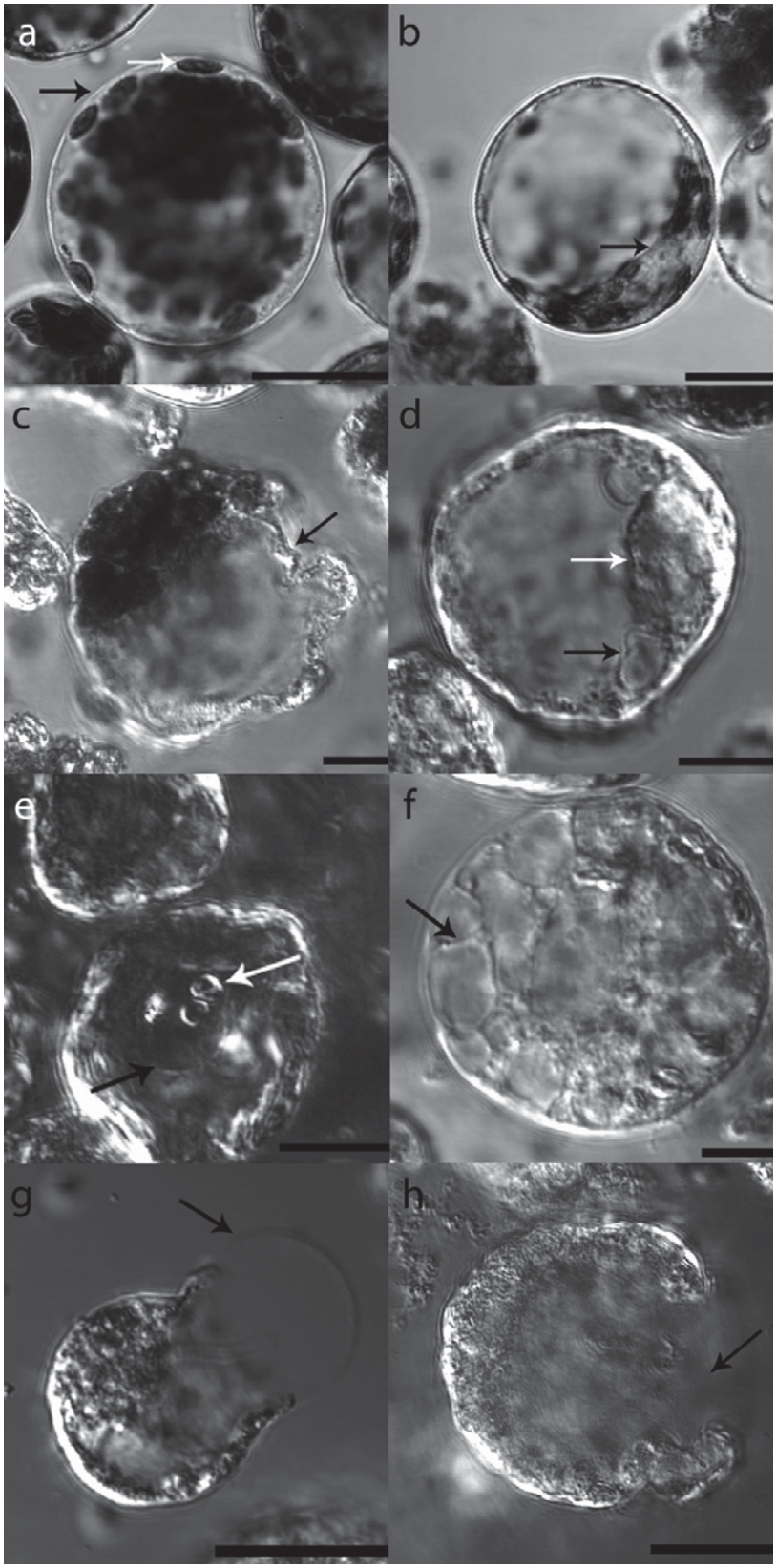

Figure 3.3 Micrographs of Individual Lace Plant Protoplasts 1 Hr Post-Isolation for Controls, and 1 Hr Post-HS for PCD and Necrotic Cells

Figure 3.4 Transmission Electron Micrographs of Lace Plant Protoplasts

Control (a–d), and HS (e–h) lace plant protoplasts. Healthy protoplast displaying intact plasma membrane (PM; red arrow) and tonoplast (black arrow, a). Healthy nucleus showing no signs of condensation or chromatin flocculation (b). Healthy chloroplast depicting intact inner and outer membrane, thylakoids, intact stroma (red arrow) and starch granules (black arrow, c). Healthy dividing mitochondria (black arrow) showing intact outer and inner membranes, and clearly non-degraded cristae; no mitochondrial swelling present (d). HS-treated protoplasts depicting PM blebbing (black arrow) and permeabilized tonoplast (red arrow, e). Magnified nucleus displaying condensation and chromatin flocculation (black arrow, f). Chloroplasts with intact inner and outer membranes, but degraded inner thylakoid membranes (black arrow) and decreases in starch granules (g). Slightly swollen and degraded mitochondria depicting degraded cristae and association with chloroplasts (h). Scale bars 2 μm (a, e, f), 1 μm (b, c, g), 0.5 μm (h), 200 nm (d).

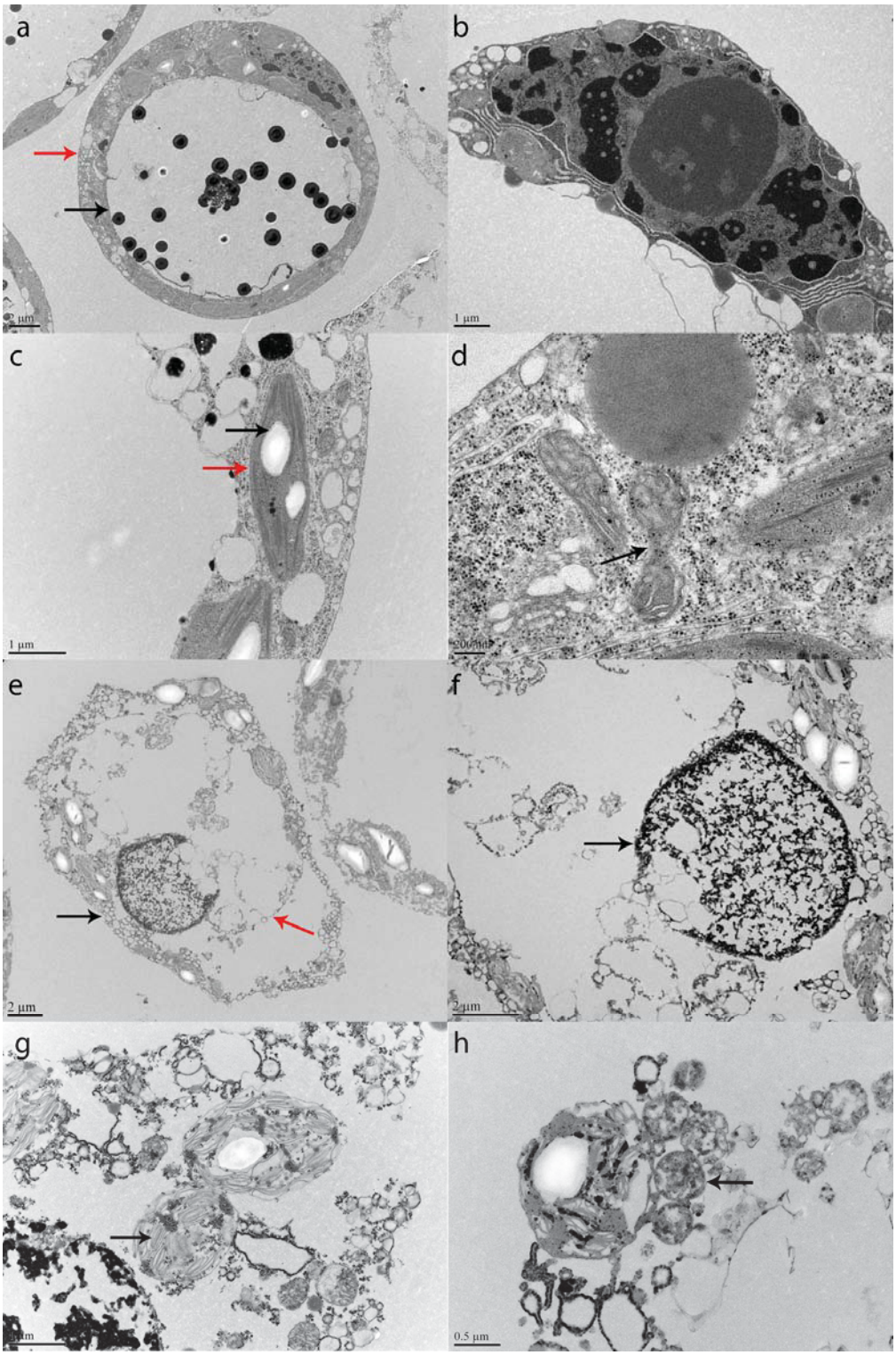

Figure 3.4 Transmission Electron Micrographs of Lace Plant Protoplasts

Figure 3.5 Percentage of Dead Protoplasts Following HS at 55°C for 20 min, Compared to Control and CsA + HS-Treated Protoplasts Over a 2 Hr Period as Determined by PI Staining

Control, CsA + HS and HS- treated protoplasts illustrating PI-stained nuclei at time 0 and 2 hr with corresponding DIC images. Control protoplasts show less cell death symptoms then HS-treated protoplasts, while CsA + HS-treated protoplasts show an intermediate amount of cell death (a). Cell death was tracked via PI staining at 30 min intervals for 2 hr, followed by counting of PI- stained nuclei. Control protoplasts show a significantly lower amount of cell death then HS-treated protoplasts at all-time intervals, while CsA + HS-treated protoplasts depict a statistically significant lower amount of cell death at 30, 60, 90, and 120 min compared to the HS treatment. Overall, CsA treatment decreased the amount of cell death seen in HS-treated protoplasts. Data represent mean ± standard error of four replicates (b). All scale bars 70 μm.

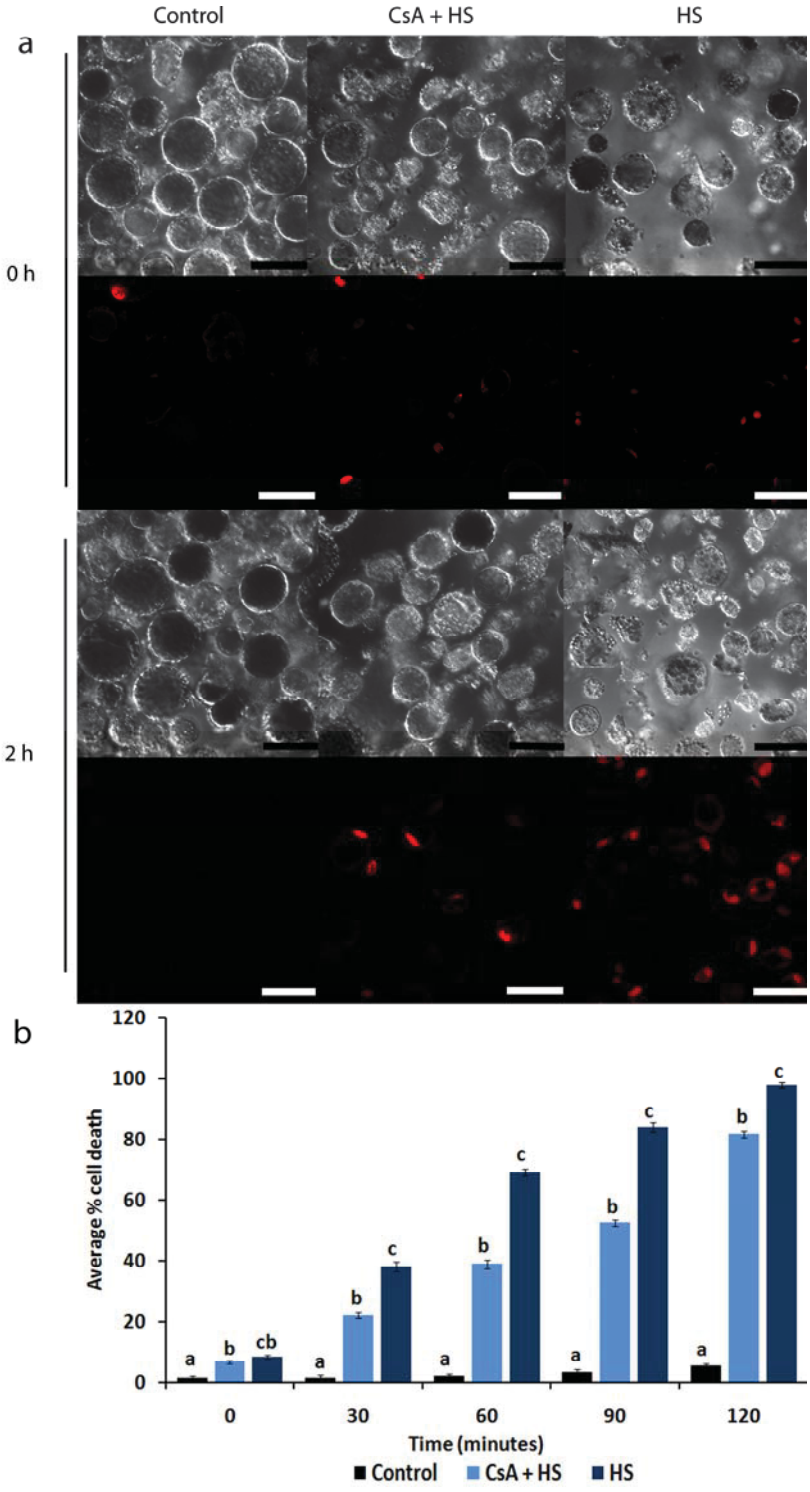

Figure 3.5 Percentage of Dead Protoplasts Following HS at 55°C for 20 min, Compared to Control and CsA + HS-Treated Protoplasts Over a 2 Hr Period as Determined by PI Staining

Figure 3.6 Quantification of Changes in CMXRos-Stained Mitochondrial Fluorescence Intensity

Image of un-treated control (a) and HS-treated (b) protoplasts taken from video clip. The value of CMXRos fluorescence inside each of the three selected areas in each photograph was plotted over 400 s. Fluorescence intensities were recorded with EZ-C1 3.80 imaging software and normalized with excel software. Scale bars 25 μm.

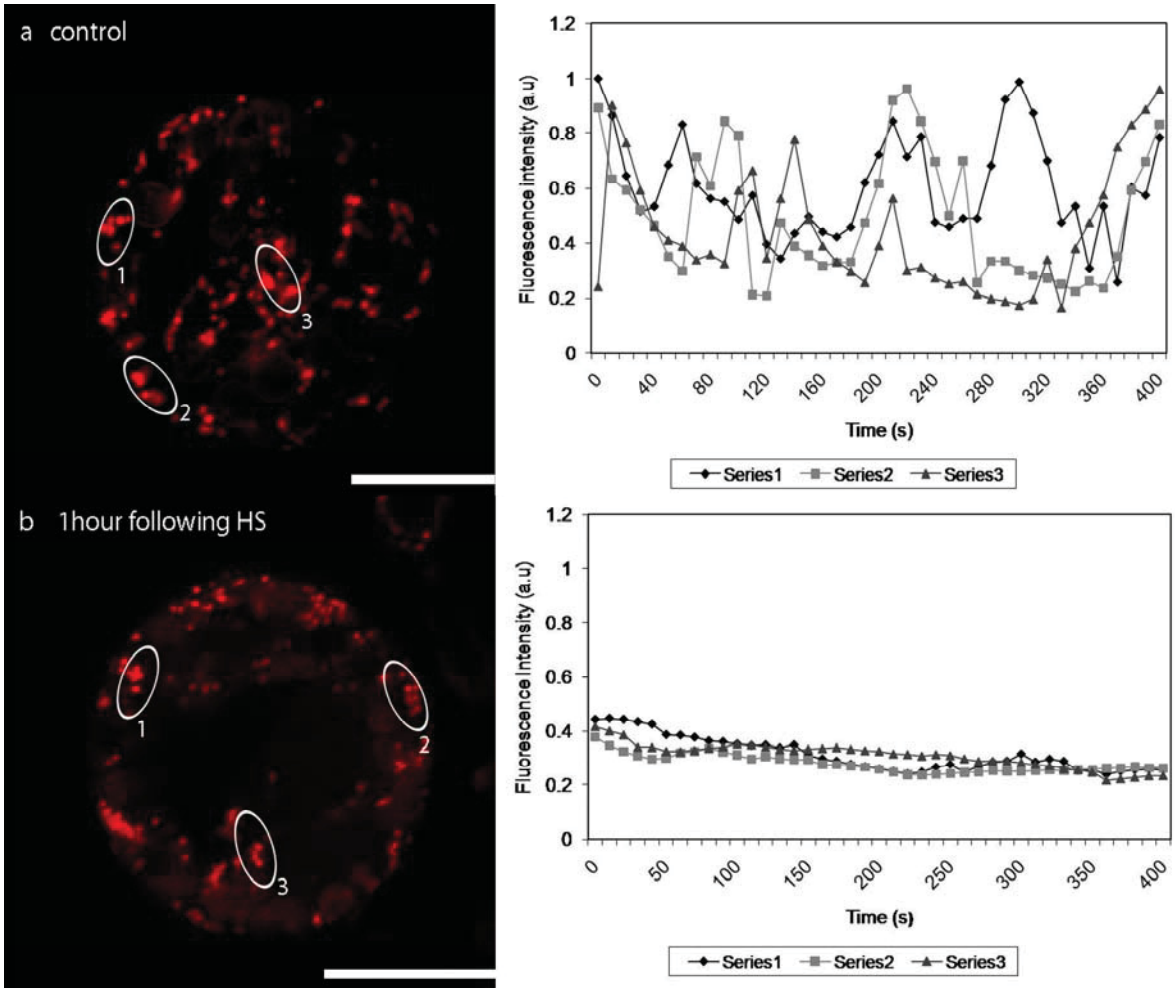

Figure 3.6 Quantification of Changes in CMXRos-Stained Mitochondrial Fluorescence Intensity

Figure 3.7 Visualization of Representative Protoplasts Mitochondrial Membrane Depolarization During Control, CsA + HS, and HS Treatment

Control protoplasts at time 0, 60, and 120 min show intense CMXRos mitochondrial staining. CsA + HS-treated protoplasts at the same time intervals show slightly decreased CMXRos staining, indicating a slight loss of mitochondrial $\Delta\Psi_m$. HS-treated protoplasts illustrate mitochondrial staining at time 0, but rapid decreases in CMXRos staining following 60 and 120 min. This loss of CMXRos staining in HS-treated cells depicts a rapid decrease in mitochondrial $\Delta\Psi_m$ as compared to both control and CsA + HS-treated cells. Note the most rapid loss of mitochondrial $\Delta\Psi_m$ can be seen between 60 and 120 min in HS challenged cells. Scale bars 25 μm.

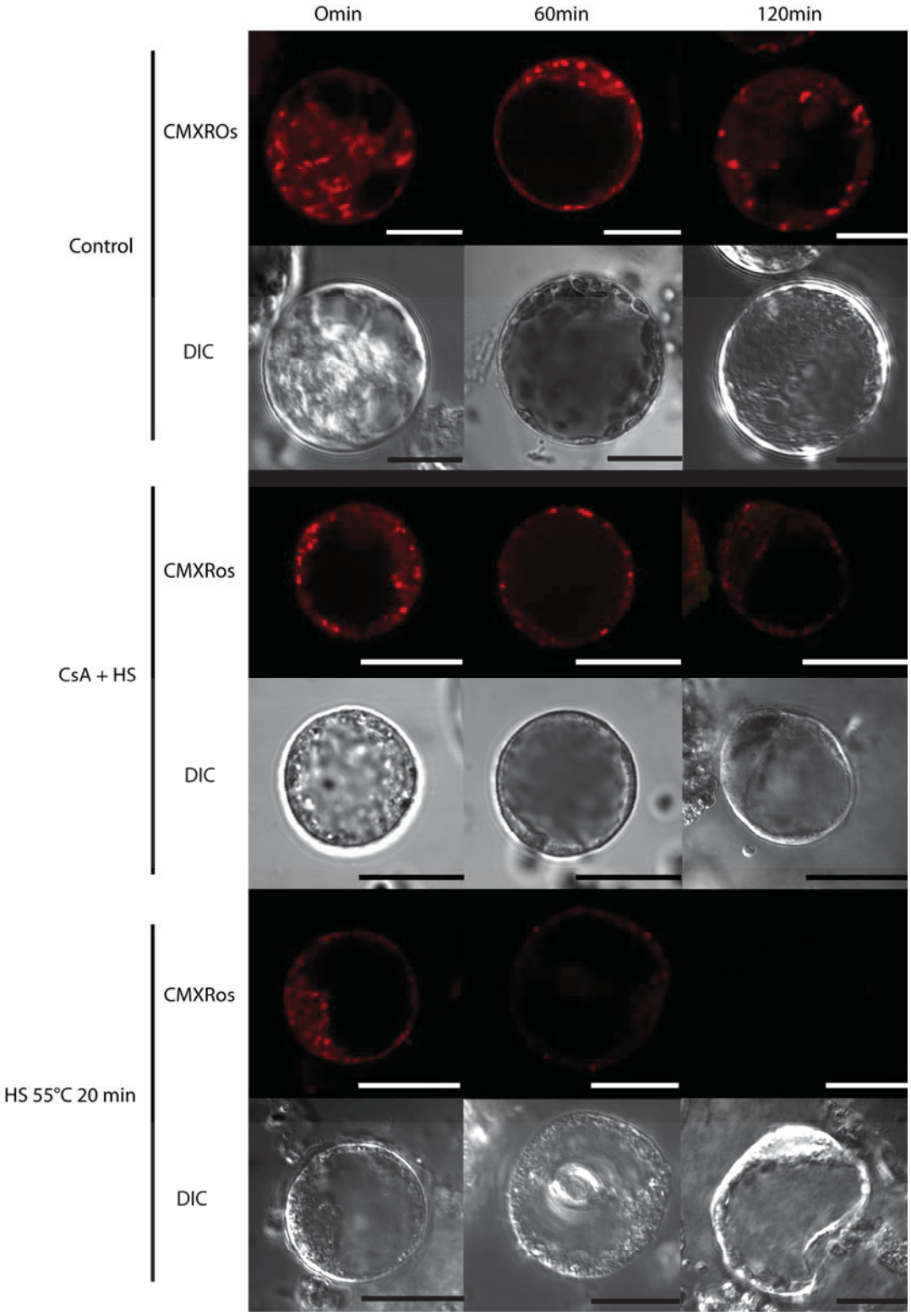

Figure 3.8 Visualization of Representative Protoplasts Mitochondrial Membrane Depolarization During Control, CsA + HS, and HS Treatment

Figure 3.9 LM-TUNEL Positive Protoplasts. DIC, Fluorescent and Overlay Images

Control protoplasts were isolated, allowed to rest for 2 hr, fixed, and labeled with fluorescent TUNEL. No TUNEL positive nuclei are present in control protoplasts (a-c). CsA + HS-treated protoplasts were pre-treated with CsA, followed by heating at 55°C for 20 min, allowed to rest for 2 hr, fixed, and labelled with fluorescent TUNEL. Approximately 20% of CsA + HS-treated cells depicted TUNEL positive nuclei (d–f). HS-treated protoplasts were heated at 55°C for 20 min and allowed to rest for 2 hr, fixed, and labelled with fluorescent TUNEL. Approximately 55% of protoplasts depicted TUNEL positive nuclei (g‑l). These results suggest that DNA fragmentation does not occur in control cells, occurs at an intermediate level in CsA + HS cells, and occurs in slightly more than half HS-treated cells. Scale bars 25 μm (a–c, g–l), 50 μm (d–f).

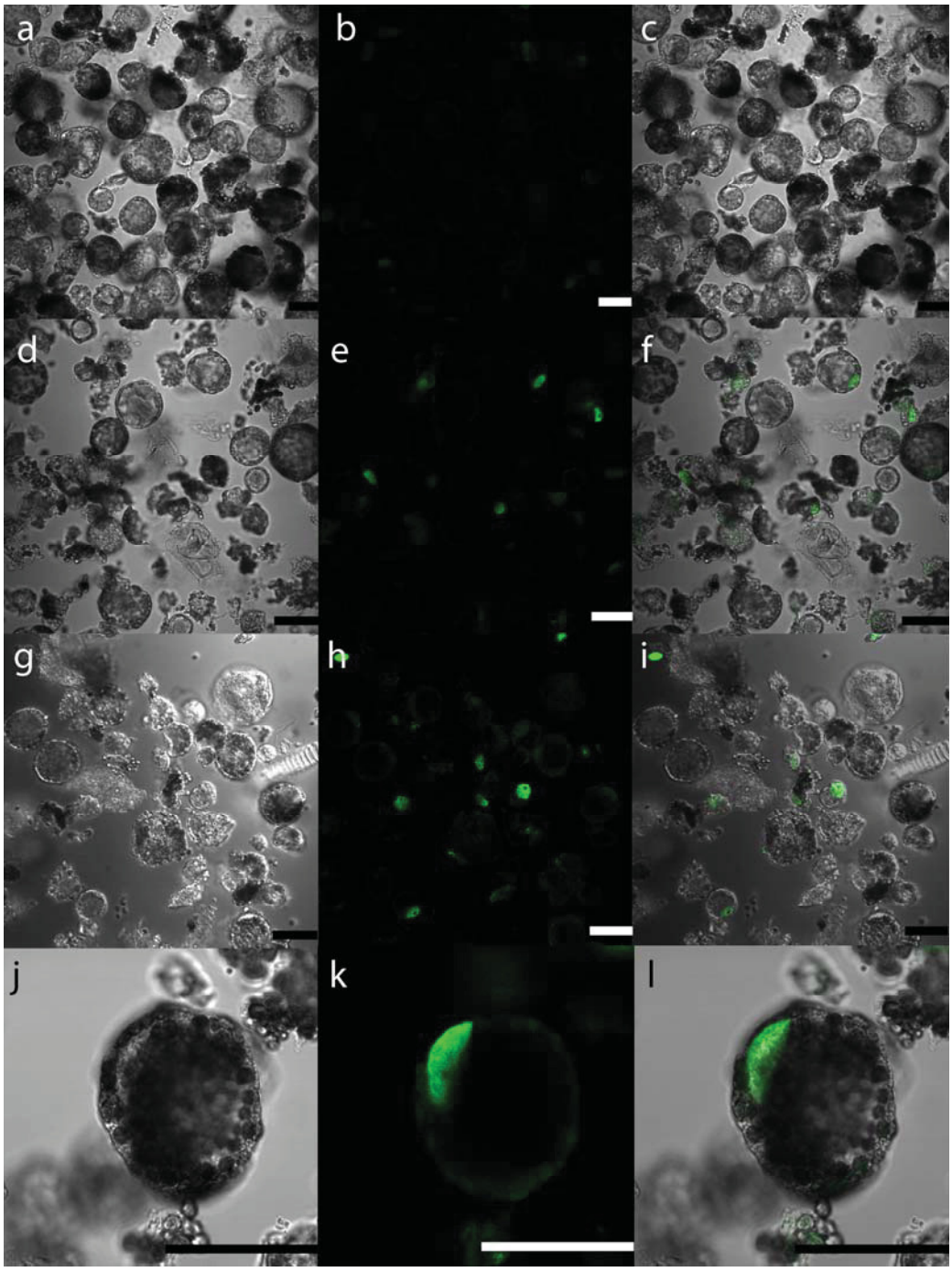

Figure 3.8 LM-TUNEL Positive Protoplasts. DIC, Fluorescent and Overlay Images

Chapter 4 Do Mitochondria Play a Role in Remodelling Lace Plant Leaves During Programmed Cell Death?

Published as:

Lord CEN, Wertman JN, Lane S and Gunawardena AHLAN. Do Mitochondria Play a Role in Remodelling Lace Plant Leaves During Programmed Cell Death? BMC Plant Biology 11: (2011) 102

4.1 Abstract

Background: Programmed cell death (PCD) is the regulated death of cells within an organism. The lace plant (*Aponogeton madagascariensis*) produces perforations in its leaves through PCD. The leaves of the plant consist of a latticework of longitudinal and transverse veins enclosing areoles. PCD occurs in the cells at the center of these areoles and progresses outwards, stopping approximately five cells from the vasculature. The role of mitochondria during PCD has been recognized in animals; however, it has been less studied during PCD in plants.

Results: The following paper elucidates the role of mitochondrial dynamics during developmentally regulated PCD *in vivo* in *A. madagascariensis*. A single areole within a window stage leaf (PCD is occurring) was divided into three areas based on the progression of PCD; cells that will not undergo PCD (NPCD), cells in early stages of PCD (EPCD), and cells in late stages of PCD (LPCD). Window stage leaves were stained with the mitochondrial dye Mito Tracker Red CMXRos and examined. Mitochondrial dynamics were delineated into four categories (M1-M4) based on characteristics including distribution, motility, and membrane potential ($\Delta\Psi_m$). A TUNEL assay showed fragmented nuclear DNA in a gradient over these mitochondrial stages. Chloroplasts and transvacuolar strands (TVS) were also examined using live cell imaging. The possible importance of mitochondrial permeability transition pore (MPTP) formation during PCD was indirectly examined via *in vivo* cyclosporine A (CsA) treatment. This treatment resulted in lace plant leaves with a significantly lower number of perforations compared to controls, and that displayed mitochondrial dynamics similar to that of non-PCD cells.

Conclusions: Results depicted mitochondrial dynamics *in vivo* as PCD progresses within the lace plant, and highlight the correlation of this organelle with other organelles during developmental PCD. To the best of our knowledge, this is the first report of mitochondria and chloroplasts moving on TVS to form a ring structure surrounding the nucleus during developmental PCD. Also, for the first time, we have shown the feasibility for the use of CsA in a whole plant system. Overall, our findings implicate the mitochondria as playing a critical and early role in developmentally regulated PCD in the lace plant.

4.2 Introduction

4.2.1 Programmed Cell Death in Plants

Programmed cell death (PCD) is the regulated death of a cell within an organism (reviewed by Sanmartin et al. 2005). In plant systems, developmentally regulated PCD is thought to be triggered by internal signals and is considered to be a part of typical development. Examples of developmentally regulated PCD include, but are not limited to, deletion of the embryonic suspensor (Giuliani et al. 2002), xylem differentiation (Fukuda, 2000; Gunawardena et al. 2004), and leaf morphogenesis (Elliott and Gunawardena, 2010; Gunawardena, 2008; Gunawardena et al. 2004, 2005, 2006, 2007; Lord and Gunawardena, 2010; Wright et al. 2009) as is seen in the lace plant (*A. madagascariensis*) and *Monstera obliqua*. Mitochondria are known to function during PCD in animal systems and the role of the organelle has been largely elucidated within this system; conversely, less is known regarding the mitochondria and PCD in plants (reviewed by Jones 2000; reviewed by Vianello et al. 2007).

4.2.2 The Role of the Mitochondria During Developmental Programmed Cell Death (PCD)

Within animal systems, mitochondria appear to undergo one of two physiological changes leading to the release of intermembrane space (IMS) proteins, allowing for the membrane permeability transition (MPT), inevitably aiding in PCD signalling. One hypothesized strategy involves the permeability transition pore (MPTP), a multi-protein complex consisting of the voltage dependent ion channel (VDAC), the ANT, and cyclophilin D (CyP-D[12]; Diamond and McCabe, 2007). The formation of the MPTP can be initiated by a number of factors including, but not limited to: cell injury (Balk et al. 1999; Yao et al. 2004; Zhang et al. 2009), oxidative stress (Diamond and McCabe, 2007; Zhang et al. 2009), the accumulation of calcium (Ca^{2+}) in the cytosol or mitochondrial matrix (reviewed by Crompton 1999; reviewed by Jones 2000), increases in ATP, ROS, and phosphate, as well changes in pH (Arpagaus et al. 2002; reviewed by Jacobson, 1996). In addition, evidence suggests that cyclosporine A (CsA) can act in disrupting the MPTP by displacing the binding of CyP-D to ANT (reviewed by Crompton 1999) within animal systems. The theory that CsA can inhibit MPTP formation has led to key advances in understanding the second pathway through which mitochondria can release IMS proteins.

The second strategy is proposed to involve the Bcl-2 family of proteins and utilizes only the VDAC. The Bcl- 2 family can be divided into two distinct groups based

---

[12] CyD has been replaced with CyP-D in the remainder of this manuscript in order to be consistent throughout this dissertation.

on functionality: the anti-apoptotic proteins including Bcl-2 and Bcl-xL, and the pro-apoptotic proteins including Bax, Bak, Bad and Bid (Balk and Leaver, 2001; Balk et al. 1999). If the amount of pro-apoptotic Bcl-2 family proteins increase or the amount of anti-apoptotic Bcl-2 family proteins decreases, the VDAC will then work independently to release IMS proteins to aid in PCD signalling.

4.2.3 The Lace Plant and Programmed Cell Death

The aquatic freshwater lace plant (*A. madagascariensis*) is an excellent model system for the study of developmental PCD in plants. It is one of forty species in the monogeneric family Aponogetonaceae, and is the only species in the family that forms perforations in its leaves via the PCD process (Elliott and Gunawardena, 2010; reviewed by Gunawardena, 2008; Gunawardena et al. 2004, 2007, 2006; Lord and Gunawardena, 2010; Wright et al. 2009). The leaves of the plant are very thin and transparent, facilitating long-term live cell imaging of the cell death process. A well-developed method for sterile culture of the plant also provides plant material with no microbial contamination (Figure 4.1A; Elliott and Gunawardena, 2010; reviewed by Gunawardena, 2008; Gunawardena et al. 2004, 2007, 2006; Lord and Gunawardena, 2010; Wright et al. 2009).

Perforation formation within the plant is also predictable, with perforations consistently forming in areoles of photosynthetic tissue, between longitudinal and transverse veins over the entire leaf surface (Figure 4.1B). On a whole plant level, leaf development can be divided into five stages (stage 1-5; Gunawardena et al. 2004). Initially, stage 1 (pre-perforation) involves longitudinally rolled, often pink leaves where

no perforations are present. This pink coloration is due to the pigment anthocyanin, which is found in the vacuole of the mesophyll cells (Figure 4.1B). Stage 2 ("window") is characterized by distinct transparent regions in the centre of the vascular tissue, due to the loss of pigments such as chlorophyll and anthocyanin (Figure 4.1C). Stage 3 (perforation formation) involves the degradation of the cytoplasm and the cell wall of the cell, resulting in the loss of transparent cells in the centre of the window (Figure 4.1D). Stage 4 (perforation expansion) is characterized by the expansion of the perforation within the areole (Figure 4.1E). Lastly, stage 5 (complete perforation) results in a completed perforation (Figure 4.1F; Gunawardena et al. 2004); these tiny perforations will continue to increase in size as the leaf blade grows.

4.2.4 Organelles Involved in Developmental Programmed Cell Death (PCD) Within Lace Plant Leaves

The mechanisms of developmentally regulated PCD at a cellular level within the lace plant have begun to be elucidated. Common characteristics of PCD have been previously described during leaf morphogenesis in the lace plant and include: the loss of anthocyanin and chlorophyll, chloroplast degradation, cessation of cytoplasmic streaming, increased vesicle formation and plasma membrane (PM) blebbing (reviewed by Gunawardena, 2008; Gunawardena et al. 2004, 2007, 2006; Wright et al. 2009). Preliminary results indicate indirect evidence for the up-regulation of ETR1 receptors, as well as for the involvement of Caspase 1-like activity during the PCD process in the lace plant (unpublished). To date, little research has been conducted on TVS and no research has been conducted specifically on the mitochondria within this developmentally

regulated cell death system (reviewed by Gunawardena, 2008; Gunawardena et al. 2004, 2007, 2006; Wright et al. 2009).

4.2.5 Objective

The following paper will aim to elucidate the role of mitochondrial dynamics with relation to other organelles, during developmentally regulated PCD in the novel model species *A. madagascariensis*, using live cell imaging techniques.

4.3 Materials and Methods

4.3.1 Plant Materials

All plant materials were grown and subcultured as described in section 2.3.1 within Chapter 2. All chemicals were purchased from Sigma-Aldrich (St Louis, MO, USA), unless otherwise stated. All experiments were completed at least three times unless otherwise stated.

4.3.2 Light Microscopy

All light microscopy observations were performed as described in section 2.3.4 within Chapter 2. This microscope was also used to acquire several of the Online Resource live cell imaging videos, all of which are in real time unless otherwise stated.

4.3.3 Confocal Laser Scanning Microscopy

Confocal observations were performed using a Nikon Eclipse T*i* confocal microscope (Nikon, Canada, Mississauga, Ontario, Canada) fitted with a digital camera

(Nikon DS-Fi1) and using EZ-C1 3.80 imaging software and T*i*-Control. Confocal microscope observations were performed using DIC optics with complimentary fluorescent images taken via a fluorescein isothiocyanate (FITC; excitation 460-500 nm emission 510-560 nm) or Tetramethyl Rhodamine Isothiocyanate (TRITC; excitation 527-552 nm emission 577-632 nm) laser. Following MitoTracker Red (CMXRos) staining, 30 sec time-lapse videos were acquired of mitochondrial streaming. False color images were prepared by selecting still images from time 0 and time 30 sec of these videos. Time 0 sec images were left their normal red colour while 30 sec images were false coloured green and overlaid onto time 0 images to demonstrate mitochondrial motility. This microscope was also used to acquire several of the Online Resource live cell imaging videos, all of which are in real time unless otherwise stated. All composite plates were assembled using Adobe Photoshop Elements version 6.0.

4.3.4 Transmission Electron Microscopy

Tissue pieces approximately 2 mm^2 were excised from window stage leaves and fixed in 2% glutaraldehyde in 0.05 M sodium cacodylate buffer, pH 6.9, for 24 hr in a vacuum (20 psi). Following overnight incubation, samples were rinsed in buffer and post fixed in 2.5% aqueous osmium tetroxide for 4 hr at room temperature. Tissues were then dehydrated in a graded ethanol series, and placed through ethanol:Spurr resin mixtures. Tissues were finally embedded in pure Spurr resin and polymerized at 70°C for 9 hr. Gold sections were prepared on a Reichert-Jung ultra-microtome, collected onto formvar coated grids and stained with lead citrate and uranyl acetate. Observations were made using a Philips 201 transmission electron microscope (TEM; Eindhoven, The

Netherlands) or a Philips Tecnai 12 TEM (Philips Electron Optics, Eindhoven, Netherlands) operated at 80 kV and fitted with a Kodak (Rochester, New York, USA) Megaview II camera with software (AnalySIS, Soft Imaging System, Münster, Germany).

4.3.5 Terminal Deoxynucleotidyl Transferase-Mediated dUTP Nick-End Labeling (TUNEL)

Tissue pieces approximately 5 mm^2 were excised from window stage leaves and fixed in FAA for 2 hr, followed subsequently by 3 washes in phosphate buffered saline (PBS). The terminal deoxynucleotidyl transferase- mediated dUTP nick end labeling (TUNEL) assay was performed according to the manufacturer's instructions (Roche Diagnostics, Mannheim, Germany). Nuclei were counterstained by incubation in 3% (w/v) propidium iodide for 2 min. Samples were observed via confocal microscopy. A negative control was performed without the terminal deoxynucleotidyl transferase enzyme, and a positive control was performed with DNase1 (Data not shown).

4.3.6 Mitochondrial Staining

Tissue pieces approximately 5 mm^2 were excised from window stage leaves and stained for 1 hr in 0.2 μM, 0.3 μM, 0.5 μM, 0.6 μM, 1 μM, and 2 μM CMXRos (Invitrogen, Eugene, OR, USA; dissolved in dimethylsulfoxide, DMSO). Leaf sections were then rinsed with ddH_2O 8 times and shaken for 90 min in ddH_2O at approximately 100 rpm. Leaf sections were then mounted on slides and excited with the TRITC cube (excitation 527-552 nm and emission 577-632 nm) to view mitochondrial fluorescence

and the FITC cube (excitation 460-500 nm emission 510-560 nm) to view the corresponding chlorophyll auto fluorescence using the confocal microscope. The optimal dye loading concentration and incubation time period was determined to be 0.6 μM CMXRos for 1 hr at room temperature in the dark. Following an intensive rinsing procedure, leaf pieces stained via this method displayed intense mitochondrial staining with little background staining, although it can be noted that a small amount of CMXRos dye is sequestered to the cell wall despite the presence or absence of mitochondria.

Four stages of mitochondrial dynamics (M1-M4) were consistent within a window stage leaf when viewing the surface of epidermal cells where mitochondria are pushed up against the PM. However, when looking deeper into an epidermal cell, where mitochondria are found within the thin ring of cytoplasm between the PM and tonoplast membrane, due to the differing focal plane and orientation, mitochondrial dynamics can vary in appearance. It was important therefore, that for quantitative measurements, that the videos and images were taken from the very top portion of epidermal cells. Mitochondrial staining was completed at least 15 times.

4.3.7 Cyclosporine A

Healthy plants between three to four weeks of age, containing at least two perforated leaves, were selected for use in CsA trials. Plants were divided at random into experimental or control groups and under sterile conditions, liquid medium was poured out of each magenta box and replaced with 200 mL of fresh liquid medium. For the treatment groups, CsA stock dissolved in 90% ethanol was added to the liquid medium to make a final concentration of 2 μM, 4 μM, 10 μM, 15 μM, or 20 μM CsA in the boxes.

For control plants, an equivalent volume of ethanol was added to the liquid medium. The plants were then returned to the growth racks under normal light conditions until they were at the proper stage for harvesting. Digital photographs acquired with a Nikon Coolpix P5000 camera (Nikon Canada Inc., Mississauga, ON, Canada) were taken of each plant for each concentration at least twice a week in order to track growth of newly emerging leaves. For the examination of mitochondria in leaves that had been treated with CsA, CMXRos staining was carried out as described above.

4.3.8 Harvesting Plants

Plants were considered ready to harvest following approximately three to four weeks from the initiation of the inhibitor experiment. Using the successive images, which were taken each week, and labeled by means of Adobe Photoshop Elements 6, version 6.0, each leaf was identified and removed from the respective magenta box. The petiole of each leaf was cut to 1 cm in length and the number of perforations per leaf was counted as an indicator of PCD. Leaf length was also measured as an indicator of normal leaf development. Number of perforations in an individual leaf was then divided by individual leaf length to obtain the variable 'ratio of number of perforations per cm of leaf length'. This variable is a more inclusive measure of PCD than solely number of perforations due to it accounting for the assumption that number of perforations depends in part on leaf length i.e. the longer the leaf the more perforations that can possibly form. Each leaf was then individually blotted dry, flattened by hand, and aligned in chronological order of emergence for photography purposes.

4.3.9 Statistical Analysis

All data were assessed as described in section 2.3.6 within Chapter 2.

4.4 Results

Within a stage 2, or window stage leaf (Figure 4.2A), developmental PCD is least advanced at the leaf blade edge and most advanced closest to the midrib (Figure 4.2B; Wright et al. 2009). In order to further elucidate organelle changes during PCD, an individual areole within a window stage leaf has been subdivided into three different areas based on the progression of cell death. Non-PCD cells (NPCD; previously regarded as 1b by Wright et al. 2009) line the inside border of a window and consist of cells which will never undergo developmental cell death; these cells are normally markedly pink in color due to the pigment anthocyanin. This area is denoted in Figure 4.2C, and consists of all cells between the white and red lines. The cells adjacent to the NPCD cells will die via PCD, but are in the earliest stages of the cell death process (EPCD; previously regarded as 2b by Wright et al. 2009). They generally contain no anthocyanin and are green in color due to aggregations of chloroplasts within the cells, sometimes surrounding the nucleus. These cells are denoted in Figure 4.2C, and consist of all cells between the red and green lines. The next delineation of cells are those found in the center of the window that are at the latest stage of cell death (LPCD; previously regarded as 3b by Wright et al. 2009). These cells are represented in Figure 4.2C, and consist of cells within the green lines. The presence of these differing stages of PCD within one areole provides a convenient gradient of cell death through which whole leaf observations are facilitated.

4.4.1 Mitochondrial Distribution and Motility

CMXRos staining allowed the distribution of mitochondria to be easily identified within the cells, and also permitted for the analysis of changes in mitochondria motility. Analysis of mitochondrial motility was completed by selecting still images from time-lapse videos of single epidermal cells at time 0 sec and 30 sec. Mitochondria at time 0 sec remain red, while mitochondria at time 30 sec were false coloured green. These images were then overlaid to provide information on mitochondrial movement.

Within a single areole of a stage 2 (window stage) leaf, mitochondrial dynamics were delineated into four categories (M1-M4) based on the gradient of PCD. It is important to note that although these stages are seen simultaneously in a window stage leaf areole, if one was to examine a pre-perforation (stage 1) window, in which no cell death is yet visible, only stage M1 mitochondria would be present (data not shown). Stage M1 mitochondria were consistently found in healthy, NPCD cells (Figure 4.2C, between white and red lines). These mitochondria were generally seen individually, appeared to have intact membranes and cristae, and illustrated active streaming within the cytosol (Figure 4.3A-C; 4.4A-C; Table 4.1; see Online Resource 4.1). Stage M2 mitochondria were generally found within EPCD window stage cells (Figure 4.2C, between red and green lines), surrounding the interior border of the NPCD cells. These mitochondria were generally seen clustered into several small aggregates, with individual mitochondria in the surrounding cytosol (Figure 4.3D-F; Table 4.1). The movement of stage M2 mitochondrial aggregates (Figure 4.4D-F) was more sporadic, random and quicker than M1 stage mitochondria (Figure 4.4A-C; see Online Resource 4.2). Stage M3 mitochondria were generally found within LPCD window stage cells (Figure 4.2C, between green lines and green asterisks). These mitochondria were again seen in

aggregate(s) with few to no individual mitochondria within the surrounding cytosol (Figure 4.3G and H). M3 mitochondria begin to display degraded cristae and unclear inner and outer membranes (Figure 4.3I). Stage M3 mitochondrial aggregates also showed little to no movement as compared to M1 and M2 stage mitochondria (Figure 4.4A-I; Table 4.1; see Additional Files 4.3 and 4.4). Lastly, stage M4 mitochondria were also generally located within LPCD cells, but closest to the center of the areole (Figure 4.2C, denoted by asterisk) and showed absolutely no staining (Figure 4.3J and K). These mitochondria appeared to have dramatically degraded cristae and nearly indistinguishable membranes via TEM imaging and also displayed no movement (Figure 4.3L; Figure 4.4J-L; Table 4.1; see Online Resource 4.5).

4.4.2 Decrease in Mitochondrial $\Delta\Psi_m$

Window stage leaf pieces stained with CMXRos were also used to make inferences regarding mitochondrial $\Delta\Psi_m$ during developmentally regulated PCD. A reduction in $\Delta\Psi_m$ is hypothesized to allow subsequent release of IMS proteins and the continuation of PCD signalling. This shift in $\Delta\Psi_m$ can be visualized via changes in CMXRos fluorescence. Stage M1-M3 mitochondria displayed vivid CMXRos staining, providing indirect evidence of the intact $\Delta\Psi_m$ (Figure 4.4A-I; Table 4.1). Stage M4 mitochondria showed little to no mitochondrial staining, and are thus expected to have undergone the MPT (Figure 4.4J-L; Table 4.1). It should be noted that despite the lack of mitochondrial fluorescence in M4 stage mitochondria, a ruptured inner or outer mitochondrial membrane was not observed.

4.4.3 Terminal Deoxynucleotidyl Transferase Mediated dUTP Nick-End Labeling (TUNEL)

Further analysis of mitochondrial dynamics during developmentally regulated PCD was completed by the execution of a TUNEL assay and counter staining with propidium iodide (PI) to aid in co-localization (Figure 4.5). Previously it has been shown that TUNEL-positive nuclei are present in stages 2-4 (window stage to perforation expansion) of leaf development (Gunawardena et al. 2004). When examining a single areole within a stage 2 (window stage) leaf, there appeared to be a gradient of TUNEL positive nuclei that corresponded with the progression of mitochondrial death (Figure 4.5A-D). NPCD cells that contained M1 stage mitochondria showed no TUNEL positive nuclei (Figure 4.5E-H). EPCD cells that contained M2 stage mitochondria also contained no TUNEL positive nuclei (Figure 4.5I-L). LPCD cells that contained M3 stage mitochondria showed TUNEL positive nuclei (Figure 4.5M-P). LPCD cells that contained M4 stage mitochondria consistently showed intense TUNEL positive staining (Figure 4.5Q-T).

4.4.4 Mitochondrial Movement and Transvacuolar Strands

Our results indicate that mitochondria, as well as associated chloroplasts, appear to be moving on TVS (Figure 4.6, see Online Resource 4.6-4.8), possibly allowing for more rapid and organized movements within the cell. Figure 4.6 illustrates still images taken from a successive Z-stack progression through an EPCD stage single cell. Mitochondria and chloroplasts appear to have distinct associations with one another, and in most instances appear to be congregated around the nucleus (Figure 4.6A-D). These

images also illustrate both mitochondria and chloroplasts moving in clear lines with a trajectory towards the nucleus, along what appear to be TVS (Figure 4.6E-H). At this stage the cells are still healthy and do not show any sign of PM shrinkage. Transvacuolar strands were examined in NPCD, EPCD and LPCD window stage leaf cells. There appeared to be several TVS present in NPCD cells (Figure 4.7A, Online Resource 4.6), an increase in TVS occurrence in EPCD cells (Figure 4.7B, Online Resource 4.7) and a dramatic decrease in TVS in LPCD cells (Figure 4.7C, Online Resource 4.8).

4.4.5 Cyclosporine A Treatment

4.4.5.1 Qualitative Analysis

Figure 4.8 illustrates the effect of the optimal concentration of CsA (10 μM) on *in vivo* perforation formation within the lace plant. Photographs of boxed plants and harvested leaves of control (just ethanol), and CsA (10 μM) treated plants clearly display a decrease in perforation formation (Figure 4.8A-D). Concentrations of 2 μM, 4 μM, 15 μM, and 20 μM CsA were also examined (data not shown), with 10 μM being chosen as the minimum concentration to statistically reduce perforation number and not cause a toxic effect. The 20 μM treatment was considered toxic and was not included within the remainder of experiments. The effect of CsA seemed to dissipate following the growth of three new leaves from the SAM, indicating initial rapid uptake of CsA or possibly a rapid disintegration of CsA overtime (Figure 4.8).

4.4.5.2 Quantitative Analysis

The GLM ANOVA revealed significant differences in the ratio of number of perforations per cm of leaf length between the CsA treated plants at 10 μM ($P = 0.0035$)

and 15 μM ($P = 0.0007$) compared to control plants ($P < 0.05$; Figure 4.9). There was no significant difference in the ratio of number of perforations per cm of leaf length between CsA treated plants at 2 μM ($P = 0.1572$) and 4 μM ($P = 0.0545$) compared to control plants ($P > 0.05$; Figure 4.9). CsA treatments at 2 μM and 4 μM differed significantly from CsA treatments at 10 μM and 15 μM ($P < 0.05$). The analysis also revealed that there was no overall significant difference in leaf length between control and any CsA treated plants ($P > 0.05$).

4.4.6 Mitochondrial Dynamics Following CsA Treatment

Following the conclusion that 10 μM was the optimal concentration to prevent PCD and perforation formation within the lace plant, CsA treated leaves were stained with CMXRos to examine mitochondrial dynamics (Figure 4.10 and 4.11). Mitochondrial dynamics were again examined within one areole, between vascular tissue, where PCD would have occurred in control leaves. Mitochondria were examined in areas that would be equal to NPCD, EPCD and LPCD areas within a control window stage leaf. CsA treated mitochondria appeared to remain individual, rounded, and evenly distributed from NPCD-LPCD cellular areas (Figure 4.10B-G). Several small aggregates did appear in some LPCD cells, but were not consistent in every cell. The mitochondria also appeared to remain actively streaming in the cytosol, and showed no loss of membrane potential within similar cellular areas examined within window stage leaves (NPCD-LPCD; Figure 4.11A-I; see Online Resource 4.9-4.11).

4.5 Discussion

4.5.1 Developmentally Regulated Programmed Cell Death

The unique and predictable system of developmentally regulated PCD within the lace plant offers an excellent model for the study of organelle changes during this process. Within this study, we showed the importance of the mitochondria within the early stages of PCD. In addition, we have illustrated the possible strong correlation between the mitochondria and other organelles including the chloroplasts, nuclei and TVS.

4.5.2 Variation in Mitochondrial Distribution, Dynamics and $\Delta\Psi_m$

The observation that the chloroplasts formed a ring formation around the nucleus in the lace plant in the mid to late stages of PCD has been reported previously by (Wright et al. 2009); however, this is the first report of the association of mitochondria with these chloroplasts surrounding the nucleus. The reasons for the above are not known, however, it is possible they congregate due to a structure-function relationship, to aid in the PCD process. Given the active movement of mitochondria and chloroplasts on TVS towards the nucleus, as seen through live cell imaging (see Online Resource 4.7) we can confirm that this association is not due to PM shrinkage, given none is present. A phenomenon noted in cucumber, pea and rye plants following induced cell death with ethylene illustrated that mitochondria located in parenchyma cells were attracted to the nuclear envelope during PCD. Authors reported that this attraction led to the condensation of chromatin at the sites where the organelles were in contact, and was thus considered to be a structural mechanism for PCD promotion (Selga et al. 2005).

The aggregation of mitochondria appears to be the first visible shift in mitochondrial dynamics during developmentally regulated PCD in the lace plant. This

aggregation of mitochondria has also been demonstrated during induced cell death systems by Scott and Logan (2008), Yao et al. (2004) and Gao et al. (2008) in *Arabidopsis* protoplasts, and also by Lord and Gunawardena (2011) in lace plant protoplasts. The reason for the formation of aggregates is unknown. Previous studies report that these mitochondrial aggregates during PCD in *Arabidopsis* (Gao et al. 2008), lace plant (Lord and Gunawardena 2011) and tobacco protoplasts (Lin et al. 2005) are located in the cytosol of the cells. However, recent data (unpublished) from the Gunawardena lab suggest that this aggregate may be inside the vacuole at later stages of PCD. These recent findings, along with the rapid and random movements of the aggregate, suggest that this aggregate may move from the cytosol to the vacuole during late PCD, possibly to be degraded. Also, this study never observed the aggregates moving along TVS, suggesting that they may be in the vacuole at this time. Previous studies by Wright et al. (2009) on developmental PCD in the lace plant provide evidence of similar aggregates, containing chloroplasts and possibly mitochondria, inside the vacuole undergoing Brownian motion during the later stages of PCD (see Online Resource 4.6 in Wright et al. 2009). However, whether these aggregates are first in the thin layer of cytoplasm and then move into the vacuole requires further investigation.

Following aggregation, mitochondria displayed a subsequent reduction in streaming. This cessation of streaming has also been demonstrated in mitochondria during several induced cell death examples in *Arabidopsis* protoplasts (Gao et al. 2008; Zhang et al. 2009), *Arabidopsis* leaf discs (Yoshinaga et al. 2005), tobacco BY-2 cells (Vacca et al. 2004; Vacca et al. 2006), and lace plant protoplasts (Lord and Gunawardena 2011). This impairment of mitochondrial movement is commonly seen following the

induction of cell death, and is thought to be highly correlated with the acute change in cellular redox status, as well as the remainder of the cell death process (Vacca et al. 2004, 2006; Zhang et al. 2009).

Following mitochondrial aggregation and cessation of streaming, they appear to undergo the MPT, characterized by a loss of CMXRos staining. The decrease in $\Delta\Psi_m$ appeared to occur between M3 and M4 mitochondria, possibly indicating that this is the first visible indication of membrane transition, and thus, possibly the first release of IMS proteins. The release of these IMS components at this time would correlate with the apparent degradation of the inner mitochondrial structure at this stage of PCD. This decrease in mitochondrial $\Delta\Psi_m$ has been noted as a key characteristic of cell death in animal systems, and has also been demonstrated in a variety of other plant examples including induced cell death in *Arabidopsis* protoplasts (Gao et al. 2008; Scott and Logan, 2008; Yao et al. 2004), isolated oat mitochondria (Curtis and Wolpert 2002), lace plant protoplasts (Lord and Gunawardena 2011) and also during developmentally regulated cell death in isolated Zinnia treachery element (TE) cells (Yu et al. 2002).

4.5.3 Terminal Deoxynucleotidyl Transferase Mediated dUTP Nick-End Labeling (TUNEL)

A trend was noted within a single areole of a stage 2 (window stage) leaf; cells that contained TUNEL positive nuclei were generally correlated with cells that contained M3 and M4 stage mitochondria. TUNEL positive nuclei were not seen in NPCD cells that contained stage M1 mitochondria; this result was expected given that these cells are not pre-disposed to undergo developmental cell death. TUNEL positive nuclei were also

absent in EPCD cells that contain stage M2 mitochondrial aggregates. This result clearly indicates that mitochondrial changes have begun prior to the fragmentation of nuclear DNA leading to TUNEL positive nuclei. TUNEL positive nuclei were consistently seen within LPCD cells that contained either M3 or M4 stage mitochondria. This trend also allows us to conclude that mitochondrial changes, particularly those seen in stage M3 and M4 stage mitochondria, including the cessation of mitochondrial streaming and complete loss of $\Delta\Psi_m$ are probably occurring simultaneously with the fragmentation of nuclear DNA, as noted by the presence of TUNEL positive nuclei within these areas.

4.5.4 Transvacuolar Strands

An increased number of TVS was noted in window stage leaf cells that were in the early stages of PCD (EPCD cells). This increased instance of TVS is a common characteristic of PCD and has been noted previously during developmental cell death in the lace plant (Wright et al. 2009), in induced cell death in lace plant protoplasts (Lord and Gunawardena 2011), and also during induced cell death by osmotic stress in tobacco suspension cultures (Reisen et al. 2005). Increases in TVS could aid in the movement of organelles such as chloroplasts and mitochondria within plant cells. Within this system, both of these organelles have been seen traveling along thin strands spanning the vacuole of the cell and sometimes appearing to be moving towards the nucleus. The appearance of these strands decreases as PCD progresses, with few to no TVS present in LPCD stage cells.

4.5.5 Cyclosporine A

The application of the MPTP antagonist CsA to the lace plant system marks the first time, to our knowledge, that this inhibitor has ever been applied *in vivo* within a plant system. This inhibitor has been used previously during induced cell death in suspension cultures (Contran et al. 2007; Tiwari et al. 2002), isolated protoplasts (Lin et al. 2005; Lord and Gunawardena, 2011; Scott and Logan, 2008; Yao et al. 2004), and isolated mitochondria (Arpagaus et al. 2002; Fortes et al. 2001; Lin et al. 2006; Oliveira et al. 2007; Pavlovskaya et al. 2007). The only other developmentally regulated PCD example in which CsA had been employed was during TE differentiation in *Zinnia*, but this example is considered *in vitro* due to the cells being isolated from the plant prior to CsA treatment (Yu et al. 2002).

The application of CsA to lace plants in magenta boxes led to a reduction in perforation formation in leaves produced following the addition of the inhibitor. This significant decrease in perforation formation within the lace plant via CsA application indirectly indicates that the MPTP pathway may play a role in cellular death within this system. Although the involvement of the MPTP in animal PCD is well supported, it is controversial if a similar complex has a role in the release of IMS proteins in plant PCD, as shown by the following authors. Studies examining tobacco protoplasts (Lin et al. 2005), sycamore cells (Contran et al. 2007) or mitochondria isolated from either winter wheat (Pavlovskaya et al. 2007) or potato tubers (Arpagaus et al. 2002), as well as developing tracheary elements (Yu et al. 2002) provide evidence suggesting that CsA effectively inhibits or delays PCD; this, arguably, suggests a role for the MPTP in plant PCD. However, there have also been studies that demonstrate the insensitivity of plant PCD to CsA (Fortes et al. 2001). Lin et al. (2006) report a delay or reduction in PCD, and

suggest that this may provide evidence for an alternate pathway. In animal systems, there is an alternate pathway for the release of IMS proteins that involves the Bcl-2 family of proteins, however, to date there is no direct evidence of Bcl-2 family proteins in plants. Inhibitor experiments, however, provide indirect evidence for Bcl-2-like family protein activity in plants (reviewed by Lam 2004). In contrast to this study, our experiment reports a significant reduction in PCD following CsA pre-treatment, suggesting the absence of an alternative pathway in this system. This provides indirect evidence for the role played by the MPTP in lace plant PCD. However, further studies are required to examine the role of the MPTP in the release of the IMS proteins from the mitochondria into the cytosol.

CsA concentrations in the lower range (2 μM and 4 μM) did not result in a significantly lower amount of perforations as compared to the controls (data not shown). This observation was expected, given that the inhibitor is dissolved in liquid and being applied to whole plants; therefore, higher concentrations may be required in order to affect the MPTP. CsA at 10 μM significantly reduced the amount of perforations in the lace plant as compared to the control, but also maintained a healthy leaf appearance. The observations that no perforations formed at the 15 μM concentration, but did form in the controls, and that some transient leaf clearing occurred, indicates that this may be the lower limit of toxicity for CsA in the lace plant. The 20 μM CsA treatment resulted in brown and/ or cleared leaves and therefore this concentration was considered very toxic and was not included in the subsequent statistical analysis. Overall, for further research it has been concluded that 10 μM CsA is the ideal concentration to inhibit the opening of the MPTP during lace plant developmentally regulated PCD. This concentration has also

been utilized as an optimal concentration in other plant examples, including sycamore cells (Contran et al. 2007).

For this reason, 10 μM CsA treated leaves, 4 days following their emergence from the SAM, were chosen for examination; these leaves were therefore a similar developmental age as window stage leaves examined previously. CsA treated leaves depicted numerous, round mitochondria, which generally remained individual within the cytosol, and formed few aggregates in all cell types equal to NPCD-LPCD. These mitochondria also remained streaming within the entire areole and did not appear to undergo a membrane permeability transition causing loss of membrane potential and CMXRos staining. Given that treatment with CsA is hypothesized to block the release of IMS proteins from the mitochondria, we would anticipate variations in mitochondrial dynamics within this system. Intense mitochondrial fluorescence was anticipated, as this drug is hypothesized to inhibit the MPTP and possibly the subsequent MPT. A round, and or swollen appearance of mitochondria following CsA treatment was also noted, although the reason behind this is unknown and needs to be further investigated. Overall, CsA treated mitochondria display characteristics that most closely resemble M1 mitochondrial dynamics, where no PCD is occurring.

4.6 Conclusions

The results presented here elucidate organelle dynamics, focused on mitochondria, during developmentally regulated PCD in the lace plant *A. madagascariensis*. Developing leaves in which PCD was initiated (window stage) were stained with the mitochondrial membrane potential sensitive dye CMXRos and were examined via live cell imaging and confocal fluorescent microscopy. Observations of

mitochondrial aggregation, motility and $\Delta\Psi_m$ lead to the classification of mitochondria into one of four stages (M1- M4) based on their location in a window stage leaf areole. Our findings also indicated that within a single areole of a stage 2 (window stage) leaf a gradient of TUNEL positive nuclei staining existed. TUNEL positive nuclei were not seen in cells containing M1 and M2 stage mitochondria and were seen in cells with M3 and M4 stage mitochondria. These correlations suggest that the mitochondrial aggregation occurs prior to DNA fragmentation, whereas cessation of mitochondrial streaming and the membrane permeability transition resulting in complete loss of $\Delta\Psi_m$, based on CMXRos staining, probably occurs concurrently with the fragmentation of nuclear DNA. Mitochondria and chloroplasts were examined via live cell imaging, highlighting the role of TVS in the movement of the organelles into a ring formation around the nucleus. The function of the mitochondrial MPTP during PCD in developing lace plant leaves was also indirectly examined via CsA pre-treatment. Examination of CsA treated mitochondria revealed individual organelles, continued mitochondrial streaming and no loss in membrane potential over the same cellular areas (NPCD-LPCD) within one areole. Overall, results presented here detail organelle dynamics during developmentally regulated PCD in whole lace plant tissue and suggest that the mitochondria plays an important role in the early stages of PCD.

4.7 Acknowledgements

The authors thank Dr. Nancy Dengler (University of Toronto, Canada) for critical review of the manuscript and Harrison Wright (Dalhousie University, Canada) for providing TEM images. The authors also greatly acknowledge the Sarah Lawson Botanical Research Scholarship (Dalhousie University) for summer funding for J.W, the

Canadian Foundation for Innovation (CFI) for the Leaders Opportunity Fund, the Natural Sciences and Engineering Research Council (NSERC) for discovery and equipment grants for A.G. and Dalhousie University for partial doctoral funding for C.L.

4.8 Authors' Contributions

CENL and JW carried out all experiments: pharmacological application and harvest, light, fluorescent, confocal and DIC microscopic observations and measurements, along with conceptual mitochondrial staging. CENL completed the statistical analysis, drafted and revised the final manuscript. JW also contributed to final manuscript revisions. SL completed TVS observations using light microscopy, and live cell-imaging. AHLANG conceived the study, participated in its design and coordination, helped in drafting and revising the manuscript, and supervised all experimental work. All authors read and approved the final manuscript.

4.9 Online Resources

Online Resource 4.1 Stage M1 Mitochondrial Dynamics

CMXRos stained NPCD cell, highlighting stage M1 mitochondrial dynamics. Note individual mitochondria actively streaming within the cytosol.

Online Resource 4.2 Stage M2 Mitochondrial Dynamics

CMXRos stained EPCD cell, highlighting stage M2 mitochondrial dynamics. Note the aggregation of mitochondria along with several individual mitochondria, all of which appear to be moving.

Online Resource 4.3 Stage M2-M3 Mitochondrial Transition

CMXRos stained EPCD cell and DIC overlay. Video highlights the transition from stage M2 to stage M3 mitochondria. Note mitochondrial aggregate moving towards the nucleus, followed by cessation of movement. Video is 15× normal speed.

Online Resource 4.4 Stage M3 Mitochondrial Dynamics

CMXRos stained LPCD cell, highlighting stage M3 mitochondrial dynamics. Note the absence of movement of the mitochondrial aggregate.

Online Resource 4.5 Stage M4 Mitochondrial Dynamics

CMXRos stained LPCD cell, aimed at highlighting stage M4 mitochondrial dynamics. Note the lack of mitochondrial staining by CMXRos possibly due to complete loss of $\Delta\Psi_m$.

Online Resource 4.6 Transvacuolar Strands in NPCD Stage Cells

NPCD stage cells showing several transvacuolar strands, and highlighting the close association and possible movement of mitochondria and chloroplasts along them. Video 20× normal speed.

Online Resource 4.7 Transvacuolar Strands in EPCD Stage Cells

EPCD stage cells showing increased transvacuolar strand activity and highlighting the close association and possible movement of mitochondria and chloroplasts along them.

Note the trajectory of most strands and organelles towards the nucleus. Video 20× normal speed.

Online Resource 4.8 Transvacuolar Strands in LPCD Stage Cells

LPCD stage cells showing a decrease in the number of transvacuolar strands and absence of organelles. Note that although mitochondrial streaming in often ceased at this point, slight cytoplasmic streaming can be visualized in mesophyll cells below the point of focus. Video 20× normal speed.

Online Resource 4.9 Mitochondrial Dynamics in CsA Treated NPCD Stage Cells

CsA treated leaf subsequently stained with CMXROS, depicting a single cell that corresponds with an NPCD window stage cell. Note, individual mitochondria that are rapidly moving within the cytosol.

Online Resource 4.10 Mitochondrial Dynamics in CsA Treated EPCD Stage Cells

CsA treated leaf subsequently stained with CMXROS, depicting a single cell that corresponds with an EPCD window stage cell. Note, individual mitochondria that are rapidly moving in the cytosol.

Online Resource 4.11 Mitochondrial Dynamics in CsA Treated LPCD Stage Cells

CsA treated leaf subsequently stained with CMXROS, depicting a single cell that corresponds with an LPCD window stage cell. Note, many individual mitochondria, and several small aggregates that are rapidly moving.

Table 4.1 Mitochondrial Stage, Distribution, Dynamic State, and ΔΨm, as Compared to Window Stage Cell Staging

Window Leaf Stage	NPCD	EPCD	LPCD	
Mitochondrial Stage	M1	M2	M3	M4
Mitochondrial distribution	Individual	Aggregates	Aggregates	Aggregates
Mitochondrial dynamics	Streaming	Streaming	Cessation of movement	Cessation of movement
Mitochondrial $\Delta\Psi_m$ intactness	Intact	Intact	Intact	Lost

Figure 4.1 Progression of Developmental PCD Within a Lace Plant Leaf, Stages (1-5)

Delineation of leaf morphogenesis in lace plant leaves as PCD progresses. (A) Whole plant growing in sterile culture in a magenta box filled with liquid and solid Murashige and Skoog (MS) medium. (B) Stage 1, or pre-perforation lace plant leaf, note the abundance of the pink pigment anthocyanin within most cells of the leaf. Also note that one full areole is shown bound by vascular tissue. (C) Stage 2, or "window" stage lace plant leaf, note the distinct cleared area in the center of the vasculature tissue indicating a loss of pigments anthocyanin and chlorophyll. (D) Stage 3, or perforation formation lace plant leaf. The cells in the center of the cleared window have begun to break away, forming a hole in the center of the areole. (E) Stage 4, or perforation expansion lace plant leaf, note that cell death has stopped approximately four-five cells from the vascular tissue. (F) Stage 5, or a completed perforation in a lace plant leaf. The cells bordering the perforation have transdifferentiated to become epidermal cells. Scale bars (A) = 1 cm; (B) = 200 μm; (C-F) = 500 μm.

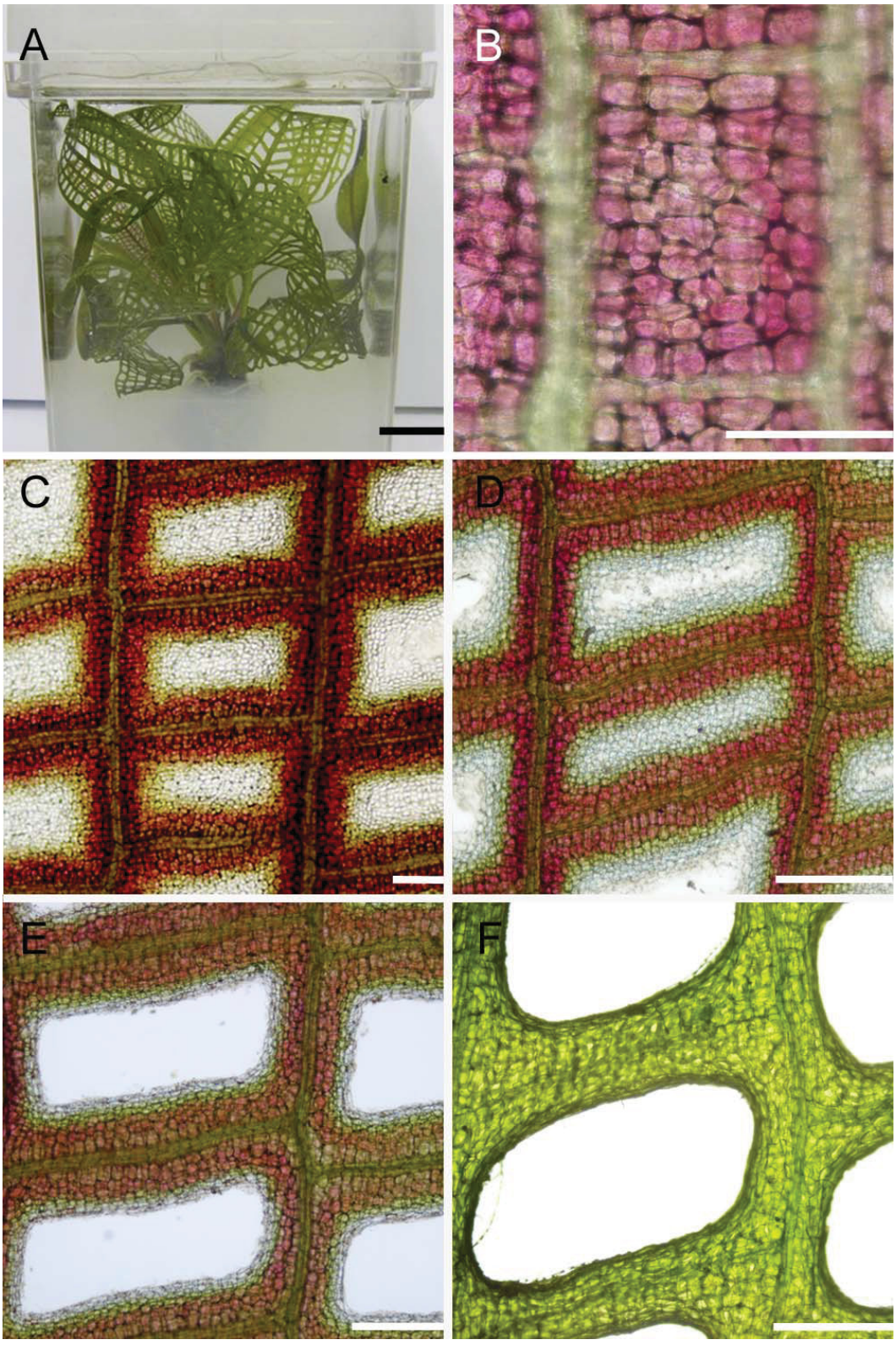

Figure 4.1 Progression of Developmental PCD Within a Lace Plant Leaf, Stages (1-5)

Figure 4.2 Description of the PCD Gradient Within a Window Stage Lace Plant Leaf

The three-part differentiation of an areole within a stage 2, or window stage leaf. (A) A detached stage 2, or "window" stage leaf. Note the green and pink coloration, which is due to the presence of the pigments chlorophyll and anthocyanin, respectively. (B) Single side of a window stage leaf, cut at the midrib. Note the gradient of PCD, in that PCD is most advanced closest to the midrib (bottom) and least advanced towards to leaf edge (top). (C) PCD has also been delineated at the level of a single areole. Within a single areole of a stage 2, or window stage leaf, cells closest to the vasculature tissue (between white and red lines) will not undergo developmental PCD and are known as non-PCD cells (NPCD); NPCD cells often contain a marked amount of the pigment anthocyanin. The next group of cells (between red and green lines) are in very early stages of PCD and are known as early PCD cells (EPCD); EPCD cells often contain a marked amount of the pigment chlorophyll. The centermost cells (green lines inward) are cells in late stages of PCD, and are known as late PCD cells (LPCD); LPCD cells have lost most of their pigment, and are clear in nature. Scale bars (A) = 25 mm; (B) = 750 μm; (C) = 250 μm.

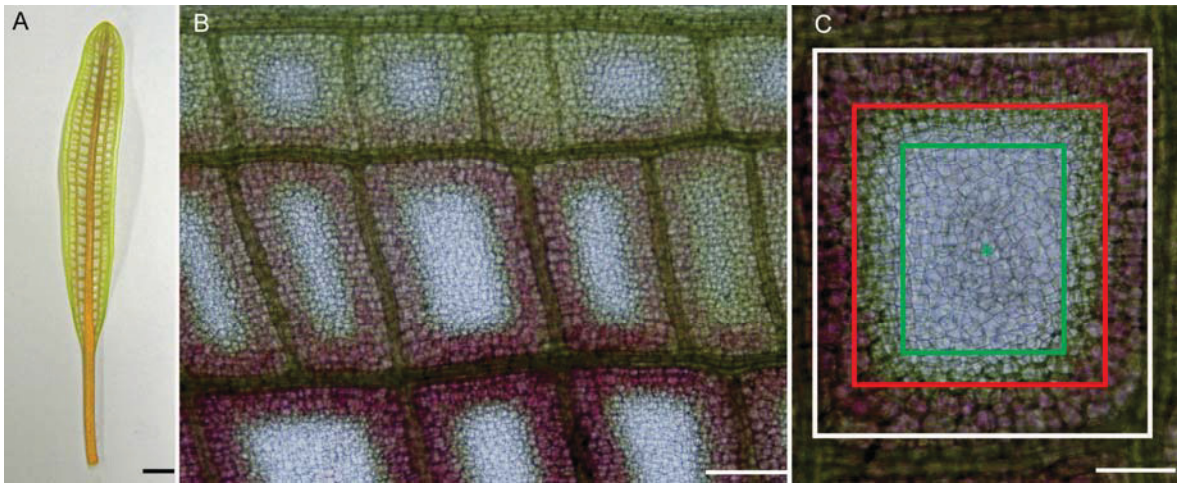

Figure 4.2 Description of the PCD Gradient Within a Window Stage Lace Plant Leaf

Figure 4.3 Mitochondrial Distribution (stage M1-M4) Within a Window Stage Lace Plant Leaf

Mitochondria within a window stage leaf stained with CMXRos and examined via confocal microscopy to view organelle distribution throughout the PCD gradient within individual cells. (A and B) Stage M1 DIC and corresponding CMXRos fluorescent images, respectively. (C) TEM micrograph of healthy mitochondria depicting intact mitochondrial membranes and cristae. (D) and (E) Stage M2 DIC and corresponding CMXRos fluorescent images, respectively. Note mitochondria most have aggregated within the cell with several individual mitochondria still present in the cytosol. (F) TEM micrograph of mitochondria within dying cell depicting what appears to be a healthy mitochondria with intact cristae and clear membranes. (G) and (H) Stage M3 DIC and corresponding CMXRos fluorescent images, respectively. Mitochondria are still aggregated within the cell. (I) TEM micrograph of degrading mitochondria, mitochondrial cristae appear to be degraded, with less clear inner and outer membranes as compared to controls. (J) and (K) Stage M4 DIC and corresponding CMXRos fluorescent images, respectively. Note mitochondria have lost membrane potential entirely and are no longer visible in the fluorescent image. Mitochondria are now considered unviable. (L) TEM micrograph of presumably dead mitochondria depicting nearly indistinguishable membranes and damaged cristae. Scale bars (A, B, D, E, G, H, J, K) = 10 μm; (C, F, I, L) = 0.5 μm.[13]

[13] Note that TEM micrographs C, F, I, and L are an addition to the manuscript published in BMC Plant Biology and were included to increase clarity of mitochondrial morphology.

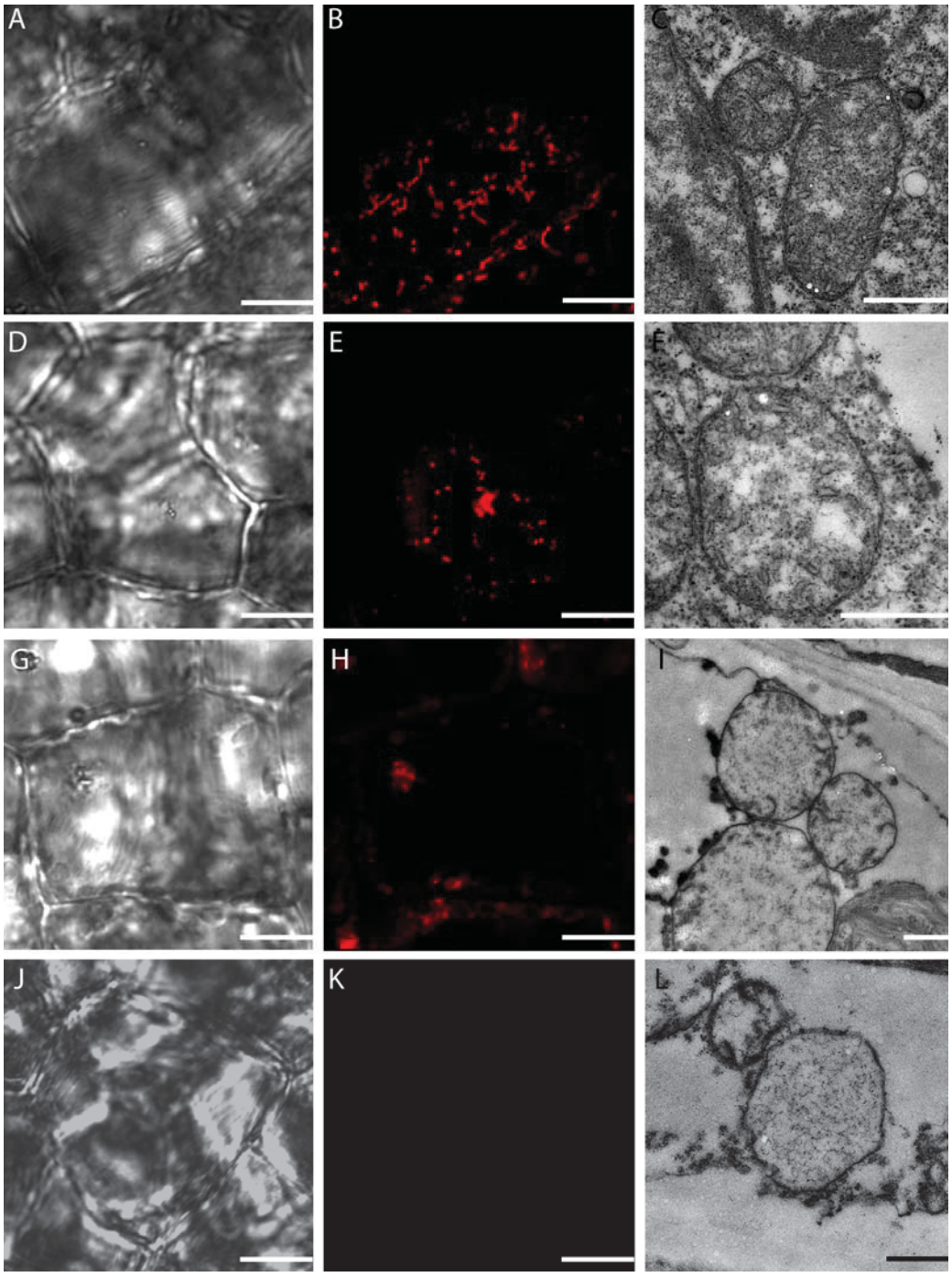

Figure 4.3 Mitochondrial Distribution (stage M1-M4) Within a Window Stage Lace Plant Leaf

Figure 4.4 *In vivo* Examination of Mitochondrial Motility and Membrane Potential in Stage M1-M4 Mitochondria Within a Single Areole of a Window Stage Lace Plant Leaf

Still images selected from time-lapse videos at time 0 and time 30 sec following CMXRos staining. Mitochondria in time 30 sec images have been false coloured green to allow for comparative overlay images to demonstrate mitochondrial motility. (A, D, G and J) time 0 sec CMXRos stained images of M1, M2, M3 and M4 mitochondria over the PCD gradient (NPCD-LPCD), respectively. (B, E, H and K) time 30 sec CMXRos stained images of M1, M2, M3 and M4 mitochondria over the PCD gradient (NPCD-LPCD), respectively. (C, F, I and L) Overlay of time 0 and 30 sec still images of M1, M2, M3 and M4 mitochondria over the PCD gradient (NPCD-LPCD), respectively. Note that when mitochondria have not moved, overlay images appear yellow. These overlay images characterize the rapid mitochondrial movement of M1 and M2 stage mitochondria, followed by the decrease in mitochondrial motility in M3 and M4 stage mitochondria. Also note the loss of mitochondrial staining in M4 mitochondria, indicating these organelles appear to have undergone a membrane permeability transition and have lost their membrane potential. Still images A, B and C taken from Online Resource 4.5. Still images D, E and F taken from Online Resource 4.6. Still images G, H and I taken from Online Resource 4.7. Still images J, K and L taken from Online Resource 4.8. Scale bars (A-I) = 10 μm.

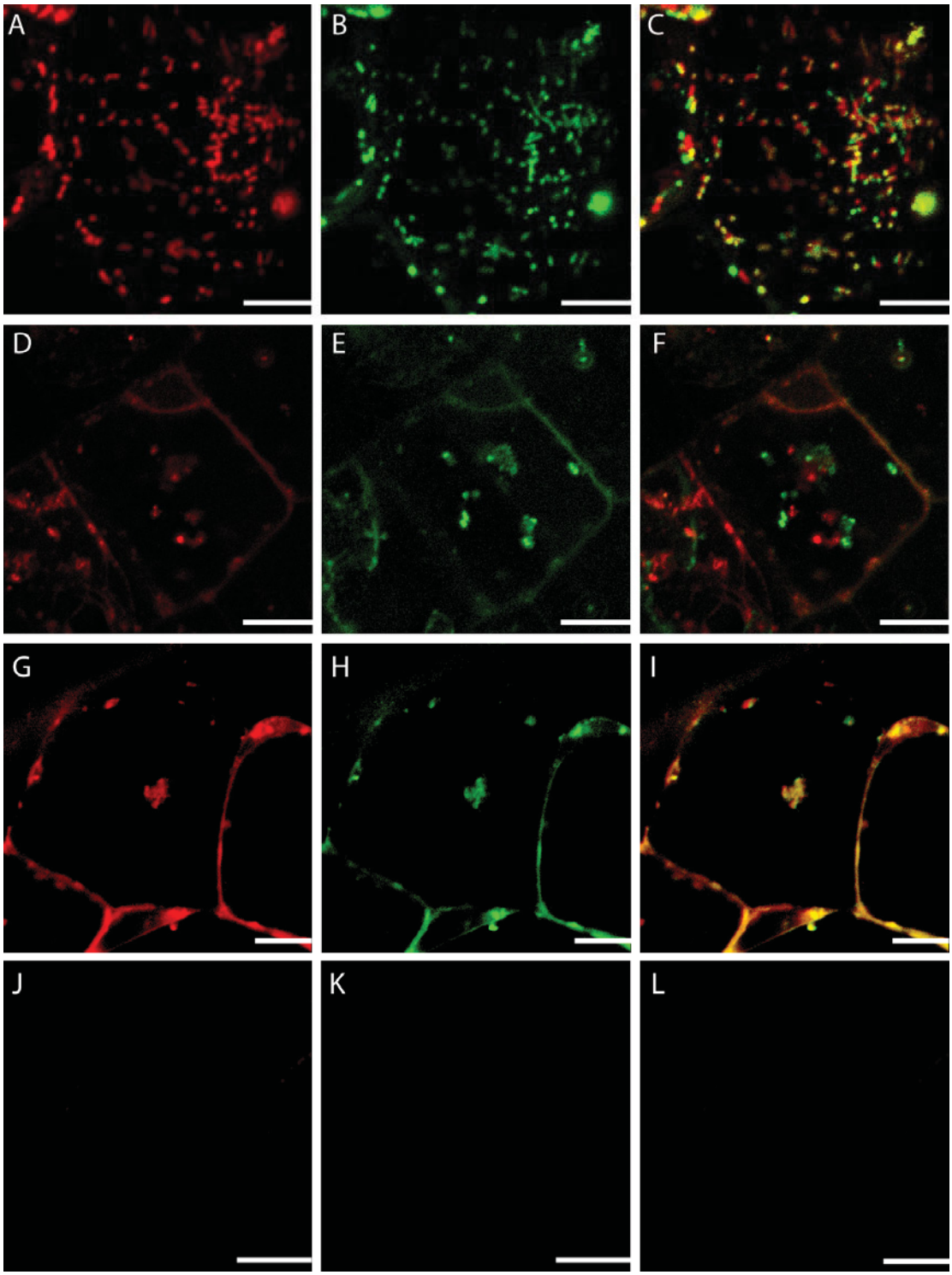

Figure 4.4 *In vivo* Examination of Mitochondrial Motility and Membrane Potential in Stage M1-M4 Mitochondria Within a Single Areole of a Window Stage Lace Plant Leaf

Figure 4.5 TUNEL Assay Portraying TUNEL Positive Nuclei Within a Single Areole of a Stage 2 or Window Stage Leaf

TUNEL positive nuclei within a single areole of a stage 2 (window stage) leaf. Note that Propidium Iodide (PI) staining is red, TUNEL positive nuclei stain green and when red and green nuclei overlap they appear yellow. (A) Low magnification differential interference contrast (DIC) image of a portion of a single areole in a window stage leaf (B) Corresponding low magnification TUNEL positive image (C) corresponding low magnification PI image (D) overlay of TUNEL positive and PI images. (E-H) High magnification images taken of NPCD cells where stage M1 mitochondria are normally found, DIC, TUNEL assay, PI and overlay of all three respectively. (I-L) High magnification images taken of EPCD cells where stage M2 mitochondria are normally found, DIC, TUNEL assay, PI and overlay of all three respectively. (M-P) High magnification images taken of LPCD cells where stage M3 mitochondria are normally found, DIC, TUNEL assay, PI and overlay of all three respectively. (Q-T) High magnification images taken of LPCD cells where stage M4 mitochondria are normally found, DIC, TUNEL assay, PI and overlay of all three respectively. Scale bars (A-D) = 60 μm; (E-T) = 15 μm.

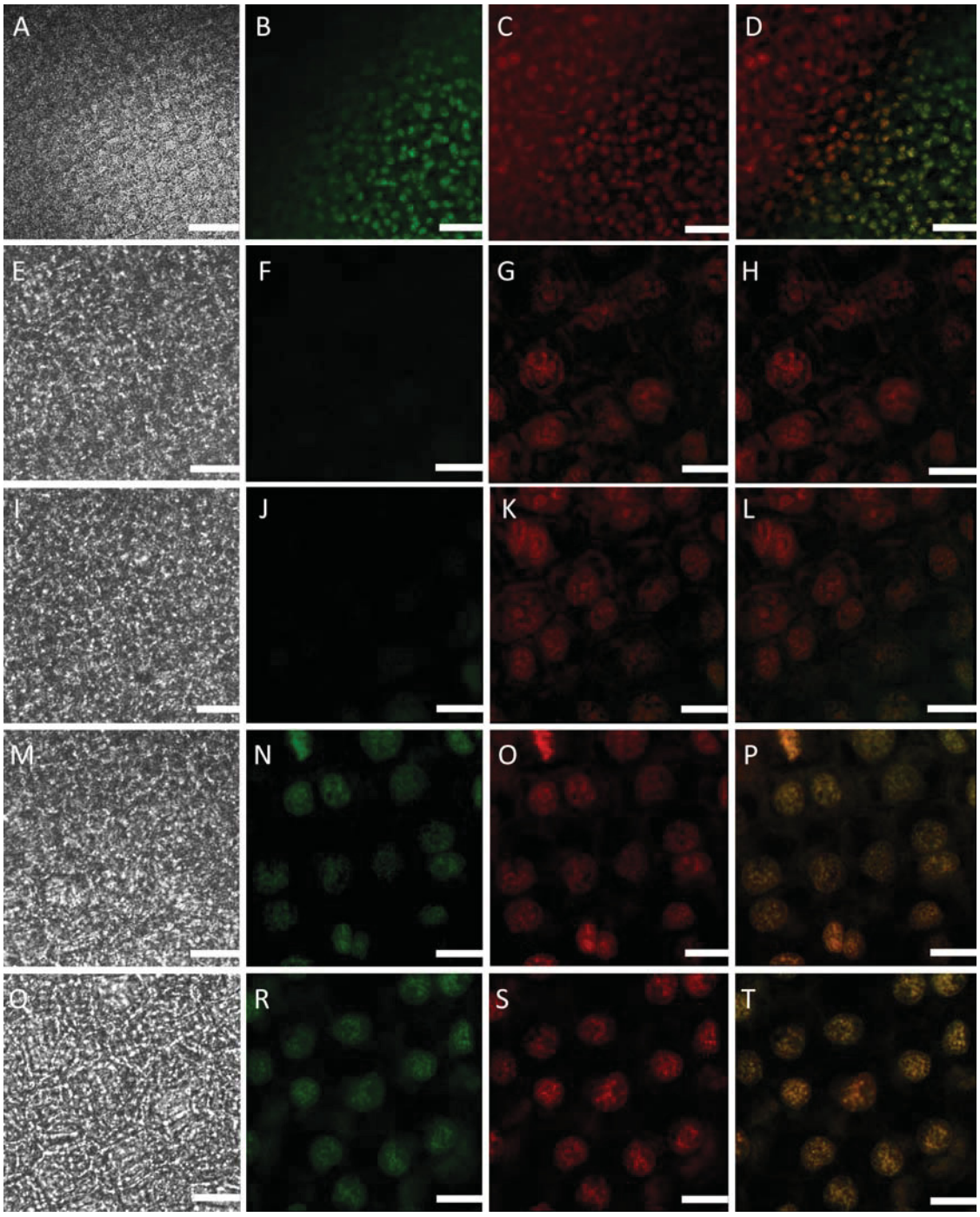

Figure 4.5 TUNEL Assay Portraying TUNEL Positive Nuclei Within a Single Areole of a Stage 2 or Window Stage Leaf

Figure 4.6 Progressive Z-Stack Series of a Single Cell, Illustrating Mitochondria and Chloroplasts Associations with Transvacuolar Strands Within a Lace Plant Window Stage Leaf

A z-stack progression consisting of four focal planes within one CMXRos stained cell in the center of a window stage leaf areole. Red fluorescence represents mitochondria while green fluorescence represents chlorophyll autofluorescence. (A) and (B) DIC and corresponding fluorescent images, respectively, in the top most plane of the cell. Note the mitochondria and chloroplasts around the nucleus. (C) and (D) DIC and corresponding fluorescent images, respectively in a lower focal plane. (E) and (F) DIC and corresponding fluorescent images, respectively in a middle focal plane within the cell. Note the continued association of chloroplasts and mitochondria around the nucleus, and the appearance of a strand in the lower right hand corner of the cell. (G) and (H) DIC and corresponding fluorescent images, respectively, displaying the lower most focal plane within this cell. Note the transvacuolar strand, which appears to have CMXRos stained mitochondria associated with it. Scale bars (A-H) = 25 μm.

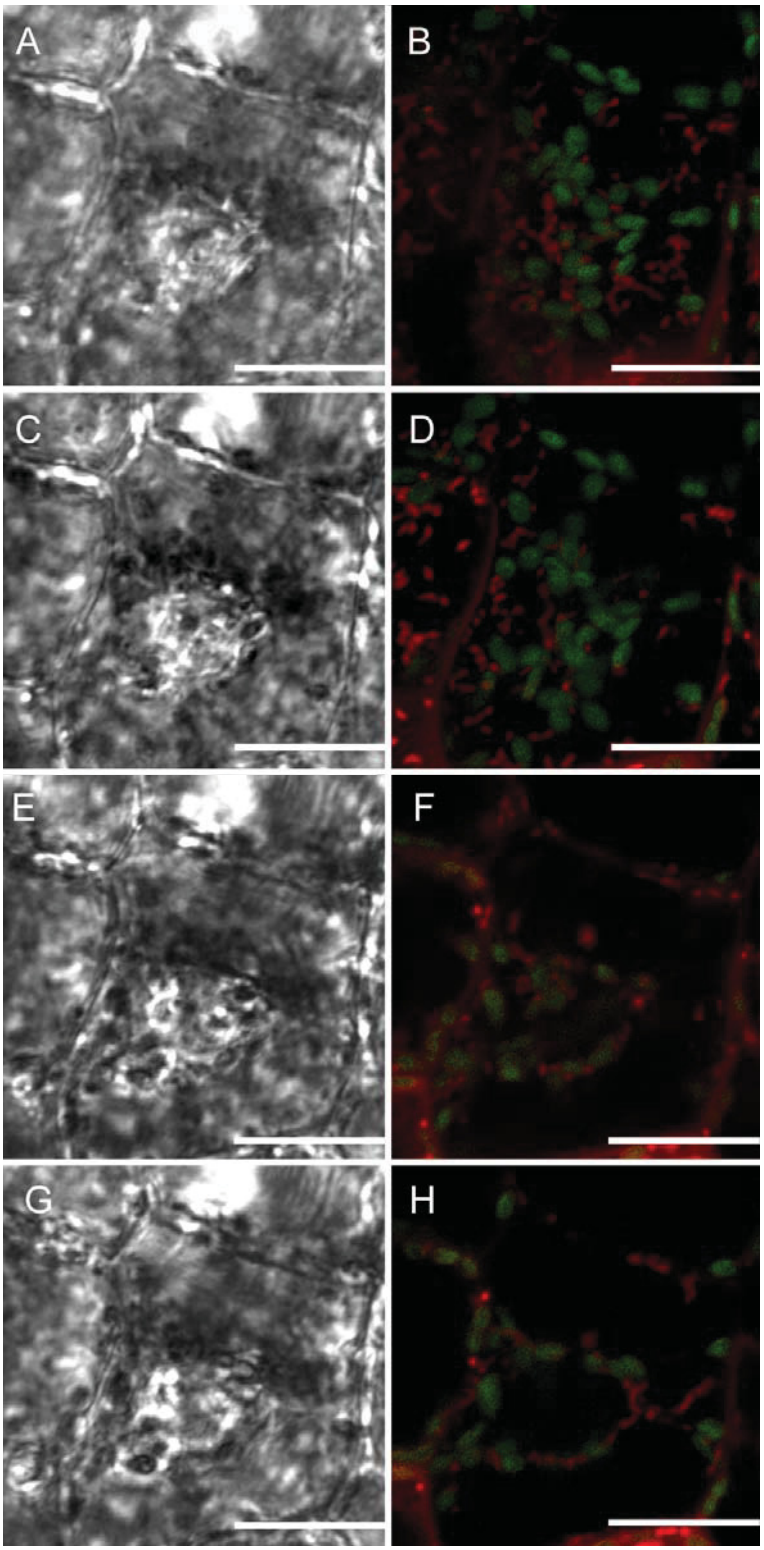

Figure 4.6 Progressive Z-Stack Series of a Single Cell, Illustrating Mitochondria and Chloroplasts Associations with Transvacuolar Strands Within a Lace Plant Window Stage Leaf

Figure 4.7 Light Micrographs of NPCD, EPCD and LPCD Stage Cells Illustrating Variation in Transvacuolar Strand Activity

(A) NPCD stage cells depicting several transvacuolar strands (black arrow), in which mitochondria and chloroplasts appeared to be associated (see Online Resource 4.6). (B) EPCD stage cells showing an increase in the number of transvacuolar strands (black arrow) and continued associations with mitochondria and chloroplasts. Depending on the focal plane of the cell, transvacuolar strands appear to be connected with the cell periphery and with the nucleus (see Online Resource 4.7). (C) LPCD stage cells illustrating a decrease in the number of transvacuolar strands with no organelle affiliations (see Online Resource 4.8).

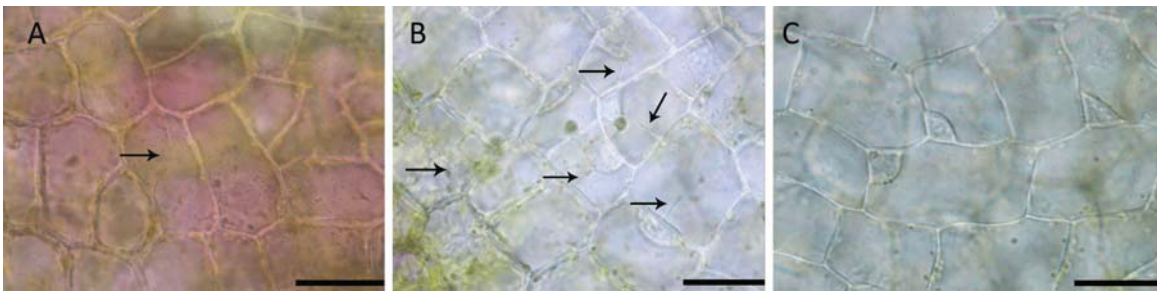

Figure 4.7 Light Micrographs of NPCD, EPCD and LPCD Stage Cells Illustrating Variation in Transvacuolar Strand Activity

Figure 4.8 Qualitative Analysis of the Effect of CsA, a Mitochondrial PTP Antagonist on Lace Plant PCD

Representative digital images of whole lace plants in magenta boxes, and harvested leaves, in the order of their emergence, from the corresponding box formed during each CsA experiment. (A) and (B) whole lace plant and corresponding leaf harvest for control plants, respectively; (C) and (D) whole lace plant and corresponding leaf harvest for 10 μM controls, respectively. For all harvested leaf images, leaves are arranged in chronological order of formation with leaf 0 representing a leaf formed prior to the initiation of the experiment, and subsequent leaves 1 through 5, or 6 having formed after the initiation of the experiment. Note that inhibition of perforation formation is primarily visible for leaves 1-3 for CsA treated plants (C-D). All scale bars = 1 cm.

Figure 4.8 Qualitative Analysis of the Effect of CsA, a Mitochondrial PTP Antagonist on Lace Plant PCD

Figure 4.9 Quantitative Analysis of the Effect of CsA, a Mitochondrial MPTP Antagonist on Lace Plant PCD

The effect of CsA on the mean ratio of number of perforations per cm of leaf length for control and treatment groups. The mean ratio of number of perforations per cm of leaf length decreased with increasing concentrations of CsA, indicating that the inhibition of the MPTP via CsA reduced the amount of PCD occurring in lace plant leaves. Significant relationships were found between the control, 10 μM and 15 μM treatment groups ($P < 0.05$). No significant relationships were found between the treatment groups ($P > 0.05$). Number of leaves per control and treatment group ranged from n = 30-60. Bars with the same letters are not significantly different.

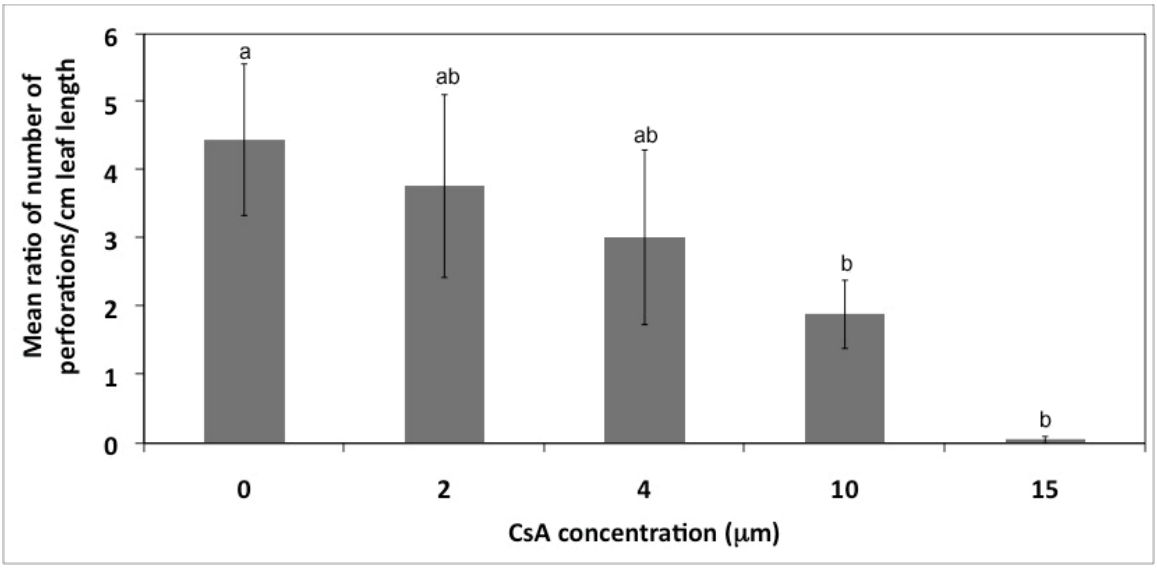

Figure 4.9 Quantitative Analysis of the Effect of CsA, a Mitochondrial MPTP Antagonist on Lace Plant PCD

Figure 4.10 *In vivo* Examination of Mitochondrial Distribution Following Pre-Treatment With the MPTP Inhibitor CsA

Changes in mitochondrial dynamics within one areole examining the same cellular areas (NPCD-LPCD) as observed within control window stage leaves. (A) A single areole within a 10 μM CsA treated leaf 4 days following its emergence from the SAM. (B and E) DIC and CMXRos images of a cell that corresponds with an NPCD window stage cell, respectively. (C and F) DIC and CMXRos images of a cell that corresponds with an EPCD window stage cell, respectively. (D and G) DIC and CMXRos images of a cell that corresponds with an LPCD window stage cell, respectively. Note even distribution of mitochondria at each stage. Scale bars (A) = 100 μm; (B and G) = 10 μm.

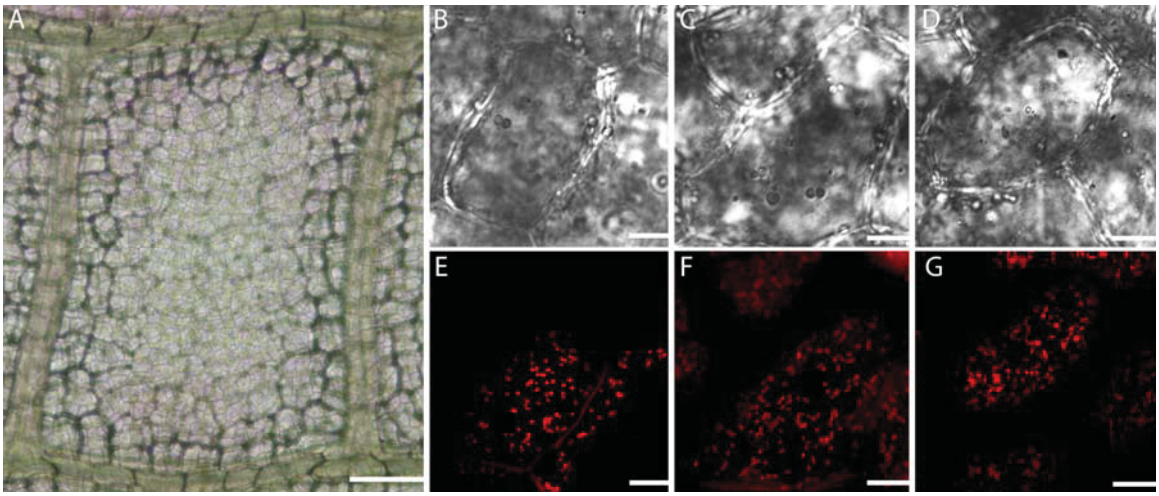

Figure 4.10 *In vivo* Examination of Mitochondrial Distribution Following Pre-Treatment With the MPTP Inhibitor CsA

Figure 4.11 *In vivo* Examination of Mitochondrial Motility and Membrane Potential Following Pre-Treatment With the MPTP Inhibitor CsA

Still images selected from time-lapse videos at time 0 and time 30 sec following 10 μM CsA treatment and subsequent CMXRos staining. Mitochondria in time 30 sec images have been false coloured green to allow for comparative overlay images to demonstrate mitochondrial motility. Note that when the red and green overlap, the mitochondria appear yellow and are presumably still. (A, D, G) time 0 sec CMXRos stained images of CsA treated leaves corresponding with NPCD, EPCD and LPCD cells, respectively. (B, E, H) time 30 sec CMXRos stained images of CsA treated leaves corresponding with NPCD, EPCD and LPCD cells, respectively. (C, F, I) Overlay of time 0 and 30 second still images corresponding with NPCD, EPCD and LPCD cells, respectively. These overlay images characterize the rapid mitochondrial movement in CsA treated leaves. Still images A, B and C taken from Online Resource 4.9. Still images D, E and F taken from Online Resource 4.10. Still images G, H and I taken from Online Resource 4.11. Scale bars (A-I) = 10 μm.

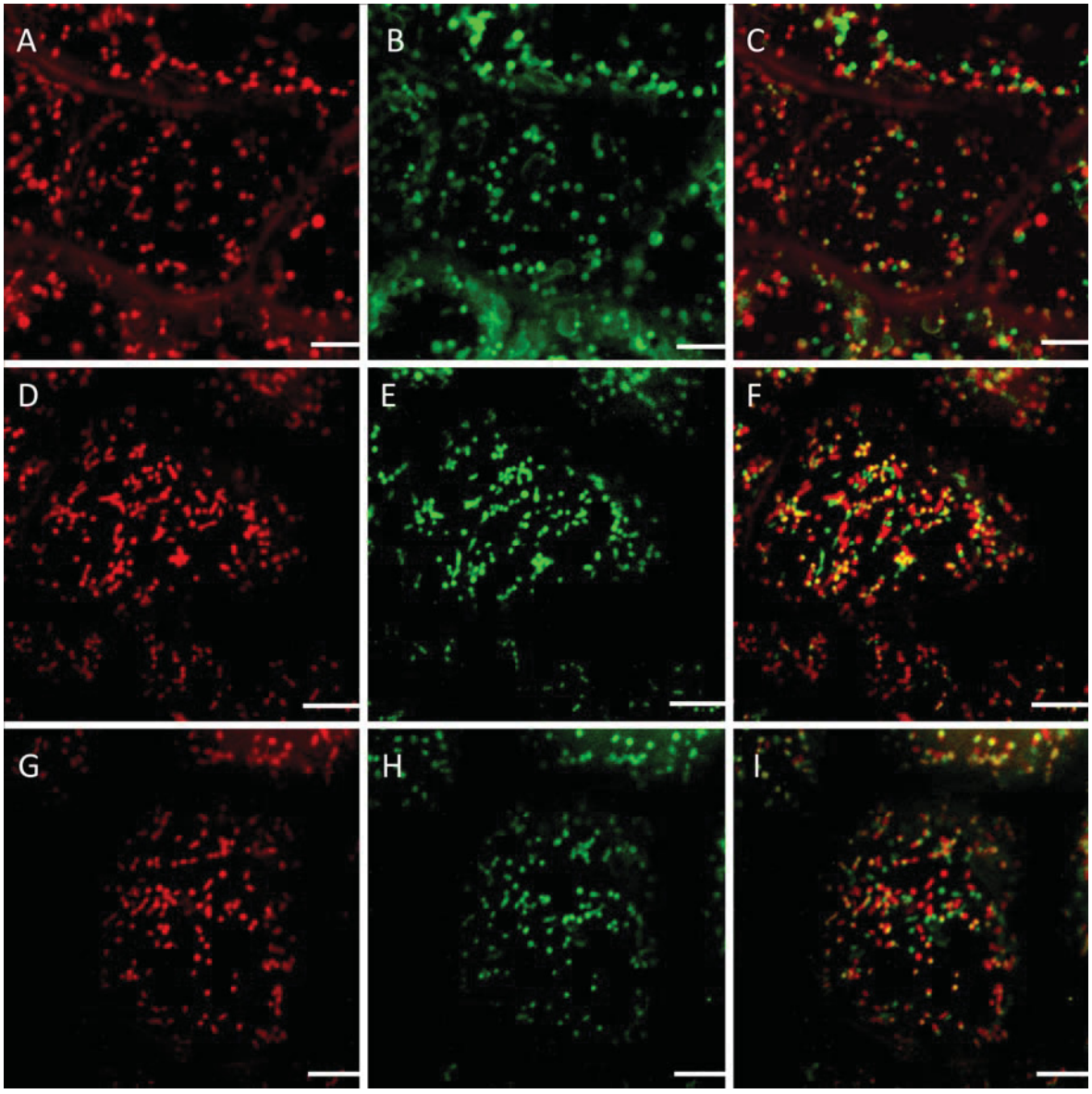

Figure 4.11 *In vivo* Examination of Mitochondrial Motility and Membrane Potential Following Pre-Treatment With the MPTP Inhibitor CsA

Chapter 5 Unveiling Interactions Among Mitochondria, Caspase-Like Proteases, and the Actin Cytoskeleton During Plant Programmed Cell Death (PCD)

Published as:

Lord CEN, Dauphinee AN, Watts RL, Gunawardena AHLAN (2013) Unveiling Interactions among Mitochondria, Caspase-Like Proteases, and the Actin Cytoskeleton during Plant Programmed Cell Death (PCD). Plos one, accepted

5.1 Abstract

Aponogeton madagascariensis produces perforations over its leaf surface via programmed cell death (PCD). PCD begins between longitudinal and transverse veins at the center of spaces regarded as areoles, and continues outward, stopping several cells from these veins. The gradient of PCD that exists within a single areole of leaves in an early stage of development was used as a model to investigate cellular dynamics during PCD. Mitochondria have interactions with a family of proteases known as caspases, and the actin cytoskeleton during metazoan PCD; less is known regarding these interactions during plant PCD. This study employed the actin stain Alexa Fluor 488 phalloidin, the actin depolymerizer Latrunculin B (Lat B), a synthetic caspase peptide substrate and corresponding specific inhibitors, as well as the mitochondrial pore inhibitor cyclosporine A (CsA) to analyze the role of these cellular constituents during PCD. Results depicted that YVADase (caspase-1) activity is higher during the very early stages of perforation formation, followed by the bundling and subsequent breakdown of actin. Actin depolymerization using Lat B caused no change in YVADase activity. *In vivo* inhibition of YVADase activity prevented PCD and actin breakdown, therefore substantiating actin as a likely substrate for caspase-like proteases (CLPs). The mitochondrial pore inhibitor CsA significantly decreased YVADase activity, and prevented both PCD and actin breakdown; therefore suggesting the mitochondria as a possible trigger for CLPs during PCD in the lace plant. To our knowledge, this is the first *in vivo* study using either caspase-1 inhibitor (Ac-YVAD-CMK) or CsA, following which the actin cytoskeleton was examined. Overall, our findings suggest the mitochondria as a possible upstream

activator of YVADase activity and implicate these proteases as potential initiators of actin breakdown during perforation formation via PCD in the lace plant.

5.2 Introduction

5.2.1 Programmed Cell Death (PCD) in Plants

Programmed cell death (PCD) is an active process resulting in the death of cells within an organism, and is pervasive throughout eukaryotes. Within plant systems, developmentally regulated PCD occurs throughout the life cycle (reviewed by Rogers 2005; reviewed by Kacprzyk et al. 2011). Examples of developmentally regulated PCD include the deletion of the embryonic suspensor (Giuliani et al. 2002; reviewed by Rogers 2005) self-incompatibility (SI) in pollen (Thomas and Franklin-Tong 2004; reviewed by Rogers 2005; reviewed by Kacprzyk et al. 2011) and leaf morphogenesis, as is seen in the lace plant (*Aponogeton madagascariensis;* Gunawardena et al. 2004; reviewed by Gunawardena 2008; Wright et al. 2009). The mitochondria (reviewed by Jones 2000; reviewed by Wang and Youle 2009), caspases (reviewed by Denault and Salvesen 2002; Potten and Wilson 2004; *C*ysteine *ASP*artate-specific prote*ASES),* and the actin cytoskeleton (reviewed by Franklin-Tong and Gourlay 2008) have been implicated in animal PCD, though less is known regarding the dynamics of these cellular components during PCD in plants.

5.2.2 The Mitochondria and PCD

In Metazoans, mitochondria aid in PCD via the release of intermembrane space (IMS) proteins, including cytochrome *c* (cyt-*c*), into the cytosol (reviewed by Jones 2000;

reviewed by Wang and Youle 2009). IMS proteins are often released via rupture or permeabilization of the outer mitochondrial membrane (OMM), usually as a consequence of mitochondrial permeability transition pore (MPTP) formation (Potten and Wilson 2004; reviewed by Kroemer et al. 2007; reviewed by Wang and Youle 2009). Mitochondria have also been implicated in plant PCD (Arpagaus et al. 2002; Yao et al. 2004; Diamond and McCabe 2007; Scott and Logan 2007, 2008; reviewed by Kacprzyk et al. 2011; Lord et al. 2011) where the release of IMS proteins, including cyt-*c,* has been detected in a number of systems (Curtis and Wolpert 2002; Balk et al. 2003; Yao et al. 2004; Vacca et al. 2006; Contran et al. 2007). The MPTP inhibitor cyclosporine A (CsA) has been shown to prevent PCD in a variety of animal (reviewed by Crompton 1999; Potten and Wilson 2004) and plant (Contran et al. 2007; Scott and Logan 2008; Lord and Gunawardena 2011) systems.

Following the release of cyt-*c* in animal cells, it binds with the apoptosis activating factor-1 (Apaf-1) in the cytosol forming the apoptosome, a complex that is capable of activating caspases to further PCD. Work completed by van der Biezen and Jones (1998) suggested the role of an apoptosome-like structure in plants, one which is hypothesized to activate downstream caspase-like proteases (CLPs; van der Biezen and Jones 1998). Although additional research on the topic is scarce, it is suggested that plant resistance gene (R-gene) products may act analogously as controlling adaptors in a plant protein structure (reviewed by Hoeberichts and Woltering 2003).

5.2.3 Caspases and Caspase-Like Proteases (CLPs)

Caspases play a fundamental role during PCD in animals, cleaving protein substrates adjacent to aspartate (Asp) residues (reviewed by Denault and Salvesen 2002; reviewed by Hoeberichts and Woltering 2003; Potten and Wilson 2004). Caspase-1 possesses a substrate specificity for the peptide sequence Tyr-Val-Ala-Asp (YVAD), while caspase-3 has been shown to have an affinity for Asp-Glu-Val-Asp (DEVD; reviewed by Piszczek and Gutman 2007). Currently, no true caspases have been found within plant systems, although evidence suggests that CLPs exist (reviewed by Sanmartin et al. 2005; reviewed by Piszczek and Gutman 2007; reviewed by Bonneau et al. 2008). A main group of CLPs, cysteine endopeptidases, are further subdivided into two groups: vacuolar processing enzymes (VPEs; reviewed by Chowdhury et al. 2008; reviewed by Bonneau et al. 2008) and metacaspases (Hara-Nishimura et al. 2005; Bozhkov et al. 2005; reviewed by Chowdhury et al. 2008; Bonneau et al. 2008). VPEs resemble true caspases in protein structure and recognize Asp when it is part of a YVAD sequence, analogous to caspase-1 (reviewed by Chowdhury et al. 2008). Synthetic caspase inhibitors have been used to stop PCD in both plant (reviewed by Bonneau et al. 2008) and animal (reviewed by Denault and Salvesen 2002) systems and provide further evidence for CLPs in plants.

5.2.4 The Cytoskeleton

Globular actin (G-actin) monomers assemble to form filamentous actin (F-actin); two F-actin filaments produce a single microfilament, the main component of the actin cytoskeleton. Actin has been implicated in the plant PCD process (Bozhkov et al. 2004; reviewed by Smertenko and Franklin-Tong 2011) where it undergoes a variety of

morphological changes including: depolymerization followed by subsequent aggregation into punctate foci during SI in both *Papaver rhoeas* (Poppy; Poulter et al. 2010) and *Pyrus pyrifolia* pollen (Liu et al. 2007); as well as bundling into dense cables during the hypersensitive response (HR) in tobacco By-2 cells (Higaki et al. 2007).

The actin cytoskeleton has been shown to be an effector as well as a target during PCD signalling (Staiger and Franklin-Tong 2003; Gourlay and Ayscough 2005). In animals, caspases have been shown to cleave cytoplasmic proteins including actin (reviewed by Hoeberichts and Woltering 2003; Liu et al. 2007; Higaki et al. 2007; reviewed by Franklin-Tong and Gourlay 2008). Conversely, in plants these associations are not as easily discernible. In 2006, Thomas et al. concluded that actin depolymerization using Latrunculin B (Lat B) induced caspase-3-like activity in *Papaver rhoeas* pollen. This pathway of induction was confirmed in 2008 by Franklin-Tong and Gourlay, (reviewed by Franklin-Tong and Gourlay 2008) where it was demonstrated that actin depolymerization using Lat B was sufficient to trigger CLP activity. However, in 2007 Vercammen et al. proposed that the metacaspase gene *mcII-Pa* may, like animal caspases, regulate actin organization during *Picea abies* suspensor differentiation.

5.2.5 The Lace Plant and Programmed Cell Death (PCD)

The lace plant (*Aponogeton madagascariensis*) is an aquatic monocot that forms perforations between longitudinal and transverse veins in spaces known as areoles, over its entire leaf surface via PCD (Gunawardena et al. 2004; Wright et al. 2009). PCD begins in the center of these areoles and radiates outwards, stopping four to five cells from the veins. The lace plant provides an ideal system for studying PCD for several

reasons including: a developed method for sterile culture, nearly transparent leaves, as well as a predictable pattern of perforation formation (Gunawardena et al. 2004, 2007; Wright et al. 2009; Wertman et al. 2012; reviewed by Lord and Gunawardena 2012). The process of perforation formation has been previously divided into the five following stages: 1. Pre-perforation, 2. Window, 3. Perforation formation, 4. Perforation expansion, 5. Mature perforation (Gunawardena et al. 2004). Within a single areole of a window stage leaf, cell death has been further subdivided based on the progression of PCD, and is visibly discernable by colour differences (Lord et al. 2011). The cells closest to the vasculature are control cells or non-PCD (NPCD); these cells are initially pink in colour due to the pigment anthocyanin found in the vacuole. The next division contains cells in the early stages of PCD (EPCD); green pigmentation is notable in these cells due to the abundance of chloroplasts and loss of anthocyanin. The third area is comprised of cells in the late stages of PCD (LPCD), which are nearly void of both pigments. Using this cell death gradient, the dynamics of organelles including the mitochondria, chloroplasts, actin cytoskeleton, nucleus and vacuole have been investigated throughout PCD. These observations were used to establish the order of cellular events during lace plant PCD (Wertman et al. 2012).

This paper attempts to shed light on the interactions among the mitochondria, CLPs and the actin cytoskeleton during developmentally regulated PCD in the novel model species *A. madagascariensis*; biochemical analyses, pharmacological experimentation and advanced microscopy techniques were used to achieve this aim.

5.3 Materials and Methods:

5.3.1 Plant Materials

All plant materials were grown and subcultured as described in section 2.3.1 within Chapter 2. All chemicals were purchased from Sigma-Aldrich (St Louis, MO, USA), unless otherwise stated. All experiments were completed at least three times unless otherwise stated.

5.3.2 Light Microscopy

Micrographs of leaf stages and representative half areoles following treatments were acquired as described in section 2.3.4 within Chapter 2. All composite plates were assembled using Adobe Photoshop version 10.0 (Adobe Systems Inc., San Jose, California, USA).

5.3.3 Confocal Laser Scanning Microscopy

Confocal investigations were performed as described in section 4.3.3 within Chapter 4.

5.3.4 Pharmacological Treatments

5.3.4.1 Caspase-1 Inhibitor

Caspase-1 inhibitor II (Ac-YVAD-CMK; Cat # 400012, Calbiochem, Darmstadt, Germany) is a cell permeable irreversible L-1β Converting Enzyme (ICE) inhibitor. Five mg of the inhibitor was dissolved in 108.2 µl DMSO (final concentration 92.42 mM) and added directly into 20 mL sterile Murashige and Skoog (MS) medium (final concentration 0.462 mM), the solution was then filter sterilized. Healthy plants approximately 4 weeks of age with at least two perforated leaves were divided at random

into experimental or control groups. The plants were then transferred aseptically into 40 mL glass growth vials (one per vial), into which the sterile caspase inhibitor + MS solution was added. Plants were allowed to grow for 7 days at which time the leaf that was produced was excised, photographed and stained with Alexa Fluor 488 phalloidin as described below.

5.3.4.2 Latrunculin B

A gradient of concentrations and incubation times for Lat B treatments were tested. Concentrations of 1 µM, 5 µM, 10 µM, 25 µM and 75 µM were tested at 3 and 6 hr incubation, following which 25 µM and 75 µM were concluded to be toxic. Subsequently, 1 µM, 5 µM and 10 µM were tested at 10 min, 30 min, and 1 hr incubation. The combination of 1 µM in dH_2O for 30 min was determined to be suitable. Window stage leaves were excised from whole plants and were treated with a Lat B solution (stock dissolved in dimethyl sulfoxide DMSO) at the time and concentration noted above in 20 mL Petri dishes; control leaves received an equal amount of DMSO. Leaves were then rinsed thoroughly with dH_2O and either stained with Alexa Fluor 488 phalloidin to examine the cytoskeleton, or pre-perforation leaves were assayed for CLP activity using the flourometric assay as described below. To ensure growth, development and experimental outcomes were accurate from excised leaf samples, whole plant experiments were also completed with Lat B. These experiments were completed in vials as described for caspase-1 inhibitor treatments above. No observable differences in parameters were noted between the excised leaf and whole plant Lat B experiments (data not shown).

5.3.4.3 CsA

Healthy plants approximately 4 weeks of age, containing at least two perforated leaves, were divided at random into experimental or control groups. Under aseptic conditions, liquid medium was poured out of each magenta box and replaced with 200 mL of fresh liquid medium; treatment groups received CsA stock solution (dissolved in 90% ethanol) to a final concentration of 10 μM (as optimized in Lord et al. 2011) and control plants received an equal volume of ethanol. Plants were then returned to growth racks under normal light conditions for 7 days until the first representative window stage leaf had formed, at which time the leaf was harvested, photographed and stained with Alexa Fluor 488 phalloidin as described below.

5.3.5 In Vitro Caspase Substrate Cleavage Assay

Lace plant leaves taken from varying stages of perforation formation (pre-perforation, window and mature; six independent experiments, two replicates per experiment), had their midribs removed, weighed, and then frozen overnight in liquid nitrogen. CsA or Lat B treated leaves (three independent experiments, two replicates per experiment) used for the assay were at the pre-perforation stage of leaf development for comparison with non-treated samples. Samples were then ground in assay buffer (100mM HEPES, 10% sucrose, 0.1% CHAPS, 5mM DTT, pH 6.5) on ice. The tissue homogenate was centrifuged at 15,000 rpm at 4°C for 15 min and the supernatant was collected. Protein concentration in the cell extract was determined by Bradford assay (BioRad, Hercules, CA, USA). Proteolytic activity was measured in 160 μl reaction solution containing approximately 200 μg of protein and 50 μM of AFC-conjugated peptide

(BioVision, Cat #K110-100, Milpitas, CA, USA) specific to mammalian caspase-1. Double reactions were incubated for 1.5 hr at 37°C and fluorescence readings of ice-cold samples were taken at 5 min intervals with an excitation of 390/20 nm and an emission of 510/10 nm (Fluoroskan Ascent, Thermo Scientific, Marietta, OH, USA). Readings were measured and compared against a blank containing assay buffer and AFC-conjugated peptide, without protein. Kinetics of substrate hydrolysis were linear throughout the first hour of the reaction, following which the curve plateaued. A 0.005-0.5 μM AFC standard, diluted in assay buffer, was used to conclude the amount of fluorochrome released. Final proteolytic activity is expressed in pmol/min/mg protein cleaved. Active caspase-1 (BioVision, Cat.# 1081-25) was used as a positive control (data not shown). Each CsA and Lat B experiment contained two controls. The first being an experimental control, in which leaves were treated with the same solvent as the drug in use; a second control consisted of non-treated pre-perforation leaves where no solvent was used.

5.3.6 Alexa Fluor 488 Phalloidin and Propidium Iodide Staining

Leaves were obtained from sterile cultures no more than 5 hr prior to fixation. The staining protocol was modified from Wertman et al. (2012) and Poulter et al. (2008). Initially, 10 mL of a 4% paraformaldehyde (BioShop Canada Inc., Burlington, Ontario, Canada) solution was made in an actin-stabilizing buffer (ASB; 100 mM Pipes, pH 6.80), 1 mM $MgCl_2$, 1 mM $CaCl_2$, 75 mM KCl) and set aside. Next, sterile leaves were cut into 5 mm by 5 mm pieces with a razor blade and placed in 10 mL of a 0.4 mM 3-Maleimidobenzoic acid *N*-hydroxysuccinimide ester (MBS), in ASB for 10 min. After 10 min, the paraformaldehyde solution was added drop wise to the MBS solution for a final

paraformaldehyde concentration of 2% and was incubated for 3 hr at 4°C. Following fixation leaves were rinsed three times over 20 min in ASB and placed on a multi-welled slide. For leaf samples from all stages excluding mature, a staining solution containing 0.1 μM Alexa Fluor 488 phalloidin (Invitrogen Canada Inc., Burlington, Ontario, Canada) and 0.1% Triton X-100 in ASB was used. For mature stage leaf samples, a staining solution containing 0.2 μM Alexa Fluor 488 phalloidin (Invitrogen) and 0.1% Triton X-100 in ASB was used. Samples were placed in a humidity chamber, wrapped in tinfoil and incubated overnight at 4°C. Following overnight incubation, staining solution was aspirated off, samples were rinsed in ASB and subsequently stained with 0.5 mg/mL propidium iodide (PI) for approximately 5 min. Samples were again rinsed in ASB and mounted in Gel/Mount™ (Biomeda Corp., Foster City, California, USA) on glass slides, cover slipped, sealed with clear nail polish, and viewed via confocal microscopy as described above.

5.3.7 Actin Width and Intensity Quantification

Both actin width and intensity were quantified given that the parameter width (measured within a single micrograph of a z-stack series) took into account the thickness of actin and alone was not a strong indicator of actin breakdown. This was evident from actin staining in LPCD cells that often retained actin thickness, but had been dramatically degraded at both ends. Intensity (measured in maximum projected z-stack micrographs) was able to take into account the degradation of actin microfilament bundles from the ends.

Actin width was measured by acquiring micrographs with the confocal microscope as described above. For non-treated control leaves approximately 50 images (approximately 25 z-stacks per image) were acquired for each stage of PCD. Approximately 150 filaments (three filaments per image) for each stage were measured (five independent experiments were completed, approximately three leaves utilized per experiment). For Lat B treated leaves approximately 20 images (25 z-stacks per image) were acquired for each stage of PCD. Approximately 50 individual filaments (approximately 2.5 filaments per image) for each stage were measured (five independent experiments were completed, approximately two leaves utilized per experiment). For caspase-1 inhibitor treated leaves approximately 40 images (25 z-stacks per image) were acquired for each stage of PCD. Approximately 160 individual filaments (four filaments per image) for each stage were measured (three independent experiments were completed, approximately three leaves utilized per experiment). For CsA treated leaves approximately 20 images (25 z-stacks per image) were acquired for each stage of PCD. Approximately 80 individual filaments (four filaments per image) for each stage were measured (three independent experiments were completed, approximately 3 leaves utilized per experiment). For more accurate width measurements, images from each stage of PCD, for each treatment were magnified using an after-capture zoom function on EZ-C1 3.80 analysis software. The mean of all widths from each treatment for each stage were then calculated for statistical analysis.

Actin intensity was measured by acquiring micrographs with the confocal microscope as described above. In all cases maximum projected micrographs were cropped to 1300 μm^3 and intensity was measured in a.u. using EZ-C1 3.80 analysis

software. For non-treated leaves approximately 40 images (40 z-stacks per maximum projected image) were acquired for each stage of PCD (5 independent experiments were completed, approximately three leaves utilized per experiment). For Lat B trials approximately 25 images (40 z-stacks per maximum projected image) were acquired for each stage of PCD (five independent experiments were completed, approximately three leaves utilized per experiment). For caspase-1 inhibitor trials, approximately 20 images (40 z-stacks per maximum projected image) were acquired for each stage of PCD (three independent experiments were completed, approximately three leaves utilized per experiment). Lastly, for CsA trials approximately 30 images (40 z-stacks per maximum projected image) were acquired for each stage of PCD (three independent experiments were completed, approximately three leaves utilized per experiment). The means of all intensities for each treatment for each stage were then calculated for statistical analysis.

The data for width and intensity for each treatment (Lat B, caspase-1 inhibitor and CsA) from each stage of PCD (NPCD, EPCD and LPCD) was compared to two sets of control data; non-treated controls, and experimental controls, that were given an equal volume of the solvent used to dissolve the corresponding treatment.

5.3.8 Statistical Analysis

All data were assessed as described in section 2.3.6 within Chapter 2.

5.4 Results

5.4.1 Caspase-Like Activity During PCD in the Lace Plant

To determine if and when CLP activity occurred during PCD in the lace plant, the ability of pre-perforation, window and mature stage leaves to cleave the synthetic peptide substrate YVAD-AFC was compared. The cleavage rates of the substrate varied significantly among all three stages of leaf development ($P \leq 0.05$; Figure 5.1).

5.4.2 The Actin-Cytoskeleton During PCD in the Lace Plant

Lace plant leaves were stained with Alexa Fluor 488 phalloidin to visualize actin and examined over the five stages of leaf development (Figure 5.2). In pre-perforation stage leaves actin appeared thin and organized, with no bundling or visual breakdown (Figure 5.2A, F and K). Conversely, in window stage leaves there appeared to be variations in actin organization across the gradient of PCD within an areole (Wertman et al. 2012; Figure 5.2B, G and L). Actin breakdown in the center of areoles was extensive in perforation formation leaves (Figure 5.2C, H and M) and continued to progress to the perforation border throughout leaf development, from perforation expansion (Figure 5.2D, I and N) to mature leaves (Figure 5.2E, J and O).

The gradient of PCD within a single areole of a window stage leaf was used to quantify actin dynamics during PCD on a detailed level (Figure 5.3). Both actin width and intensity were quantified. All mean actin widths varied significantly between NPCD (0.38 μm), EPCD (1.17 μm) and LPCD (0.82 μm; $P \leq 0.05$; Figure 5.3B-E). Groupings of actin within NPCD cells were thin, and often organized in a parallel fashion (Figure 5.3B; highlighted in inset). Actin organized into thick bundles during EPCD (Figure 5.3C; highlighted in inset) and began to breakdown during LPCD (Figure 5.3D; highlighted in inset). All mean actin intensities varied significantly among NPCD (848.72 a.u.), EPCD

(717.70 a.u.) and LPCD (240.86 a.u.; $P \leq 0.05$; Figure 5.3F-I). NPCD cells illustrated a thin layer of actin that underlayed the PM in a fine mesh (Figure 5.3F). Actin within EPCD cells was less consistent and bundling of microfilaments caused gaps or breaks in the coating (Figure 5.3G). LPCD cells depicted actin that was severely broken down and often missing in particular cells. Less frequently, actin within LPCD cells was visualized as small punctate foci (Figure 5.3H; highlighted in inset).

Following actin depolymerization with Lat B treatment, leaves were stained with Alexa Fluor 488 phalloidin and actin was quantified (Figure 5.4). Figure 5.4A displays half of a single representative areole following Lat B treatment; note that the areole appears as if it will produce a perforation as denoted by pigment loss in EPCD and LPCD stage cells. Both mean actin width and intensity were quantified. The mean actin width for NPCD cells (0.44 μm; Figure 5.4B and E) following Lat B treatment did not vary significantly from NPCD non-treated controls (0.38 μm; $P \geq 0.05$; Figure 5.4E). However, mean actin width for EPCD cells (0.68 μm; Figure 5.4C and E) and LPCD cells (0.50 μm; Figure 5.4D and E) following Lat B treatment did vary significantly from their non-treated controls ($P \leq 0.05$; Figure 5.4E). Examining mean actin intensities following Lat B treatment, NPCD (19.5 a.u.; Figure 5.4F and I), EPCD (34.35 a.u.; Figure 5.4G and I) and LPCD (13.0 a.u.; Figure 4H and I) all varied significantly from their non-treated controls ($P \leq 0.05$; Figure 5.4I). Lat B experimental controls did not vary significantly from non-treated controls for the same stage ($P \geq 0.05$; Figure 5.4I).

Additionally, pre-perforation leaves were treated with Lat B and CLP activity was measured using a caspase-1 flourometric assay. We observed that cleavage rates of the synthetic peptide substrate (YVAD-AFC) did not diverge significantly from non-treated

pre-perforation controls ($P \geq 0.05$; Figure 5.5). Mitochondria were also examined using Mito Tracker Red (CMXRos) following Lat B treatment and depicted normal mitochondrial staining (data not shown).

5.4.3 Caspase-1 Inhibitors and Lace Plant PCD

A caspase-1 inhibitor was applied *in vivo* and whole plants were then grown for 7 days. Leaves that emerged post-treatment contained no perforations; these leaves were subsequently stained with Alexa Fluor 488 phalloidin to observe actin (Figure 5.6). Figure 5.6A displays half of a representative areole following caspase-1 inhibitor treatment; note that a loss of pigmentation is not present in this areole, indicating a perforation will not form. Both mean actin width and intensity were quantified. The mean actin width for NPCD cells (0.33 μm; Figure 5.6B and E) following caspase-1 inhibitor treatment did not vary significantly from NPCD non-treated controls ($P \geq 0.05$; Figure 5.6E). However, mean actin width for EPCD cells (0.33 μm; Figure 5.6C and E) and LPCD cells (0.35 μm; Figure 5.6D and E) did vary significantly from non-treated controls ($P \leq 0.05$; Figure 5.6E). EPCD and LPCD mean actin widths did not vary significantly from NPCD non-treated controls (0.38 μm; $P \geq 0.05$; Figure 5.6E). Likewise, NPCD, EPCD and LPCD mean actin widths did not vary significantly from one another ($P \leq 0.05$; Figure 5.6E). Examining mean actin intensities following caspase-1 inhibitor treatment, NPCD (860.77 a.u.; Figure 5.6F and I) and EPCD (874.40 a.u.; Figure 5.6G and I) did not vary significantly from non-treated controls ($P \geq 0.05$; Figure 5.6I). However, LPCD (838.37 a.u.; Figure 5.6H and I) varied significantly from non-treated controls ($P \leq 0.05$; Figure 5.6I). EPCD and LPCD mean actin intensities did not

vary significantly from NPCD non-treated controls ($P \geq 0.05$; Figure 5.6I). Likewise, NPCD, EPCD and LPCD mean actin intensities did not vary significantly from one another ($P \leq 0.05$; Figure 5.6I).

Additionally, all caspase-1 inhibitor treatment controls did not vary significantly from non-treated controls for the same stage ($P \geq 0.05$). Mitochondria were also examined via Mito Tracker Red (CMXRos) following caspase inhibition and depicted normal mitochondrial staining (data not shown).

5.4.4 The Mitochondria, Actin and CLPs in the Lace Plant

To determine the role of the mitochondria in conjunction with CLPs and the actin cytoskeleton during lace plant PCD, plants were treated *in vivo* with CsA. Leaves that emerged following treatment contained no perforations; these leaves were subsequently stained with Alexa Fluor 488 phalloidin to quantify actin (Figure 5.7). Figure 5.7A displays half of a representative areole following CsA treatment. The typical gradient of cell death is not present indicating a perforation will not form (note: CsA treated leaves showed a different colouration from typical lace plant window stage leaves; perhaps due to the ethanol solvent). Both mean actin microfilament width and intensity were quantified. The mean actin width for NPCD cells (0.39 μm; Figure 5.7B and E) following CsA treatment did not vary significantly from NPCD non-treated controls ($P \geq 0.05$; Figure 5.7E). However, mean actin width for EPCD cells (0.39 μm; Figure 5.7C and E) and LPCD cells (0.38 μm; Figure 5.7D and E) did vary significantly from non-treated controls within their groups ($P \leq 0.05$; Figure 5.7E). EPCD and LPCD mean actin widths did not vary significantly from NPCD non-treated controls ($P \geq 0.05$; Figure 5.7E).

Likewise, NPCD, EPCD and LPCD mean actin widths did not vary significantly from one another ($P \leq 0.05$; Figure 5.7E). Examining mean actin intensities following CsA treatment, NPCD (844.50 a.u.; Figure 5.7F and I) and EPCD (836.31 a.u.; Figure 5.7G and I) did not vary significantly from non-treated controls ($P \geq 0.05$; Figure 5.7I). However, LPCD (858.30 a.u.; Figure 5.7H and I) varied significantly from non-treated controls ($P \leq 0.05$; Figure 5.7I). EPCD and LPCD mean actin intensities did not vary significantly from NPCD non-treated controls ($P \geq 0.05$; Figure 5.7I). Likewise, NPCD, EPCD and LPCD mean actin widths did not vary significantly from one another ($P \leq 0.05$; Figure 5.7I). Additionally, all CsA treatment controls did not vary significantly from non-treated controls for the same stage ($P \geq 0.05$).

Following treatment of whole plants with CsA, leaves at the pre-perforation stage of development were assayed for CLP activity using a caspase-1 flourometric assay. Cleavage rates of the synthetic peptide substrate (YVAD-AFC) diverged significantly from non-treated control pre-perforation leaves ($P \leq 0.05$; Figure 5.5).

5.5 Discussion

5.5.1 Caspase-Like Activity During PCD in the Lace Plant

Data presented here suggests that perforation formation within lace plant leaves requires the activation of a protease or group of proteases, which preferentially cleave YVAD sequence-containing substrates. Cleavage of a substrate containing YVAD mimics activity of caspase-1 during mammalian apoptosis (Bonneau et al. 2008; reviewed by Lord and Gunawardena 2012). CLP (caspase-1) activity was determined to be the highest during the pre-perforation stage of leaf development, as compared to

window and mature stage leaves (Figure 5.1). Thus it is likely that CLP activity is higher prior to the visible initiation of PCD as compared to mature stage leaves, where the process is complete. This hypothesis would be better concretized via CLP activity measurements in leaf primordia found surrounding the shoot apical meristem, prior to the pre-perforation stage of leaf development; however obtaining sufficient protein concentrations from these small leaf primordia is not feasible. This early initiation of CLP activity was also noted during Norway spruce autophagic cell death in embryonal tube cells where *in vivo* studies identified VEIDase (caspase-3) activity at the beginning of the execution phase of cell death (Bozhkov et al. 2004).

5.5.2 The Actin-Cytoskeleton During PCD in the Lace Plant

The actin cytoskeleton has been implicated in plant PCD (reviewed by Smertenko and Franklin-Tong 2011) and therefore was examined extensively in the present study. Across the five stages of leaf development it was apparent that visible alterations in actin did not begin to occur until the window stage of leaf development (Figure 5.2); this evidence indicates that CLPs (highest during the pre-perforation stage), are likely upstream of actin microfilament modifications. The thin linear actin seen in NPCD (Figure 5.3B) is essential as a framework for cellular structure, and allows myosin-based motors to transport organelles throughout the cytosol (Liu et al. 2007). The bundling of actin seen in EPCD (Figure 5.3C) is comparable to the longitudinal thick fibres found during embryogenesis in *Picea abies* (Smertenko et al. 2003; Schwarzerová et al. 2010; Mishra et al. 2011) or the bundles of actin directed towards infection sites following the HR in *Arabidopsis* (Takemoto et al. 2003). The reason for this bundling within the lace

plant system is still not well understood and requires further investigation. The breakdown of actin, followed by its subsequent aggregation into punctate foci seen in LPCD (Figure 5.3H, highlighted in inset) is reminiscent of actin dynamics during SI in both *Papaver rhoeas* (Poulter et al. 2010) and *Pyrus pyrifolia* pollen (Liu et al. 2007). However, in *Papaver rhoeas* this depolymerization was necessary and sufficient for triggering PCD (Staiger and Franklin-Tong 2003; reviewed by Franklin-Tong and Gourlay 2008).

The application of the actin depolymerization drug Lat B (1μM) showed normal leaf growth and PCD processes (data not shown). Therefore, it can be concluded that actin microfilaments may not be crucial executors of PCD as described in poppy pollen, (Staiger and Franklin-Tong 2003; reviewed by Franklin-Tong and Gourlay 2008) but may be downstream substrates for CLPs. Figure 5.4 displays cytoskeleton dynamics following Lat B treatment. Actin width and intensity varied significantly between treatments and non-treated controls at every point except for NPCD actin width. This reduction in the breakdown of filamentous actin in NPCD cells suggests a limited effect of the depolymerization agent, and infers the presence of very stable microfilaments, perhaps as a consequence of these cells not being genetically primed to die. No punctate foci were present within Lat B treated samples, signifying that foci produced during lace plant PCD may not be as resistant as those found in *Papaver rhoeas* (Poulter et al. 2010), where it was reported that foci were extremely stable and unaffected by treatment with actin depolymerizers. Within metazoan PCD, it has been demonstrated that caspases act upon the actin cytoskeleton. In the lace plant system, actin was depolymerized via Lat B within pre-perforation leaves and CLP activity measured. Results suggest that

cytoskeleton depolymerization (1 μM for 30 min) has no effect on CLP activity (Figure 5.5) thus providing additional evidence for CLPs upstream of actin cytoskeleton breakdown. As noted above this sequence of events is in contrast to the pathway recognized in *Papaver rhoeas,* where actin is thought to be the trigger of CLP activity (Staiger and Franklin-Tong 2003; Liu et al. 2007; reviewed by Franklin-Tong and Gourlay 2008); however our results are in agreement with evidence from animal systems where caspases cleave filamentous actin (reviewed by Hoeberichts and Woltering 2003; Liu et al. 2007; Higaki et al. 2007; reviewed by Franklin-Tong and Gourlay 2008). The authors speculate that the use of a higher concentration of Lat B may be able to induce CLP activity, possibly through a non-developmental PCD pathway, although this requires further investigation.

5.5.3 Caspase-1 Inhibitor and the Lace Plant

To determine if CLPs were acting upon the actin cytoskeleton, causing breakdown, as is seen within metazoan PCD, caspase-1 inhibitor (Acetyl-YVAD-aldehyde or Ac-YVAD-CMK) experiments were completed. To the best of these authors knowledge this is the first example in which a whole plant has been treated *in vivo* with such an inhibitor. Ac-YVAD-CMK is a commonly used inhibitor within plant systems with, Ac-YVAD-CHO shown to suppress cell death in tobacco mosaic virus (TMV) induced PCD, while Ac-DEVD-CHO had no effect (Hatsugai et al. 2004). On the contrary, during PCD in *Papaver rhoeas* pollen SI, Ac-DEVD-CHO was shown to suppress PCD while Ac-YVAD-CHO did not (Hatsugai et al. 2004; Thomas and Franklin-Tong 2004). Additionally, for the first time within the literature, actin width and

intensity were quantified following CLP inhibition. Results depicted that all NPCD, EPCD and LPCD treatments did not vary significantly from NPCD non-treated controls (Figure 5.6); this suggests that the inhibition of YVADase activity blocked actin dynamic changes. Overall, these *in vivo* experiments further support the notion that YVADase activity may play a role in actin breakdown during leaf morphogenesis in the lace plant.

5.5.4 The Mitochondria, Actin and CLPs in the Lace Plant

Within metazoan PCD it has been demonstrated that the release of cyt-*c* and other IMS proteins from the mitochondria have the ability to activate caspases. CsA has been shown in the past to prevent perforation formation in lace plant leaves (Lord et al. 2011), and therefore it was used in this study within pre-perforation leaves (where CLP activity was originally determined to be the highest) following which CLP activity was measured. Subsequent to CsA application, YVADase activity was determined to be significantly lower than controls (Figure 5.5), indicating that the mitochondria act upstream of YVADase activation. Following CsA treatment actin dynamics were also quantified (Figure 5.7). Lower CLP activation via the mitochondria presumably meant fewer CLPs affecting the actin cytoskeleton; this hypothesis was supported by results indicating that the actin cytoskeleton of CsA treated samples did not differ significantly from NPCD controls, or among stages (Figure 5.7). It should be noted however that although cyt-*c* release has been described in a variety of plant species, that this release does not appear to be the sole trigger for PCD in plants (Balk et al. 2003). Therefore further investigation is required in order to understand how CsA prevents PCD in the lace plant.

5.6 Acknowledgments

We thank Dr. Veronica Franklin-Tong (University of Birmingham) for helpful correspondence and discussion throughout this work. The authors thank Kendra Sauerteig (Guelph University) for the original optimization of the actin staining protocol, Jaime Wertman for critical review of the final manuscript and Dr. Brent Johnston (Dalhousie University) for the kind use of his bench top fluorometer.

5.7 Authors' Contributions[14]

CENL and RLW carried out Latrunculin B experiments, including drug application followed by subsequent Alexa Fluor 488 phalloidin staining and quantification of actin-microfilament width and intensity. CENL and AND carried out cyclosporine A (CsA) whole plant applications; CENL carried out subsequent Alexa Fluor 488 phalloidin staining and quantification of actin-microfilament width and intensity for CsA treated plants. CENL carried out caspase-1 inhibitor experiments including whole plant application followed by subsequent Alexa Fluor 488 phalloidin staining and quantification of actin-microfilament width and intensity. CENL carried out Alexa Fluor 488 phalloidin staining for the five stages of leaf development. CENL also carried out Alexa Fluor 488 phalloidin staining for the examination of the actin cytoskeleton over the gradient of PCD within a single areole of a non-treated window stage leaf (EPCD-LPCD), as well as the quantification of actin-microfilament width and intensity for these stages. CENL also completed the *in vitro* caspase-1 substrate cleavage

[14] Authors contributions are an addition to the manuscript published in Plos one, and were added to clarify the contribution of each author within the manuscript.

assay. AND compiled figures and completed all statistical analyses; AND also contributed to final manuscript revisions. AHLANG conceived the study, participated in its design and organization, helped in drafting and revising the manuscript, and supervised all experimental work.

Figure 5.1 Kinetics of YVADase Activity in Non-Treated Control Leaves

Leaf samples from pre perforation leaves (PCD not visibly detected), window stage leaves (PCD visibly occurring in central cells) and mature leaves (PCD complete) were used. Data are expressed as mean ± S.E.M. (n= 6). Data represented by different letters are significantly different ($P \leq 0.05$ ANOVA).

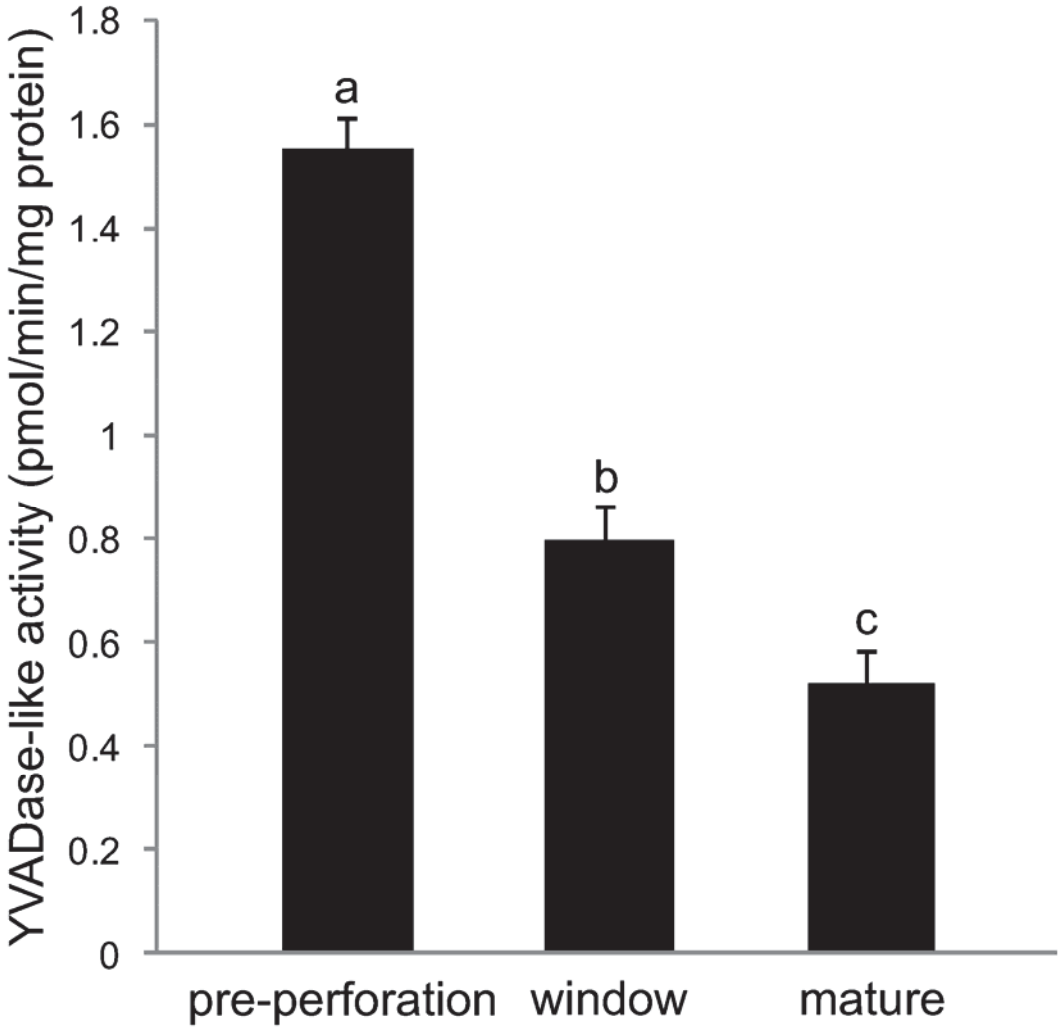

Figure 5.1 Kinetics of YVADase Activity in Non-Treated Control Leaves

Figure 5.2 Rearrangement of the Actin Cytoskeleton During Leaf Morphogenesis Over Five Stages of Leaf Development in the Lace Plant

Each image depicts a piece of a single corner of an areole (A-E). Coloured differential interference contrast (DIC) images of (A) pre perforation (B) window (C) perforation formation (D) perforation expansion and (E) mature stage leaf areoles. (F-J) Black and white DIC images of (F) pre perforation (G) window (H) perforation formation (I) perforation expansion and (J) mature stage leaves. (K-O) Fluorescent images of Alexa Fluor 488 phalloidin (green) stained areoles counterstained with propidium iodide (PI; red) of (K) pre-perforation (L) window (M) perforation formation (N) perforation expansion and (O) mature stage leaves. Please note that images A-E do not correspond with images F-O. These images are representative micrographs to illustrate the five stages of leaf development. DIC images F-J are corresponding to K-O. There is a consistent gradient of actin microfilament staining over the pre perforation areole; conversely there is variation (bundling followed by breakdown) in actin microfilament dynamics over the gradient of PCD (NPCD-LPCD) found within the single areole of the window stage leaf. Note the complete degradation and disappearance of actin microfilament staining as the perforation becomes larger, from perforation formation to the mature stage of leaf development. Scale bars = 70 μm.

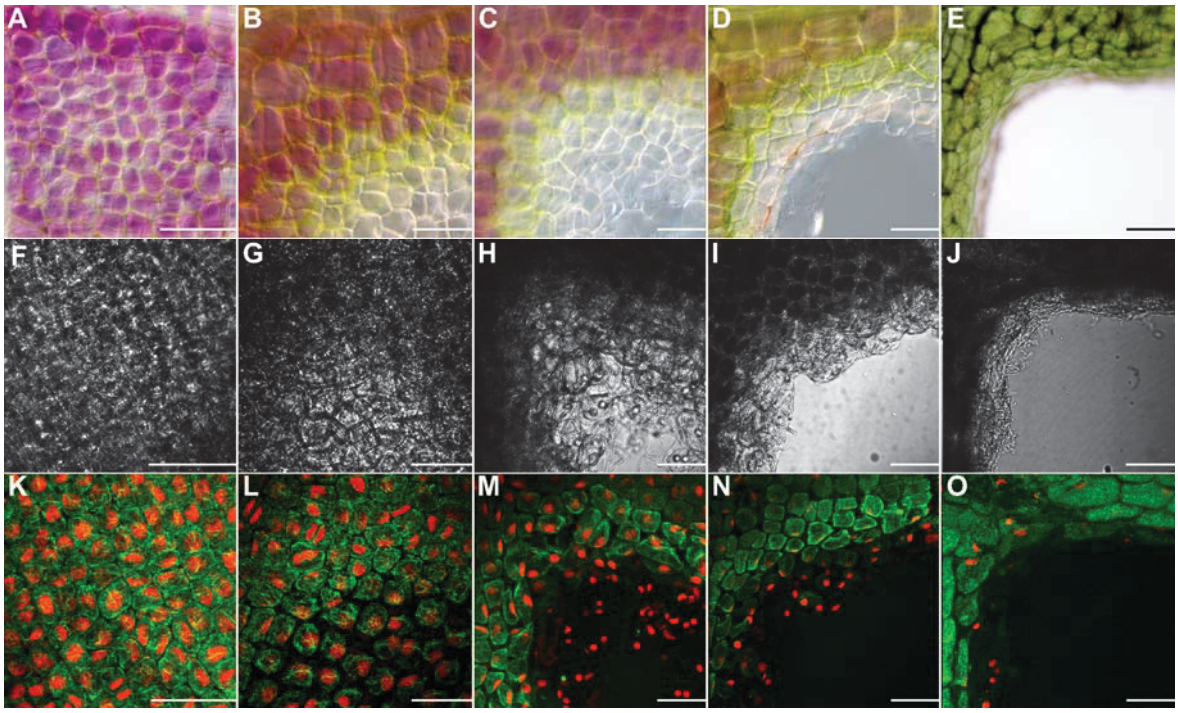

Figure 5.2 Rearrangement of the Actin Cytoskeleton During Leaf Morphogenesis Over Five Stages of Leaf Development in the Lace Plant

Figure 5.3 Rearrangement of the Actin Cytoskeleton Over a Gradient of PCD Within a Single Areole of a Non-Treated Window Stage Leaf

Cells within the lower portion of this figure (B-D and F-H) are stained with fluorescent Alexa Fluor 488 phalloidin (green) for actin and counterstained with propidium iodide (PI; red) for nuclei; tissues are fixed. (A) A representative DIC micrograph of half of a single areole of a window stage leaf demonstrating the gradient of PCD that exists over this region. Cells between the border of the image and the red line are NPCD cells and do not undergo PCD during perforation formation, cells between the red line and the blue line are in the early stages of PCD (EPCD) and cells between the blue line and the bottom of the image are in the late stages of PCD (LPCD). (B-D) Characteristic single z-stack micrographs of actin width within NPCD, EPCD and LPCD stage cells (0.38μm, 1.17μm and 0.82μm, respectively; see insets). (E) Mean widths of actin microfilaments. (F-H) Representative maximum projection micrographs of actin intensity within NPCD, EPCD and LPCD stage cells (848.72 a.u, 717.70 a.u. and 240.86 a.u, respectively). Note inset in panel H highlights punctate actin foci. All actin intensity measurements were acquired within 1300μm^3 of maximum projected z-stacks tissue. (I) Mean intensities of actin microfilaments. All error bars are representative of standard error and all data represented by different letters are significantly different within individual graphs ($P \leq 0.05$ ANOVA). Scale bars (A) = 50μm, (B-D) = 15μm, (F-H) = 25 μm.

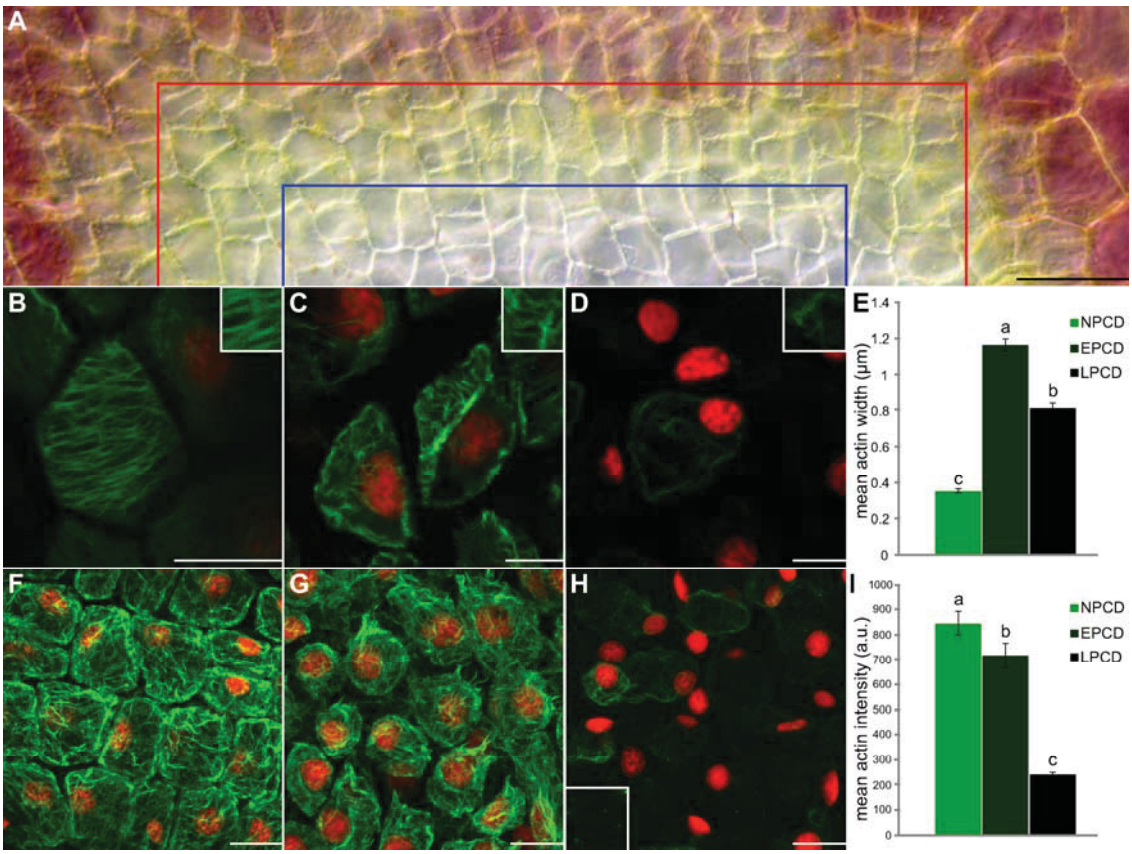

Figure 5.3 Rearrangement of the Actin Cytoskeleton Over a Gradient of PCD Within a Single Areole of a Non-Treated Window Stage Leaf

Figure 5.4 Actin Depolymerization Following Treatment With Latrunculin B (Lat B)

Cells within the lower portion of this Figure (B-D and F-H) are stained with fluorescent Alexa Fluor 488 phalloidin (green) for actin and counterstained with propidium iodide (PI; red) for nuclei; tissues are fixed (A) A representative DIC micrograph of a half of a single areole of a window stage leaf following Lat B treatment. Cells between the border of the image and the red line are representative NPCD cells, cells between the red line and the blue line are representative EPCD cells and cells between the blue line and the bottom of the image are representative LPCD cells. (B-D) Characteristic single z-stack micrographs of actin width within NPCD, EPCD and LPCD stage cells (0.44μm, 0.68μm, 0.5μm, respectively; see insets) following Lat B treatment (E) Lat B experimental data compared to non-treated leaves (control; data extracted from Figure 3) and treated controls (Lat B con). (F-H) Representative maximum projection micrographs of actin intensity within NPCD, EPCD and LPCD stage cells (19.52 a.u., 34.35 a.u. and 13.0 a.u. respectively) following Lat B treatment. All actin intensity measurements were acquired within 1300μm^3 of maximum projected z-stacks tissue. (I) Mean actin intensities for each stage of PCD. Data for non-treated controls were extracted from Figure 3. All error bars are representative of standard error and all data represented by different letters are significantly different within individual graphs ($P \leq 0.05$ ANOVA). Scale bars (A) = 45 μm, (B-D) = 20 μm, (F-H) = 25 μm.

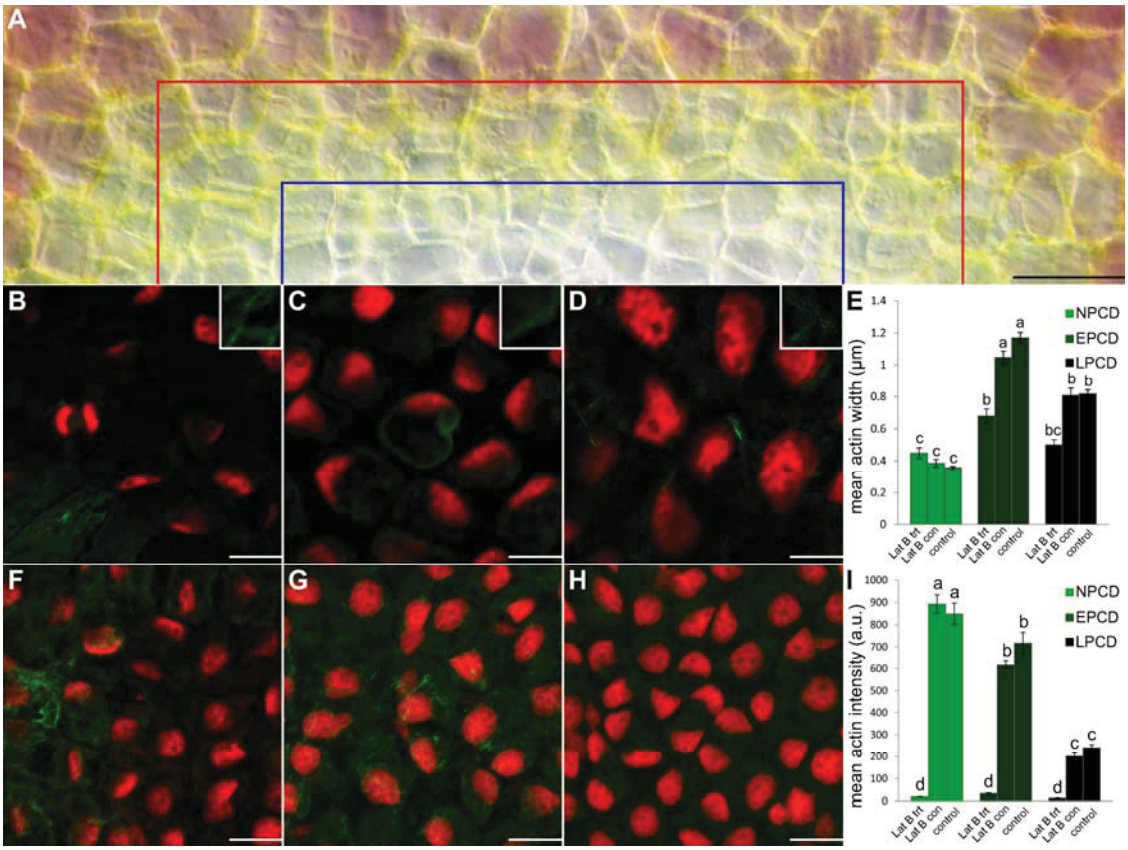

Figure 5.4 Actin Depolymerization Following Treatment With Latrunculin B (Lat B)

Figure 5.5 Kinetics of YVADase Activity for Cyclosporine A (CsA) and Latrunculin B (Lat B) Treated Leaves

CsA and Lat B pre-perforation stage leaf data as compared to their respective experimental and non-treated controls. Data are expressed as mean ± S.E.M. (n= 3). Data represented by different letters are significantly different ($P \leq 0.05$ ANOVA).

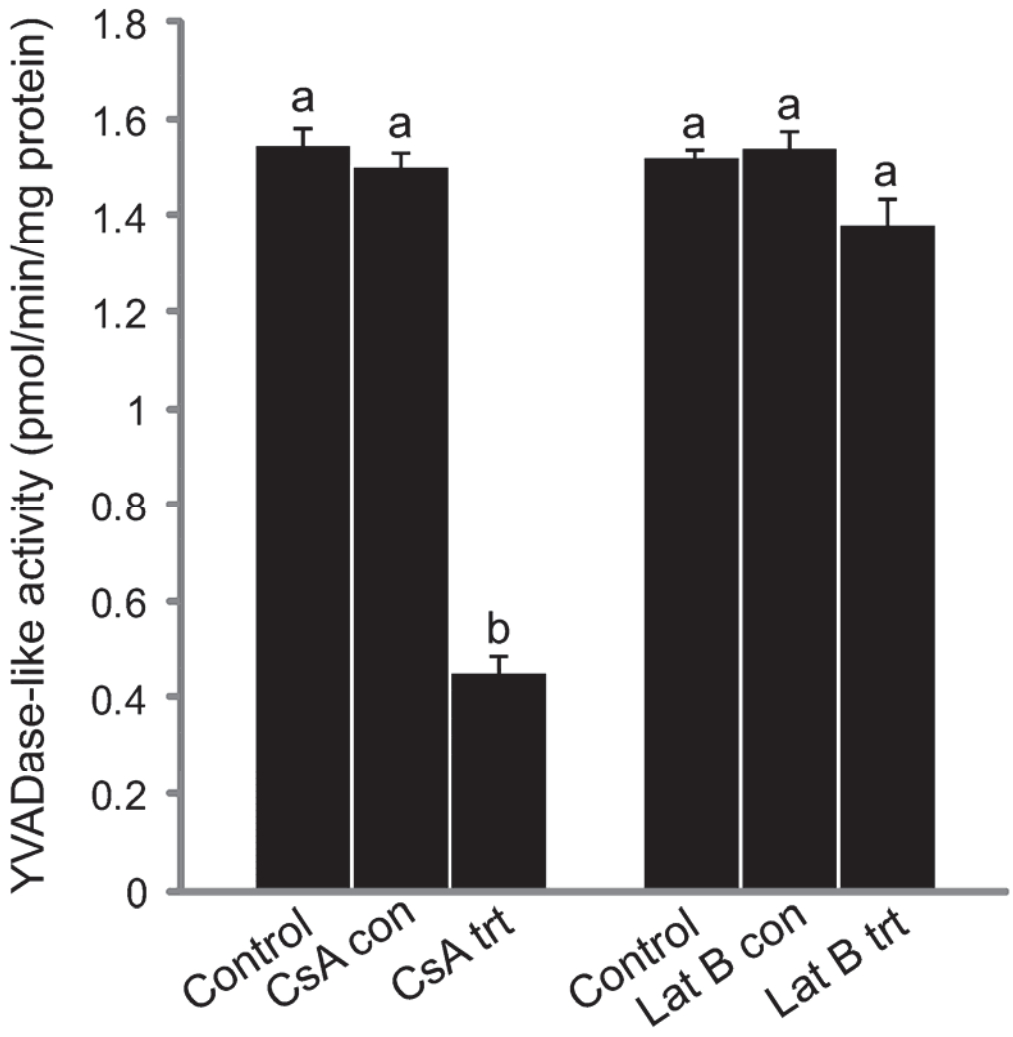

Figure 5.5 Kinetics of YVADase Activity for Cyclosporine A (CsA) and Latrunculin B (Lat B) Treated Leaves

Figure 5.6 Actin Dynamics Following *In vivo* Treatment With 0.462M Caspase-1 Inhibitor for 7 Days in Sterile Culture

Cells within the lower portion of this figure (B-D and F-H) are stained with fluorescent Alexa Fluor 488 phalloidin (green) for actin and counterstained with propidium iodide (PI; red) for nuclei; tissues are fixed. (A) A representative DIC micrograph of a half of a single areole of a window stage leaf following caspase-1 inhibitor treatment; note that a loss of pigmentation is not present in this areole, indicating a perforation will not form. Cells between the border of the image and the red line are representative NPCD cells, cells between the red line and the blue line are representative EPCD cells and cells between the blue line and the bottom of the image are representative LPCD cells. (B-D) Characteristic single z-stack micrographs of actin width within NPCD, EPCD and LPCD stage cells (0.33µm, 0.33µm and 0.35µm, respectively; see insets) following caspase-1 inhibitor treatment. (E) Caspase-1 inhibitor experimental data compared to non-treated leaves (control; data extracted from Figure 3) and treated controls (CASP con). (F-H) Representative maximum projection micrographs of actin intensity within NPCD, EPCD and LPCD stage cells (860.78 a.u., 874.10 a.u., 838.37 a.u. respectively) following caspase-1 inhibitor treatment. All actin intensity measurements were acquired within 1300µm^3 of maximum projected z-stacks tissue. (I) Mean actin intensities for each stage of PCD. Data for non-treated controls were extracted from Figure 3. All error bars are representative of standard error and all data represented by different letters are significantly different within individual graphs ($P \leq 0.05$ ANOVA). Scale bars (A) = 45 µm, (B-D) = 20 µm, (F-H) = 25 µm.

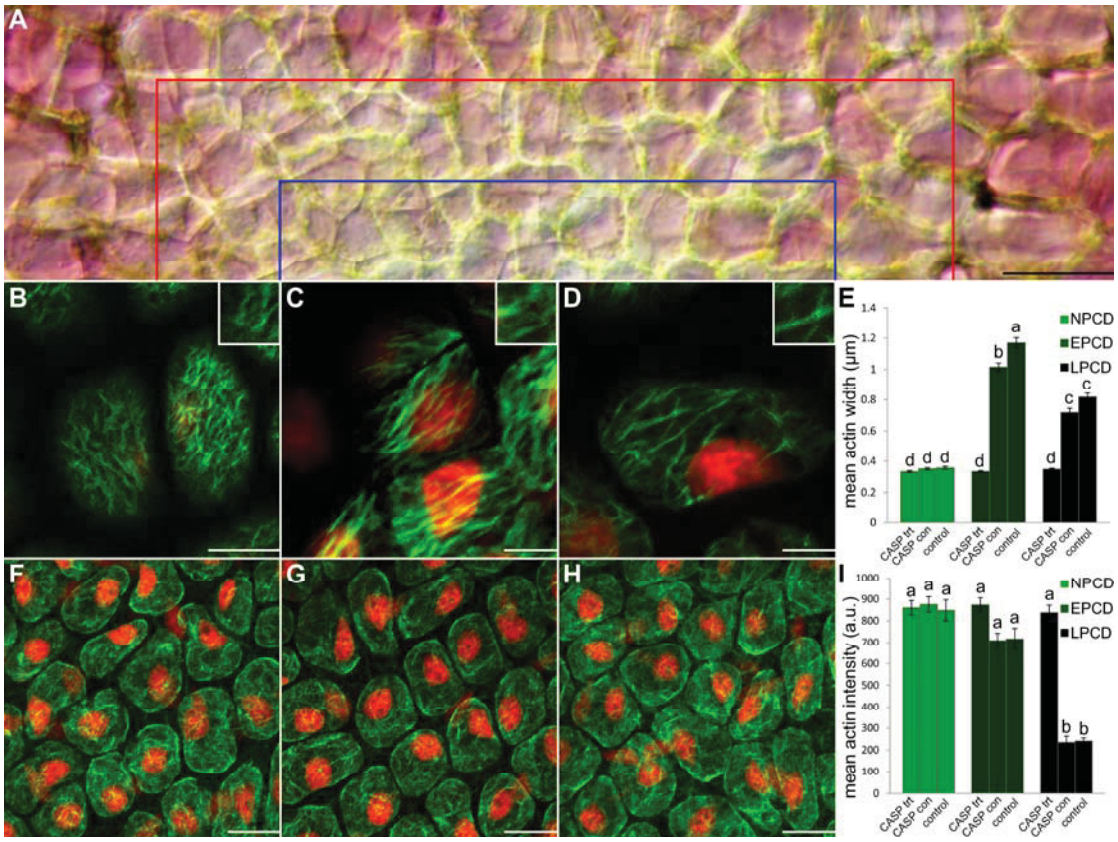

Figure 5.6 Actin Dynamics Following *In vivo* Treatment With 0.462M Caspase-1 Inhibitor for 7 Days in Sterile Culture

Figure 5.7 Actin Dynamics Following Treatment With 10 µM CsA for 3 Days in Sterile Culture

Cells within the lower portion of this figure (B-D and F-H) are stained with fluorescent Alexa Fluor 488 phalloidin (green) for actin and counterstained with propidium iodide (PI; red) for nuclei; tissues are fixed (A) A representative DIC micrograph of a half of a single areole of a window stage leaf following CsA treatment; note that the typical gradient of cell death is not present. Cells between the border of the image and the red line are representative NPCD cells, cells between the red line and the blue line are representative EPCD cells and cells between the blue line and the bottom of the image are representative LPCD cells. (B-D) Characteristic single z-stack micrographs of actin width within NPCD, EPCD and LPCD stage cells (0.39µm, 0.39µm and 0.38µm, respectively; see insets) following CsA treatment. (E) CsA experimental data compared to non-treated leaves (control; data extracted from Figure 3) and treated controls (CsA con). (F-H) Representative maximum projection micrographs of actin intensity within NPCD, EPCD and LPCD stage cells (844.50 a.u., 836.31 a.u., 858.30 a.u. respectively) following CsA treatment. All actin intensity measurements were acquired within $1300\mu m^3$ of maximum projected z-stacks tissue. (I) Mean actin intensities for each stage of PCD. Data for non-treated controls was extracted from Figure 3. All error bars are representative of standard error and all data represented by different letters are significantly different within individual graphs ($P \leq 0.05$ ANOVA). Scale bars (A) = 45 µm, (B-D and F-H) = 25 µm.

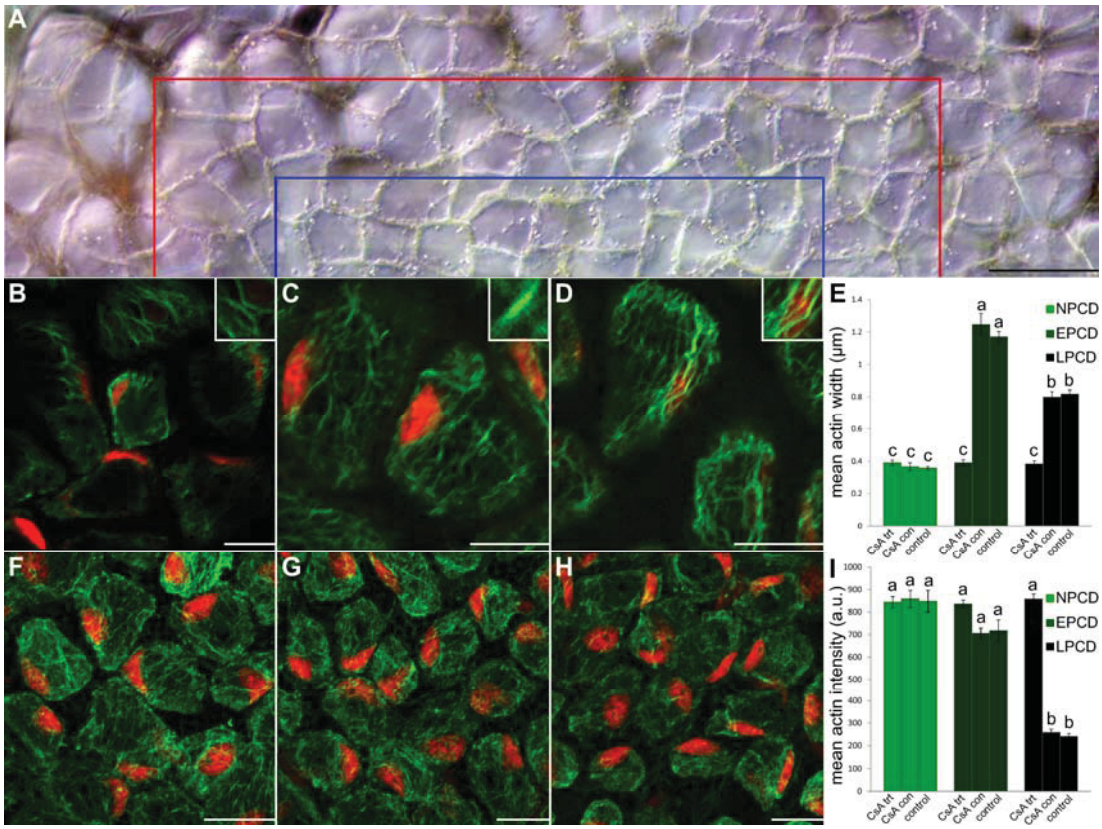

Figure 5.7 Actin Dynamics Following Treatment With 10 µM CsA for 3 Days in Sterile Culture

Chapter 6 The Pathway of Cell Dismantling During Programmed Cell Death in Lace Plant (*Aponogeton madagascariensis*) Leaves

Published as:

Wertman JN*, Lord CEN*, Dauphinee AN, Gunawardena AHLAN. The Pathway to Cell Dismantling During Programmed Cell Death in Lace Plant (*Aponogeton madagascariensis*) leaves. BMC Plant Biology 12: (2012) 115

*Both authors contributed equally to this manuscript

6.1 Abstract

Background: Developmentally regulated programmed cell death (PCD) is the controlled death of cells that occurs throughout the life cycle of both plants and animals. The lace plant (*Aponogeton madagascariensis*) forms perforations between longitudinal and transverse veins in spaces known as areoles, via developmental PCD; cell death begins in the center of these areoles and develops towards the margin, creating a gradient of PCD. This gradient was examined using both long- and short-term live cell imaging, in addition to histochemical staining, in order to establish the order of cellular events that occur during PCD.

Results: The first visible change observed was the reduction in anthocyanin pigmentation, followed by initial chloroplast changes and the bundling of actin microfilaments. At this stage, an increased number of transvacuolar strands (TVS) was evident. Perhaps concurrently with this, increased numbers of vesicles, small mitochondrial aggregates, and perinuclear accumulation of both chloroplasts and mitochondria were observed. The invagination of the tonoplast membrane and the presence of vesicles, both containing organelle materials, suggested evidence for both micro- and macro autophagy, respectively. Mitochondrial aggregates, as well as individual chloroplasts were subsequently seen undergoing Brownian motion in the vacuole. Following these changes, fragmentation of nuclear DNA, depolymerization of actin microfilaments and early cell wall changes were detected. The vacuole then swelled, causing nuclear displacement towards the plasma membrane (PM) and tonoplast rupture followed closely, indicating mega-autophagy. Subsequent to tonoplast rupture, cessation of Brownian motion occurred, as well as the loss of mitochondrial membrane potential ($\Delta\Psi_m$), nuclear

shrinkage and PM collapse. Timing from tonoplast rupture to PM collapse was approximately 20 min. The entire process from initial chlorophyll reduction to PM collapse took approximately 48 hr. Approximately 6 hr following PM collapse, cell wall disappearance began and was nearly complete within 24 hr.

Conclusion: Results showed that a consistent sequence of events occurred during the remodelling of lace plant leaves, which provides an excellent system to study developmental PCD *in vivo*. These findings can be used to compare and contrast with other developmental PCD examples in plants.

6.2 Introduction

6.2.1 Programmed Cell Death

Programmed cell death (PCD) occurs in both plants and animals, and is a highly regulated process that happens either as a part of normal development or in response to environmental influences (reviewed by Jones 2001; reviewed by Gunawardena 2008). Examples of environmentally induced PCD include, but are not limited to: heat shock (Lord and Gunawardena 2011) and the hypersensitive response (HR; Groover et al. 1997; reviewed by Kuriyama and Fukuda, 2002; reviewed by Pennell and Lamb, 1997; reviewed by Reape et al. 2008). Examples of developmentally regulated PCD include, but are not limited to: deletion of the embryonic suspensor (Filonova et al. 2000; Giuliani et al. 2002; Liu et al. 2005; Vuosku et al. 2009) tracheary element (TE) differentiation (reviewed by Fukuda 1997), leaf senescence (reviewed by Lim et al. 2007), and leaf morphogenesis (Gunawardena, 2008; Gunawardena, et al. 2004, 2005, 2006, 2007; Lord et al. 2011; Wright et al. 2009).

The classification of plant PCD into categories based on morphological characteristics has been challenging in the past (reviewed by Jones, 2001; reviewed by Reape et al. 2008; reviewed by van Doorn and Woltering, 2005). In 2000 Fukuda defined three different forms of plant PCD 1. Apoptotic-like 2. Cell death during senescence and 3. PCD in which the vacuole plays a central role. In 2005 van Doorn and Woltering compared plant PCD with three previously established morphological categories of metazoan cell death 1. Apoptosis 2. Autophagy and 3. Non-lysosomal PCD; these authors found that no plant examples conformed to the apoptotic type (reviewed by van Doorn and Woltering 2005). In 2008 Reape and McCabe, reverted to the use of Fukudas` (2000) term, apoptotic-like cell death, referring to examples from both induced and developmentally regulated PCD. Recently, plant PCD has been classified into two main categories based on morphological characteristics: necrotic and vacuolar cell death (reviewed by van Doorn et al. 2011). However, these authors agree with van Doorn et al. 2011, that biochemical and molecular data are needed to classify the categories of plant PCD more accurately.

Autophagy is known to play a major role in the regulation of death in animal cells, but the extent to which autophagy is involved in plant PCD has yet to be concretized (reviewed by Denton et al. 2012; reviewed by Edinger and Thompson, 2004; reviewed by Kwon and Park, 2008; reviewed by van Doorn and Woltering, 2005). Autophagy has been divided into three forms within plants: micro-, macro-, and mega-autophagy (reviewed by van Doorn and Woltering 2005; reviewed by Elmore 2007; reviewed by van Doorn and Yoshimoto 2010). Micro-autophagy is the uptake of organelles or other cellular contents by a lytic compartment, usually the vacuole in plant

cells. Macro-autophagy involves the creation of a double membraned structure containing cytosolic contents, called an autophagosome; this organelle will then fuse with a compartment, such as the vacuole, containing lytic enzymes. Lastly, mega-autophagy involves the permeabilization or rupture of the tonoplast and the release of hydrolytic enzymes into the cell, causing total degradation (reviewed by van Doorn and Woltering 2005; reviewed by van Doorn and Yoshimoto 2010).

Processes such as leaf senescence, TE differentiation, and the deletion of the embryonic suspensor have emerged as valuable examples used to study plant cell death (Bozhkov et al. 2005; reviewed by Lim et al. 2007; Obara and Fukuda, 2004). However, to date very little research has been conducted *in vivo* to understand the order of organelle changes, which occur during developmentally regulated PCD *in Planta*. Therefore, this study focused on establishing the sequence of cellular changes during plant PCD, to begin understanding cause and effect relationships between plant organelles.

6.2.2 The Lace Plant as a Novel Model Organism to Study PCD In vivo

The aquatic lace plant is a submerged monocot endemic to Madagascar (Sergueff 1907; Kasselmann 2003), that acquires its name from its' unique perforated leaf morphology. In lace plant leaves, PCD begins in the center of areas known as areoles, between transverse and longitudinal veins and continues outwards, stopping four to five cells from the vasculature (Gunawardena et al. 2007, 2006, 2005). This system lends predictability to both the time and location of cell death, and in combination with its' transparent and thin leaf, makes the plant an ideal specimen for live cell imaging (Gunawardena et al. 2006; Lord et al. 2011; Wright et al. 2009). As well, a technique has

been developed to culture the lace plant in sterile conditions, providing ample experimental material without contamination (Figure 6.1A; Gunawardena et al. 2006). Collectively, these qualities make the lace plant an excellent system to study developmentally regulated plant PCD *in vivo* (Gunawardena 2008; reviewed by Lord and Gunawardena 2012).

The process of perforation formation in lace plant leaves has been divided into five stages, as outlined in Gunawardena et al. (2004). The present study will focus on stage 2, or window stage leaves, where PCD is actively occurring (Figure 6.1B). This window stage leaf is then examined at the level of a single areole (Figure 6.1C). The window stage areole is subdivided into three groups of cells along a gradient of PCD, based on morphological characteristics (Lord et al. 2011). These groups include: non-PCD or control cells (NPCD; Figure 6.1C, between white and red lines), early-PCD cells (EPCD; Figure 6.1C, between red and blue lines) and late-PCD cells (LPCD; Figure 6.1C, inside blue rectangle). NPCD stage cells possess pink colouration, indicating the presence of the pigment anthocyanin. EPCD cells display chlorophyll pigmentation but no longer display large amounts of anthocyanin, indicating that this is one of the earliest changes in lace plant PCD (Gunawardena et al. 2004; Lord et al. 2011). The length of time between anthocyanin disappearance and chlorophyll reduction is still under investigation. Note that the leaves used in this study have previously lost most visible anthocyanin, as this is a precise way to ensure that the area of interest will perforate. In the lace plant, various cellular morphological characteristics have been examined throughout the process of cell death (Lord et al. 2011; Wright et al. 2009), however the detailed characterization of the order of events occurring throughout the entire process

has not yet been investigated. The aim of this paper is to use the novel lace plant system to delineate the possible order of organelle changes that occur throughout developmental PCD using both *in vivo* short- and long-term live cell imaging. This study will also employ experiments using fixed tissue samples in order to supplement this data. As a subset of this goal, this paper will provide visual evidence for autophagy during developmental PCD in the lace plant.

6.3 Materials and Methods

6.3.1 Plant Material and Selection

All plant materials were grown and subcultured as described in section 2.3.1 within Chapter 2. All chemicals were purchased from Sigma-Aldrich (St Louis, MO, USA), unless otherwise stated. All experiments were completed at least five times unless otherwise stated. Additionally, all image plates were composed using Adobe Photoshop Elements version 6.0.

Experiments used window stage, or stage 2, lace plant leaves (Figure 6.1B). Areoles in which the pigments had already cleared from the centermost cells were chosen. This was done to ensure that the given areole would in fact perforate, as some never do. In addition, windows were chosen in which there was a clear delineation between NPCD, EPCD and LPCD stage cells. These stages, represented by the rectangles in Figure 6.1C, served as a gradient through which all stages of the PCD process could be observed simultaneously. Cells within four to five cells of the vasculature were denoted as non-PCD cells (NPCD; Figure 6.1C, between white and red lines). These cells were prominently pink in colour due to the pigment anthocyanin found in their vacuole, were

not pre-disposed to undergo developmental PCD, and were therefore used as control cells. Cells interior to the control cells were in the early stages of cell death and were regarded as early-PCD cells (EPCD; Figure 6.1C, between red and blue lines); anthocyanin in these cells had disappeared and they were green in colour due to the abundance of chlorophyll containing chloroplasts within them. In the center of the areole, the cells were in the latest stage of cell death, were generally cleared of all pigments, and were called late-PCD cells (LPCD; Figure 6.1C, inside blue rectangle). It is important to note, however, that LPCD stage cells were once EPCD stage cells and all EPCD stage cells will develop into LPCD stage cells. Although EPCD cells, which contain anthocyanin, are similar in appearance to NPCD cells, NPCD stage cells differ in that they do not undergo PCD during perforation formation. Therefore, NPCD cells remain viable, whereas both the EPCD and LPCD actively undergo PCD.

6.3.2 Light Microscopy

All light microscopy observations were performed as described in section 2.3.4 within Chapter 2. NIS-Elements AR Version 3.0 software was used for both imaging and analysis on this microscope. All slides were prepared as wet mounts.

6.3.3 Confocal Microscopy

All confocal microscopy observations were performed as described in section 4.3.3 within Chapter 4. Maximum projection images were composed of approximately 30 to 50 successive z-stack images compiled using NIS-Elements AR version 3.0 software.

6.3.4 Transmission Electron Microscopy(TEM)

All transmission electron microscopy observations were performed as described in section 4.3.4 within Chapter 4.

6.3.5 Long and Short Term Live Cell Imaging

Videos were acquired on a compound light microscope using the audio video interleave (AVI) capture function in NIS-Elements AR software version 3.0. Long term live cell imaging (~72 hr) experiments were carried out using window stage leaves where PCD was not visibly initiated, as denoted by central cells of the areoles still possessing green colour due to the presence of chloroplasts. The leaves were mounted on a custom slide, submerged in 400 µl of distilled water, covered with a coverslip, and then sealed with petroleum jelly to prevent evaporation. Every 6 hr, the samples were rinsed three times with distilled water, re-mounted, and refocused to the appropriate cells.

Following the determination of the basic timeline of the cellular changes in PCD, it was necessary to obtain high-magnification videos for particular events. Videos were taken of carefully chosen window stage leaves, containing areoles in which the centermost cells were about to undergo membrane blebbing. The leaves were placed in between a slide and a coverslip and mounted as mentioned above. Samples were viewed for 1–6 hr (short-term), with constant supervision to prevent changes in focal plane.

All videos were compressed using the Radius Cinepak Codec and kept at full length and size until subsequent analysis. Videos were shortened to the desired length using either QuickTime Pro (Version 10.0), IMovie (Version 9.0.2) or Adobe Premiere Pro CS5 (Version 5.0) software. Arrows and text were inserted into the videos using Adobe Premiere Pro CS5 (Version 5.0) or QuickTime Pro (Version 10.0). Videos

captured throughout individual long-term live cell imaging experiments were trimmed, compiled and edited using Adobe Premiere Pro CS5 (Version 5.0).

6.3.6 Staining

6.3.6.1 Alexa Fluor 488 Phalloidin

Staining was performed as described in section 5.3.6 within Chapter 5. Leaf pieces were excited with the FITC cube (excitation 460-500 nm emission 510-560 nm) on the confocal microscope.

6.3.6.2 MitoTracker Red (CMXRos)

CMXRos stain was dissolved initially in DMSO and further in dH_2O to a final concentration of 0.6 μM. Window stage leaves were removed from lace plants, the mid rib was removed and the leaf was cut into segments of approximately 5 mm^2. These leaf sections were incubated in CMXRos at room temperature in the dark for 60 min. Following this, the leaves were rinsed 8 times in dH_2O and shaken at 100 rpm for 90 min. The leaf sections were then mounted in dH_2O and excited with the TRITC cube (excitation 527-552 nm and emission 577-632 nm) of the confocal microscope.

6.3.6.3 Terminal Deoxynucleotidyl Transferase–Mediated dUTP Nick-End Labeling (TUNEL)

All TUNEL observations were performed as described in section 4.3.5 within Chapter 4. All samples were then excited with the FITC cube (excitation 460-500 nm emission 510-560 nm) on the confocal microscope.

6.3.6.4 FM1-43

Window stage leaf segments were cut into approximately 5 mm^2 pieces and incubated in a 5 μg/mL FM1-43 solution dissolved in ice cold PBS. Leaf pieces were then incubated in a vacuum at 20 psi for 4 hr. These leaf segments were not rinsed, but counterstained immediately with 3% (w/v) PI for 3 min and subsequently mounted in Fluorogel (Electron Microscopy Sciences, Hatfield, PA, USA). These segments were then excited with the FITC cube (excitation 460-500 nm emission 510-560 nm) on the confocal microscope.

To conduct the vesicle counting trials, window stage leaves were stained as above. Cells from each stage of PCD were captured with z-stack imaging and compiled into a maximum projection image, to simultaneously show all planes. The total number of whole cells seen in each image was counted. The number of cells in each image that contained at least one vesicle was counted. The number of cells containing vesicles was then divided by the total number of cells and multiplied by 100 in order to obtain a percentage of cells containing vesicles per stage. This value was averaged over at least 120 cells per stage. Data was analyzed using a general linear model of variance ANOVA and the average percentages were compared using the Tukey test at 95% confidence intervals ($P < 0.05$). Statistical analysis was carried out using Minitab 16 statistical software (Minitab Inc., State College, PA, USA, 1972).

Three-dimensional image analysis was performed on window stage leaves stained with FM1-43, as described above. Confocal microscopy was employed to capture 30–50 successive z-stack images of cells from an areole of a window stage leaf. Files from the EZ-C1 software were exported and opened with NIS-Elements AR (Version 3.0),

containing the Deconvolution Demonstration from Nikon. Images were compiled and edited with the Volume View function and the Deconvolution Demonstration Package.

6.3.6.5 Evans Blue

Window stage leaves were cut from lace plants and had their midribs removed. The leaf segments were then stained for 1 hr in a 0.5% (w/v) solution of Evans Blue dissolved in dH_2O. Leaves were then washed in distilled water, mounted on a slide and viewed with the compound light microscope.

6.4 Results

6.4.1 Window Formation

The gradient of cell death seen simultaneously in one areole of a window stage leaf was used to classify cells into groups (NPCD, EPCD and LPCD). Thus, each cell that underwent PCD during perforation formation transitioned from EPCD to LPCD (See Materials and Methods section for more details). Therefore, long-term live cell imaging was used to focus on individual cells (Arrows, Figure 6.1D-G; Online Resource 6.1) initially containing chlorophyll pigmentation in EPCD (Figure 6.1D) until the collapse of the plasma membrane (PM) in LPCD (Figure 6.1G). The time between the reduction in visible chlorophyll in EPCD (Figure 6.1E) to PM collapse in LPCD (Figure 6.1G) in a typical individual cell was determined to be approximately 48 hr.

6.4.2 Changes in F-Actin, Chloroplasts, Mitochondria and Nuclei

Following anthocyanin loss, evidence depicted an initial reduction in chlorophyll content, as well as a reduction in the size and number of chloroplasts (Figure 6.1D-G). The actin cytoskeleton also underwent changes at this time, as demonstrated by Alexa Fluor 488 Phalloidin staining (Figure 6.2A). Control, or NPCD cells, displayed thin groups of actin filaments that appeared to underlay each PM (Figure 6.2B). Cells in the early stages of PCD displayed the first visible changes in actin arrangement; notably, the filaments re-organized into thicker cables (Figure 6.2C). There was also an increased number of visible transvacuolar strands (TVS) in EPCD stage cells (Online Resource 6.2). The arrangement of the actin looked increasingly haphazard until LPCD, at which point there was less visible overall cytoskeleton stained (Figure 6.2D).

Figure 6.3A depicts a gradient of cell death that is seen in lace plant windows. The image is sectioned into three stages, the right most section being NPCD, the middle being EPCD and the left most being LPCD (Figure 6.3A). It was noted that, in EPCD stage cells, individual chloroplasts and/or small groups of mitochondria could be seen moving along TVS in a seemingly orderly fashion (Online Resource 6.2). In EPCD stage cells, it was common to see chloroplasts in a ring-like formation surrounding the nucleus, shown in Figure 6.3B. The gradient of CMXRos staining seen in Figure 6.3C corresponds with the gradient delineated in Figure 6.3A. During EPCD there was also an increase in the associations between mitochondria, causing small groupings of mitochondria within the cytosol (Figure 6.3C). EPCD cells also contained aggregates of chloroplasts and mitochondria undergoing Brownian motion in the vacuole (Online Resource 6.1). It should be noted that these aggregates became visibly larger as PCD advanced (Online Resource 6.1). The gradient of TUNEL positive nuclei that could be seen in a lace plant

areole began at the border of EPCD to LPCD cells, indicating that it is one of the earlier cell death characteristics occurring in the LPCD stage (Figure 6.3D); note that the gradient division seen in Figure 6.3D corresponds to that seen in Figure 6.3A. Also at this time, organelle aggregates were still seen undergoing Brownian motion in the vacuole until tonoplast rupture initiated the cessation of movement during the late stages of cell death (Online Resource 6.3). Later, mitochondria exhibited the loss of mitochondrial membrane potential ($\Delta\Psi_m$), as denoted by the lack of CMXRos staining (Figure 6.3C). Overall, the presence of TUNEL positive nuclei supports the notion that LPCD cells contain fragmented nuclear DNA (Figure 6.3D).

6.4.3 Evidence For Autophagy and Aggregate Formation

Window stage leaves stained with FM1-43 displayed vivid staining of the tonoplast and PMs (Figure 6.4A-C, H). Small amounts of this stain also localized to the outside of organelles such as mitochondria and chloroplasts, due to their surrounding phospholipid membranes. Vesicle-like objects were rarely present in NPCD stage cells (Figure 6.4A), and increased in number from the early stages (Figure 6.4B) to the later stages (Figure 6.4C) of PCD. To support the notion that vesicles were more commonly seen in LPCD cells than EPCD or NPCD cells, the percentage of cells that contained vesicles was quantified (Figure 6.4D). These results depicted that the percent of cells containing vesicles differed significantly between each group ($P < 0.05$), with 66% of LPCD stage cells, 38% of EPCD and 22% of NPCD cells containing vesicles.

In order to more closely examine these vesicles, lace plant cells in later stages of PCD were observed via TEM and similar membrane-bounded bodies were found (Figure

6.4E-G). Rarely, results displayed double-membraned bodies, sometimes containing organelle material (Figure 6.4E, F). Additionally, in several instances, vesicles, with or without contents, appeared to be fusing with the tonoplast membrane (Figure 6.4F). Further evidence of autophagic-like processes was seen using live-cell imaging; FM1-43 staining displayed the vesiculation of LPCD lace plant cells that occasionally contained organelle material (Figure 6.4H).

In this study, aggregates were observed with DIC optics, TEM imaging, FM1-43, CMXRos staining and via long and short-term live cell imaging (Figure 6.5; Online Resource 6.1, 6.4 and 6.3). Aggregates appeared to be formed within EPCD cells, and were most prominent in LPCD stage cells. They were irregularly shaped and seemed to be composed of organelle materials. Live cell imaging suggested that these aggregates are chloroplasts or chlorophyll-containing objects due to their colour (Figure 6.5A, B; Online Resource 6.1). Within individual cells, the size of the aggregate appeared to increase as PCD progressed. Individual or small groups of organelles undergoing Brownian motion independently of the aggregate were seen to attach to the aggregate and then move in unison with the cluster (Online Resource 6.1). Also, it is important to note that Brownian motion was also seen in NPCD stage cells, albeit to a much lesser extent (data not shown). Using TEM imaging, it was apparent that the aggregates were mostly electron-dense (Figure 6.5C, D). Using FM1-43, it was confirmed that these aggregates consisted of organelles surrounded by phospholipid bilayers (Figure 6.5E, F). Using the mitochondria-specific stain CMXRos, it was also apparent that there were mitochondria present within the aggregates (Figure 6.5G, H; Online Resource 6.4).

Through the use of 3D analysis it was revealed that the aggregates (indicated by the arrows) were in the vacuole in later stages of cell death (Figure 6.5I, J). These aggregates of mitochondria and chloroplasts were also infrequently observed within vesicles (Figure 6.4H, 6.5C, D). In addition, TEM imaging depicted organelle material in an invagination of the tonoplast (Figure 6.4E, G) and within the vacuole (Figure 6.5C, D). In contrast, in NPCD stage cells, these organelles were normally dispersed throughout the cytosol and less commonly seen in the vacuole (Online Resource 6.1).

6.4.4 Tonoplast Rupture to Cell Wall Degradation

In late PCD, nuclei were observed to be displaced, visibly smaller and pushed against the PM (Online Resource 6.1, 6.3 and 6.5). This was followed by rupture of the tonoplast and vacuolar collapse (Online Resource 6.5). Following vacuolar collapse, the nucleus was liberated and then shrunk, the aggregate of organelles stopped moving (Online Resource 6.3), and the PM collapsed (Online Resource 6.3, 6.5 and 6.6); the process from tonoplast rupture to PM collapse took approximately 20 min (Online Resource 6.5; Appendix B). Plasma membrane collapse is visualized in Online Resource 6.6. At this stage, PM collapse was also made apparent by positive Evans Blue staining (Figure 6.6A, B). In late LPCD cells, it was apparent that mitochondria had lost their $\Delta\Psi_m$, as evident in Figure 6.3C. Initial cell wall changes were also observed early in LPCD via lightening of cell walls in the centermost cells (Figure 6.7A). Additionally, live cell imaging depicted visual evidence of cell wall disappearance occurred within 24 hr following PM collapse (Figure 6.7A-D; Appendix B). It is important to note that this

experiment began with cells with intact PMs and followed them throughout cell wall degradation.

6.5 Discussion

The lace plant window provides a spatially and temporally predictable system within which to study developmental PCD *in vivo*. Similar studies have used mesophyll cells isolated from *Zinnia elegans* to study developmentally regulated PCD in the past; however, these studies are considered *in vitro* as differentiation into TEs was induced following cell isolation (Groover et al. 1997). Therefore, these authors consider the live-cell imaging reported within this manuscript as a unique data set. Results presented here elucidate the sequence of cellular events occurring during developmentally regulated PCD in the lace plant using long- and short-term live cell imaging techniques (Summarized in Figure 6.8; Online Resource 6.1).

The first visible change noted in lace plant cells undergoing PCD is the reduction/disappearance of anthocyanin (Gunawardena et al. 2004). It is unclear whether this reduction is due to early changes in the pH of the vacuole following variations in tonoplast permeability, as seen in petal senescence (reviewed by Van Doorn 2004), or due to the actual degradation of the pigment. More research is needed to determine the reason for these colour changes that occur early in the PCD process. This loss of pigment in the center of a perforation occurs very early in the PCD process, and is often already reduced when the leaf unfurls. Following this, the pigment chlorophyll becomes less abundant (Gunawardena et al. 2004; Wright et al. 2009). This is due to the decrease in chlorophyll within the chloroplasts and the significant reduction in both chloroplast size and number (Wright et al. 2009) that is seen in EPCD cells (Online Resource 6.1). Lim et

al. (2007) also reported that loss of chlorophyll is a characteristic of leaf senescence, where initial changes occur within the chloroplasts.

Perhaps concurrently with chlorophyll reduction, actin filament organization begins to change. The actin filaments of the cytoskeleton are known to play major roles in cell expansion, division and differentiation; however, less is known about their role in PCD (reviewed by Smith and Oppenheimer 2005; reviewed by Smertenko and Franklin-Tong 2011). At the border of NPCD-EPCD, filaments changed from thin, organized structures coating the periphery of each protoplast (Figure 6.2B), to thicker cables that are more haphazard in arrangement (Figure 6.2C); this was also seen in *Picea abies* embryos (reviewed by Smertenko and Franklin-Tong 2011). Also at this stage an increase in the number of TVS becomes apparent. This increase in TVS has been reported during developmentally regulated PCD in the lace plant and during induced cell death in both lace plant protoplasts and tobacco suspension cultures (Lord and Gunawardena, 2011; Reisen et al. 2005; Wright et al. 2009). Previous work in the Gunawardena lab showed organelles moving along TVS (Lord et al. 2011); additional evidence of this is provided in the present study (Online Resource 6.2). The movement of organelles along these TVS may result in the perinuclear accumulation of organelles seen in EPCD stage lace plant cells (Figure 6.3B; Lord et al. 2011).

It was determined via FM1-43 staining that vesicles begin increasing in prevalence in EPCD stage cells. The majority of observed vesicle structures were membrane-bound bodies that may or may not contain organelle material. It is probable that the vesicles seen via FM1-43 staining and confocal imaging are the same vesicles seen in the cytosol and joining with the tonoplast via TEM imaging (Figure 6.4E-G). The

present study also noted several instances of multi-membraned structures that sometimes contained organelle material. Similar swirled cytoplasmic membranes were seen by Filonova et al. (2000) during PCD in embryogenesis in Norway spruce and were called 'whorls'. Liu et al. (2005) also observed similar vesicle-containing membranous structures as seen in lace plant PCD, during the HR response in *Nicotiana* plants. In addition, it has been determined that autophagy is necessary for developmental PCD in TE formation in *Arabidopsis*, which may provide further evidence for the role autophagy plays in plant PCD (reviewed by Denton et al. 2012). Overall, these membrane-bound structures represent evidence for autophagy during lace plant PCD.

As PCD progresses lace plant cells display aggregation of organelles. The early aggregation of mitochondria in cells undergoing PCD has been noted previously during induced cell death in *Arabidopsis* (Scott and Logan, 2008; Yao et al. 2004) and also in previous developmental PCD studies within the lace plant (Lord and Gunawardena 2011; Lord et al. 2011). The various forms of microscopy used here depict chlorophyll-containing organelles, as well as mitochondria in these aggregates. The association among and between mitochondria and plastids has been observed previously, where mitochondria were often seen touching and embedded within chloroplasts of senescing wheat leaves (Wittenbach et al. 1982).

Long-term live cell imaging provides evidence suggesting that the aggregates, characteristic of EPCD and LPCD stage cells, visibly increased in size, perhaps through the accumulation of individual organelles as PCD progresses (Online Resource 6.1). Wright et al. (2009) previously noted aggregates in the vacuole of lace plant cells undergoing PCD that displayed distorted thylakoid membranes, thus indicating the

presence of chloroplasts; these aggregates appeared to be undergoing Brownian motion as seen in Online Resources 6.1, 6.3, 6.4 and 6.6 of this manuscript. Through the use of confocal z-stack imaging and NIS-Elements Volume View Software, the present authors were able to determine that these aggregates were positioned in the vacuole during the later stages of PCD. Presumably, these organelles are in the vacuole to be degraded; however, it is as of yet unknown how and exactly when this movement into the vacuole occurs. The authors believe that small aggregates of mitochondria, and perhaps individual chloroplasts, are brought to the vacuole independently, potentially aided by TVS, following which aggregation would occur (Online Resources 6.1, 6.3, 6.4 and 6.6). Alternatively, the aggregate could be assembled in the cytosol and then brought into the vacuole as a whole. Regardless, this phenomenon of organelles in the vacuole is likely indicative of some form of autophagy (reviewed by van Doorn and Woltering 2005).

In LPCD stage cells, it is also discernible in Figure 6.3C and D that there are cells that have both CMXRos staining and TUNEL positive nuclei. In addition, Figure 6.3C and D also display cells, to the far left (late LPCD), that contain TUNEL positive nuclei without CMXRos staining. Therefore, it was deduced that DNA fragmentation occurs prior to the loss of mitochondrial $\Delta\Psi_m$ indicated by a loss in CMXRos staining. Perhaps concurrently with the appearance of TUNEL positive nuclei, the actin cytoskeleton appeared to break down or depolymerize. Re-organization of actin into thick cables followed by its' depolymerization is a common feature of developmentally regulated plant PCD (reviewed by Smertenko and Franklin-Tong 2011). Some authors have proposed cytoskeleton alterations as a trigger for the onset of PCD in *Arabidopsis* during the HR (Tian et al. 2009). However recent work in our lab suggests that cysteine-

aspartate specific protease-like proteases (caspase-like proteases, CLPs) may act upon the actin cytoskeleton, suggesting the cytoskeleton may not be an initial trigger for PCD but instead a target of an upstream signal, although further research is required (data not shown)[15]. In addition to cytoskeletal changes in LPCD stage cells, the current study provides live cell imaging evidence of visible cell wall changes, as reported originally by Gunawardena et al. (2007) via TEM.

Following the appearance of TUNEL positive nuclei and the breakdown of actin, visible changes in tonoplast dynamics became apparent. It is unknown whether this marks the first change in tonoplast integrity, as it is also possible that an early change in selective permeability of the tonoplast could have caused the subsequent anthocyanin colour change. The rupture of the tonoplast is known to be involved in several examples of plant PCD including TE differentiation and aerenchyma formation (reviewed by Drew et al. 2000; Lord et al. 2011; Obara et al. 2001). The present study demonstrates, to the best of these authors' knowledge, the first *in vivo* video recording of tonoplast rupture and subsequent visible cellular events (Online Resource 6.5). The rarity of the above observations is explained by the quick succession in which these events occur.

Online Resource 6.5 depicts swelling of the vacuole resulting in the flattening of the nucleus against the PM, a characteristic also seen in TE differentiation (Obara et al. 2001). In lace plant cells, this step is followed closely by tonoplast rupture, visible nuclear liberation, and subsequent cessation of organelle aggregate Brownian motion (Online Resource 6.3), loss of mitochondrial $\Delta\Psi_m$ (Figure 6.3C) and rapid nuclear shrinkage. Although it was not possible to view CMXRos stained cells and also see

[15] This work was presented within Chapter 5 of this dissertation.

tonoplast rupture at the same time, the order for cessation of organelle aggregate movement and loss in mitochondrial $\Delta\Psi_m$ was discerned from Lord et al. (2011). This maintenance of mitochondrial integrity until late in lace plant PCD is reminiscent of leaf senescence and xylem differentiation (Inada et al. 1999; reviewed by Lim et al. 2007; Yu et al. 2002; reviewed by van Doorn and Woltering, 2005). A similar process is also seen in TE differentiation, where studies report liberation of the nucleus followed by complete nuclear degradation 20 min post tonoplast rupture due to nucleases being released from the vacuole (Obara et al. 2001). However, the current study does not provide evidence of complete nuclear degradation, as intact condensed nuclei can still be seen following cell wall degradation (Figure 6.7; Gunawardena et al. 2004, 2007).

Tonoplast rupture is regarded as the decisive moment during plant PCD in which cytoplasmic streaming stops and the cell is considered dead (reviewed by Jones, 2001; Wright et al. 2009; reviewed by van Doorn and Woltering, 2005); more recently, tonoplast rupture has also been coined as the process of 'mega-autophagy' by van Doorn and Woltering (2005). Within this manuscript we have presented evidence supporting van Doorn's latest classification of the lace plant into vacuolar type PCD, especially with regards to the presence of autophagy characteristics. However, it is still unclear whether mega-autophagy by van Doorn and Woltering (2005) definition applies to the lace plant given that most organelles have been degraded prior to tonoplast rupture.

Following tonoplast rupture within the lace plant system, PM collapse is observed (Figure 6.7 inset; Online Resources 6.5 and 6.6). Additional evidence of PM collapse is seen via positive Evans Blue staining, that is only able to enter cells with compromised PMs (Figure 6.6). In the lace plant, there is approximately 48 hr between initial

chlorophyll reduction and PM collapse (Online Resource 6.1; Figure 6.1D-G). Depending on the form of PCD, PM collapse may or may not be followed by cell wall degradation (Filonova et al. 2000; Gunawardena et al. 2007; Obara et al. 2001; reviewed by Pennell and Lamb 1997). During TE differentiation, the cell wall is partially degraded and modified, leaving an empty tube (Filonova et al. 2000). Conversely, during leaf senescence in *Arabidopsis,* increasing leaf weight is seen up until approximately 30 days following sowing, suggesting no visible wall degradation (Breeze et al. 2011). In contrast to both of these systems, Gunawardena et al. (2007) showed changes in wall structure as early as in stage 2, or in window stage leaves during lace plant leaf morphogenesis via TEM. These results were complemented by results presented in this manuscript in which cell wall disappearance was shown to occur within 24 hr of PM collapse using live cell imaging (Figure 6.7A-D; Gunawardena et al. 2007). The inset in Figure 6.7 displays an LPCD stage cell with a blebbed PM and intact cell wall, indicating PM collapse precedes visible cell wall degradation. However, the extent of cell wall degradation was examined only qualitatively here and thus represents a possible area for future research.

6.6 Conclusions

This study aimed to employ the novel *in vivo* system of a single areole in a window stage lace plant leaf, to elucidate the sequence of organelle changes occurring throughout developmentally regulated PCD in plants. The first visible change observed was the reduction in visible anthocyanin, then initial reduction of chlorophyll pigmentation within chloroplasts along with changes in chloroplast size and number. Perhaps concurrently with chloroplast changes, actin filaments re-organized into bundles, and there were increased numbers of TVS and additional instances of organelles

travelling along TVS. Mitochondria then tended to form small groupings in the cytosol, and cells often possessed rings of chloroplasts surrounding the nucleus. Live cell imaging revealed single-layered membranous structures while TEM imaging revealed both single and multi-layered membranous structures; each of which were seen to occasionally contain organelle material. In addition, images depicting invaginations of the tonoplast and double membrane-bound vesicles indicating a role for micro- and macro- autophagy in lace plant PCD were also presented. Later, the aggregate of mitochondria and chloroplasts could be seen within the vacuole undergoing Brownian motion, and this aggregate visibly increased in size as PCD progressed. This study shows, for the first time, an *in vivo* video during developmentally regulated PCD, of vacuole swelling and tonoplast collapse, resembling mega-autophagy. This paper provided evidence of these events leading to the cessation of organelle aggregate movement, loss of mitochondrial $\Delta\Psi_m$, nuclear shrinkage and PM collapse. Total time from reduction in visible chlorophyll to PM collapse is approximately 48 hr. Cell wall disappearance followed the collapse of the PM within 24 hr. This study reports a consistent order of events that occur in lace plant cells undergoing PCD, in addition to providing visual evidence of autophagy.

6.7 Acknowledgments

The authors greatly acknowledge Dr. Peter Bozhkov (Swedish University of Agricultural Sciences) for critical review of this MS. Thank you to Stephanie Lane (Dalhousie University) for live cell imaging assistance. We would also like to thank Nikon Canada for allowing us to use the deconvolution demonstration for NIS-Elements to prepare two micrographs for this work. Additionally, the authors acknowledge the

Sarah Lawson Research Scholarship (Dalhousie University) for funding for JW. The authors also wish to thank the National Sciences and Engineering Research Council of Canada (NSERC) for doctoral funding for CENL. Lastly, thank you to the Canadian Foundation for Innovation (CFI) for the Leaders Opportunity Fund along with NSERC for discovery and equipment grants for AHLANG.

6.8 Authors' Contributions

JW and CENL both contributed equally to manuscript preparation. JW carried out experiments including: selected short-term imaging, all FM1-43 staining and 3D analysis, selected CMXRos and all Evans blue staining, as well as selected TUNEL staining and imaging. CENL carried out experiments including: selected short-term imaging, all cytoskeleton staining, selected TUNEL staining and imaging, selected CMXRos staining, all statistical analysis, as well as cell wall degradation light microscopy. AND completed selected CMXRos staining, long-term live cell imaging, video editing and flow-chart compilation. JW drafted the first manuscript while JW, AND and CENL all contributed to final manuscript revisions. AHLANG, conceived the study, participated in its design and coordination, and helped in manuscript revisions as well as supervised all experimental work.

6.9 Online Resources

Online Resource 6.1 Video Clip Compilation Showing the Development of a Window Over a Period of 72 Hours

Note that this video focused initially on early-PCD (EPCD) stage cells. Chloroplast pigmentation, movement and size differ between cells in different stages of PCD. Small

aggregates become larger as PCD advances and individual organelles are seen attaching to the aggregate. Transvacuolar strands (TVS) can be seen within cells and are most frequent in EPCD. Note the advancement of EPCD visibly denoted by a decrease in chloroplast size and number, resulting in a reduction in chlorophyll pigmentation. The two cells of interest show a loss of chloroplast pigmentation, individual organelles and aggregates undergoing Brownian motion, and near the final stages of PCD, nuclear displacement followed by PM collapse. Approximately 100X sped up.

Online Resource 6.2 Transvacuolar Strands (TVS) in EPCD Stage Lace Plant Cells

Video displays chloroplasts and mitochondria (small, round, grey-coloured objects) within lace plant cells, in addition to the occurrences of visible TVS. Note the instances of organelle movement along TVS. Also note the perinuclear accumulation of some chloroplasts. Note the visible reduction in anthocyanin from the top right corner to the bottom left corner. Approximately 100X sped up.

Online Resource 6.3 Aggregate Cessation of Brownian Motion

This video shows a gradient of cell death: control cells on the left, early-PCD (EPCD) stage cells in the center and late-PCD (LPCD) stage cells to the right. Video depicts perinuclear accumulation of chloroplasts. Note the moving organelle aggregates at the beginning of the movie. Note visible vacuole swelling, causing displacement of the nucleus and subsequent tonoplast rupture. Following tonoplast rupture, the organelle aggregate stops Brownian motion; PM collapse quickly follows this process. Approximately 200X sped up.

Online Resource 6.4 Mitochondrial Aggregates Stained With CMXRos

Video displays that the aggregate of organelles contains CMXRos stained, mitochondria. This video demonstrates that the aggregate is moving within the cells vacuole via Brownian motion. Refer to Figure 6.5 for histological analysis of this aggregate. Approximately 10X sped up.

Online Resource 6.5 LPCD Stage Cells Displaying Tonoplast Rupture and Subsequent Events

This video depicts vacuolar swelling, displacing the nucleus toward the PM. Following this, the tonoplast ruptures, allowing the nucleus to be temporarily liberated. The nucleus then condenses. Following this, the tonoplast shrinks and PM collapse follows closely. Approximately 200 X sped up.

Online Resource 6.6 Visualizing the Process of PM Collapse

Note that the mesophyll cells' PMs begin collapse prior to the epidermal cells. Also note the synchronicity of PM collapse. Approximately 200X sped up.

Figure 6.1 The Lace Plant, or *Aponogeton madagascariensis*

(A) Experimental lace plant in a magenta box containing liquid and solid MS medium. (B) Stage 2, or 'window' stage leaf. Note the pink colouration, due to the pigment anthocyanin in the plant cell vacuole. (C) Subdivision of a single areole of a window stage leaf. Surrounding the areole is vascular tissue, or the veins of the leaf (outside the white square). The first delineation is cells that will not undergo PCD, or the NPCD cells, and are used as control cells (between the white and the red rectangles). These cells are markedly pink due to the pigment anthocyanin. The next grouping of cells are those in the earliest stage of PCD, or the EPCD stage cells (between the red and the blue rectangles). These cells are normally green, marking the presence of chlorophyll. Finally, the cells in the latest stage of PCD, or LPCD stage cells, are in the centre of the areole (inside the blue rectangle). These cells are usually transparent, indicating that pigments have been degraded. (D-G) Progression of window development within a section of an areole captured approximately at times 0, 12, 36 and 60 hr, during long-term live cell imaging respectively. Arrows indicate cells that were initially seen with chlorophyll pigmentation (D), reduced pigmentation (E and F) and collapsed PM (G). Microscope settings remained constant throughout observation. Scale bars: A-B = 1 cm, C = 250 μm, D-F = 30 μm, G = 40 μm.

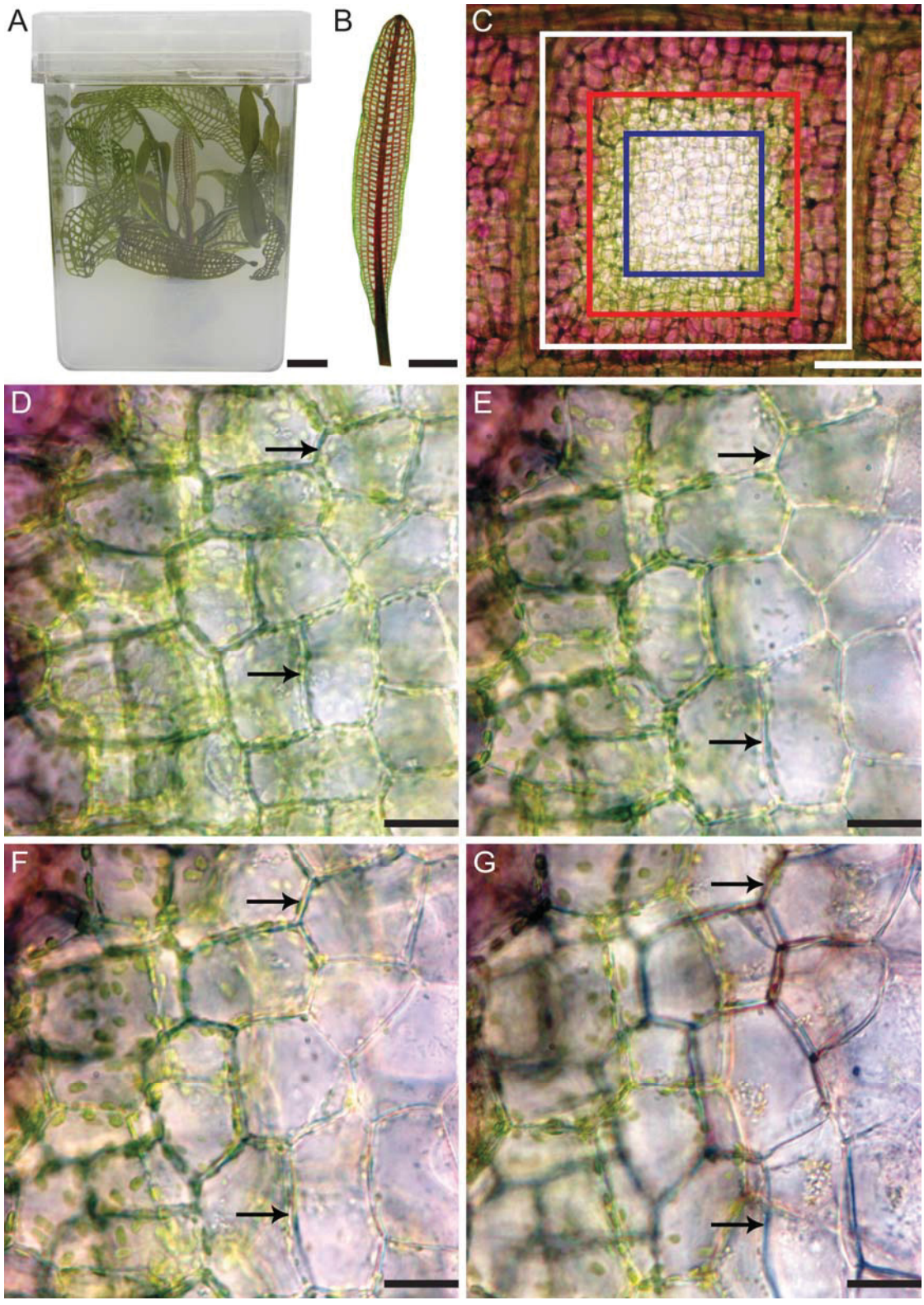

Figure 6.1 The Lace Plant, or *Aponogeton madagascariensis*

Figure 6.2 Alterations in Cytoskeletal Dynamics Within a Single Areole of a Window Stage Leaf

Each image represents a maximum projection of approximately 50 z-stack images. (A) Half of a single areole of a window stage leaf, displaying the gradient of non-PCD (NPCD), early-PCD (EPCD) and late-PCD (LPCD). Actin microfilaments are stained green with Alexa Fluor 488 Phalloidin, while nuclei are stained red with propidium iodide. Note the variation in cytoskeletal dynamics across this gradient. (B) NPCD cells displaying a thin layer of actin microfilaments underlying the PM. (C) EPCD cells displaying actin microfilament bundling. Note the bundles of actin found in several cells within the field of view (arrow). (D) LPCD cells displaying actin microfilament breakdown. Note the loss of actin staining within these cells and the discontinuous nature of the filaments that are still present. Scale bars: A-D = 100 μm.

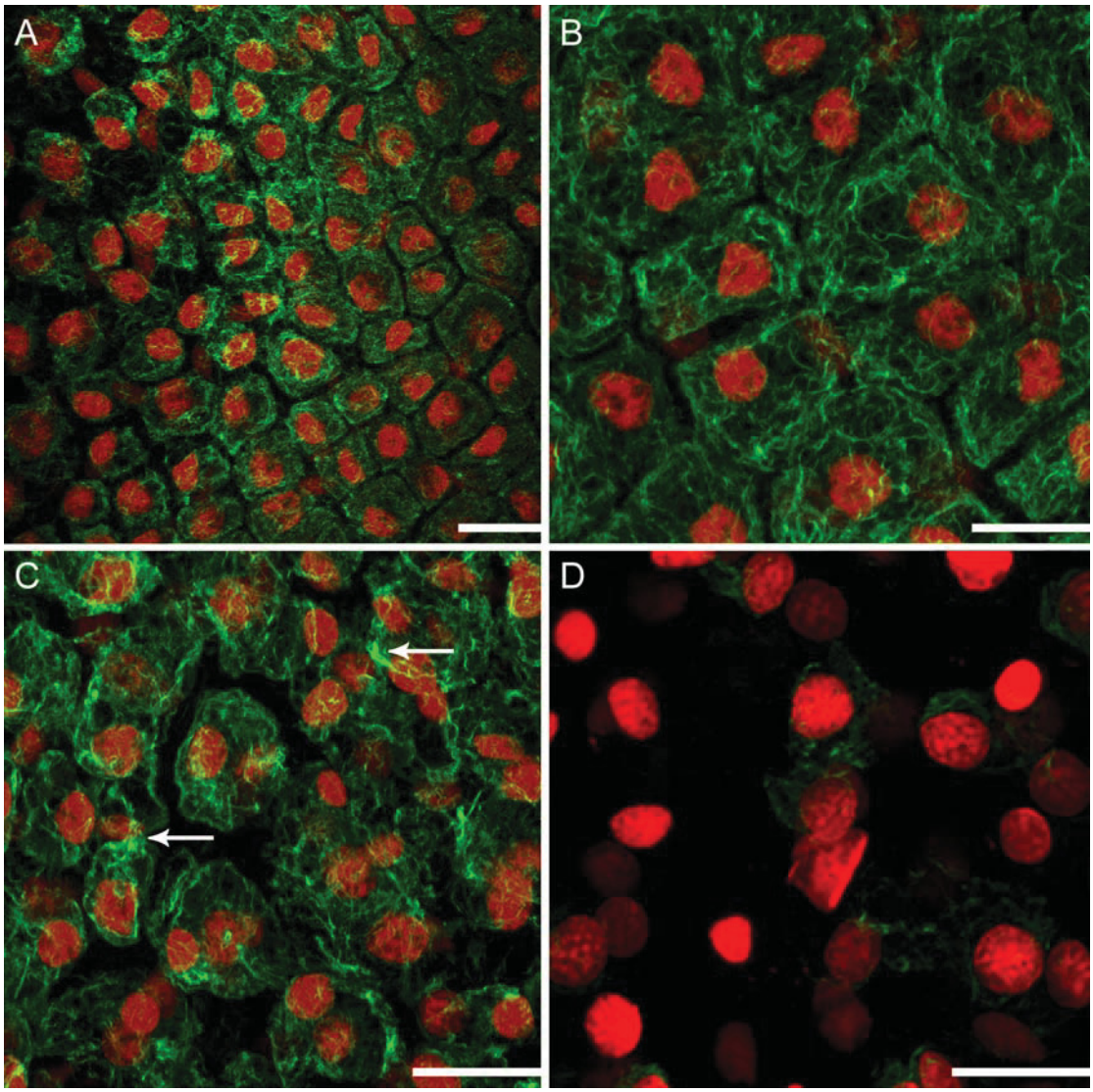

Figure 6.2 Alterations in Cytoskeletal Dynamics Within a Single Areole of a Window Stage Leaf

Figure 6.3 Organelle Dynamics Within a Single Areole of a Stage 2 or Window Stage Lace Plant Leaf

(A) Half of a single areole of a window stage leaf. Note that the image is sectioned into three stages, the right most section being NPCD, the middle being EPCD and the left most being LPCD. (B) Perinuclear accumulation of chloroplasts. (C) Mitochondrial dynamics over the gradient of PCD, visualized via CMXRos. Note that this gradient corresponds with that seen in panel A. NPCD stage cells contain many individual mitochondria in the cytosol. EPCD stage cells contain mitochondrial aggregates (arrows), along with some individual mitochondria. LPCD stage cells depict either aggregates of mitochondria, or a lack of staining, indicating the loss of $\Delta\Psi m$ (mitochondrial membrane potential). (D) Gradient of TUNEL positivity, indicating the cleavage of DNA by endonucleases throughout PCD in the lace plant. Note that this gradient corresponds with that in panel A. NPCD and EPCD stage cells do not contain TUNEL positive nuclei, indicating intact nuclear DNA. LPCD stage cells do contain TUNEL positive nuclei, signifying DNA cleavage by endonucleases. Scale bars: A = 100 μm, B = 25 μm, C-D = 100 μm.

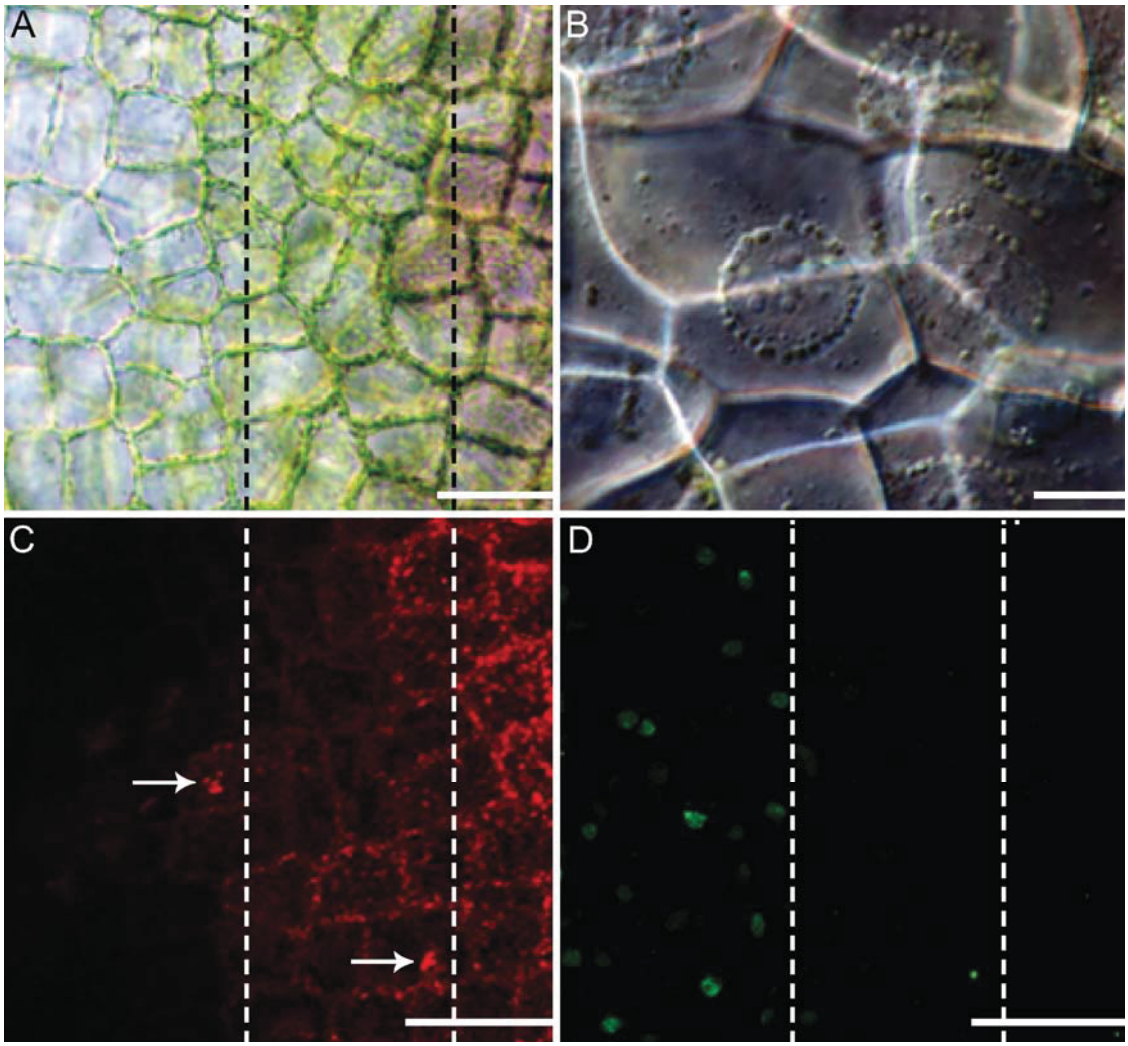

Figure 6.3 Organelle Dynamics Within a Single Areole of a Stage 2 or Window Stage Lace Plant Leaf

Figure 6.4 Presence of Autophagic Vesicles Throughout Lace Plant PCD

(A) Non-PCD (NPCD) stage cells co-stained with FM1-43 (green), a dye that localizes to phospholipid bilayers, and PI (red), a dye that localizes to the nucleus. Staining of the PM and possibly the tonoplast, in addition to several small round organelles can be seen. The absence of PI staining indicated healthy nuclei. (B) EPCD stage cells co-stained with FM1-43 and PI. Note stained PMs, some tonoplast staining, in addition to several autophagic vesicles. Organelle aggregates were present and stained with FM1-43. Again recognize the absence of PI staining, indicating healthy nuclei. (C) LPCD stage cells co-stained with FM1-43 and PI. Note PM, tonoplast and organelle staining as well as the multiple, variable sized vesicles. Most nuclei in LPCD cells are stained with PI, indicating non-viable nuclei (D) Percentage of cells containing vesicles by stage. NPCD, EPCD and LPCD stages had 22, 38 and 66 percent of their cells containing vesicles, respectively. Bars with different letters differed significantly ($P < 0.05$). Error bars represent standard error of a minimum of 120 cells per category. (E) TEM micrograph of a late stage lace plant leaf. Double-membraned vesicular structures, some of which contain organelle material can be seen (marked by black arrow). (F) TEM micrograph of a late stage lace plant cell. Note multiple vesicles, including one double membraned vesicle containing organelle material. (G) TEM image of late stage PCD cell depicting invagination of the tonoplast, possibly indicating micro-autophagy. Electron dense material in the invagination that is possibly composed of organelles can be seen (marked by black arrow). (H) LPCD stage cell stained with FM1-43. Note the stained PM, organelles and vesicles. White arrow points to an aggregate that appears to be within a small vacuole. Scale bars: A = 50 μm, B-C = 100 μm, E = 0.4 μm, F = 1 μm, G = 0.8 μm, H = 100 μm.

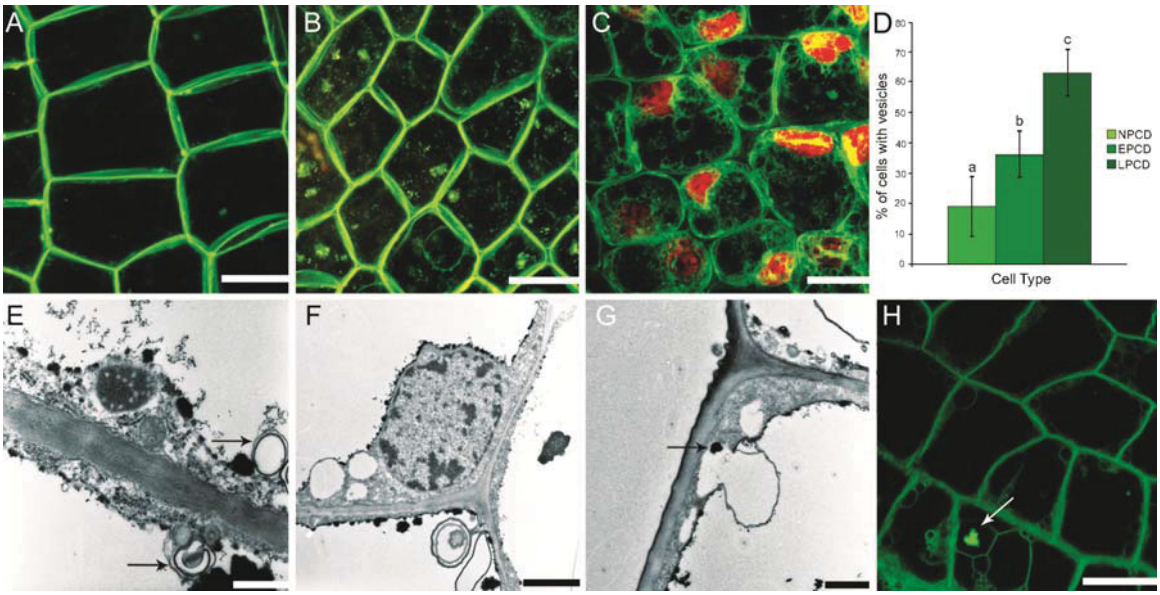

Figure 6.4 Presence of Autophagic Vesicles Throughout Lace Plant PCD

Figure 6.5 Visualization of the Organelle Aggregate Seen in EPCD and LPCD Stage Cells

(A) DIC image depicting aggregates of mitochondria and chloroplasts in early-PCD (EPCD) stage cells. (B) Higher magnification DIC image from EPCD stage cells. Aggregate marked by black arrow. (C) TEM image of EPCD stage cells depicting an aggregate of electron dense material inside the vacuole of a lace plant cell; note the membranous body in the vacuole. (D) Higher magnification TEM image of an EPCD stage cell, displaying aggregate of electron dense material in the vacuole, marked with a black arrow. Also note the organelle material was bound by a single membrane in the vacuole, marked with a red arrow. (E) Low magnification confocal micrograph displaying EPCD stage cells stained with FM1-43, sequestered to the phospholipid bilayer. Note the aggregates of membrane-bound organelles within each cell. (F) High magnification confocal micrograph depicting LPCD stage cells stained with FM1-43. Note the presence of the organelle aggregate and some vesiculation in the cells. (G) Confocal micrograph of EPCD stage cells stained with CMXRos, which stains mitochondria with intact $\Delta\Psi m$ (mitochondrial membrane potential). Note the aggregates are stained red, indicating the presence of mitochondria. (H) High magnification confocal micrograph of EPCD cells stained with CMXRos. Note that the aggregates are stained red, indicating the presence of viable mitochondria. (I) 3D volume view confocal image of LPCD stage cells co-stained with FM1-43 and PI. Fifty successive z-stack images were compiled into a single 3D image using the deconvolution demonstration from Nikon Instruments. Note the presence of the aggregate within the vacuole of the cell, denoted with white arrow. Also note surrounding vesicles. (J) Secondary view of panel I, also depicting the aggregate, stained with FM1-43 within the vacuole of LPCD lace plant cells, denoted by white arrow. Scale bars: A = 100 μm, B = 10 μm, C = 50 μm, D = 25 μm E = 150 μm, F = 25 μm, G = 50 μm, H- J = 25 μm.

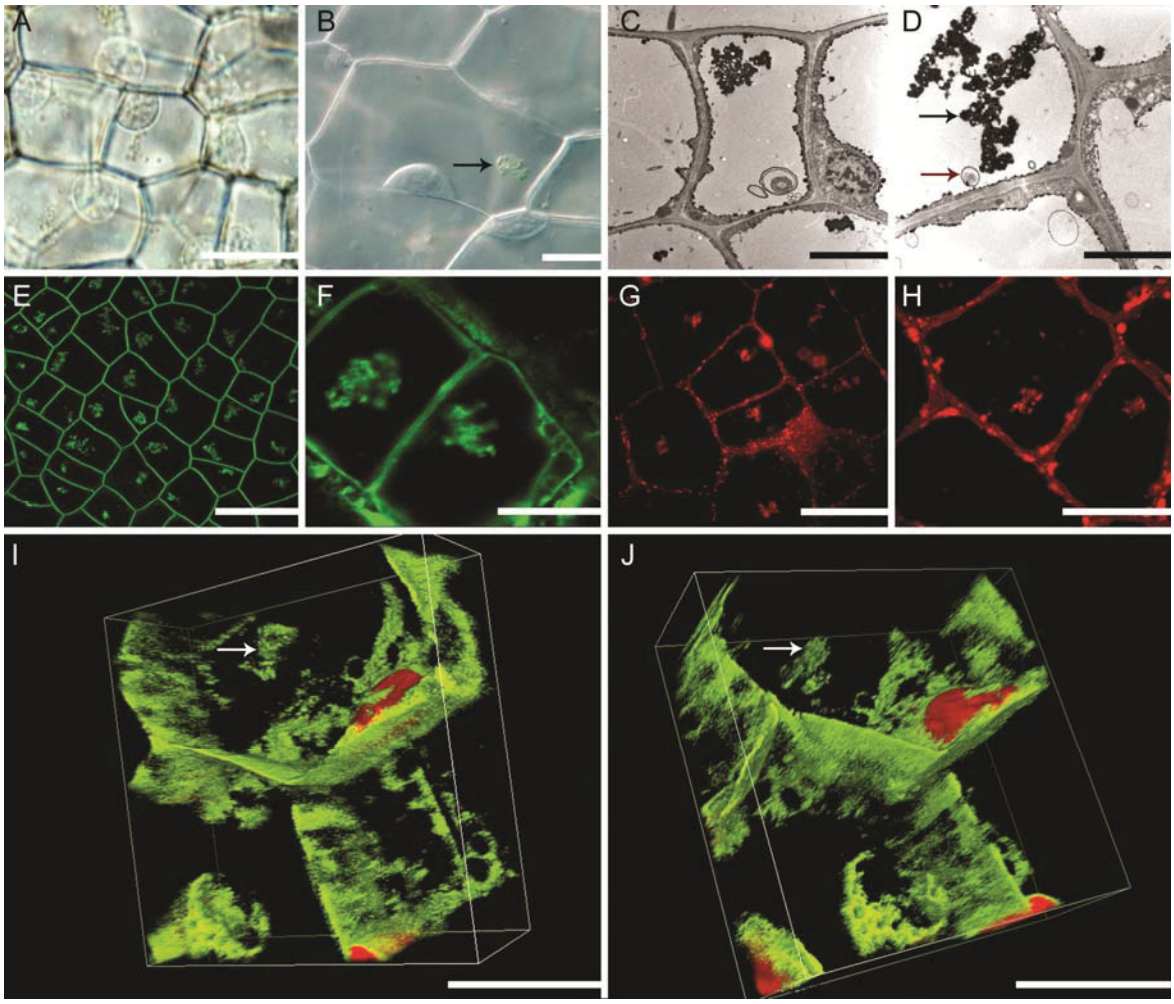

Figure 6.5 Visualization of the Organelle Aggregate Seen in EPCD and LPCD Stage Cells

Figure 6.6 Plasma Membrane Intactness, Demonstrated by Evans Blue Staining

(A) Window stage leaf stained with Evans Blue. Note the gradient of PCD that exists, with the outermost cells being non-PCD (NPCD) stage cells and the centermost being late-PCD (LPCD) stage cells. Also note that only LPCD stage cells, with collapsed PMs, stain blue. (B) Higher magnification of a similar leaf as shown in panel A, again note that only cells with collapsed PMs possess blue staining. Scale Bars: A = 100 μm, B = 50 μm.

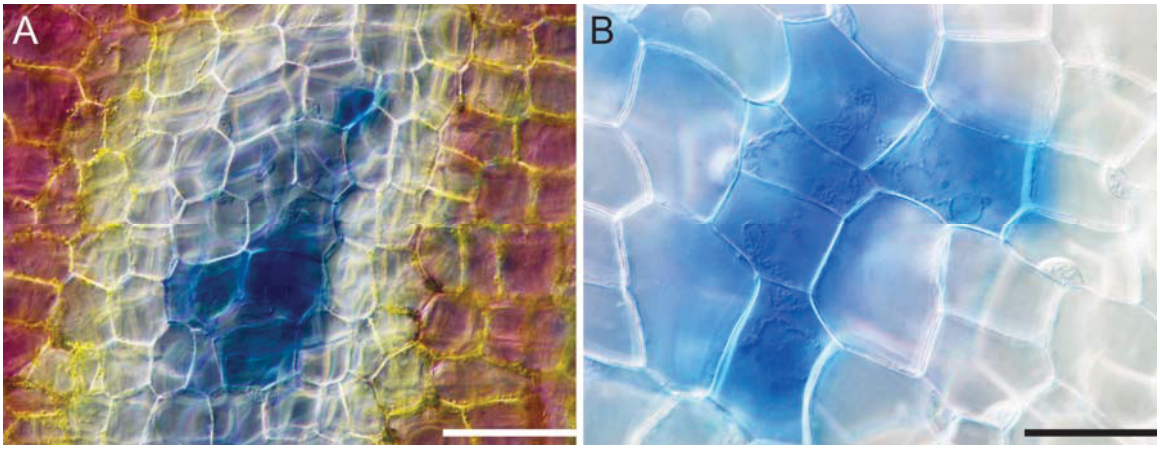

Figure 6.6 Plasma Membrane Intactness, Demonstrated by Evans Blue Staining

Figure 6.7 Time Course Analysis of Cell Wall Degradation

The blue ellipse highlights a single cell for focus. (A) Time 0, has an intact PM. Also note the characteristic aggregate of mitochondria and chlorophyll containing material within the cell, indicated by the black arrow. Inset: Late-PCD (LPCD) stage cell with a collapsed PM and visibly intact cell wall. The collapse of the PM occurs between the stages shown in panels A and B. (B) Time 6 hr, recognize that within this 6 hr time span, the PM of the cell of interest has collapsed, and some cell wall degradation has begun to occur. (C) Time 12 hr, note the cell of interest now has little visible cell wall content. (D) Time 24 hr, note the cell of interest now appears to have very little visible cell wall content and cellular wall degradation is nearly complete. Scale bars: A-D = 100 μm, Inset = 20 μm.

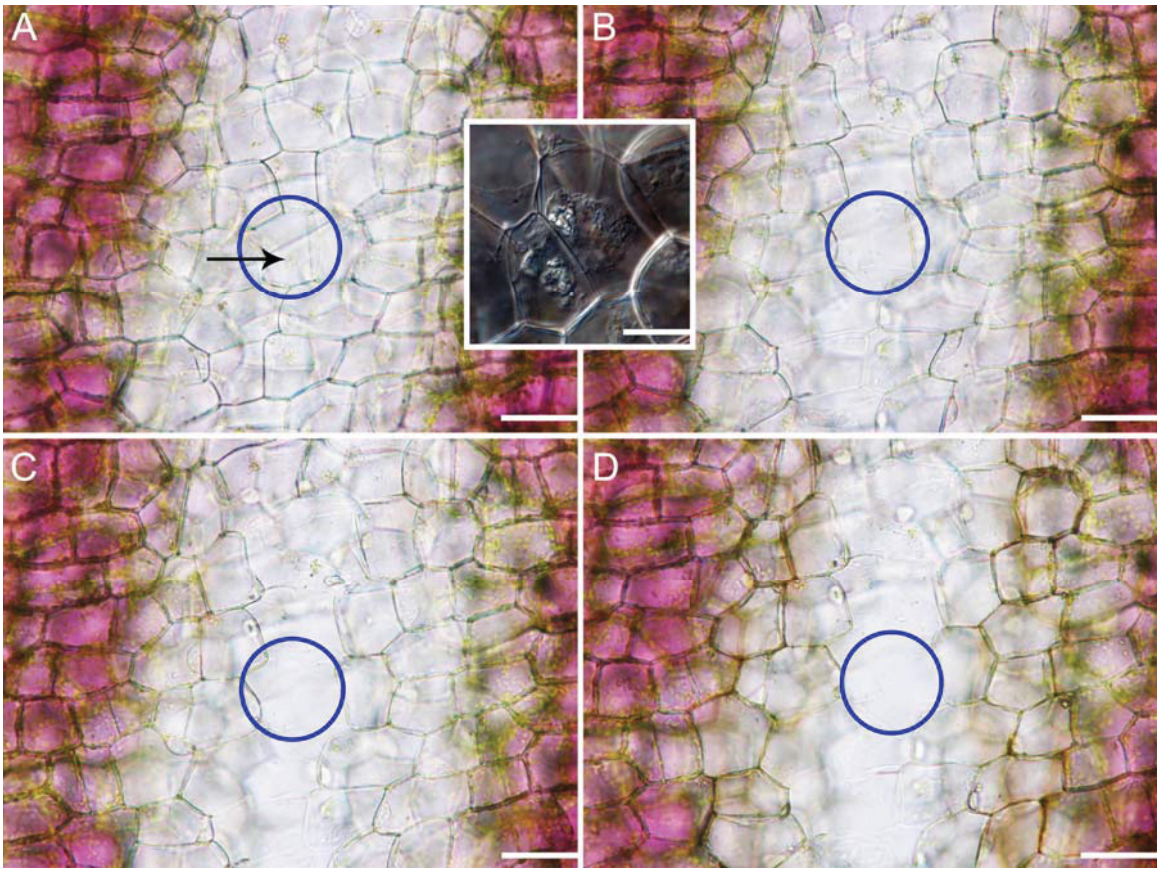

Figure 6.7 Time Course Analysis of Cell Wall Degradation

Figure 6.8 Summary Flowchart

Proposed timeline for cellular changes during developmental PCD throughout lace plant leaf morphogenesis. Note that control, or NPCD stage cells, do not undergo PCD, but instead appear to undergo normal cellular processes throughout the development of the perforation.

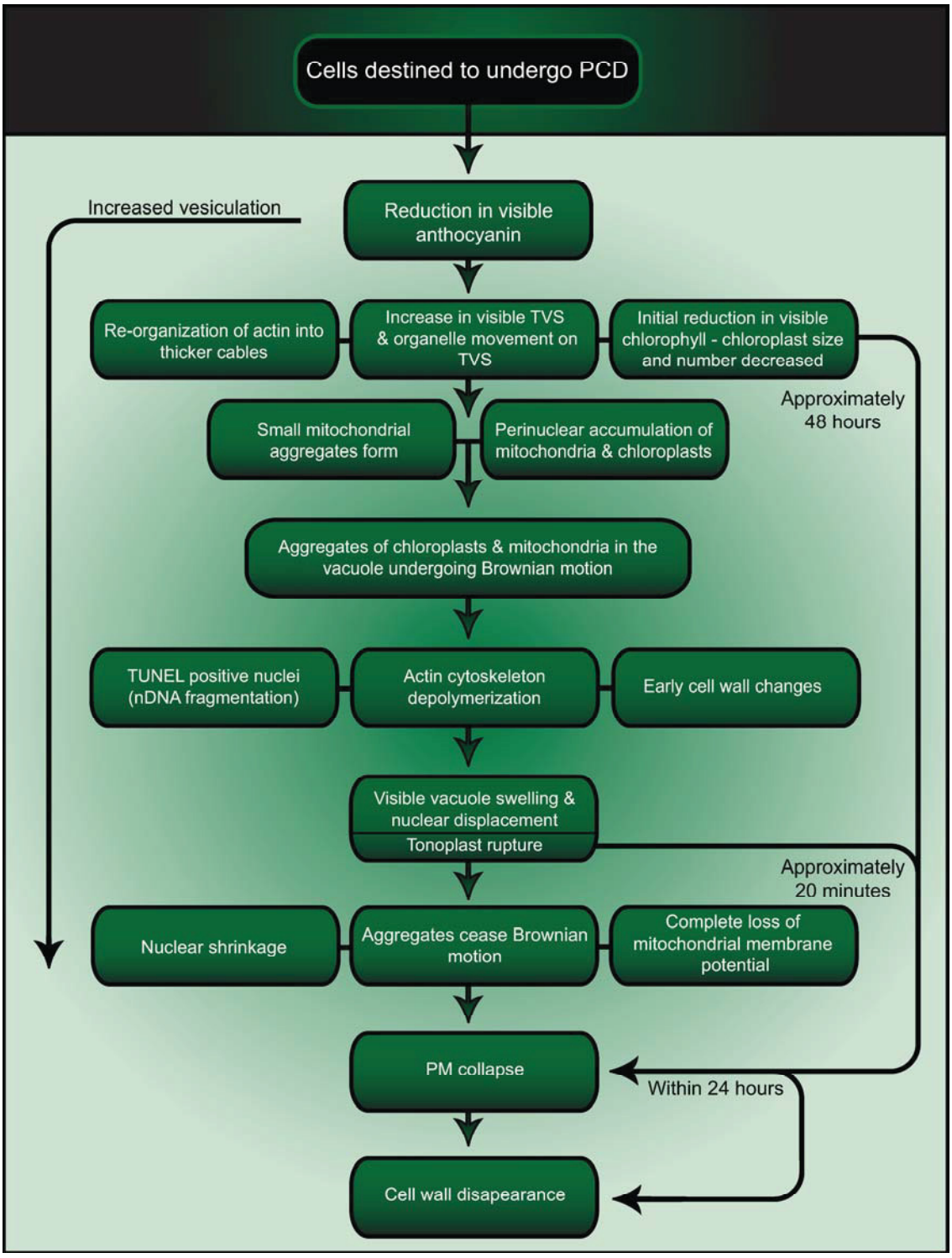

Figure 6.8 Summary Flowchart

Chapter 7 Conclusions

Work presented within the previous chapters' explored the lace plant as an excellent new model system with which to study plant PCD. Large portions of the introduction are aimed at highlighting the significant, but often underestimated similarities between plant and metazoan PCD. The introduction also presents a relevant argument regarding the over-classification of plant PCD, which will be further addressed later in this chapter. This thesis explored the processes of environmentally induced and developmentally regulated programmed cell death (PCD), within the lace plant; data presented within the five primary Chapters (2-6) revealed various commonalities between these two forms of cell death.

This dissertation documented the first successful protocol for protoplast isolation from *Aponogeton madagascariensis*. Leaf stage, carbohydrate source, enzyme solution and incubation time were all determined to have significant impacts on isolation. This work represents one of the few examples of protoplast isolation from a new-model species and demonstrates the difficulties that can be presented when working with non-canonical organisms. Furthermore, these protoplasts were successfully heat shocked (HS) at 55°C for 20 min to induce PCD; similarly HS was also used at 75°C for 20 min to induce necrosis. This induction of cell death in control lace plant protoplasts provided the first ever opportunity to compare both forms of PCD within one plant species. Through this comparison it was revealed that these two forms of PCD shared many common morphological characteristics. Some of these characteristic include: Terminal deoxynucleotidyl transferase mediated dUTP nick-end labeling (TUNEL) positive nuclei, condensed chromatin, increases in vesicles as well as Brownian motion, and plasma

membrane blebbing. The aggregation of mitochondria, cessation of mitochondrial streaming and loss in mitochondrial $\Delta\Psi_m$ was also a common feature of both forms of PCD. Additionally, through the use of the MPTP inhibitor cyclosporine A (CsA) in both cell death systems PCD was halted or significantly delayed; this indirectly suggesting a possible role for the MPTP during both forms of PCD in the lace plant. A detailed comparison of organelle dynamics and timing of both forms of PCD (regulated and induced) is available within Appendix B.

These similarities depict that regardless of the origin of the initial stimulus (internal or external) PCD within the lace plant follows a comparable progression. This knowledge is pertinent to researchers in the field who complete induced cell death research or whose systems warrant only this type of PCD be investigated. Given the systems appear to progress so similarly, inferences made within an induced cell death system could be applied to a regulated counterpart and vs.

Although lace plant protoplasts provide an excellent model to study induced PCD, the lace plants naturally thin and nearly transparent leaves, as well as the extremely predictable pattern of perforation formation, make the plant an even more valuable system within which to study developmentally regulated cell death. Consequently, a focus was placed on the developmental PCD system within this thesis. This focus allowed for not only comparisons between it and the induced counterpart but also permitted for the examination of organelles during regulated PCD on a closer level. Originally a single areole within a window stage leaf was subdivided onto three levels, based on a gradient of cell death; these areas were delineated non-PCD cells (NPCD), early-PCD cells (EPCD) and late-PCD cells (LPCD). This gradient of PCD on both a

spatial and temporal level has also been detailed in spruce embryogenesis (Bozhkov et al. 2004) but lacks this specific naming terminology. Through the use of this gradient an order of organelle events during PCD in the lace plant was determined. Organelle events included the reduction in visible anthocyanin and chlorophyll pigmentation. Perhaps concurrently actin filaments re-organized into bundles. Through the use of live cell imaging and TEM incidences of micro-, macro- and mega autophagy in lace plant PCD were presented. Through the use of the phospholipid bilayer specific dye FM1-43 it was also determined that the aggregates of mitochondria and chloroplasts seen within previous publications were actually within the vacuole undergoing Brownian motion; most likely brought in through micro- or macro- autophagy. Evidence gathered also pointed to tonoplast rupture as a definitive moment in which the cessation of organelle aggregate movement, loss of mitochondrial $\Delta\Psi$m, nuclear shrinkage and PM collapse occur. Total time from reduction in visible chlorophyll to PM collapse was calculated to take approximately 48 hr. Cell wall disappearance followed the collapse of the PM within 24 hr.

Information gathered from Chapter 4 and amalgamated within Chapter 6 detailed mitochondrial dynamics into four distinct categories, linked with the gradient of PCD (NPCD-LPCD). M1 and M2 mitochondria found in EPCD cells were never associated with TUNEL positive nuclei, while M3 and M4 mitochondria were. Given that within M3 and M4 mitochondria cessation of mitochondrial streaming and loss in $\Delta\Psi_m$ is noted, as well as TUNEL positive nuclei, it is accurate to assume that DNA fragmentation occurs after mitochondrial aggregation and perhaps concurrently with cessation of streaming and loss in $\Delta\Psi_m$.

Chapter 5 presented the first plant specific article detailing the link between mitochondria, CLPs and the actin cytoskeleton through the use of pharmacological applications, biochemical analysis and advanced microscopy. This work also revealed the first report of *in vivo* whole plant treatment with caspase inhibitors, and CsA following which the actin cytoskeleton was examined. Results depicted that YVADase (caspase-1) activity is higher during the very early stages of leaf development as compared to mature stage leaves. *In vivo* inhibition of YVADase activity prevented PCD and actin breakdown, while actin depolymerization using Latrunculin B (Lat B) caused no change in YVADase activity, therefore substantiating actin as a likely substrate for caspase-like proteases (CLPs). This link between the actin cytoskeleton and CLPs has been demonstrated within mammalian systems in the past but has not been detailed within plants previously. Finally this work illustrates that the cytoskeleton may not be a crucial executor of PCD within the lace plant but perhaps a downstream substrate for enzymatic activity.

Prior to the work presented in Chapter 6 little research has been conducted *in vivo* to understand the order of organelle changes, which occur during developmentally regulated PCD *in Planta*; therefore the data presented within that manuscript were considered new and unique data sets. This detailed order of events and timing of the PCD process could be utilized as a tool aiding in the classification of cell death in the future. Given several cell death systems are often described based on length and/or order of organelle events (ex. leaf senescence being a lengthy process initially involving chlorophyll degradation and tracheary element (TE) differentiation being extremely expedited and relaying heavily on mega-autophagy) this time course analysis could assist

when making comparisons between the forms of cell death and perhaps shed light on the morphological classifications presented earlier in the introduction.

Overall, as stated in the opening line of van Doorn (2011) “relatively little is known about programmed cell death (PCD) in plants.” This author believes work presented within this dissertation adds indispensable information to the area of PCD research in plants and can be used as a springboard to continue this work in the future. Furthermore, this author feels researchers in this field should be cautious when ascribing stringent categories to partially described systems until further evidence is available. Allowing biochemical and molecular data to accumulate regarding these examples in the future will undoubtly offer an evidence enabling us to classify these systems with increased accuracy. Lets stop filling the fields of the discipline with haphazard definitions and classifications that only confuse newcomers and complicate things for experts, lets keep it simple.

References

Alnemri ES, Livingston D, Nicholson D, Salvesen G, Thornberry N, Wong W, Yuan J. **1996**. Human ICD/CED-3 protease nomenclature. *Cell* **87**: 171.

Arpagaus S, Rawyler A, Braendle R. **2002**. Occurrence and characteristics of the mitochondrial permeability transition in plants. *The Journal of Biological Chemistry* **277**: 1780–1787.

Bajt ML, Cover C, Lemasters JJ, Jaeschke H. **2006**. Nuclear translocation of endonuclease G and apoptosis-inducing factor during acetaminophen-induced liver cell injury. *Toxicological Sciences: An Official Journal of the Society of Toxicology* **94**: 217–225.

Balk J, Chew SK, Leaver CJ, McCabe PF. **2003**. The intermembrane space of plant mitochondria contains a DNase activity that may be involved in programmed cell death. *The Plant Journal* **34**: 573–583.

Balk J, Leaver CJ. **2001**. The PET1-CMS mitochondrial mutation in sunflower is associated with premature programmed cell death and cytochrome c release. *The Plant Cell* **13**: 1803–1818.

Balk J, Leaver CJ, McCabe PF. **1999**. Translocation of cytochrome c from the mitochondria to the cytosol occurs during heat-induced programmed cell death in cucumber plants. *FEBS Letters* **463**: 151–154.

Battraw M, Hall TC. **1991**. Stable transformation of *Sorghum bicolor* protoplasts with chimeric neomycin phosphotransferase II and -glucuronidase genes. *Theoretical and Applied Genetics* **82**: 161–168.

Benítez-Rangel E, García L, Namorado MC, Reyes JL, Guerrero-Hernández A. **2011**. Ion channel inhibitors block caspase activation by mechanisms other than restoring intracellular potassium concentration. *Cell Death and Disease* **2**: 1–8.

Bonneau L, Ge Y, Drury GE, Gallois P. **2008**. What happened to plant caspases? *Journal of Experimental Botany* **59**: 491–499.

Bozhkov P, Jansson C. **2007**. Autophagy and cell-death proteases in plants: Two wheels of a funeral cart. *Autophagy* **3**: 136–138.

Bozhkov PV, Filonova LH, Suarez MF, Helmersson A, Smertenko AP, Zhivotovsky B, Von Arnold S. **2004**. VEIDase is a principal caspase-like activity involved in plant programmed cell death and essential for embryonic pattern formation. *Cell Death and Differentiation* **11**: 175–182.

Bozhkov PV, Smertenko AP, Zhivotovsky B. **2010**. Aspasing out metacaspases and caspases: proteases of many trades. *Science Signaling* **3**: pe48.

Bozhkov PV, Suarez MF, Filonova LH, Daniel G, Zamyatnin AA, Rodriguez-Nieto S, Zhivotovsky B, Smertenko A. **2005**. Cysteine protease mcII-Pa executes programmed cell death during plant embryogenesis. *Proceedings of the National Academy of Sciences of the United States of America* **102**: 14463–14468.

Bratton SB, Salvesen GS. **2010**. Regulation of the Apaf-1-caspase-9 apoptosome. *Journal of Cell Science* **123**: 3209–3214.

Breeze E, Harrison E, McHattie S, Hughes L, Hickman R, Hill C, Kiddle S, Kim Y-S, Penfold CA, Jenkins D, Zhang C, Morris K, Jenner C, Jackson S, Thomas B, Tabrett A, Legaie R, Moore JD, Wild DL, Ott S, Rand D, Beynon J, Denby K, Mead A, Buchanan-Wollaston V. **2011**. High-resolution temporal profiling of transcripts during Arabidopsis leaf senescence reveals a distinct chronology of processes and regulation. *The Plant Cell* **23**: 873–894.

Browder L, Iten L. **1998**. Programmed cell death in development- dynamic development. *University of Calgary*: http://people.ucalgary.ca/~browder/apoptosis.html.

Chen S, Dickman MB. **2004**. Bcl-2 family members localize to tobacco chloroplasts and inhibit programmed cell death induced by chloroplast-targeted herbicides. *Journal of Experimental Botany* **55**: 2617–2623.

Chinnaiyan AM. **1997**. Interaction of CED-4 with CED-3 and CED-9: A molecular framework for cell death. *Science* **21**: 1122–1126.

Chowdhury I, Tharakan B, Bhat GK. **2008**. Caspases— An update. *Comparative Biochemistry and Physiology, Part B* **151**: 10–27.

Coffeen WC, Wolpert TJ. **2004**. Purification and characterization of serine proteases that exhibit caspase-like activity and are associated with programmed cell death in *Avena sativa*. *The Plant Cell* **16**: 857–873.

Conradt B. **2009**. Genetic control of programmed cell death during animal development. *Annual Review of Genetics* **43**: 493–523.

Conradt B, Xue D. **2005**. Programmed cell death. *WormBook : the Online Review of C. elegans Biology*: 1–13.

Contran N, Cerana R, Crosti P, Malerba M. **2007**. Cyclosporin A inhibits programmed cell death and cytochrome c release induced by fusicoccin in sycamore cells. *Protoplasma* **231**: 193–199.

Crompton M. **1999**. The mitochondrial permeability transition pore and its role in cell death. *The Biochemical Journal* **341**: 233–249.

Curtis MJ, Wolpert TJ. **2002**. The oat mitochondrial permeability transition and its implication in victorin binding and induced cell death. *The Plant Journal* **29**: 295–312.

Danon A, Delorme V, Mailhac N, Gallois P. **2000**. Review plant programmed cell death: A common way to die. *Plant Physiology Biochemistry* **38**: 647–655.

Danon A, Gallois P. **1998**. UV-C radiation induces apoptotic-like changes in Arabidopsis thaliana. *FEBS letters* **437**: 131–136.

Darland-Ransom M, Wu Y-C, Xue D. **2009**. Programmed cell death in *C. elegans*. *In: Essentials of Apoptosis* (Dong Z, Yin X-M, Ed). Totowa, NJ: Humana Press, 355–373.

Denault J-B, Salvesen GS. **2002**. Caspases: keys in the ignition of cell death. *Chemical Reviews* **102**: 4489–500.

Denton D, Nicolson S, Kumar S. **2012**. Cell death by autophagy: facts and apparent artefacts. *Cell Death and Differentiation* **19**: 87–95.

Diamond M, McCabe PF. **2007**. The mitochondrion and plant programmed cell death. *Plant Mitochondria- Annual Plant Reviews* (Logan DC, Ed). Blackwell Publishing, 308–334.

Dickman MB, Park YK, Oltersdorf T, Li W, Clemente T, French R. **2001**. Abrogation of disease development in plants expressing animal antiapoptotic genes. *Proceedings of the National Academy of Sciences of the United States of America* **98**: 6957–6962.

Dion M, Chamberland H, St-Michel C, Plante M, Darveau A, Lafontaine JG, Brisson LF. **1997**. Detection of a homologue of bcl-2 in plant cells. *Biochemistry and Cell Biology* **75**: 457–461.

Drew MC, He CJ, Morgan PW. **2000**. Programmed cell death and aerenchyma formation in roots. *Trends in Plant Science* **5**: 12312–12317.

Edinger AL, Thompson CB. **2004**. Death by design: apoptosis, necrosis and autophagy. *Current Opinion in Cell Biology* **16**: 663–669.

Eichmann R, Schultheiss H, Kogel K-H, Hückelhoven R. **2004**. Bax inhibitor-1 compromises nonhost penetration resistance of barley to the inappropriate pathogen *Blumeria graminis* f. sp. tritici. *Molecular Plant-Microbe Interactions* **17**: 484–490.

Elliott A, Gunawardena A H L A N. **2010**. Calcium inhibition halts developmental programmed cell death in the lace plant, *Aponogeton madagascariensis*? *Botany*: 206–210.

Ellis HM, Horvitz RH. **1986**. Genetic control of programmed cell death in nematod *C. elegans*. *Cell* **44**: 817–829.

Elmore S. **2007**. Apoptosis: A review of programmed cell death. *Toxicologic Pathology* **35**: 495–516.

Enoksson M, Salvesen GS. **2010**. Metacaspases are not caspases--always doubt. *Cell Death and Differentiation* **17**: 1221.

Evans DE. **2004**. Programmed cell death in response to abiotic stress. In: Programmed Cell Death in Plants (J Gray, Ed). Blackwell.

Filonova LH, Bozhkov PV, Brukhin VB, Daniel G, Zhivotovsky B, Arnold SV. **2000**. Two waves of programmed cell death occur during formation and development of somatic embryos in the gymnosperm, Norway spruce. *Journal of Cell Science* **113**: 4399–4411.

Filonova LH, Suárez MF, Bozhkov PV. **2008**. Detection of programmed cell death in plant embryos. *Methods in Molecular Biology* **427**: 173–179.

Fortes F, Castilho RF, Catisti R, Carnieri EGS, Vercesi AE. **2001**. Ca2+ induces a cyclosporine A-insensitive permeability transition pore in isolated potato tuber mitochondria mediated by reactive oxygen species. *Journal of Bioenergetics and Biomembranes* **33**: 43–51.

Franklin-Tong VE, Gourlay CW. **2008**. A role for actin in regulating apoptosis/programmed cell death: evidence spanning yeast, plants and animals. *The Biochemical Journal* **413**: 389–404.

Fukuda H. **1997**. Tracheary element differentiation. *The Plant Cell* **9**: 3–7.

Fukuda H. **2000**. Programmed cell death of tracheary elements as a paradigm in plants. *Plant Molecular Biology* **44**: 245–253.

Fukuda H, Watanabe Y, Kuriyama H, Aoyagi S, Sugiyama M, Yamamoto R, Demura T, Minami A. **1998**. Programming of cell death during xylogenesis. *Journal of Plant Research* **111**: 253–256.

Gao C, Xing D, Li L, Zhang L. **2008**. Implication of reactive oxygen species and mitochondrial dysfunction in the early stages of plant programmed cell death induced by ultraviolet-C overexposure. *Planta* **227**: 755–767.

Gartner A, Alpi A, Schumacher B. **2003**. Programmed cell death in *C. elegans* (Grimm S, Ed). *Genetics of Apoptosis*: 155–175.

Genescà M, Sola A, Hotter G. **2006**. Actin cytoskeleton derangement induces apoptosis in renal ischemia/reperfusion. *Apoptosis* **11**: 563–571.

Giuliani C, Consonni G, Gavazzi G, Colombo M, Dolfini S. **2002**. Programmed cell death during embryogenesis in maize. *Annals of Botany* **90**: 287–292.

Golstein P, Kroemer G. **2007**. Cell death by necrosis: towards a molecular definition. *Trends in Biochemical Sciences* **32**: 37–43.

Gourlay CW, Ayscough KR. **2005**. The actin cytoskeleton: a key regulator of apoptosis and ageing? *Nature Reviews. Molecular Cell Biology* **6**: 583–589.

Gray J. **2004**. Paradigms of the evolution of programmed cell death. *In: Programmed Cell Death in Animals and Plants* (Gray J, Ed). Blackwell Publishing, 1–25.

Green DR, Reed JC. **1998**. Mitochondria and apoptosis. *Science* **281**: 1309–1312.

Groover A, DeWitt N, Heidel A, Jones A. **1997**. Programmed cell death of plant tracheary elements differentiating *in vitro*. *Protoplasma* **196**: 197–211.

Gross A, Mcdonnell JM, Korsmeyer SJ. **1999**. BCL-2 family members and the mitochondria in apoptosis. *Genes & Development* **13**: 1899–1911.

Gunawardena A H L A N. **2008**. Programmed cell death and tissue remodelling in plants. *Journal of Experimental Botany* **59**: 445–451.

Gunawardena A H L A N, Dengler NG. **2006**. Alternative modes of leaf dissection in monocotyledons. *Botanical Journal of the Linnean Society*: 25–44.

Gunawardena A H L A N, Greenwood JS, Dengler NG. **2004**. programmed cell Death remodels lace plant leaf shape during development. *The Plant Cell* **16**: 60–73.

Gunawardena A H L A N, Greenwood JS, Dengler NG. **2007**. cell wall degradation and modification during programmed cell death in lace plant, *Aponogeton madagascariensis* (Aponogetonaceae). *American Journal of Botany* **94**: 1116–1128.

Gunawardena A H L A N, Navachandrabala C, Kane M, Dengler NG. **2006**. Lace plant: A novel system for studying developmental programmed cell death. In: Teixeira da Silva JA, ed. *Floriculture, Ornamental and Plant Biotechnology: Advances and Topical issues*. Global Science Books, 157–162.

Gunawardena A H L A N, Pearce DME, Jackson MB, Hawes CR, Evans DE. **2001**. Rapid changes in cell wall pectic polysaccharides are closely associated with early stages

of aerenchyma formation , a spatially localized form of programmed cell death in roots of maize (*Zea mays* L.) promoted by ethylene. *Plant, Cell and Environment* **212**: 1369–1375.

Gunawardena A H L A N, Sault K, Donnelly P, Greenwood JS, Dengler NG. **2005**. Programmed cell death and leaf morphogenesis in *Monstera obliqua* (Araceae). *Planta* **221**: 607–618.

Gunter TE, Buntinas L, Sparagna G, Eliseev R, Gunter K. **2000**. Mitochondrial calcium transport: mechanisms and functions. *Cell Calcium* **28**: 285–296.

Halestrap AP, Gillespie JP, Otoole A, Doran E. **2000**. Mitochondria and cell death: a pore way to die? *In*:*Programmed Cell Death in Animals and Plants* (Bryant JA, Hughes SG, Garland JM, Ed). BIOS Scientific Publishers, 65–80.

Hara-Nishimura I, Hatsugai N, Nakaune S, Kuroyanagi M, Nishimura M. **2005**. Vacuolar processing enzyme: an executor of plant cell death. *Current Opinion in Plant Biology* **8**: 404–408.

Harris R, Wright M, Byrne M, Varnum J, Brightwell B, Schubert K. **1988**. Callus formation and plantlet regeneration from protoplasts derived from suspension cultures of wheat (*Triticum aestivum* L.). *Plant Cell Reports* **7**: 337–340.

Hatsugai N, Kuroyanagi M, Nishimura M, Hara-Nishimura I. **2006**. A cellular suicide strategy of plants: vacuole-mediated cell death. *Apoptosis* **11**: 905–911.

Hatsugai N, Kuroyanagi M, Yamada K, Meshi T, Tsuda S, Kondo M, Nishimura M, Hara-Nishimura I. **2004**. A plant vacuolar protease, VPE, mediates virus-induced hypersensitive cell death. *Science* **305**: 855–858.

He R, Drury GE, Rotari VI, Gordon A, Willer M, Farzaneh T, Woltering EJ, Gallois P. **2008**. Metacaspase-8 modulates programmed cell death induced by ultraviolet light and H_2O_2 in Arabidopsis. *The Journal of Biological Chemistry* **283**: 774–783.

Helmersson A, Von Arnold S, Bozhkov PV. **2008**. The level of free intracellular zinc mediates programmed cell death/cell survival decisions in plant embryos. *Plant Physiology* **147**: 1158–1167.

Hengartner MO. **2000**. The biochemistry of apoptosis. *Nature* **407**: 770–776.

Hengartner MO, Bryant JA. **2000**. Apoptotic cell death: from worms to wombats . . . but what about the weeds? *In: Programmed Cell Death in Animals and Plants* (Bryant JA, Hughes SG, Garland JM, Ed). BIOS Scientific Publishers, 1–12.

Hetz C, Glimcher L. **2007**. The daily job of night killers: alternative roles of the BCL-2 family in organelle physiology. *Trends in Cell Biology* **18**: 38–44.

Higaki T, Goh T, Hayashi T, Kutsuna N, Kadota Y, Hasezawa S, Sano T, Kuchitsu K. **2007**. Elicitor-induced cytoskeletal rearrangement relates to vacuolar dynamics and execution of cell death: in vivo imaging of hypersensitive cell death in tobacco BY-2 cells. *Plant & Cell Physiology* **48**: 1414–1425.

Hoeberichts FA, Woltering EJ. **2003**. Multiple mediators of plant programmed cell death: interplay of conserved cell death mechanisms and plant-specific regulators. *BioEssays* **25**: 47–57.

Iakimova ET, Woltering EJ, Kapchina-Toteva VM, Harren FJM, Cristescu SM. **2008**. Cadium toxicity in cultured tomato cells- role of ethylene, proteases and oxidative stress in cell death signalling. *Cell Biology International* **32**: 1521–1529.

Inada N, Sakai A, Kuroiwa H, Kuroiwa T. **1999**. Senescence program in rice (*Oryza sativa* L.) leaves : analysis of the blade of the second leaf at the tissue and cellular levels. *Protoplasma*: 222–232.

Inohara N, Ogura Y, Nuñez G. **2002**. Nods: a family of cytosolic proteins that regulate the host response to pathogens. *Current Opinion in Microbiology* **5**: 76–80.

Jabbour AM, Puryer MA, Yu JY, Lithgow T, Riffkin CD, Ashley DM, Vaux DL, Ekert PG, Hawkins CJ. **2006**. Human Bcl-2 cannot directly inhibit the *Caenorhabditis elegans* Apaf-1 homologue CED-4, but can interact with EGL-1. *Journal of Cell Science* **119**: 2572–2582.

Jacobson MD. **1996**. Reactive oxygen species and programmed cell death. *TIBS*: 83–86.

Jan N, Hussain M-U, Andrabi KI. **2008**. Programmed cell death or apoptosis: Do animals and plants share anything in common. *Biotechnology and Molecular Biology Reviews* **3**: 111–126.

Jones A. **2000**. Does the plant mitochondrion integrate cellular stress and regulate programmed cell death? *Trends in Plant Science* **5**: 225–230.

Jones AM. **2001**. Programmed cell death in development and defense. *Plant Physiology* **125**: 94–97.

Joza N, Susin SA, Daugas E, Stanford WL, Cho SK, Li CY, Sasaki T, Elia AJ, Cheng HY, Ravagnan L, Ferri KF, Zamzami N, Wakeham A, Hakem R, Yoshida H, Kong YY, Mak TW, Zúñiga-Pflücker JC, Kroemer G, Penninger JM. **2001**. Essential role of the mitochondrial apoptosis-inducing factor in programmed cell death. *Nature* **410**: 549–554.

Kacprzyk J, Daly CT, McCabe PF. **2011**. The Botanical Dance of Death: Programmed Cell Death in Plants. *In: Advances in Botanical Research* (Kader J-C, Delseny M, Ed). Elsevier Ltd., 169–261.

Kasselmann C. **2003.** *Aquarium Plants*. Malabar: Krieger Publishing Co, 132–133.

Kawai-Yamada M, Jin L, Yoshinaga K, Hirata A, Uchimiya H. **2001**. Mammalian Bax-induced plant cell death can be down-regulated by overexpression of Arabidopsis Bax Inhibitor-1 (AtBI-1). *Proceedings of the National Academy of Sciences of the United States of America* **98**: 12295–12300.

Kim H-E, Du F, Fang M, Wang X. **2005**. Formation of apoptosome is initiated by cytochrome c-induced dATP hydrolysis and subsequent nucleotide exchange on Apaf-1. *Proceedings of the National Academy of Sciences of the United States of America* **102**: 17545–17550.

Kinchen JM, Cabello J, Klingele D, Wong K, Feichtinger R, Schnabel H, Schnabel R, Hengartner MO. **2005**. Two pathways converge at CED-10 to mediate actin rearrangement and corpse removal in *C. elegans*. *Nature* **434**: 93–99.

Kinoshita T, Nishimura M, Hara-nishimura I. **1995**. Homologues of a vacuolar processing enzyme that are expressed in different organs in *Arabidopsis thaliana*. *Plant Molecular Biology* **61393**: 81–89.

Kroemer G, Galluzzi L, Brenner C. **2007**. Mitochondrial membrane permeabilization in cell death. *Physiological Reviews* **87**: 99–163.

Kroemer G, Galluzzi L, Vandenabeele P, Abrams J, Alnemri ES, Baehrecke EH, Blagosklonny MV, El-Deiry WS, Golstein P, Green DR, Hengartner M, Knight RA, Kumar S, Lipton SA, Malorni W, Nuñez G, Peter ME, Tschopp J, Yuan J, Piacentini M, Zhivotovsky B, Melino G. **2009**. Classification of cell detah: recommendations of the nomenclature committee on cell death 2009. *Cell Death and Differentiation* **16**: 3–11.

Kroemer G, Zamzami N, Susin SA. **1997**. Mitochondrial control of apoptosis. *Immunology Today* **18**: 44–51.

Kuriyama H, Fukuda H. **2002**. Developmental programmed cell death in plants. *Current Opinion in Plant Biology* **5**: 568–573.

Kuroyanagi M, Nishimura M, Hara-Nishimura I. **2002**. Activation of Arabidopsis vacuolar processing enzyme by self-catalytic removal of an auto-inhibitory domain of the C-terminal propeptide. *Plant & Cell Physiology* **43**: 143–151.

Kuwana T, Newmeyer DD. **2003**. Bcl-2-family proteins and the role of mitochondria in apoptosis. *Current Opinion in Cell Biology* **15**: 1–9.

Kwon SI, Park OK. **2008**. Autophagy in plants. *Journal of Plant Biology* **51**: 313–320.

Lam E. **2004**. Controlled cell death, plant survival and development. *Nature Reviews. Molecular Cell Biology* **5**: 305–315.

Lam E, Kato N, Lawton M. **2001**. Programmed cell death, mitochondria and the plant hypersensitive response. *Nature* **411**: 848–853.

Lam E, Del Pozo O. **2000**. Caspase-like protease involvement in the control of plant cell death. *Plant Molecular Biology* **44**: 417–428.

Lettre G, Hengartner MO. **2006**. Developmental apoptosis in *C. elegans:* a complex CEDnario. *Nature Reviews. Molecular Cell Biology* **7**: 97–108.

Lim PO, Kim HJ, Nam HG. **2007**. Leaf senescence. *Annual Review of Plant Biology* **58**: 115–136.

Lin J, Wang Y, Wang G. **2005**. Salt stress-induced programmed cell death via Ca2+-mediated mitochondrial permeability transition in tobacco protoplasts. *Plant Growth Regulation* **45**: 243–250.

Lin J, Wang Y, Wang G. **2006**. Salt stressed-induced programmed cell death in tobacco protoplasts is mediated by reactive oxygen species and mitochondrial permeability transition pore status. *Journal of Plant Physiology* **163**: 2006.

Liu Y, Schiff M, Czymmek K, Tallóczy Z, Levine B, Dinesh-Kumar SP. **2005**. Autophagy regulates programmed cell death during the plant innate immune response. *Cell* **121**: 567–577.

Liu Z-Q, Xu G-H, Zhang S-L. **2007**. *Pyrus pyrifolia* stylar S-RNase induces alterations in the actin cytoskeleton in self-pollen and tubes in vitro. *Protoplasma* **232**: 61–67.

Lord CEN, Gunawardena A H L A N. **2010**. Isolation of leaf protoplasts from the submerged aquatic monocot *Aponogeton madagascariensis*. *The Americas Journal of Plant Science and Biotechnology* **4**: 6–11.

Lord CEN, Gunawardena A H L A N. **2011**. Environmentally induced programmed cell death in leaf protoplasts of *Aponogeton madagascariensis*. *Planta* **233**: 407–21.

Lord CEN, Gunawardena A H L A N. **2012a**. Programmed cell death in *C. elegans*, mammals and plants. *European Journal of Cell Biology* **91**: 603–613.

Lord CEN, Gunawardena A H L A N. **2012b**. Erratum to: Environmentally induced programmed cell death in leaf protoplasts of *Aponogeton madagascariensis*. *Planta*: 1825.

Lord CEN, Gunawardena AHAN. **2012**. The lace plant: a novel model system to study plant proteases during developmental programmed cell death in vivo. *Physiologia Plantarum*.

Lord CEN, Wertman JN, Lane S, Gunawardena A H L A N. **2011**. Do mitochondria play a role in remodelling lace plant leaves during programmed cell death? *BMC Plant Biology* **11**: 102.

McCabe PF, Leaver CJ. **2000**. Programmed cell death in cell cultures. *Plant Molecular Biology* **44**: 359–368.

McCabe PF, Levine A, Maijer P-J, Tapon NA, Pennell RI. **1997**. A programmed cell death pathway activated in carrot cells cultured at low cell density. *The Plant Joural* **12**: 267–280.

Michele R De, Formentin E, Schiavo F Lo. **2009**. Legume leaf senescence. *Plant Signaling and Behavior*: 319–320.

Minamikawa T, Toyooka K, Okamoto T, Hara-Nishimura I, Nishimura M. **2001**. Degradation of ribulose-bisphosphate carboxylase by vacuolar enzymes of senescing French bean leaves: immunocytochemical and ultrastructural observations. *Protoplasma* **218**: 144–153.

Mishra S, Tyagi A, Dwivedi SP. **2011**. Regulation of apoptosis in living organisms : A biotechnological approach. *Biotechnology, Bioinformatics and Bioengineering* **1**: 1–18.

Mittler R, Lam E. **1997**. Characterization of nuclease activities and DNA fragmentation induced upon hypersensitive response cell death and mechanical stress. *Plant Molecular Biology* **34**: 209–221.

Nehme R, Conradt B. **2009**. Egl-1: a key activator of apoptotic cell death in *C. elegans*. *Oncogene* **27**: S30–S40.

Newman JR, Raven JA. **1999**. CO_2 is the main inorganic C species entering photosynthetically active leaf protoplasts of the freshwater macrophyte *Ranunculus penicillatus* ssp. pseudofluitans. *Plant, Cell and Environment*: 1019–1026.

Obara K, Fukuda H. **2004**. Programmed cell death in xylem differentiation. *In: Programmed Cell Death in Plants* (Gray J, Ed). Blackwell Publishing, 131–154.

Obara K, Kuriyama H, Fukuda H. **2001**. Direct evidence of active and rapid nuclear degradation triggered by vacuole rupture during programmed cell death in *Zinnia*. *Plant Physiology* **125**: 615–626.

Odaka C, Sanders ML, Crews P. **2000**. Jasplakinolide induces apoptosis in various transformed cell lines by a caspase-3-like protease-dependent pathway. *Clinical and Diagnostic Laboratory Immunology* **7**: 947–952.

Oliveira H, Saviani E, Oliveira J, Salgado I. **2007**. Cyclosporin A inhibits calcium uptake by *Citrus sinensis* mitochondria. *Plant Science* **172**: 665–670.

Parrish J, Li L, Klotz K, Ledwich D, Wang X, Xue D. **2001**. Mitochondrial endonuclease G is important for apoptosis in *C. elegans*. *Nature* **412**: 90–94.

Pavlovskaya NS, Savinova OV, Grabel'nykh OI, Pobezhimova TP, Koroleva NA, Voinikov VK. **2007**. The cyclosporine-A-sensitive mitochondrial permeability transition pore in winter wheat at a low temperature and under oxidative stress. *Doklady Biological Sciences* **417**: 446–448.

Pennell RI, Lamb C. **1997**. Programmed cell death in plants. *The Plant Cell* **9**: 1157–1168.

Pepper C, Bentley P. **2000**. The role of the Bcl-2 family in the modulation of apoptosis. *In: Programmed Cell Death in Animals and Plants* (Bryant JA, Hughes SG, Garland JM, Ed). BIOS Scientific Publishers, 43–54.

Piszczek E, Gutman W. **2007**. Caspase-like proteases and their role in programmed cell death in plants. *Acta Physiologiae Plantarum* **29**: 391–398.

Pongchawee K, Na-nakorn U, Lamseejan S, Poompuang S, Phansiri S. **2007**. Protoplast isolation and culture of aquatic plant *Cryptocoryne wendtii* De Wit. : 300–310.

Pongchawee K, Na-nakorn U, Lanseejan S, Poompuang S, Phansiri S. **2006**. Factors affecting the protoplast isolation and culture of *Anunias nana* Engler. *International Journal of Botany* **2**: 193–200.

Potokar M, Kreft M, Chowdhury HH, Vardjan N, Zorec R. **2006**. Subcellular localization of Apaf-1 in apoptotic rat pituitary cells. *American Journal of Physiology. Cell Physiology* **290**: C672–C677.

Potten C, Wilson J. **2004**. *Apoptosis- The life and death of cells*. Cambridge: Cambridge University Press.

Poulter NS, Staiger CJ, Rappoport JZ, Franklin-Tong VE. **2010**. Actin-binding proteins implicated in the formation of the punctate actin foci stimulated by the self-incompatibility response in *Papaver*. *Plant Physiology* **152**: 1274–1283.

Poulter NS, Vatovec S, Franklin-tong VE. **2008**. Microtubules are a target for self-incompatibility signaling in *Papaver* pollen. *Plant Physiology* **146**: 1358–1367.

Pourkarimi E, Greiss S, Gartner A. **2011**. Evidence that CED-9 / Bcl2 and CED-4 / Apaf-1 localization is not consistent with the current model for *C. elegans* apoptosis induction. *Cell Death and Differentiation*: 1–10.

Del Pozo O, Lam E. **1998**. Caspases and programmed cell death in the hypersensitive response of plants to pathogens. *Current Biology* **8**: 1129–1132.

Reape TJ, McCabe PF. **2008**. Apoptotic-like programmed cell death in plants. *The New Phytologist* **180**: 13–26.

Reape TJ, Molony EM, McCabe PF. **2008**. Programmed cell death in plants: distinguishing between different modes. *Journal of Experimental Botany* **59**: 435–444.

Reisen D, Marty F, Leborgne-Castel N. **2005**. New insights into the tonoplast architecture of plant vacuoles and vacuolar dynamics during osmotic stress. *BMC Plant Biology* **5**: 13.

Rogers HJ. **2005**. Cell death and organ development in plants. *In:Current Topics in Developmental Biology* (Schatten GP, Ed). Elsevier, 225–261.

Rogers HJ. **2006**. Programmed cell death in floral organs: how and why do flowers die? *Annals of Botany* **97**: 309–315.

Rojo E, Martı R, Carter C, Zouhar J, Pan S, Plotnikova J, Jin H, Paneque M, Sa J, Baker B, Ausubel FM, Raikhel Natasha V. **2004**. VPE exhibits a caspase-like activity that contributes to defense against pathogens. *Current Biology* **14**: 1897–1906.

Ryerson DE, Heath MC. **1996**. Cleavage of nuclear DNA into oligonucleosomal fragments during cell death induced by fungal infection or by abiotic treatments. *The Plant Cell* **8**: 393–402.

Sanmartin M, Jaroszewski L, Raikhel N V, Rojo E. **2005**. Caspases. Regulating death since the origin of life. *Plant Physiology* **137**: 841–847.

Schwartz HT. **2007**. A protocol describing pharynx counts and a review of other assays of apoptotic cell death in the nematode worm *Caenorhabditis elegans*. *Nature Protocols* **2**: 705–14.

Schwarzerová K, Vondráková Z, Fischer L, Boríková P, Bellinvia E, Eliásová K, Havelková L, Fiserová J, Vágner M, Opatrný Z. **2010**. The role of actin isoforms in somatic embryogenesis in Norway spruce. *BMC Plant Biology* **10**: 89.

Scott I, Logan DC. **2007**. Mitochodnrial dynamics: the control of mitochondrial shape, size, number, motility, and cellular inheritance. *In:Programmed Cell Death in Plants* (Gray J, Ed.). Blackwell Publishing, 1–35.

Scott I, Logan DC. **2008**. Mitochondrial morphology transition is an early indicator of subsequent cell death in Arabidopsis. *The New Phytologist* **177**: 90–101.

Selga T, Selga M, Pāvila V. **2005**. Death of mitochondria during programmed cell death of leaf mesophyll cells. *Cell Biology International* **29**: 1050–1056.

Senatore A, Trobacher CP, Greenwood JS. **2009**. Ricinosomes predict programmed cell death leading to anther dehiscence in tomato. *Plant Physiology* **149**: 775–790.

Sergueff M. **1907**. Contribution á la Morphologie et la Biologie des Aponogetonacees.: 1907. PhD dissertation.

Shabala S. **2009**. Salinity and programmed cell death: unravelling mechanisms for ion specific signalling. *Journal of Experimental Botany* **60**: 709–12.

Sheen J. **1993**. Protein phosphatase activity is required for light-inducible gene expression in maize. *The EMBO Journal* **12**: 3497–505.

Shi Y. **2001**. A structural view of mitochondria-mediated apoptosis. *Nature Structural Biology* **8**: 394–401.

Smertenko A, Franklin-Tong VE. **2011**. Organisation and regulation of the cytoskeleton in plant programmed cell death. *Cell Death and Differentiation* **18**: 1263–1270.

Smertenko AP, Bozhkov PV, Filonova LH, Von Arnold S, Hussey PJ. **2003**. Re-organisation of the cytoskeleton during developmental programmed cell death in *Picea abies* embryos. *The Plant Journal* **33**: 813–824.

Smith LG, Oppenheimer DG. **2005**. Spatial control of cell expansion by the plant cytoskeleton. *Annual Review of Cell and Developmental Biology* **21**: 271–295.

Snowman BN, Kovar DR, Shevchenko G, Franklin-Tong VE, Staiger CJ. **2002**. Signal-mediated depolymerization of actin in pollen during the self-incompatibility response. *The Plant Cell* **14**: 2613–2626.

Staal M, Prins HBA, Harmelen M, Helder RJ. **1988**. The isolation of leaf protoplasts from the submerged aquatic angiosperm *Potamogeton lucens* L. *Plant, Cell and Environment* **11**: 715–719.

Staiger CJ, Franklin-Tong VE. **2003**. The actin cytoskeleton is a target of the self-incompatibility response in *Papaver rhoeas*. *Journal of Experimental Botany* **54**: 103–113.

Stennicke HR. **2000**. Caspases- at the cutting edge of cell death. In: Programmed cell death in animals and plants. *In: Programmed Cell Death in Animals and Plants* (Bryant JA, Hughes SG, Garland JM, Ed). BIOS Scientific Publishers, 13–30.

Stennicke HR, Salvesen GS. **2000**. Caspases- controlling intracellular signals by protease zymogen activation. *Biochimica et Biophysica Acta* **1477**: 299–306.

Sulston JE, Horvitz HR. **1977**. Post-embryonic cell lineages of the nematode, *Caenorhabditis elegans*. *Developmental Biology* **56**: 110–56.

Takemoto D, Jones DA, Hardham AR. **2003**. GFP-tagging of cell components reveals the dynamics of subcellular re-organization in response to infection of Arabidopsis by oomycete pathogens. *The Plant Journal* **33**: 775–792.

Thomas SG, Franklin-Tong VE. **2004**. Self-incompatibility triggers programmed cell death in *Papaver* pollen. *Nature* **429**: 305–309.

Thomas SG, Huang S, Li S, Staiger CJ, Franklin-Tong VE. **2006**. Actin depolymerization is sufficient to induce programmed cell death in self-incompatible pollen. *The Journal of Cell Biology* **174**: 221–229.

Tian M, Chaudhry F, Ruzicka DR, Meagher RB, Staiger CJ, Day B. **2009**. Arabidopsis actin-depolymerizing factor AtADF4 mediates defense signal transduction triggered by the *Pseudomonas syringae* effector AvrPphB. *Plant Physiology* **150**: 815–824.

Tiwari BS, Belenghi B, Levine A. **2002**. Oxidative stress increased respiration and generation of reactive oxygen species, resulting in ATP depletion, opening of mitochondrial permeability transition, and programmed cell death. *Plant Physiology* **128**: 1271–1281.

Tristán CA. **2008**. Gene expression profile of Nicotiana tabacum plants expressing *Caenorhabditis elegans*' programmed cell death genes. *Gene Expression*: 24.

Uren AG, O'Rourke K, Aravind LA, Pisabarro MT, Seshagiri S, Koonin EV, Dixit VM. **2000**. Identification of paracaspases and metacaspases: two ancient families of caspase-like proteins, one of which plays a key role in MALT lymphoma. *Molecular Cell* **6**: 961–967.

Utsumi T, Sakurai N, Nakano K, Ishisaka R. **2003**. C-terminal 15 kDa fragment of cytoskeletal actin is posttranslationally N-myristoylated upon caspase-mediated cleavage and targeted to mitochondria. *FEBS Letters* **539**: 37–44.

Vacca RA, Pinto MCD, Valenti D, Passarella S, Marra E, Nazionale C, A VA, Vegetale P, Orabona V, Bari I, Sanctis VD, Campobasso I, Interdipartimentale C. **2004**. Production of reactive oxygen species, alteration of cytosolic ascorbate peroxidase,

and impairment of mitochondrial metabolism are early events in heat shock-induced programmed cell death in tobacco bright-yellow 2 Cells. *Plant Physiology* **134**: 1100–1112.

Vacca RA, Valenti D, Bobba A, Merafina RS, Passarella S. **2006**. Cytochrome c is released in a reactive oxygen species-dependent manner and is degraded via caspase-like proteases in tobacco bright-yellow 2 cells en route to heat shock-induced cell eeath 1. *Plant Physiology* **141**: 208–219.

van der Biezen EA, Jones JD. **1998**. The NB-ARC domain: a novel signalling motif shared by plant resistance gene products and regulators of cell death in animals. *Current Biology* **8**: R226–227.

van Doorn W G. **2004**. Update on senescence is petal senescence due to sugar starvation? *Plant Physiology* **134**: 35–42.

van Doorn W G. **2011**. Classes of programmed cell death in plants, compared to those in animals. *Journal of Experimental Botany* **62**: 4749–4761.

van Doorn W G, Beers EP, Dangl JL, Franklin-Tong VE, Gallois P, Hara-Nishimura I, Jones AM, Kawai-Yamada M, Lam E, Mundy J, Mur LAJ, Petersen M, Smertenko A, Taliansky M, Van Breusegem F, Wolpert T, Woltering E, Zhivotovsky B, Bozhkov PV. **2011**. Morphological classification of plant cell deaths. *Cell Death and Differentiation* **18**: 1241–1246.

van Doorn W G, Woltering EJ. **2005**. Many ways to exit? Cell death categories in plants. *Trends in Plant Science* **10**: 117–122.

van Doorn W G, Yoshimoto K. **2010**. Role of chloroplasts and other plastids in ageing and death of plants and animals: a tale of Vishnu and Shiva. *Ageing Research Reviews* **9**: 117–30.

Vasil V, Vasil IK. **1974**. Regeneration of tobacco and petunia plants from protoplasts and culture of corn protoplasts. *In Vitro Cellular & Developmental Biology - Plant* **10**: 83–96.

Vaux DL, Weissman IL, Kim SK. **1992**. Prevention of programmed cell death in *Caenorhabditis elegans* by human bcl-2. *Science (New York, N.Y.)* **258**: 1955–1957.

Vianello A, Zancani M, Peresson C, Petrussa E, Casolo V, Krajňáková J, Patui S, Braidot E, Macrì F. **2007**. Plant mitochondrial pathway leading to programmed cell death. *Physiologia Plantarum* **129**: 242–252.

Vuosku J, Sarjala T, Jokela A, Sutela S, Sääskilahti M, Suorsa M, Läärä E, Häggman H. **2009**. One tissue, two fates: different roles of megagametophyte cells during Scots pine embryogenesis. *Journal of Experimental Botany* **60**: 1375–1386.

Wada S, Ishida H, Izumi M, Yoshimoto K, Ohsumi Y, Mae T, Makino A. **2009**. Autophagy plays a role in chloroplast degradation during senescence in individually darkened leaves. *Plant Physiology* **149**: 885–893.

Wang C, Youle RJ. **2009**. The role of mitochondria in apoptosis*. *Annual Review of Genetics* **43**: 95–118.

Wang W, Pan J, Zheng K, Chen H, Shao H, Guo Y, Bian H, Han N, Wang J, Zhu M. **2009**. Ced-9 inhibits Al-induced programmed cell death and promotes Al tolerance in tobacco. *Biochemical and Biophysical Research Communications* **383**: 141–145.

Wertman J, Lord CEN, Dauphinee AN, Gunawardena A H L A N. **2012**. The pathway of cell dismantling during programmed cell death in lace plant (*Aponogeton madagascariensis*) leaves. *BMC Plant Biology* **12**: 115.

Widlak P, Garrard WT. **2005**. Discovery, regulation, and action of the major apoptotic nucleases DFF40/CAD and endonuclease G. *Journal of Cellular Biochemistry* **94**: 1078–1087.

Wilson ZA, Song J, Taylor B, Yang C. **2011**. The final split: the regulation of anther dehiscence. *Journal of Experimental Botany* **62**: 1633–1649.

Wittenbach VA, Lin W, Hebert RR. **1982**. Vacuolar localization of proteases and degradation of chloroplasts in mesophyll protoplasts from senescing primary wheat leaves. *Plant Physiology* **69**: 98–102.

Wright H, van Doorn Wouter G, Gunawardena A H L A N. **2009**. *In vivo* study of developmental programmed cell death using the lace plant (*Aponogeton madagascariensis*; Aponogetonaceae) leaf model system. *American Journal of Botany* **96**: 865–876.

Xu P, Rogers SJ, Roossinck MJ. **2004**. Expression of antiapoptotic genes bcl-xL and ced-9 in tomato enhances tolerance to viral-induced necrosis and abiotic stress. *Proceedings of the National Academy of Sciences of the United States of America* **101**: 15805–15810.

Xu Q, Reed JC. **1998**. Bax inhibitor-1, a mammalian apoptosis suppressor identified by functional screening in yeast. *Molecular Cell* **1**: 337–346.

Yakimova ET, Kapchina-Toteva VM, Woltering EJ. **2007**. Signal transduction events in aluminum-induced cell death in tomato suspension cells. *Journal of Plant Physiology* **164**: 702–708.

Yamada Y, Zhi-qi Y, Ding-tai T. **1986**. Plant regeneration from protoplast-derived callus of rice (*Oryza sativa* L.). *Plant Cell Reports* **5**: 85–88.

Yan Xiu Z, Harris PJC, Dun-yi Y. **1995**. Plant regeneration from protoplasts isolated from cotyledons of Sesbania bispinosa. *Plant Cell, Tissue and Organ Culture* **40**: 119–123.

Yao N, Eisfelder BJ, Marvin J, Greenberg JT. **2004**. The mitochondrion-an organelle commonly involved in programmed cell death in *Arabidopsis thaliana*. *The Plant Journal* **40**: 596–610.

Yoo SD, Cho YH, Sheen J. **2007**. Arabidopsis mesophyll protoplasts: a versatile cell system for transient gene expression analysis. *Nature* **2**: 1565–1572.

Yoshinaga Keiko, Arimura S, Niwa Y, Tsutsumi N, Uchimiya Hirofumi, Kawai-Yamada Maki. **2005**. Mitochondrial behaviour in the early stages of ROS stress leading to cell death in *Arabidopsis thaliana*. *Annals of Botany* **96**: 337–342.

Yu X-H, Perdue TD, Heimer YM, Jones a M. **2002**. Mitochondrial involvement in tracheary element programmed cell death. *Cell Death and Differentiation* **9**: 189–198.

Zamzami BN, Marchetti P, Castedo M, Zanin C, Vayssi J, Petit PX, Kroemer G. **1995**. Reduction in mitochondrial potential constitutes an early irreversible step of programmed lymphocyte death *In vivo*. *The Journal of Experimental Medicine* **181**: 1661–1672.

Zhang J, Dong M, Li L, Fan Y, Pathre P, Dong J, Wells JM, Olivares-villagómez D, Kaer LV, Wang X, Xu M, Lit L, Lou D, Olivares-villagmez D. **2003**. Endonuclease G is required for and normal apoptosis in mice early embryogenesis. *Proceedings of the National Academy of Science* **100**: 15782–15787.

Zhang L, Li Y, Xing D, Gao C. **2009**. Characterization of mitochondrial dynamics and subcellular localization of ROS reveal that HsfA2 alleviates oxidative damage caused by heat stress in Arabidopsis. *Journal of Experimental Botany* **60**: 2073–2091.

Appendix A Copyright Permission Letters

A large portion of the introduction was published in *The European Journal of Cell Biology* by the Elsevier publishing company. Chapter 2 was published in *The Americas Journal of Plant Science and Biotechnology* by the Global Science Books publishing company. Chapter 3 was published in *Planta* by the Springer publishing company. Chapter 4 was published in *BMC Plant Biology* by BioMed Central publishing company; this publication is "open access". Chapter 5 was published in PLOS ONE; this publication is also "open access". Chapter 6 was also published in *BMC Plant Biology* by BioMed Central publishing company; again this publication is "open access". Chapter 7 is original content.

Appendix A.1 Copyright Permission for Chapter 1

ELSEVIER LICENSE
TERMS AND CONDITIONS

Jul 26, 2012

This is a License Agreement between Christina EN Lord ("You") and Elsevier ("Elsevier") provided by Copyright Clearance Center ("CCC"). The license consists of your order details, the terms and conditions provided by Elsevier, and the payment terms and conditions.

All payments must be made in full to CCC. For payment instructions, please see information listed at the bottom of this form.

Supplier	Elsevier Limited The Boulevard,Langford Lane Kidlington,Oxford,OX5 1GB,UK
Registered Company Number	1982084
Customer name	Christina EN Lord
Customer address	Dalhousie University Halifax , NS B3H 4R2
License number	2904330816156
License date	May 08, 2012
Licensed content publisher	Elsevier
Licensed content publication	European Journal of Cell Biology
Licensed content title	Programmed cell death in*C. elegans*, mammals and plants
Licensed content author	Christina E.N. Lord,Arunika H.L.A.N. Gunawardena
Licensed content date	16 April 2012
Licensed content volume number	
Licensed content issue number	
Number of pages	1
Start Page	
End Page	
Type of Use	reuse in a thesis/dissertation
Portion	full article
Format	both print and electronic
Are you the author of this Elsevier article?	Yes
Will you be translating?	No
Order reference number	
Title of your thesis/dissertation	Developmentally Regulated and Environmentally Induced Programmed Cell Death (PCD) in the Lace Plant (Aponogeton madagascariensis)
Expected completion date	Oct 2012
Estimated size (number of pages)	120

Appendix A.2 Copyright Permission for Chapter 2

Copyright of this manuscript is transferred to Global Science Books (GSB).

A GSB Copyright Transfer Form (CTF), which details the below, is NOT available online but is provided when the manuscript has been provisionally accepted for publication and is sent as an e-mail attachment together with the revised manuscript text.

By signing the CTF, the author authorizes GSB to publish that work, in all formats and in all languages throughout the world, and to include it in any electronic databases and retrieval systems as it deems necessary. GSB grants authors the permission to copy their work for academic, non-profit purposes only (lectures, classes, seminars), restricted to their Academic Institute, or to post the electronic version on their personal or Institutional web-page provided that full acknowledgement is provided to Global Science Books, including a link to the GSB website (www.globalsciencebooks.info). Manuscripts containing copyright content (text, tables, figures, etc.) must ensure that the file is password protected or that access to the file is password protected. Requests by third parties must be made through GSB directly, and cannot be processed by the author(s).

Additionally in an email received from Global Science Book Ltd on 09/02/12 they state

> "Dear Christina,
> We sincerely apologise for the lack of response.
> We have been over-loaded with work.
> You have full permission but please be sure to add a full reference to the source and a note of thanks to the publisher, Global Science Books, Ikenobe, Japan.
> Sincerely,
> GSB Administration"

The authors would like to specifically thank Global Science Books, Ikenobe, Japan for allowing the reproduction of this article for this dissertation.

Appendix A.3 Copyright Permission for Chapter 3

SPRINGER LICENSE
TERMS AND CONDITIONS

Aug 05, 2012

This is a License Agreement between Christina EN Lord ("You") and Springer ("Springer") provided by Copyright Clearance Center ("CCC"). The license consists of your order details, the terms and conditions provided by Springer, and the payment terms and conditions.

All payments must be made in full to CCC. For payment instructions, please see information listed at the bottom of this form.

License Number	2956620123856
License date	Jul 26, 2012
Licensed content publisher	Springer
Licensed content publication	Planta
Licensed content title	Environmentally induced programmed cell death in leaf protoplasts of *Aponogeton madagascariensis*
Licensed content author	Christina E. N. Lord
Licensed content date	Jan 1, 2010
Volume number	233
Issue number	2
Type of Use	Thesis/Dissertation
Portion	Full text
Number of copies	4
Author of this Springer article	Yes and you are the sole author of the new work
Order reference number	
Title of your thesis / dissertation	Developmentally Regulated and Environmentally Induced Programmed Cell Death (PCD) in the Lace Plant (Aponogeton madagascariensis)
Expected completion date	Oct 2012
Estimated size(pages)	120
Total	0.00 USD

Appendix A.4 Copyright Permission for Chapter 4

BioMed Central Open Access license agreement

Brief summary of the agreement

Anyone is free:

- to copy, distribute, and display the work;
- to make derivative works;
- to make commercial use of the work;

Under the following conditions: Attribution

- the original author must be given credit;
- for any reuse or distribution, it must be made clear to others what the license terms of this work are;
- any of these conditions can be waived if the authors gives permission.

Statutory fair use and other rights are in no way affected by the above.

Appendix A.5 Copyright Permission for Chapter 5

Open-Access License

No Permission Required

PLOS applies the Creative Commons Attribution License (CCAL) to all works we publish (read the human-readable summary or the full license legal code). Under the CCAL, authors retain ownership of the copyright for their article, but authors allow anyone to download, reuse, reprint, modify, distribute, and/or copy articles in PLOS journals, so long as the original authors and source are cited. No permission is required from the authors or the publishers.

In most cases, appropriate attribution can be provided by simply citing the original article (e.g., Kaltenbach LS et al. (2007) Huntingtin Interacting Proteins Are Genetic Modifiers of Neurodegeneration. *PLOS Genet* 3(5): e82. doi:10.1371/journal.pgen.0030082). If the item you plan to reuse is not part of a published article (e.g., a featured issue image), then please indicate the originator of the work, and the volume, issue, and date of the journal in which the item appeared. For any reuse or redistribution of a work, you must also make clear the license terms under which the work was published.

This broad license was developed to facilitate open access to, and free use of, original works of all types. Applying this standard license to your own work will ensure your right to make your work freely and openly available. Learn more about open access. For queries about the license, please contact us.

Appendix A.6 Copyright Permission for Chapter 6

BioMed Central Open Access license agreement

Brief summary of the agreement

Anyone is free:

- to copy, distribute, and display the work;
- to make derivative works;
- to make commercial use of the work;

Under the following conditions: Attribution

- the original author must be given credit;
- for any reuse or distribution, it must be made clear to others what the license terms of this work are;
- any of these conditions can be waived if the authors gives permission.

Statutory fair use and other rights are in no way affected by the above.

Appendix B

Table Summarizing the Differences and Similarities Between Developmentally Regulated and Environmentally Induced PCD Within the Lace Plant

Timing from the onset of anthocyanin loss is detailed for developmentally regulated PCD while the timing following 20 min HS at 55°C is given for induced PCD. Within the developmentally regulated timing column a solid line indicates that these organelle characteristics probably occur concurrently. A dashed line indicates the timing between actin bundling/ increased TVS/ reduction in chloroplast size number and PM collapse. A dotted line indicates the timing between vacuole swelling/ tonoplast rupture and PM collapse. Lastly a dashed and dotted line indicates the timing between PM collapse and cell wall disappearance. Note that evidence for each organelle characteristic is noted within its own column; this evidence was amalgamated from this entire dissertation to ensure easy reference to the organelle event in question.

	Developmentally Regulated		Environmentally Induced	
Organelle/ Cellular event	**Timing From Anthocyanin Loss**	**Evidence**	**Timing Post HS (min)**	**Evidence**
Anthocyanin reduction	-	Wertman et al. 2012, BMC plant Biol Fig 8; Additional file 2 (thesis Fig 6.8; online resource 6.2)	60-120 ?	Between 60-120 min tonoplast changes, leading to slow release of anthocyanin?
Increased vesiculation	Throughout PCD process, until PM collapse	Wertman et al. 2012 BMC Plant Biol Fig 4 and 8 (thesis Fig 6.4 and 6.8)	0-120 ?	Throughout PCD process, until PM collapse?
Actin bundling		Lord et al. 2012, Plos one Fig 2 and 3 (thesis Fig 5.2 and 5.3) Wertman et al. 2012, BMC plant Biol Fig 8 (thesis Fig 6.8)	-	-
Increased TVS		Lord et al. 2011, BMC plant Biol, Fig 6 and 7; Additional file 6 and 7 (thesis Fig 4.6 and 4,7; online resource 4.6 and 4.7) Wertman et al. 2012 BMC Plant Biol Fig 8; Additional file 1 and 2 (thesis Fig 6.8; online resource 6.1 and 6.2)	60-120	Lord and Gun 2011, Planta Fig 3f (thesis Fig 3.3f)
Reduction in chloroplast size and number/ visible chlorophyll		Lord 2011 et al. BMC plant Biol Fig 7 (thesis Fig 4.7) Wright et al. 2009 Fig 2 Wertman et al. 2012 BMC Plant Biol Fig 1 and 8; Additional file 1 (thesis Fig 6.1 and 6.8; online resource 6.1)	30-120	Lord and Gun 2011, Planta Fig 4 [120min]; Online resource 3a and 3b [30min] (thesis Fig 3.4; online resource 3.3 and 3.4) Thesis appendix C [30-120min]
Mitochondria aggregation	Approx 48 hrs Cont'd on next page	Lord et al. 2011, BMC plant Biol Fig 3 and 4 (thesis Fig 4.3 and 4.4) Wertman et al. 2012, BMC Plant Biol, Fig 3c (thesis Fig 6.3c)	30-60	Lord and Gun 2011, Planta Fig 6b [1 hour]; online resource 3b [30 min] (thesis Fig 3.6b; online resource 6.4)
Organelle* perinuclear accumulation		Lord et al. 2011, BMC plant Biol, Fig 6 (thesis Fig 4.6) Wertman et al. 2012, BMC Plant Biol Fig 3b and 8; Additional file 2 and 4 (thesis Fig. 6.3b and 6.8; online resource 6.2 and 6.4)	-	-
Organelle* Brownian motion		Lord et al. 2011, BMC plant Biol, Fig 4 (thesis Fig 4.4) Wertman et al. 2012 BMC Plant Biol Additional file 1 and 3 (thesis online resource 6.1 and 6.3)	30-60	Lord and Gun 2011, Planta online resource 1 and 2 (thesis online resource 3.1 and 3.2)

	Developmentally Regulated		Environmentally Induced	
Organelle/ Cellular event	**Timing From Anthocyanin Loss**	**Evidence**	**Timing Post HS (min)**	**Evidence**
Cessation of individual mitochondrial streaming	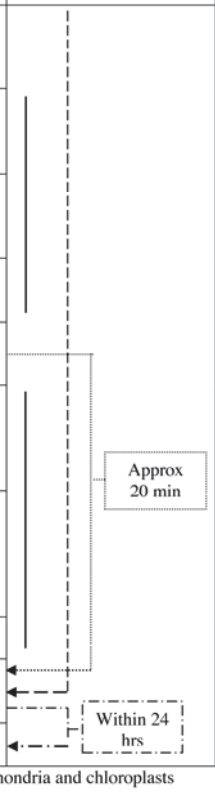	-	30-60	Lord and Gun 2011, Planta Fig 6 [1 hour]; online resource 3b [30 min] (thesis Fig 3.6; online resource 3.4)
TUNEL positive nuclei		Lord et al. 2011, BMC plant Biol, Fig 5 (thesis Fig 4.5) Wertman et al. 2012, BMC plant Biol Fig 3d and 8 (thesis Fig 6.3d and 6.8)	120	Lord and Gun 2011, Planta Fig 8 (thesis Fig 3.8)
Actin depolymerization		Lord et al. 2012, Plos one Fig 2 and 3 (thesis Fig. 5.2 and 5.3) Wertman et al. 2012, BMC plant Biol Fig 2 and 8 (thesis Fig 6.2 and 6.8)	0-120	Appendix D
Early cell wall changes		Gunawardena et al. 2004 Fig 3c Wertman et al. 2012 BMC Plant Biol Fig 7 and 8 (thesis Fig 6.7 and 6.8)	-	-
Vacuole swelling/ tonoplast rupture		Wertman et al. 2012 BMC Plant Biol Fig 8; Additional file 4 and 5 (thesis Fig 6.8; online resource 6.4 and 6.5)	60-120	Appendix C
Nuclear shrinkage		Lord et al. 2011, BMC plant Biol, Fig 7c (thesis Fig 4.7c) Wertman et al. 2012 BMC Plant Biol Fig 8; Additional file 4 and 5 (thesis Fig 6.8; online resource 6.4 and 6.5)	60-120	Lord and Gun 2011, Planta Fig 3 [1 hour] and 4 [2 hour] (thesis Fig 3.3 and 3.4)
Cessation of organelle* Brownian motion		Lord 2011, BMC plant Biol Figure 4; Additional Fig 3, 4 and 5 (thesis Fig 4.4; online resource 4.3, 4.4 and 4.5) Wertman et al. 2012 BMC Plant Biol Fig 8; Additional file 4 (thesis Fig 6.8; online resource 6.4)	60-120	Lord and Gun 2011, Planta online resource 2 (thesis online resource 3.2)
Loss of mitochondrial membrane potential		Lord 2011, BMC plant Biol Fig 3 and 4 (thesis 4.3 and 4.4)	60-120	Lord and Gun 2011, Planta Fig 7 (thesis Fig 3.7)
Plasma membrane collapse		Wertman et al. 2012 BMC Plant Biol Fig 6 and 8; Additional file 1, 4 , 5 and 6 (thesis Fig 6.6 and 6.8; online resource 6.1, 6.4, 6.5 and 6.6)	~120	Appendix C
Cell wall disappearance		Wertman et al. 2012, BMC plant Biol Fig 7 and 8 (thesis Fig 6.7 and 6.8)	-	-

* Referring to both mitochondria and chloroplasts

Appendix C

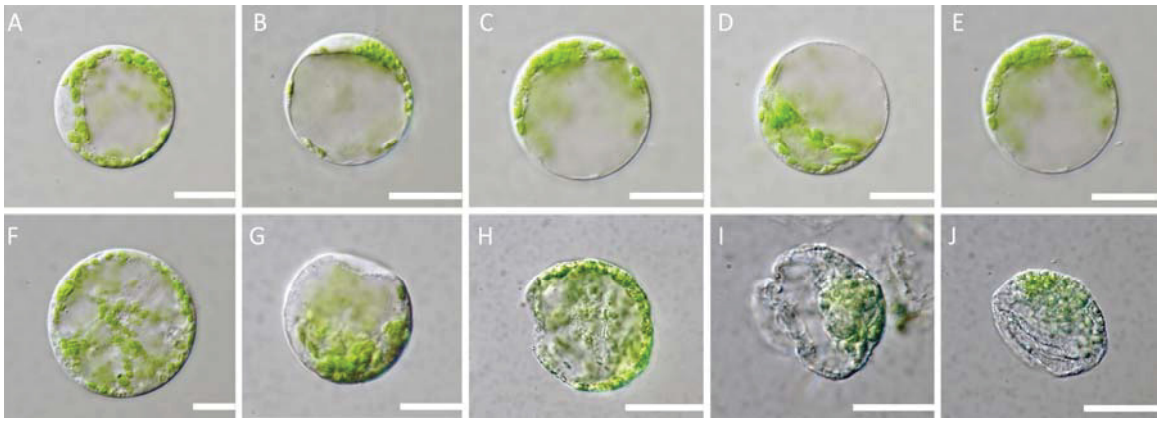

DIC Coloured Micrographs of Control and HS Treated Epidermal Protoplasts

(A-E) control protoplasts at time 0, 30, 60, 90, and 120 min respectively. Note little change in protoplast integrity in control samples. (F-J) HS treated protoplasts at time 0, 30, 60, 90 and 120 min respectively. Note decrease in chloroplast pigmentation and changes in vacuole/tonoplast dynamics between 60-120 min post HS (panels H-J). Scale bars= 40 μm.

Appendix D

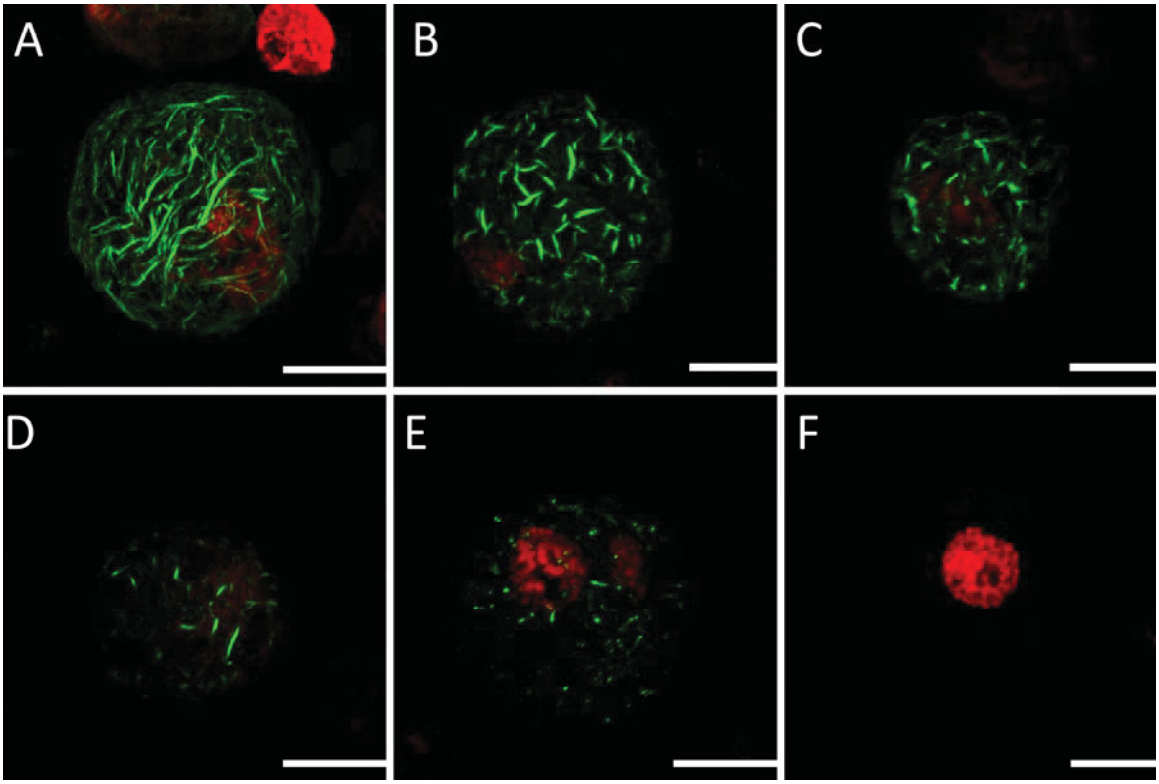

Actin Cytoskeleton Rearrangement in Control and Heat Shock Treated Individual Protoplasts

Protoplasts are stained with fluorescent Alexa Fluor 488 phalloidin (green) for actin microfilaments and counterstained with propidium iodide (PI; red) for nuclei; tissues are fixed. Each image is a representative maximum projection micrograph of approximately 25 z-stacks. (A) Control protoplast at Time 0. (B) HS treated protoplast at time 0, immediately following HS. (C) HS treated protoplast at time 30min. (D) HS treated protoplast at time 60min. (E) HS treated protoplast at time 90min. (F) HS treated protoplast at time 120min. Scale bars = 50μm.

Appendix E

Online Resource: Protoplast HS at 55°C for 20 min and Monitored for 120min Post HS

Note dark pigment in top right hand protoplast is anthocyanin found within the vacuole. Also, note tonoplast changes and vacuole shrinkage followed by plasma membrane collapse in nearly all cells. 180x sped up. Scale bar = 10μm

Appendix F

Erratum to: Environmentally induced programmed cell death in leaf protoplasts of Aponogeton madagascariensis

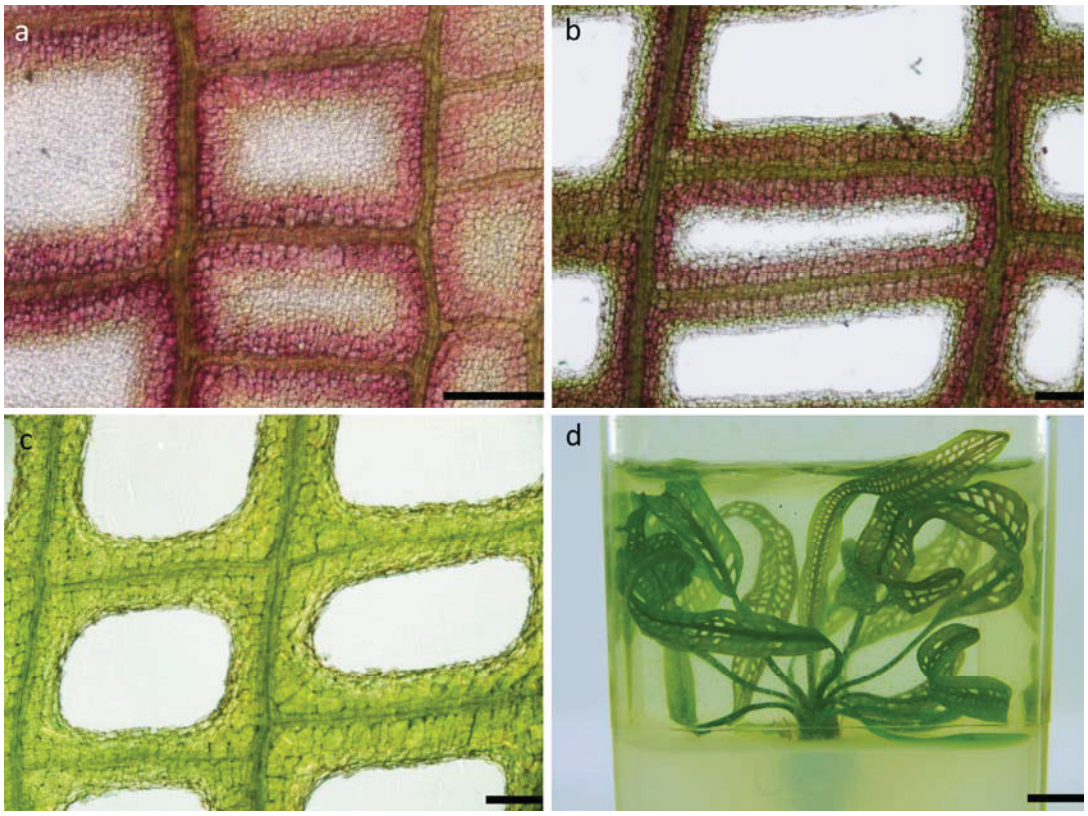

The lace plant (*Aponogeton madagascariensis*). (a) Window stage lace plant leaf, displaying transparent windows where PCD is occurring. (b) Perforation expansion lace plant leaf portraying the expansion of the perforated areole. (c) Mature lace plant leaf showing completed perforations between longitudinal and transverse veins. (d) Sterile lace plant in magenta box. Scale bars 100 μm (a–c), 1 cm (d).